



## FHR Materials, Fuels and Components White Paper

### Integrated Research Project Workshop 3

## Fluoride-Salt-Cooled High Temperature Reactor (FHR) Materials, Fuels and Components White Paper

#### Panel Members

Todd Allen (University of Wisconsin, Madison)

Mark Anderson (University of Wisconsin, Madison)

Ron Ballinger (Massachusetts Institute of Technology)

Tim Burchell (Oak Ridge National Laboratory)

Edward Blandford (University of New Mexico)

Denis Clark (Idaho National Laboratory)

William Corwin (Department of Energy)

George Flanagan (Oak Ridge National Laboratory)

Charles Forsberg (Massachusetts Institute of Technology)

Peter Hosemann (University of California, Berkeley)

David Holcomb (Oak Ridge National Laboratory)

Lin-Wen Hu (Massachusetts Institute of Technology)

John Hunn (Oak Ridge National Laboratory)

Victor Ignatiev (Kurchatov Institute)

Gordon Kohse (Massachusetts Institute of Technology)

Regis Matzie (*ret.* Westinghouse Electric Company)

Matthew Memmott (Westinghouse Electric Company)

Jim Nestell (MPR Associates)

Michael Patterson (Idaho National Laboratory)

Scott Penfield (Technology Insights)

Per Peterson (University of California, Berkeley)

Sam Sham (Oak Ridge National Laboratory)

Lance Snead (Oak Ridge National Laboratory)

Kumar Sridharan (University of Wisconsin, Madison)

Carl Stoots (Idaho National Laboratory)

Richard Vollmer (Westinghouse Electric Company)

David Williams (Oak Ridge National Laboratory)

Dane Wilson (Oak Ridge National Laboratory)

#### UW Madison Facilitators

Guoping Cao

Tyler Gerczak

Brian Kelleher

Guiqiu Zheng

#### MIT Facilitators

David Carpenter

Becky Romatoski

John Dennis Stempien

#### UC Berkeley Facilitators

Anselmo Cisneros

Lakshana Huddar

Raluca Scarlat

Nicolas Zweibaum

UCBTH-12-003

Final

July 2013

Department of Nuclear Engineering and Engineering Physics

University of Wisconsin, Madison

This research is being performed using funding received from the U.S. Department of Energy  
Office of Nuclear Energy's Nuclear Energy University Programs.



## Preamble

The University of California, Berkeley; Massachusetts Institute of Technology; and University of Wisconsin, Madison, hosted a series of four workshops during 2012 under a U.S. Department of Energy-sponsored Integrated Research Project (IRP) to review technical and licensing issues for fluoride-salt-cooled, high-temperature reactors (FHRs). The focus of the third workshop was to discuss key fuel and materials needs unique to FHRs, as well as methods for tritium and beryllium control. FHRs deliver heat at temperatures in the range of 600°C to 700°C, and thus structures and components must be designed for high-temperature service where time-dependent phenomena are important. Recently, closely related progress has been made in high-temperature design and materials as a part of U.S. research for the Next Generation Nuclear Plant and for liquid metal reactors. This white paper reviews the current status of this work, and identifies additional work needed to support FHR development.

The four workshops are a central element of developing an FHR preliminary conceptual design report to be completed in 2014. This third white paper focuses on material covered by the third workshop and is divided into six chapters. The first chapter provides an overview and discusses the unique environmental conditions that FHR structures and components experience. The second, third, and fourth chapters review FHR fuels, ceramic materials, and metallic materials respectively. The fifth chapter reviews FHR salt corrosion and chemistry control. The sixth chapter reviews tritium and beryllium control issues for FHRs.

The comments of the experts attending the workshop were also integrated into this white paper. The IRP team sincerely appreciates the input of all of the experts who attended and contributed to the third FHR workshop, as well as the hard work of the graduate students and postdoctoral scholars who organized it, facilitated the sessions, and drafted the major sections of this white paper based on their research and the review and input of the workshop experts.

## Executive Summary

The fluoride-salt-cooled, high-temperature reactor (FHR) is a new reactor concept that uses a novel combination of fuel, coolant and materials: graphite-matrix, coated particle fuel; fluoride salt coolant; graphite moderator materials; and high-temperature metallic structural materials. This white paper provides a review of the results from a two-day expert workshop held in Madison, Wisconsin, in August 2012. It reviews the state-of-the-art for these materials and fuels, and the issues that arise from their application to FHRs.

FHRs are graphite-moderated, thermal-spectrum nuclear power systems. The neutron spectrum in these systems is selected to enable negative coolant temperature reactivity feedback and maximize burnup. The neutron spectrums in FHRs are much softer than those in pressurized water reactors and slightly harder than those in high-temperature, gas-cooled reactors (HTGRs). FHR fuel utilization is quite similar to that of HTGRs, but components in FHRs are exposed to larger neutron fluxes than in HTGRs due to the much higher power density in FHRs. To deal with the radiation damages to graphite reflectors in FHRs, the inner graphite reflector is designed to be replaced once it reaches its radiation damage limit and the outer graphite reflector is protected from radiation damage by graphite pebble reflectors.

The baseline pebble fuel uses an annular fuel layer of graphite-matrix-coated particles, with a center, inert kernel of lower-density graphite. The graphite matrix is the primary reactor neutron moderator and the structural form of the fuel. These coated particle fuels have the ability to maintain their integrity up to temperatures of 1600°C or higher, which provides highly robust safety characteristics to FHRs. The fuel can be in many geometric forms including pebbles, prismatic blocks, plates, and stringers. The pebble fuel was selected as the baseline FHR fuel form because of the lowest development risk and lower fabrication costs. This white paper discusses the performance of FHR fuel, quality verification requirements and development needs.

The baseline FHR design assumes limited use of carbon fiber reinforced composites (CFRC), for example for the core barrel assembly, and silicon carbide fiber reinforced composite (SiC/SiC) for structures in high neutron rate regions of the core, for example for liners for shutdown rod channels. Experts agreed that these composite materials are likely to perform as expected in nuclear reactor environments. However, since there is no precedent for using ceramic composites within a nuclear reactor, American Society for Testing and Materials standard test procedures will be established to qualify ceramic composites for nuclear reactor applications. Since information on the compatibility of CFRC and SiC/SiC in fluoride salts is also limited, corrosion data to validate lifetime predictions of composite materials in FHRs is needed.

FHRs operate at significantly higher temperature than light water reactors and even liquid metal reactors. To ensure safe and reliable operation of FHRs for thirty or sixty years, time-dependent creep deformation of reactor structural materials must be limited. Type 316 stainless steel (SS) and Alloy N are two candidate alloys to make the reactor vessel and intermediate heater exchangers. Experts emphasized that only a single metallic structural material should be used in contact with the FHR coolant salts to prevent electro-chemical interactions. 316 SS is an

attractive candidate material for use in FHRs due to the extensive experience for nuclear applications, its good tolerance for neutron irradiation and the well developed ASME Section III code case for high temperature use. Because the code for 316 SS does not address corrosion and neutron embrittlement, some further evaluation is needed to address these effects. Alloy N is a reasonably well proven alloy for structural components that operate at temperatures up to 704°C in low neutron flux regions (up to 1 dpa). It has excellent corrosion resistance in fluoride salts. However, Alloy N is not code qualified for Subsection NH – Class 1 Components in Elevated Temperature Service. To qualify Alloy N for Subsection NH, extensive data, especially creep rupture and creep fatigue, in relevant FHR fluoride salt environment is required.

Optimizing the method to control corrosion of structural materials in fluoride salts is a key research goal for FHRs. Presence of graphite and the production of tritium fluoride (TF) due to neutron irradiation will affect the corrosion of structural materials. This white paper presents studies performed at the University of Wisconsin in recent years on corrosion of structural alloys (316 SS and Alloy N) in different salt systems, including flinak and KCl-MgCl<sub>2</sub> systems, and corrosion control by redox control. It was found that graphite can accelerate corrosion in molten salt systems and metallic redoxagents (Zr or Na) can improve the corrosion resistance of 316 SS. However, graphite damage is also observed when Zr or Na redox is added into the salt. This shows optimal redox control is important to minimize corrosion of metallic materials and also avoid graphite damage. Further study is needed on the compatibility of structural alloys, graphite and composite materials in the flibe primary coolant. Impurities in the salt, particularly moisture and oxygen, also have significant effects on corrosion. This white paper discusses purification of salts by hydrofluoric acid and hydrogen used in the Molten-Salt Reactor Experiment and alternative methods such as fluorination with NF<sub>3</sub>. Experts agreed that developing methods to control salt chemistry, on-line monitoring of salt chemistry and in-service inspection of structures are critical to the successful development of FHR technology.

Tritium production is a key issue associated with FHRs that needs to be managed. This white paper also discusses tritium production, transport and recovery. During steady state operation, Be-9 and Li-7 are major constituents in the primary salt to produce tritium through neutron interactions. Tritium permeates through high-temperature metals easily. Metallic and ceramic barriers have been studied to reduce tritium permeation through heat exchangers. Alumina (Al<sub>2</sub>O<sub>3</sub>) and SiC appear to be good candidates for advanced FHR systems, because it has very low tritium diffusivity. An alternative is to use double-walled tubes in place of the single-walled tubes, particularly for application to steam generators for FHRs. Double-walled heat exchangers with sweep flow may help to remove tritium. Many methods have been proposed to isolate and extract tritium from fluoride salts. Experts emphasized that tritium transport and management should be one of the key technology developments in an FHR test reactor.

The beryllium contained in flibe, the baseline FHR primary salt, is toxic. This white paper discusses the standards for acceptable beryllium levels in the work place, proper handling of beryllium and safety measures. It is advisable to have an in-house analytical facility capable of fast turnaround times on beryllium swipes and air monitors to avoid the long lead time associated with sending samples to off-site labs. To avoid the handling of toxic beryllium-containing salts, alternative coolants such as enriched zirconium fluoride (ZrF<sub>4</sub>) may also be used if affordable zirconium enrichment methods become available, though at the expense of less desirable neutronic and thermal hydraulic properties.



# Contents

<b>1</b>	<b>Introduction.....</b>	<b>15</b>
<b>1.1</b>	<b>Overview of the FHR Workshop Series .....</b>	<b>15</b>
<b>1.2</b>	<b>FHR Operating and Transient Conditions Relevant to Materials and Fuels.....</b>	<b>16</b>
1.2.1	Typical FHR Thermal, Pressure, and Flow Conditions .....	19
1.2.2	Typical FHR Neutron Flux and Dose Conditions .....	25
1.2.3	Typical FHR Refueling Conditions.....	27
<b>2</b>	<b>FHR Fuel Fabrication and Performance.....</b>	<b>30</b>
<b>2.1</b>	<b>Current Status of Coated-Particle Fuel Technology.....</b>	<b>30</b>
<b>2.2</b>	<b>Key Issues for FHR Fuels .....</b>	<b>34</b>
2.2.1	Candidate FHR Fuel Geometries .....	34
2.2.2	Unique FHR Operating Conditions.....	38
2.2.3	FHR Fuel Quality Verification Requirements.....	46
<b>2.3</b>	<b>Development Needs for FHR Fuel.....</b>	<b>46</b>
<b>3</b>	<b>FHR Ceramic and Ceramic Composite Components .....</b>	<b>50</b>
<b>3.1</b>	<b>FHR Graphite.....</b>	<b>50</b>
3.1.1	Current Status of Graphite Technology.....	50
3.1.2	Unique FHR Operating Conditions.....	57
<b>3.2</b>	<b>FHR Ceramic Composites.....</b>	<b>63</b>
3.2.1	Current Status of Ceramic Composites Technology .....	63
3.2.2	Unique FHR Operating Conditions.....	71
<b>3.3</b>	<b>In-Service Inspection and Component Testing for Composites.....</b>	<b>75</b>
3.3.1	In-Service Inspection.....	75
3.3.2	Component Testing Facility .....	77
<b>4</b>	<b>FHR Metallic Structural Materials.....</b>	<b>79</b>
<b>4.1</b>	<b>Current Status of Candidate Metallic Structural Materials for FHRs .....</b>	<b>79</b>
<b>4.2</b>	<b>In-Service Inspection and Components for Metallic Components .....</b>	<b>85</b>
4.2.1	In-Service Inspection.....	86
4.2.2	Component Testing Facility .....	87
<b>5</b>	<b>Salt Corrosion and Chemistry Control.....</b>	<b>89</b>
<b>5.1</b>	<b>Review of Previous Work in Salt Corrosion and Chemistry Control .....</b>	<b>90</b>
5.1.1	Corrosion in Molten Fluoride Salts.....	90
5.1.2	Effect of Additional Materials on Corrosion.....	91
5.1.3	Salt Purity Standards .....	92
5.1.4	Differences Between Flibe and Flinak .....	93
<b>5.2</b>	<b>Previous Work at UW.....</b>	<b>94</b>
5.2.1	Static Immersion Corrosion Test Overview .....	94
5.2.2	Material Corrosion and Thermal Hydraulic Studies at UW.....	94
5.2.3	Molten-Salt/Graphite Interaction Overview.....	96
<b>5.3</b>	<b>Previous MSRE/MSBR Work.....</b>	<b>99</b>
5.3.1	Passive Corrosive Control.....	99
5.3.2	Active Corrosion Control .....	100
5.3.3	MSRE Flibe Production .....	101
5.3.4	MSRE Salt Purity Analysis.....	103
<b>5.4</b>	<b>New Work Needed for Salt Corrosion and Chemistry Control.....</b>	<b>103</b>

5.4.1	Initial Operational Concerns and Pebble Treatment .....	103
5.4.2	Primary Loop Chemistry Control.....	104
5.4.3	Intermediate Loop Chemistry Control .....	105
<b>5.5</b>	<b>FHR Coolant Chemistry – Considerations for Failed Fuel and Accident Conditions.....</b>	<b>106</b>
5.5.1	Possible Fission Products of Concern .....	106
5.5.2	Data and Discussion.....	108
<b>5.6</b>	<b>In-Service Inspection and Component Testing for Salt Corrosion .....</b>	<b>115</b>
5.6.1	In-Service Inspection.....	115
5.6.2	Component Test Facility .....	116
<b>6</b>	<b>Tritium and Beryllium Control .....</b>	<b>117</b>
<b>6.1</b>	<b>FHR Tritium Control .....</b>	<b>117</b>
6.1.1	FHR Tritium Source Term .....	117
6.1.2	Comparison of Tritium Production in FHRs to PWRs and CANDUs .....	119
6.1.3	FHR Tritium Transport .....	121
6.1.4	FHR Tritium Barriers .....	123
6.1.5	FHR Tritium Management and Recovery .....	124
<b>6.2</b>	<b>FHR Beryllium Control.....</b>	<b>126</b>
6.2.1	Beryllium Health Effects and Standards .....	126
6.2.2	Beryllium Fluoride Health Effects .....	128
6.2.3	Previously Used Beryllium Fluoride Control Methods.....	131
6.2.4	Potential Beryllium Controls for the FHR .....	132
6.2.5	Expert Discussion on Beryllium Control .....	134
<b>7</b>	<b>References.....</b>	<b>135</b>
<b>Appendix A Thermal Hydraulic Modeling of the PB-AHTR Core in COMSOL</b>		
<b>Multiphysics.....</b>		<b>144</b>
<b>Appendix B Neutronic Model for FHR.....</b>		<b>148</b>
<b>Appendix C Fuel Options.....</b>		<b>155</b>
<b>Appendix D Thermal Hydraulic Modeling of the PB-AHTR Core in RELAP5 .....</b>		<b>162</b>

## List of Figures

Figure 1-1.	IRP Structure Illustrating Workshop Rationale and Key IRP Objectives (this white paper focuses on the third workshop).....	16
Figure 1-2.	2009 PB-AHTR Reactor System.....	17
Figure 1-3.	Operating Temperature Range for FHRs and LMRs, Compared to ASME Section III-Allowable Stresses for Typical Construction Materials.....	19
Figure 1-4.	Bulk Coolant Temperature (°C) Distribution in the 2009 PB-AHTR Core Under Normal Operating Conditions, Calculated in COMSOL Multiphysics.....	21
Figure 1-5.	Fuel Temperature (°C) Distribution (Average Kernel Temperature in Fuel Pebble) in the 2009 PB-AHTR Core Under Normal Operating Conditions, Calculated in COMSOL Multiphysics .....	22
Figure 1-6.	Pressure (kPa) Distribution in the 2009 PB-AHTR Core Under Normal Operating Conditions, Calculated in COMSOL Multiphysics.....	23
Figure 1-7.	Reynolds Number Distribution in the 2009 PB-AHTR Core Under Normal Operating Conditions, Calculated in COMSOL Multiphysics.....	24
Figure 1-8.	Neutron Flux of Various Nuclear Power Systems; Magenta Line Indicates Fast Flux Cutoff, 0.1 MeV .....	25
Figure 1-9.	2011 AHTR Refueling Station Components.....	28
Figure 1-10.	Temperature Evolution in a 2011 AHTR Fuel Element During Refueling Transient.....	29
Figure 2-1.	Optical Cross Section of a Fuel Particle From AGR-1 PIE Campaign (Hunn and Others 2012) .....	33
Figure 2-2.	Baseline PB-FHR Fuel Particle .....	35
Figure 2-3.	Geometry of the Baseline PB-AHTR Fuel Pebble .....	36
Figure 2-4.	Baseline 2011 AHTR Fuel Assembly with Dimensions in Centimeters.....	37
Figure 2-5.	Baseline 2011 AHTR Fuel Plate .....	38
Figure 2-6.	Power Density Evolution of Pebble at Various Locations in the 2009 PB-AHTR .....	40
Figure 2-7.	Average Fuel Kernel Temperature Evolution of Pebble at Various Locations in 2009 PB-AHTR .....	41
Figure 2-8.	Cumulative Failure Probability as a Function of Temperature and Burnup (Jeong, Jeong, and Chang 2009).....	42
Figure 2-9.	Map of Fast Flux Intensity in the Active Region of the 2009 PB-FHR .....	44
Figure 2-10.	TRISO Layer Behavior Under Irradiation (INL, Centre d'Etude Atomique, and Massachusetts Institute of Technology 2004) .....	45
Figure 2-11.	Buildup of Fission Gases in the 2009 PB-AHTR in a Single TRISO Particle.....	45
Figure 2-12.	Fuel Qualification Capsule for 2009 PB-AHTR Fuel: ATR 3-Inch Location .....	47
Figure 2-13.	Fuel Qualification Capsule for PB-AHTR Fuel: ATR 5.25-Inch Location .....	47
Figure 2-14.	Fuel Qualification Capsule for PB-AHTR Fuel: HFIR Boron Removal Location.....	48
Figure 2-15.	Few Group Neutron Energy Spectrum Comparison Between ATR (left) and HFIR (right) and the 2009 PB-AHTR in the Active Region.....	49
Figure 3-1.	Volumetric Response to Dose and Temperature of Generalized Graphite (Windes, Croson, and Roberts 2010).....	52

Figure 3-2.	Turnaround Point for Graphite (Windes, Croson, and Roberts 2010).....	52
Figure 3-3.	Tensile Strength Response to Dose and Temperature of Generalized Graphite (Windes, Croson, and Roberts 2010).....	53
Figure 3-4.	Typical Young's Modulus Response to Dose and Temperature of Generalized Graphite (Windes, Croson, and Roberts 2010).....	53
Figure 3-5.	NGNP VHTR Graphite Irradiation Test Plan (Bratton and Burchell 2005) .....	54
Figure 3-6.	2009 PB-AHTR Core Geometry with Graphite Structures Subsystem Highlighted in Red.....	58
Figure 3-7.	Energy Deposition Rate for Inner (left) and Outer (right) Graphite Reflectors as a Function of R-Z Position in the Active Region of the 2009 PB-AHTR.....	60
Figure 3-8.	Rates of dpa for Inner (left) and Outer (right) Graphite Reflectors as a Function of R-Z Position in the Active Region of the 2009 PB-AHTR.....	61
Figure 3-9.	Fast Flux in the Inner (left) and Outer (right) Graphite Reflectors as a Function of R-Z Position in the Active Region of the 2009 PB-AHTR.....	62
Figure 3-10.	Gas Production Rate in the Inner (left) and Outer (right) Graphite Reflectors as a Function of R-Z Position in the Active Region of the 2009 PB-AHTR.....	63
Figure 3-11.	2009 PB-AHTR Core Geometry with Ceramic Composites Highlighted in Red ...	72
Figure 3-12.	Peak Core Average Fuel Temperature Compared to Inlet and Outlet Core Coolant Temperatures During a 2009 PB-AHTR LOFC Transient (transient initiated at t=100s).....	73
Figure 4-1.	ASME Code-Allowable Stresses for Several Structural Materials .....	81
Figure 5-1.	Chromium Depletion Through the Thickness of the 800H Sample Exposed to Flinak at 850°C in a Graphite Crucible .....	92
Figure 5-2.	Typical Graphite Coupon Appearance Before Exposure to Flinak at 850°C for 1,000 hours (left) and After Cleaning Showing the Presence of the Chrome Carbide Coating (right) (The length is shorter because a cross section of the sample has been taken).....	96
Figure 5-3.	Cross-Sectional SEM Micrograph of Graphite Coupon Tested with 316L in Flinak at 850°C for 1,000 Hours (top) and Electron Backscatter Diffraction Analysis Phase Distribution Map of the White Dotted Rectangle on the SEM Micrograph (bottom) (Green and red phases represent Cr <sub>7</sub> C <sub>3</sub> and Mo <sub>2</sub> C, respectively).....	97
Figure 5-4.	Graphite Particle Dispersion Within Frozen Flinak in a Crucible Containing 316L, Graphite, and Metallic Sodium Held for 1,000 Hours at 850°C.....	98
Figure 5-5.	Graphite Intercalation Process by Alkali Metallics in Molten Flinak: (a) Beginning of Corrosion Test, (b) Alkali Uptake Between Layers of Graphene, (c) Complete Graphite Erosion.....	99
Figure 5-6.	ORNL's Batch Fluoride Salt Primary Chemical Reactor.....	102
Figure 5-7.	Stability of Selected Metal Fluorides (More negative indicates increasing stability of the fluoride (Beneš and Konings 2012)) .....	111
Figure 5-8.	Relative Stability of Fluoride Compounds of the Various Elements, Indicated Approximately by the Heat of Formation per Mole of Fluoride at an Unknown Temperature (Baes Jr. 1974) .....	113
Figure 5-9.	Stability via the Gibbs Free Energy of Formation of Select Fluoride Compounds (Fission products europium and cesium may not be stable	

	fluorides at all temperatures using beryllium for redox control. Calculated with HSC Chemistry v.6.0.) .....	113
Figure 6-1.	Cross Sections for (n.alpha) Reactions for <sup>6</sup> Li, <sup>7</sup> Li, and <sup>9</sup> Be.....	118
Figure 6-2.	Chest Radiographs of Worker Involved in the Production of Beryllium Metal from Beryllium Fluoride: (A) Before Being Hired; (D) Follow-Up .....	127
Figure 6-3.	Beryllium Fluoride Nugget Obtained from Materion.....	128
Figure 6-4.	Summary of Lung Function and Beryllium Exposure of Case 1 : (A) Results of Pulmonary Function Tests Before, During, and After Two Episodes of Acute Work-Related Illness. (B) Time-Weighted Average Airborne Beryllium Exposures in Patient’s Departments During This Time. ....	130
Figure 6-5.	An MSRE Employee Measuring Quantities of Salt for Production of Flibe .....	131
Figure A-1.	Geometric Configuration of the Annular PB-AHTR Core (Li et al. 2010).....	144
Figure A-2.	Geometric Configuration of the Annular PB-AHTR Core as Modeled in COMSOL Multiphysics.....	146
Figure B-1.	MCNP5 Model of TRISO Particles: (left) Pebble Scale Model with TRISO Particles in a Simple Cube Lattice; (right) a Single Unit Cell of a TRISO Particle with the TRISO Layers and Graphite Matrix Homogenized Together ....	149
Figure B-2.	FCC Pebble Unit Cell Model: (left) MCNP5 Model of Annular Fuel Pebbles: (orange) Flibe, (white) Pebble Shell, (pink) Active Region, and (grey) Inert Pebble Core; (right) Burnup States Within an FCC Unit Cell Model .....	150
Figure B-3.	Baseline PB-FHR Full Core Geometry .....	151
Figure B-4.	MCNP5 Model of Full Core PB-AHTR.....	152
Figure B-5.	Simplified Transmutation Flow Chart for a Two Burnup State System: (dark gray) Fuel Composition Flow, (white) Independent Parameters Supplied from Fuel Cycle Search and Neutron Transport, (light gray) Dependent Parameters Supplied from Transmutation Analysis .....	153
Figure B-6.	Continuous Composition Evolution Divided into Four Burnup States .....	154
Figure B-7.	BEAU Iterative Equilibrium Depletion Algorithm .....	154
Figure C-1.	Dimensional Change Contrast of CVD SiC and FCM Fuel with Nuclear Graphite ATR-2E and Matrix Graphite (C. W. Forsberg, Terrani, et al. 2012)....	156
Figure C-2.	Composition of Pebble Fuel (C. Forsberg 2008).....	157
Figure C-3.	Hexagonal Plate Fuel Assembly (Greene et al. 2010).....	158
Figure C-4.	HTTR Prismatic-Block Fuel (C. Forsberg 2008) .....	159
Figure C-5.	Pin-Type (“stringer”) Fuel (Ingersoll, Forsberg, and MacDonald 2007) .....	160
Figure D-1.	Schematic of the Modular PB-AHTR RELAP5 Model .....	162

## List of Tables

Table 1-1.	Thermal Hydraulic Comparison to Other Nuclear Power Systems.....	20
Table 1-2.	Neutron Flux Data of Various Nuclear Power Systems .....	26
Table 1-3.	Maximum Neutron Flux and Radiation Damage Values for Components of the 2009 PB-AHTR .....	26
Table 1-4.	Expected Refueling Period in the 2009 PB-AHTR .....	27
Table 2-1.	Geometric and Material Definition of the Baseline PB-FHR Coated-Fuel Particle .....	35
Table 2-2.	Geometric and Material Definition of the Baseline 2009 PB-AHTR Annular Fuel Pebble .....	37
Table 2-3.	Attainable Burnup in Various Reactors.....	38
Table 2-4.	Power in Representative Reactors .....	39
Table 2-5.	Temperatures in Various Reactors .....	40
Table 2-6.	Fast Fluence in the 2009 PB-AHTR at Various Locations.....	44
Table 2-7.	Fast Fluence in the 2009 PB-AHTR, ATR and HFIR at Various Locations.....	49
Table 3-1.	Graphite Properties (Billot et al. 2004; Chi and Kim 2008; Simpkins et al. 1989; Briggs 1964) .....	55
Table 3-2.	2009 PB-AHTR Surface Areas of the Inner and Outer Reflectors Exposed to Coolant at Temperature T.....	59
Table 3-3.	Energy Deposition Rate for the 2009 PB-AHTR Inner and Outer Graphite Reflector .....	61
Table 3-4.	Maximum Radiation Damage to the Inner and Outer 2009 PB-AHTR Graphite Reflector in Terms of dpa.....	62
Table 3-5.	Maximum Radiation Damage to Inner and Outer 2009 PB-AHTR Graphite Reflectors in Terms of Fast Flux (>0.1 MeV).....	62
Table 3-6.	Gas Production in the 2009 PB-AHTR Inner and Outer Graphite Reflector .....	63
Table 3-7.	Irradiation Effect Issues for SiC/SiC Composites (Katoh, Wilson, and Forsberg 2007).....	66
Table 3-8.	Ongoing SiC/SiC Research and Development Activities for Nuclear Applications and Their Focuses (Katoh, Wilson, and Forsberg 2007) .....	68
Table 3-9.	Radiation Damage and Gas Production Rates for Ceramic Composites in the 2009 PB-AHTR .....	74
Table 4-1.	FHR Constituents – Structural Materials.....	80
Table 4-2.	Specifications, Product Forms, Types, Grades, or Classes of 316 SS Permitted in Subsection NH (Natesan et al. 2008)* .....	83
Table 5-1.	Testing Parameters and Weight Loss for Two Static Corrosion Tests at 850°C.....	92
Table 5-2.	Acceptable Impurity Levels for the MSRE (Adhoum et al. 2006).....	93
Table 5-3.	Fission Product Inventories for Four Plants (Beahm et al. 1992) Based on the Total Core .....	108
Table 5-4.	Metallic Fission Products Known to Escape from Intact TRISO Fuel Particles in the VHTR (J. Harp) .....	108
Table 5-5.	Electrochemical Measurements of Redox Couples in Chlorides and Fluorides, Measured at 496°C (Del Cul, Williams, and Toth 2002) .....	110

Table 5-6.	Gibbs Free Energy of Formation of Fluorides at 727°C (1,000K) (Keiser, DeVan, and Manning 1977) .....	112
Table 5-7.	Approximate Relative Stability of Fluoride Indicated by the Gibbs Free Energy of Formation (Grimes 1967). These data are for the pure crystalline solid, not for the formation of molten fluorides in molten mixtures. ....	114
Table 6-1.	Equilibrium Tritium Production Rates for Different Types of Reactors.....	119
Table 6-2.	United States Regulatory Constraints on Tritium Concentration in Air and Water Effluents.....	121
Table 6-3.	Tritium Permeation Barriers and Their Associated Effectiveness .....	123
Table 6-4.	Workplace Beryllium Standards ( $\mu\text{g}/\text{m}^3$ ) as Dictated by Different Organizations.....	128
Table A-1.	Reactor Functional Requirements Related to Thermal Hydraulic Modeling of the Core.....	145
Table A-2.	Detailed Positions and Dimensions of the Outlet Ports in the COMSOL Multiphysics Model of the Annular PB-AHTR Core.....	147
Table B-1.	Geometric and Material Definition of the Baseline PB-AHTR Full Core .....	151

## Acronyms and Abbreviations

ABD – Acute Beryllium Disease  
AGC – Advanced Graphite Creep  
AGR – Advanced Gas-cooled Reactor  
AHTR – Advanced High-Temperature Reactor  
ASME – American Society of Mechanical Engineers  
ASTM – American Society for Testing and Materials International  
ATR – Advanced Test Reactor  
ATWS – Anticipated Transients Without Scram  
AVR – Arbeitsgemeinschaft Versuchsreaktor  
Be-LPT – Beryllium Lymphocyte Proliferation Test  
BPV – Boiler and Pressure Vessel (Code)  
BOL – Beginning of Life  
BWR – Boiling Water Reactor  
CBD – Chronic Beryllium Disease  
C/C – Carbon/Carbon (composites)  
CCD – Conduction Cool Down  
CFR – Code of Federal Regulations  
CFRC – Carbon Fiber-Reinforced Composite  
CTE – Coefficient of Thermal Expansion  
CVD – Chemical Vapor Deposition  
CVI – Chemical Vapor Infiltration  
DHX – DRACS Heat Exchanger  
DOE – U.S. Department of Energy  
dpa – Displacements per Atom  
DRACS – Direct Reactor Auxiliary Cooling System  
EFPD – Equivalent Full Power Days  
EFPY – Equivalent Full Power Years  
FHR – Fluoride-salt-cooled, High-temperature Reactor  
FHTR – FHR Test Reactor  
FIMA – Fissions per Initial Metal Atom  
FSVR – Fort St. Vrain Reactor  
GFR – Gas-cooled Fast Reactor  
GIF – Generation IV International Forum  
GT-MHR – Gas Turbine Modular Helium Reactor  
HFIR – High Flux Isotope Reactor  
HTGR – High-Temperature Gas-cooled Reactor  
HTTR – High-Temperature Test Reactor  
HTR – High-Temperature Reactor  
HX – Heat Exchanger  
IAEA – International Atomic Energy Agency  
IARC – International Agency for Research on Cancer  
ICP-MS – Inductively Coupled Plasma Mass Spectrometry  
ICP-OES – Inductively Coupled Plasma Optical Emission Spectrometry

IGC – Intergranular Grain-boundary Cracking  
IHX – Intermediate Heat Exchanger  
IMGA – Irradiated Microsphere Gamma Analyzer  
IPyC – Inner Pyrocarbon  
INL – Idaho National Laboratory  
IRP – Integrated Research Project  
IVFHM – In-Vessel Fuel Handling Machine  
JET – Joint European Tokamak  
LBL – Leach-Burn-Leach  
LMR – Liquid Metal Reactor  
LOCA – Loss of Coolant Accident  
LOFC – Loss of Forced Circulation  
LWR – Light-Water Reactor  
MHR – Modular Helium Reactor  
MIT – Massachusetts Institute of Technology  
MSBR – Molten Salt Breeder Reactor  
MSRE – Molten Salt Reactor Experiment  
MTS – Methyltrichlorosilane  
NAA – Neutron Activation Analysis  
NGNP – Next Generation Nuclear Plant  
NIOSH – National Institute for Occupational Safety and Health  
NITE – Nano-powder Infiltration and Transient Eutectoid  
NRC – U.S. Nuclear Regulatory Commission  
OPyC – Outer Pyrocarbon  
ORNL – Oak Ridge National Laboratory  
OSHA – Occupational Safety and Health Administration  
PARFUME – Particle Fuel Model  
PB-AHTR – Pebble Bed Advanced High-Temperature Reactor  
PBMR – Pebble Bed Modular Reactor  
PIE – Post-Irradiation Examination  
PPE – Personal Protective Equipment  
PRF – Permeability Reduction Factors  
PWR – Pressurized-Water Reactor  
RDC – Regulatory Design Criteria  
RSM – Refueling Station Manipulator  
SiC/SiC – Silicon Carbide (composites)  
SEM – Scanning Electron Microscopy  
SFR – Sodium Fast Reactor  
SS – Stainless Steel  
TEP – Transient Eutectic Phase  
THTR – Thorium High-Temperature Reactor  
TRISO – Tristructural Isotropic  
TZM – (Mo-0.5Ti-0.1Zr)  
VHTR – Very High Temperature Reactor  
UCB – University of California, Berkeley  
UW – University of Wisconsin

# 1 Introduction

Fluoride salts have unique thermophysical properties compared to other reactor coolants, which make them potentially attractive to use as coolants for high-temperature, low-pressure reactors called fluoride-salt-cooled, high-temperature reactors (FHRs). The U.S. Department of Energy (DOE) has initiated an Integrated Research Project (IRP) with the Massachusetts Institute of Technology (MIT); University of California, Berkeley (UCB); and University of Wisconsin, Madison (UW), to develop the technical basis to design, develop, and license commercially attractive FHRs. This is one of four white papers developed during the first year of the IRP to aid in identifying the technical basis and unique issues for the design and licensing of FHRs.

This white paper reviews key issues for fuel and materials for FHRs. The following section describes how this white paper integrates with the other three white papers in this series. The subsequent section reviews the environmental conditions (temperature, irradiation, chemistry) that FHR structures and components experience. Subsequent chapters review FHR fuel (Chapter 2), ceramic and composite structural materials (Chapter 3), metallic structural materials (Chapter 4), coolant chemistry and corrosion control (Chapter 5), and tritium and beryllium control (Chapter 6).

## 1.1 Overview of the FHR Workshop Series

To initiate the IRP, UCB, UW, and MIT organized a series of four workshops in 2012 to engage reactor technology experts in identifying and reviewing key FHR development issues (Figure 1-1). The first FHR workshop white paper discusses the major technical characteristics that differentiate FHRs from other power reactor technologies, the major systems and subsystems expected to be used in FHRs, high-level functional requirements for these systems and subsystems, and licensing basis events that should be considered in FHR design and licensing. The second workshop studied key thermal hydraulic, neutronic, and structural response phenomena and identified system response codes that are appropriate to predict the response of FHRs under steady-state operation and design basis events, along with experimental data needs to validate these models.

The experts who attended the third FHR workshop brought extensive experience in fuels, materials, and component testing, including the following areas:

- Coated-particle fuel fabrication, irradiation, and post-irradiation examination (PIE)
- Metallic structural materials for FHRs, with a focus on near-term options for a test reactor (FHTR), including 316 stainless steel (SS), Alloy N, and Alloy 800H, as well as practical issues of American Society of Mechanical Engineers (ASME) code qualification and design of pressure boundary structures subject to thermal creep
- Graphite response under irradiation/exposure to fluoride salt
- Composite structural materials for the response of reactor core internals [e.g., carbon/carbon (C/C) composites for core barrels, silicon carbide/silicon carbide

(SiC/SiC) composites for shutdown rod channels] under irradiation/exposure to fluoride salt

- Corrosion of structural materials in candidate primary and intermediate salts and salt chemistry control
- In-service inspection, on-line monitoring, maintenance, and replacement of components in high-temperature environments.

A draft of this white paper was made available to participants before the third workshop to provide background material on the topics to be covered during the workshop. The key goals for this workshop and white paper included the following:

- Identify the key fuel and materials needs that are unique to FHRs.
- Identify candidate materials including graphite, ceramic composites (C/C, SiC/SiC) and metallic structural materials for the FHR reactor vessel and intermediate heat exchanger (IHX).
- Identify methods for tritium and beryllium control.
- Identify additional work needed to support FHR development.

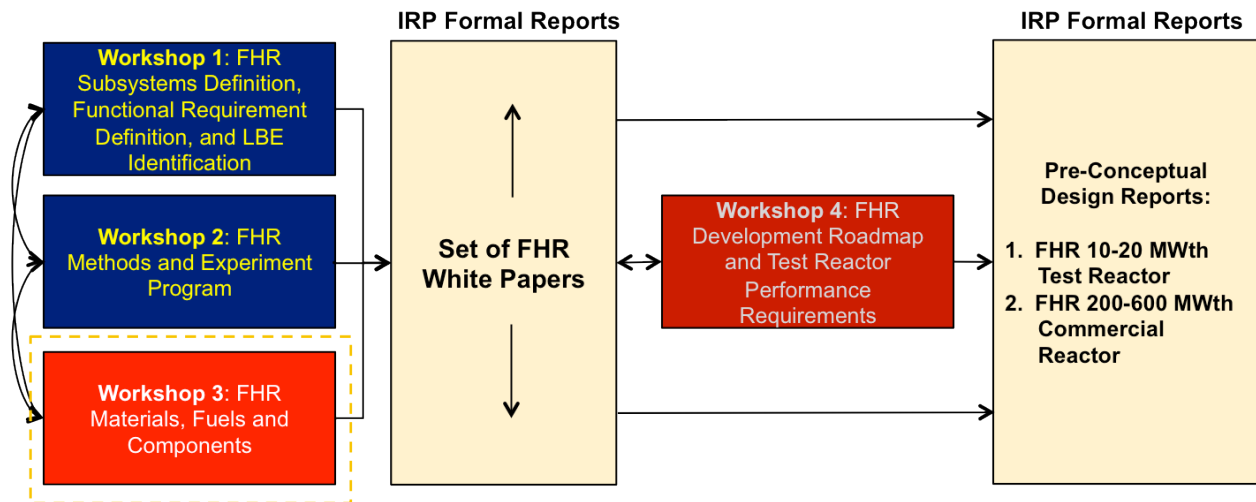


**Figure 1-1. IRP Structure Illustrating Workshop Rationale and Key IRP Objectives (this white paper focuses on the third workshop)**

## 1.2 FHR Operating and Transient Conditions Relevant to Materials and Fuels

The FHR is a new reactor concept that uses graphite-matrix coated-particle fuel and a fluoride-salt coolant. There are many design options. To provide a realistic assessment of FHR materials and components, the expected operating conditions must be defined. Discussions for the third workshop focused on the baseline operating conditions for the 900-MWt Pebble Bed Advanced High-Temperature Reactor (PB-AHTR) as a starting point because more work has been done on this specific design than other designs. Where information was available, the operating conditions of other proposed FHR designs were provided.

The website at <http://pb-ahtr.nuc.berkeley.edu/> introduces the PB-AHTR. It is a liquid-salt-cooled, high-temperature reactor design developed in 2008 and 2009 at UCB in collaboration with Oak Ridge National Laboratory (ORNL) and other national labs. Because the design is relatively detailed, the 2009 PB-AHTR is used in this white paper to provide illustrative operating conditions for FHR materials, fuels, and components. Figure 1-2 shows the reactor system schematically.

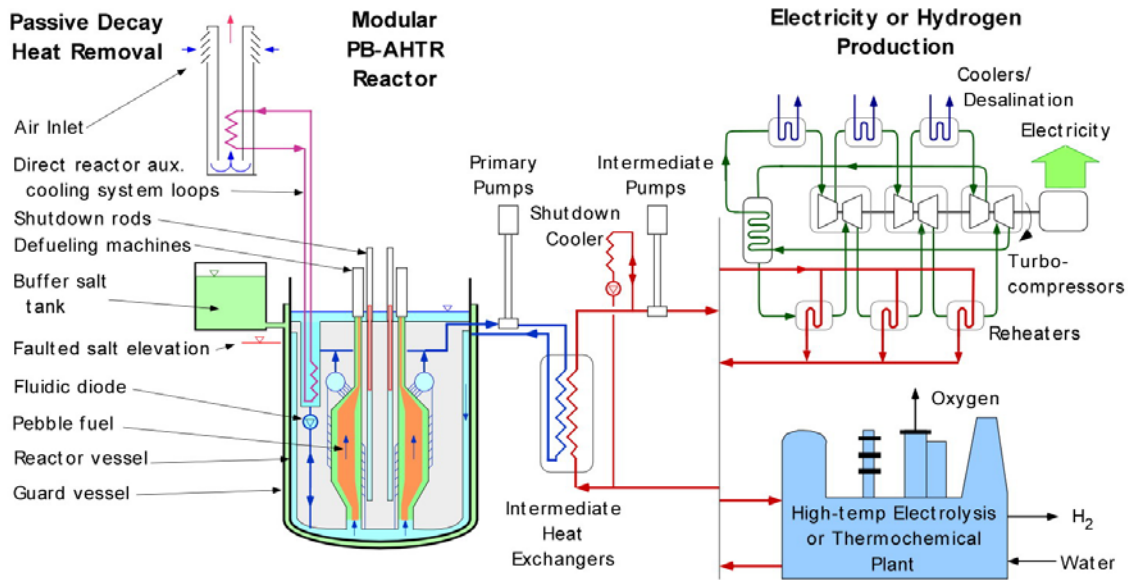


**Figure 1-2. 2009 PB-AHTR Reactor System**

The 2009 PB-AHTR has a nominal thermal power output of 900 MWth (and electrical output of 410 MWe). It differs from conventional helium-cooled high-temperature reactors (HTRs) because its liquid-salt coolant enables operation with a core power density of 20 to 30 MWth/m<sup>3</sup>, compared to the 4.8 to 6.0 MWth/m<sup>3</sup> typical of modular helium reactors (MHRs) (Bardet et al. 2008). The 2009 PB-AHTR delivers heat with a core outlet temperature of 704°C, achieving 46% thermal efficiency with a multi-reheat helium Brayton (gas-turbine) cycle. As described later, ORNL also completed a design for a fixed-fuel FHR in 2011 (Holcomb et al. 2011); this reactor is also used for reference in this white paper and is referred to as the 2011 AHTR. In both of these designs, low-pressure, chemically inert liquid-salt coolant, with its high heat capacity and capability for natural circulation heat transfer, provides two key advantages: (1) robust safety (including fully passive decay heat removal) and (2) improved economics with passive safety systems that allow higher power densities and longer-term scaling to large reactor sizes (>1,000 MWe) for central station applications.

The 2009 PB-AHTR used conventional tristructural isotropic (TRISO) high-temperature fuel in the form of pebbles slightly smaller than golf balls. The baseline PB-AHTR design uses the well understood beryllium-based salt flibe (<sup>7</sup>Li<sub>2</sub>BeF<sub>4</sub>) as its primary coolant and flinak (LiF-NaF-KF) as its intermediate coolant. Metallic structures and components like the reactor vessel are constructed using Alloy 800H, an ASME Section III code-qualified material, with Alloy N cladding for high corrosion resistance. The coolant loop of the ORNL Molten Salt Reactor

Experiment (MSRE) (Guymon 1973) operated with clean fluoride salt, like the PB-AHTR, for over 26,000 hours without any detectable corrosion to Alloy N samples studied after the reactor was shut down (Rosenthal, Haubenreich, and Briggs 1972). The major components in the 2009 PB-AHTR core are fabricated from graphite, which is chemically inert to fluoride salts.

Like FHRs in general, the PB-AHTR design combines technologies derived from earlier reactor designs to create a high-temperature reactor design with a unique combination of features:

- *Pebble bed modular helium reactors (PBMR)*: TRISO pebble fuel, nuclear-grade graphite, high-temperature metallic and C/C composite structural materials, and helium Brayton power conversion
- *Sodium fast reactors (S-PRISM/EBR-II)*: Pool-configuration reactor vessel, reactor building seismic base isolation, and direct reactor auxiliary cooling system (DRACS) for passive decay heat removal.
- *Light-water reactors (AP-1000/ESBWR)*: Integral effects test scaling and best-estimate safety code validation methods, and modern computer-aided design, manufacturing, and modular construction technologies.
- *Molten salt reactors (MSRE/MSBR)*: Liquid salt pumps, HXs, corrosion resistant alloys, and a liquid salt corrosion test and thermophysical property database.

Like modern MHRs, FHRs and the 2009 PB-AHTR use a conventional low-enriched uranium fuel cycle. But FHR technology also supports advanced fuel cycle options:

- *Deep burn fuel cycle*: FHRs can use deep burn TRISO fuels to destroy plutonium and other transuranics from commercial spent fuel.
- *Once-through seed-blanket fuel cycle*: FHRs can operate with a low-enriched uranium seed and thorium blanket fuel cycle that can reduce uranium consumption and waste generation while maintaining once-through operation.
- *Closed thorium fuel cycle*: FHRs can operate with a closed thorium-based fuel cycle with greatly reduced production of plutonium and other transuranics. Achievable conversion ratios are being studied now.
- *Liquid fluoride thorium reactors*: FHRs provide technology that can be applied to future deployment of molten salt reactors using sustainable closed thorium fuel cycles.

FHRs operate at significantly higher temperature than light-water reactors (LWRs) and even liquid metal reactors (LMRs), as illustrated in Figure 1-3. FHRs operate with lower peak temperatures than high-temperature gas-cooled reactors (HTGRs), but with similar average temperatures because of the much smaller temperature change across FHR cores compared to HTGR cores. The following subsections provide an overview of the expected typical operating conditions of key FHR structures and components.

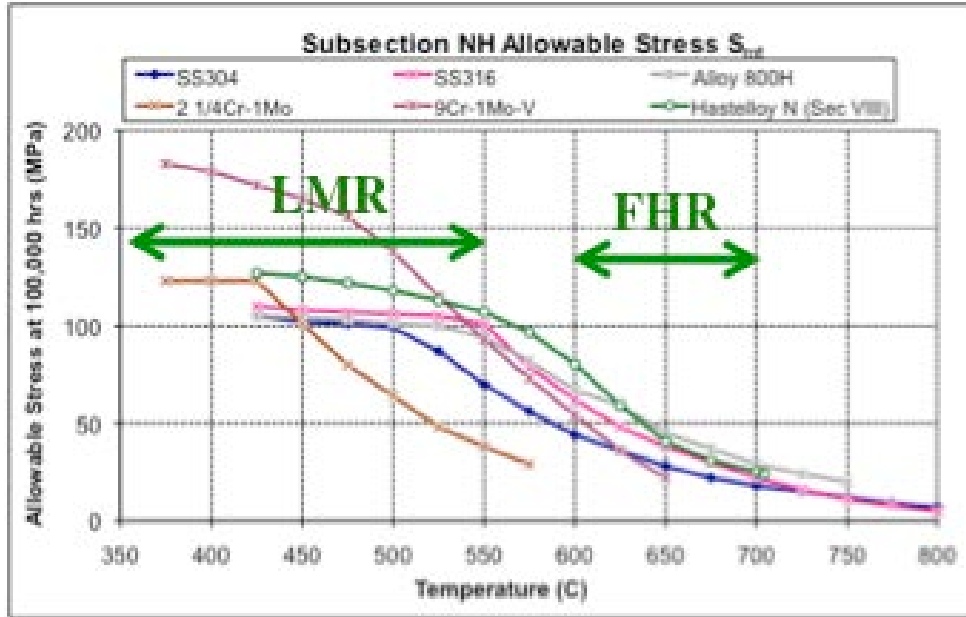


**Figure 1-3. Operating Temperature Range for FHRs and LMRs, Compared to ASME Section III-Allowable Stresses for Typical Construction Materials**

### 1.2.1 Typical FHR Thermal, Pressure, and Flow Conditions

This subsection provides an overview of typical FHR thermal, pressure, and flow conditions with a focus on the FHR core system under normal operating conditions. More details on the temperature distribution of the flibe coolant in the rest of the primary loop are provided in Chapter 4, as they are directly relevant to the degradation of metallic structural components outside of the core. Details on the temperature evolution of the fuel, coolant, and metallic structural components under a selected transient condition are also provided in Chapters 3 and 4.

Fluoride salts are low-volatility fluids with high volumetric heat capacity, melting temperatures, and boiling temperatures compared to other typical reactor coolants. The differences in thermal hydraulic phenomena in FHRs emerge from the differences in the thermophysical properties of the fluoride salts and the structural materials used with them, compared to other reactor coolants and their typical structural materials.

As can be seen in Table 1-1, although FHRs operate at significantly higher temperatures than conventional LWRs, the thermophysical properties of the fluoride salts allow for a pool-type configuration and operation at nearly atmospheric pressures (the pressure drop across the core is only a few tens of kiloPascals).

**Table 1-1. Thermal Hydraulic Comparison to Other Nuclear Power Systems**

<b>Function</b>	<b>2009 PB-AHTR</b>	<b>2011 AHTR</b>	<b>PWR</b> (Duderstadt and Hamilton 1976)*	<b>GT-MHR**</b>
Inlet, °C	600	650	300	590
Outlet, °C	700	700	332	950
Pressure, MPa	0.1	0.1	15.5	5.0
Power density, MW/m <sup>3</sup>	16.2	12.9	10.4	6.6

\* PWR=pressurized-water reactor

\*\* GT-MHR=gas turbine, modular helium reactor

The detailed design of the 2009 PB-AHTR can be used to estimate FHR-relevant operating condition parameters for corrosion and degradation analysis. Figures 1-4, 1-5, 1-6 and 1-7 present the bulk coolant temperature, fuel temperature, pressure, and Reynolds number distributions in the 2009 PB-AHTR core, respectively. The thermal hydraulic model used to calculate these parameters is described in detail in Appendix A.

As shown in Figure 1-4, the minimum coolant temperature is 600°C, and the bulk coolant temperature reaches 769°C in some regions of the core. However, the average core outlet temperature is 700°C, and designing the outlet plenum structures for proper mixing will ensure that the coolant reaching the inlet of the IHXs is well mixed, at the bulk temperature. The average coolant temperature in the core is 652°C, slightly higher than the average of the core inlet and outlet temperatures, because of bypass flow around the core.

As a result of a high heat transfer coefficient between the graphite shell of the pebbles and the salt coolant ( $h \sim 15 \text{ kW/m}^2\text{K}$  on average in the core), the temperatures of the pebble surfaces never exceed those of the surrounding coolant by more than a few tens of degrees Celsius.

Bulk Coolant Temperature: Color Surface.  
Streamlines: Gray Lines

MULTIPHYSICS

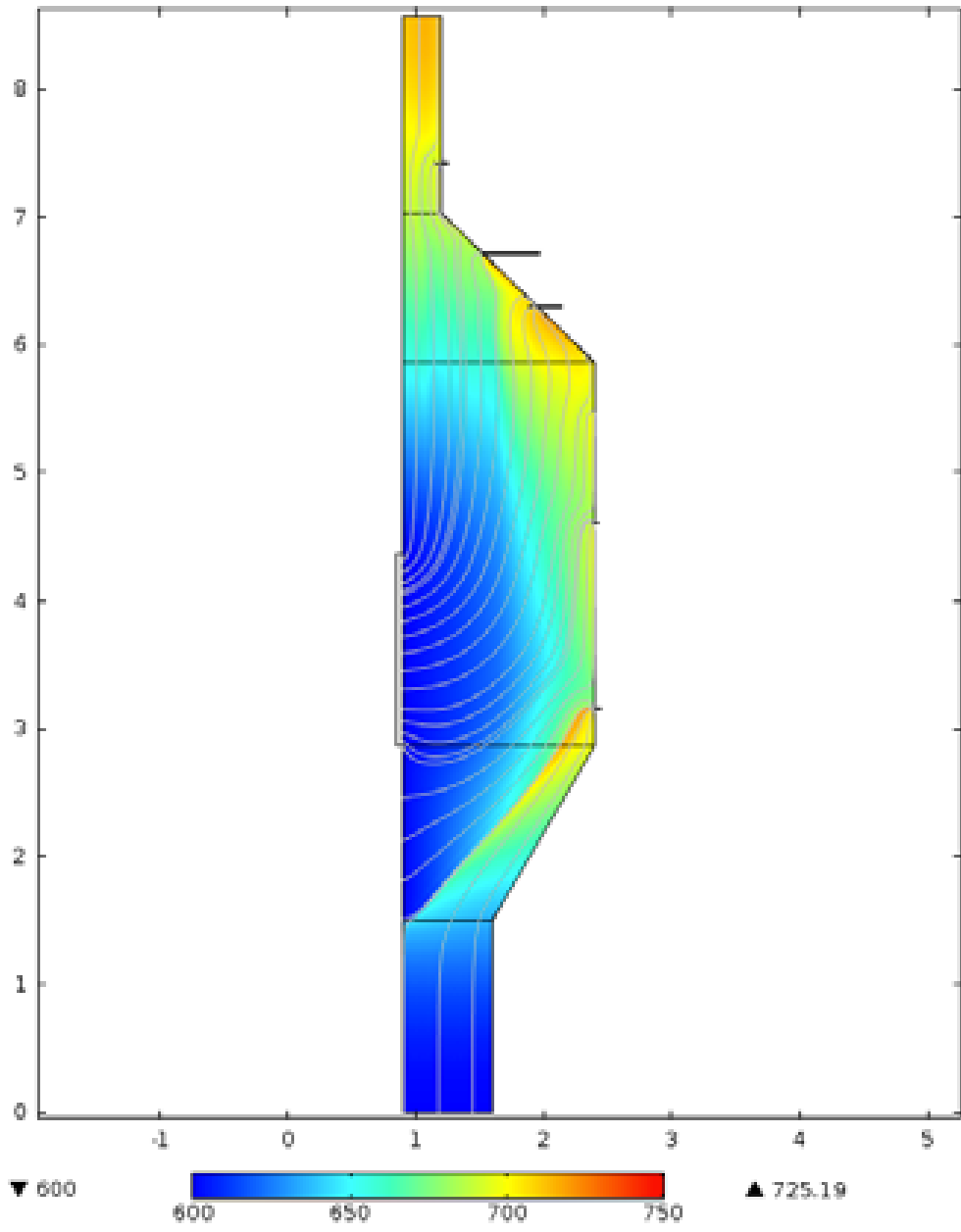


**Figure 1-4. Bulk Coolant Temperature (°C) Distribution in the 2009 PB-AHTR Core Under Normal Operating Conditions, Calculated in COMSOL Multiphysics**

## Average Fuel Kernel Temperature

COMSOL  
MULTIPHYSICS

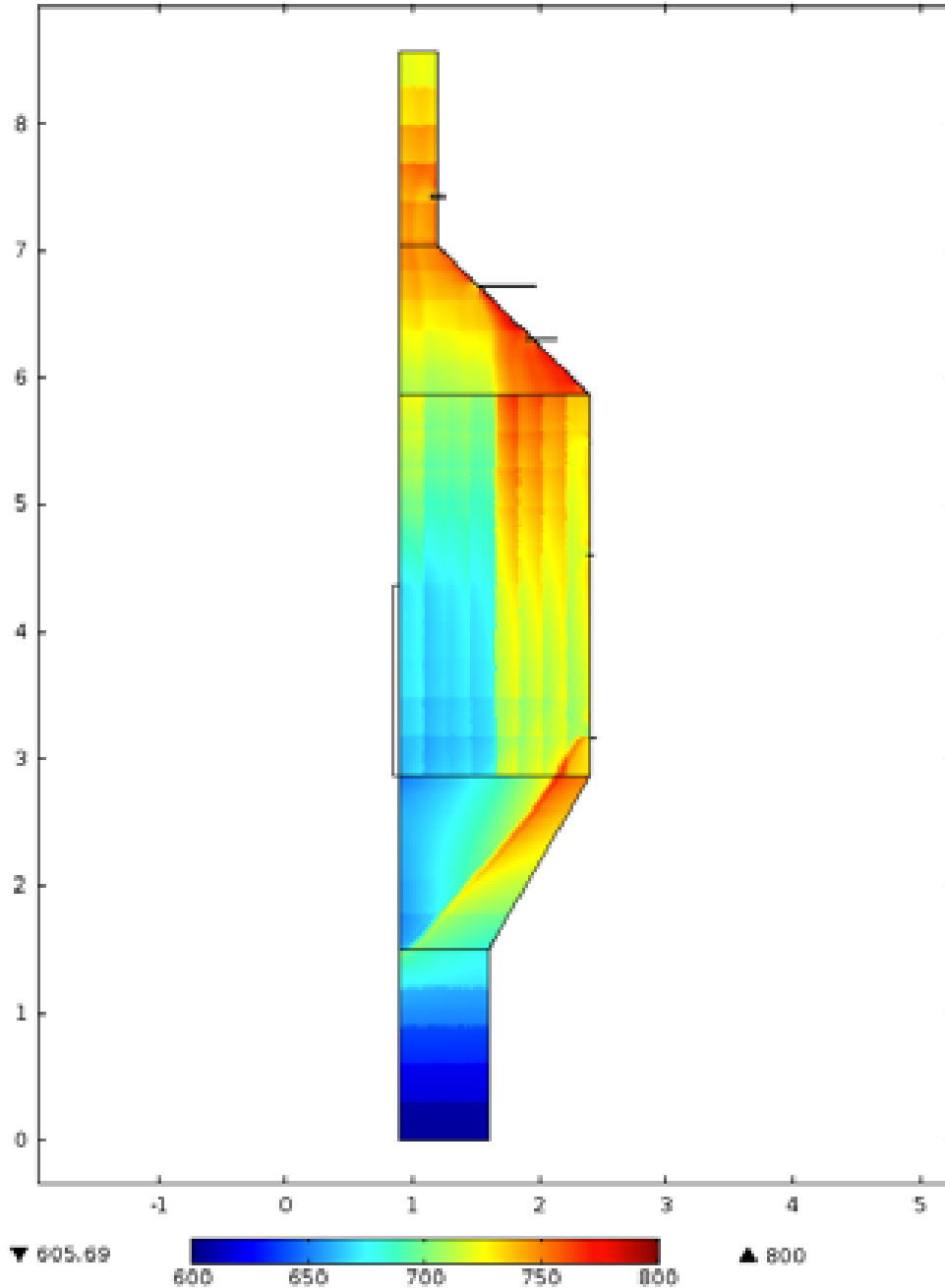


**Figure 1-5. Fuel Temperature (°C) Distribution (Average Kernel Temperature in Fuel Pebble) in the 2009 PB-AHTR Core Under Normal Operating Conditions, Calculated in COMSOL Multiphysics**

The average fuel temperature in the 2009 PB-AHTR core under normal operating conditions is 714°C, with a minimum value of 600°C and a maximum value of 1,110°C in a very small region of the core. These results will partly inform fuel performance and potential material degradation of the pebble fuel.

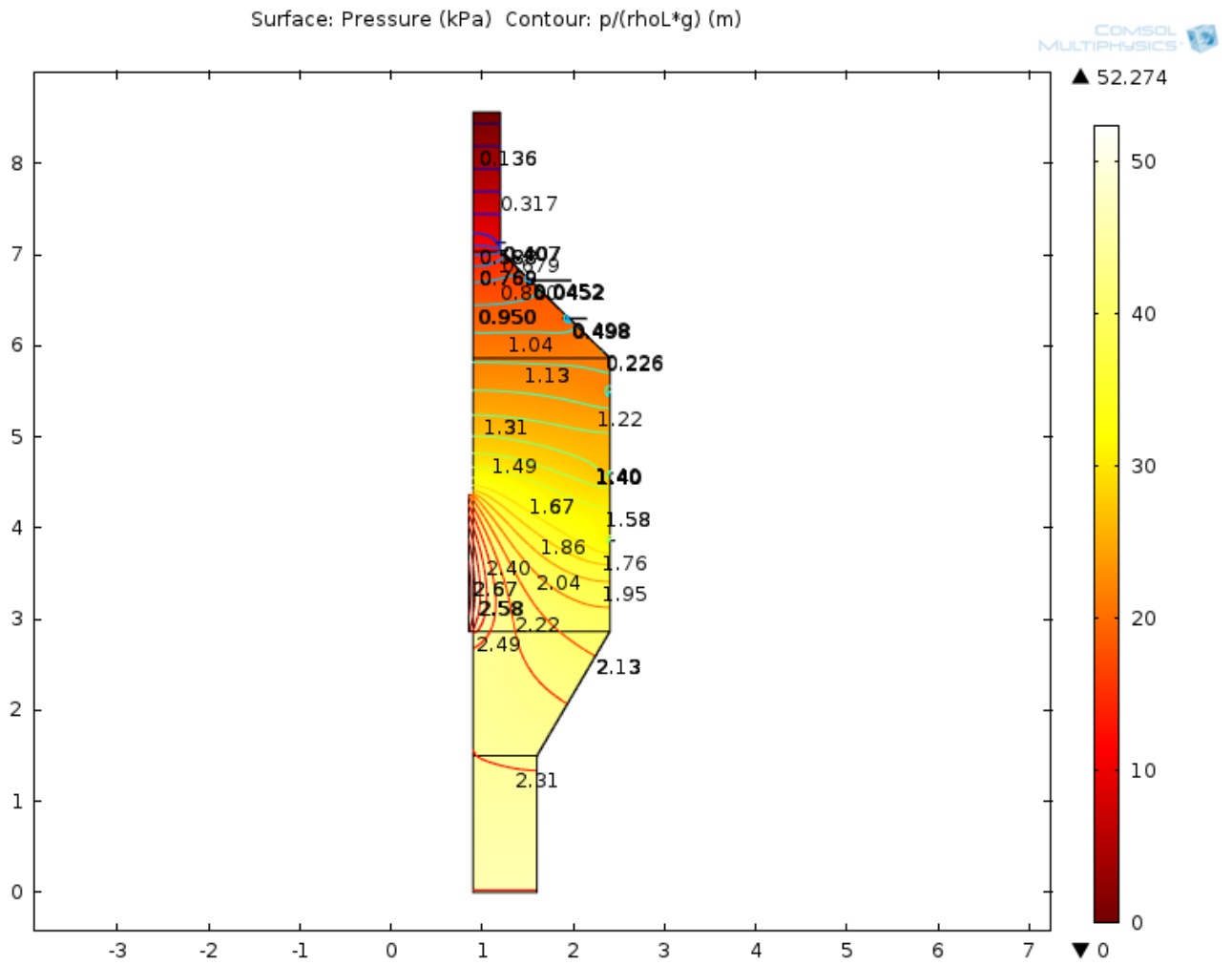


**Figure 1-6. Pressure (kPa) Distribution in the 2009 PB-AHTR Core Under Normal Operating Conditions, Calculated in COMSOL Multiphysics**

Reynolds (based on pore velocity): color map.  
Streamlines: gray lines

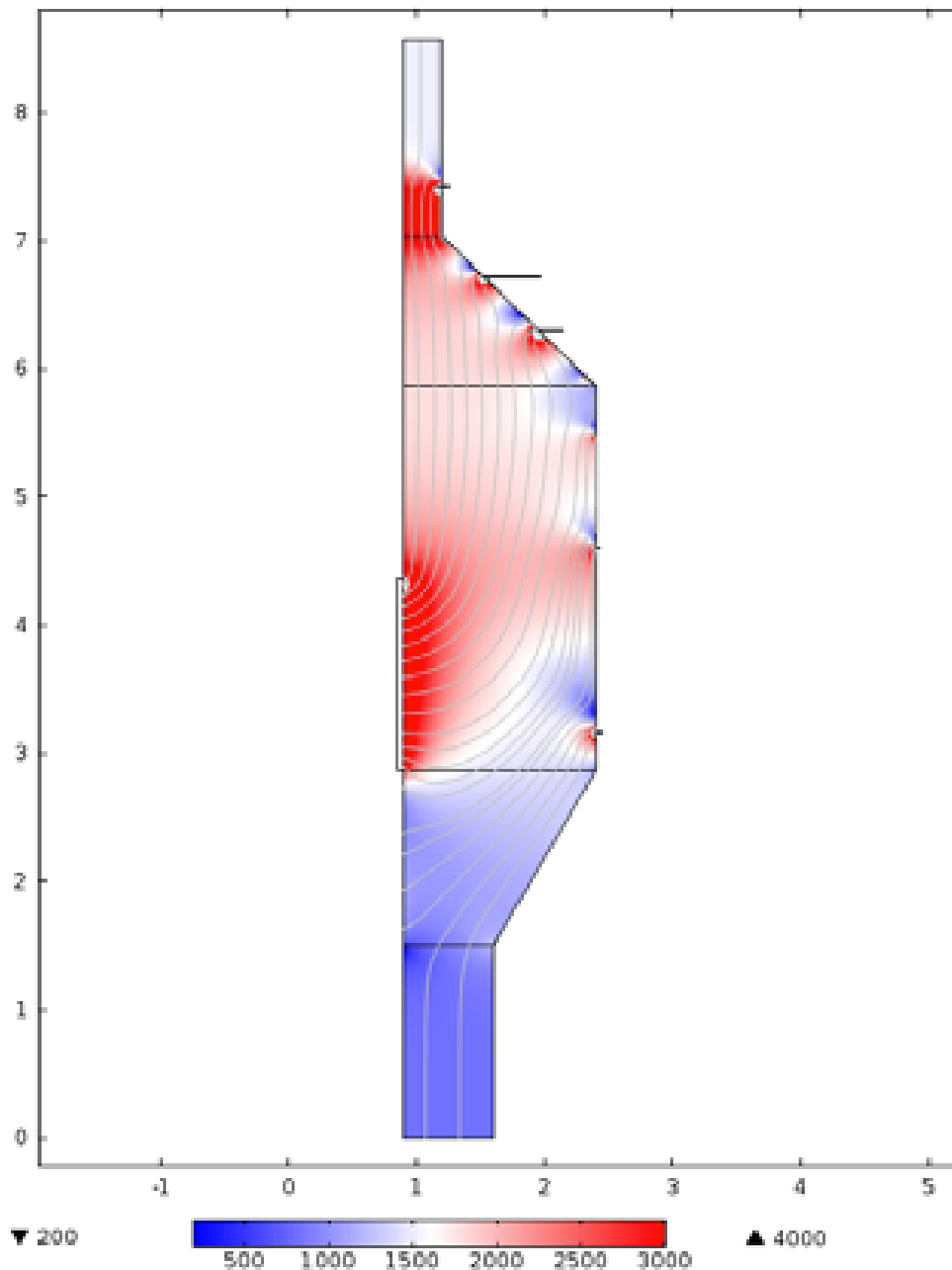


**Figure 1-7. Reynolds Number Distribution in the 2009 PB-AHTR Core Under Normal Operating Conditions, Calculated in COMSOL Multiphysics**

The pressure drop across the 2009 PB-AHTR core is only 52 kPa. Combined with a pool-type configuration, this small pressure drop allows for operation at nearly atmospheric pressures, removing the stored energy associated with pressurization in conventional systems such as LWRs and thus greatly reducing the risk of certain transients such as loss of coolant accidents (LOCA). This low pressure drop also facilitates the establishment of natural circulation for

passive decay heat removal during loss of forced circulation (LOFC) transients. This pressure distribution will eventually be used for fatigue analysis of the core components.

### 1.2.2 Typical FHR Neutron Flux and Dose Conditions

This subsection provides an overview of typical FHR neutron flux and dose conditions for different components (fuel, center and outer radial reflectors, boron shielding pins, core barrel, and reactor vessel).

FHR systems are graphite-moderated, thermal spectrum nuclear power systems. The neutron spectrum in these systems is selected to enable negative coolant temperature reactivity feedback and maximize burnup by balancing neutron economy with fissile fuel breeding. Figure 1-8 compares the neutron spectrum from unit cell models of various nuclear power systems at their beginning of life (BOL) compositions. A comparison of characteristic neutron fluxes is presented in Table 1-2.

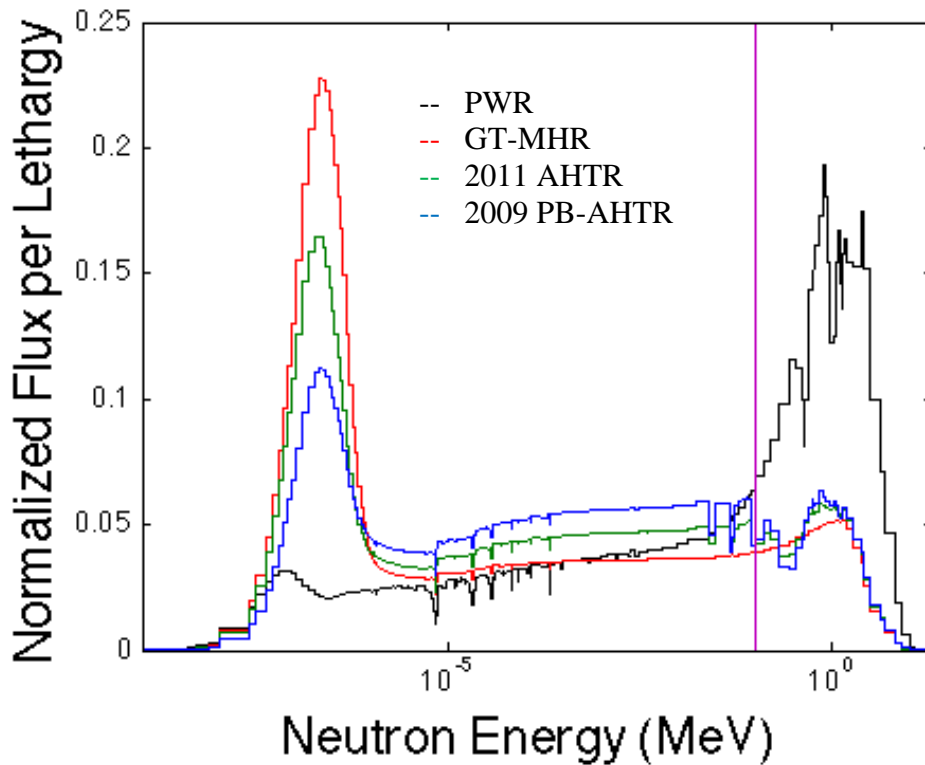


**Figure 1-8. Neutron Flux of Various Nuclear Power Systems; Magenta Line Indicates Fast Flux Cutoff, 0.1 MeV**

**Table 1-2. Neutron Flux Data of Various Nuclear Power Systems**

<b>Flux Characteristics</b>	<b>2009 PB-AHTR</b>	<b>2011 AHTR</b>	<b>PWR</b>	<b>GT-MHR</b>
Average power density, MW/m <sup>3</sup>	16.2	12.9	104	6.6
Characteristic total flux, n/cm <sup>2</sup> s*	4.03×10 <sup>14</sup>	3.62×10 <sup>14</sup>	3.44×10 <sup>14</sup>	3.03×10 <sup>14</sup>
Fast flux, n/cm <sup>2</sup> s (>0.1 MeV)	6.95×10 <sup>13</sup>	6.18×10 <sup>13</sup>	1.70×10 <sup>14</sup>	3.98×10 <sup>13</sup>
Fast flux/total flux, %	17.2	17.0	49.2	16.0

\*Calculated based on unit cell models

The neutron spectrums of graphite-moderated systems like HTGRs and FHRs are much softer than those in PWRs. FHRs tend to be a little harder than HTGRs but have similar fast fission fractions of 17% in FHRs compared to 16% in HTGRs. Furthermore, FHR components are exposed to larger neutron fluxes than components in HTGRs because they operate at two to six times the power densities.

Two strategies deal with radiation damage: (1) replace components when they are no longer useful or (2) build components to survive the irradiation conditions, shield components, and reduce the power density or life of components. The PB-AHTR can replace fuel pebbles and inert graphite reflector pebbles when they are no longer useful. Furthermore, the central graphite reflector is designed to be replaced once it reaches its radiation damage limit. Conversely, the outer graphite reflector in the PB-AHTR is protected from radiation damage by the graphite pebble reflector. The PB-AHTR also uses robust carbon fiber reinforced composite (CFRC) fuel elements to survive multiple cycles.

Table 1-3 presents the maximum values for fast flux and radiation damage rate in various components of the 2009 PB-AHTR. The neutronic model used to calculate these parameters is described in detail in Appendix B. As seen in Table 1-3, 15 dpa/yr to the inner reflector of the 2009 PB-AHTR design is high and may require a lowering of the power density in the FHR. This example emphasizes the importance of determining the dose limits and how to set them for each component in the FHR system.

**Table 1-3. Maximum Neutron Flux and Radiation Damage Values for Components of the 2009 PB-AHTR**

<b>Characteristic</b>	<b>Fast Flux, n/cm<sup>2</sup>s (&gt;0.1 MeV)</b>	<b>Damage Rate, dpa/yr</b>	<b>Temperature, °C</b>
Fuel (TRISO)*	8.25×10 <sup>13</sup>	1.91	770
Inner reflector	1.22×10 <sup>13</sup>	15.7	600

Characteristic	Fast Flux, n/cm <sup>2</sup> s (>0.1 MeV)	Damage Rate, dpa/yr	Temperature, °C
Outer reflector	3.55×10 <sup>11</sup>	0.96	700
Core barrel	1.99×10 <sup>9</sup>	4.27×10 <sup>-5</sup>	600
Shutdown rod liners	1.03×10 <sup>13</sup>	0.24	600
Reactor vessel**	1.99×10 <sup>9</sup>	3.52×10 <sup>-5</sup>	600

\* dpa rate for SiC layer, calculated by tallying the dpa cross section over the entire active region rather than specifically in the SiC layers and assuming the highest flux intensity in the active region.

\*\* Reactor vessel fast flux rate conservatively approximated as the fast flux rate in the core barrel, because the design of the downcomer is not well developed.

### 1.2.3 Typical FHR Refueling Conditions

This subsection provides an overview of the expected frequency of fuel replacement in FHRs, focusing on the two most developed FHR designs: the 2009 PB-AHTR and the 2011 AHTR, which operate with continuously refueled and multibatch fuel cycles, respectively.

#### *Refueling in the 2009 PB-AHTR*

The 2009 PB-AHTR operates with a refueling strategy similar to the PBMR, in which fresh fuel is inserted into the pebble bed and passes through the core a number of times before reaching a given discharge burnup. The fuel handling system measures each pebble's burnup after every pass through the core. If the pebble's fuel is below a burnup limit, the pebble will be recirculated. Otherwise, the pebble will be discharged and replaced by a fresh pebble. Burnup analysis is used to calculate the maximum attainable discharge burnup for the PB-AHTR. However, the pebbles burn at different rates because of variation in the flux distribution in the pebble bed and the different flux levels pebbles experience depending on their path through the core, so the residence time should be given as a range rather than any one absolute number. Table 1-4 presents characteristics of the residence time distribution for pebbles in the 2009 PB-AHTR, in equivalent full power days (EFPD).

**Table 1-4. Expected Refueling Period in the 2009 PB-AHTR**

	Average	Minimum	Maximum
Residence time, EFPD	1,071	645	1,241

The number of passes each pebble makes in the PB-AHTR and the detailed design of the external pebble handling system are still open design and development issues.

#### *Refueling in the 2011 AHTR*

The 2011 AHTR design uses fixed-fuel elements with a multibatch fuel cycle. The baseline fuel management scheme is a 180-EFPD, two-batch fuel cycle. At the end of each fuel

equilibrium fuel cycle, the twice-burned fuel is discharged from the core and replaced with fresh fuel. The process is as follows:

1. All the control blades are inserted into all the fuel assemblies and coast down the primary pumps to reduce the salt flow.
2. Access is provided to the fuel assemblies by removing the control rod drive plate as well as raising the upper-core support plate.
3. Individual fuel elements are removed from the core by the In-Vessel Fuel Handling Machine (IVFHM).
4. These fuel elements are transferred from the IVFHM to the refueling station.
5. The refueling station manipulator (RSM) robot at the refueling station receives new fuel, exchanges fuel (when fuel shuffling is required), or transfers used nuclear fuel to the used fuel canal.

The used nuclear fuel is uncovered for a few minutes while it is lifted out of the primary salt and into the storage salt in the used fuel transfer canal. While the fuel is uncovered, it will heat up at about 44 K per minute for up to 2 minutes. Figure 1-9 presents the geometry of the refueling station components, and Figure 1-10 provides an example of the temperature evolution in an AHTR fuel assembly during a refueling transient.

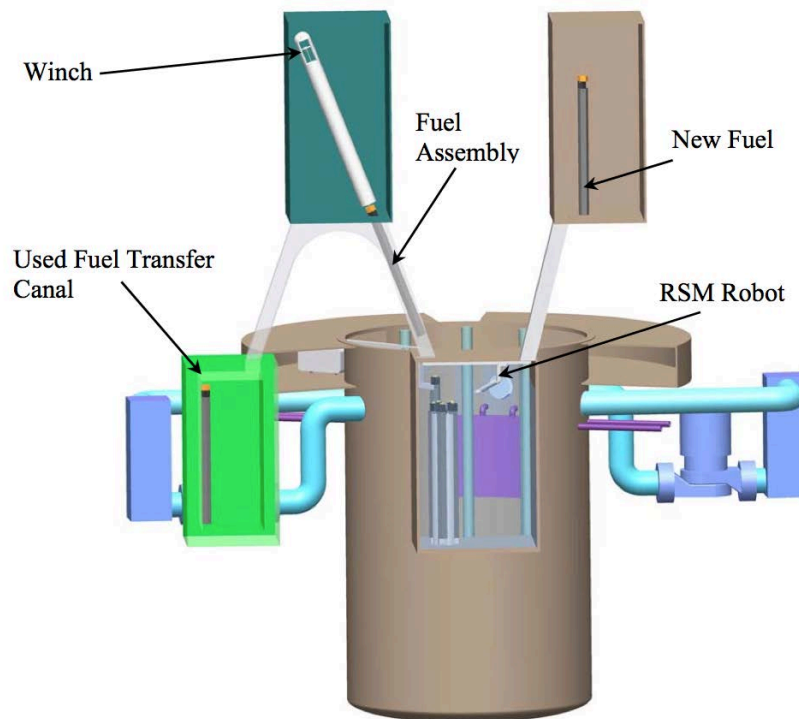


**Figure 1-9. 2011 AHTR Refueling Station Components**

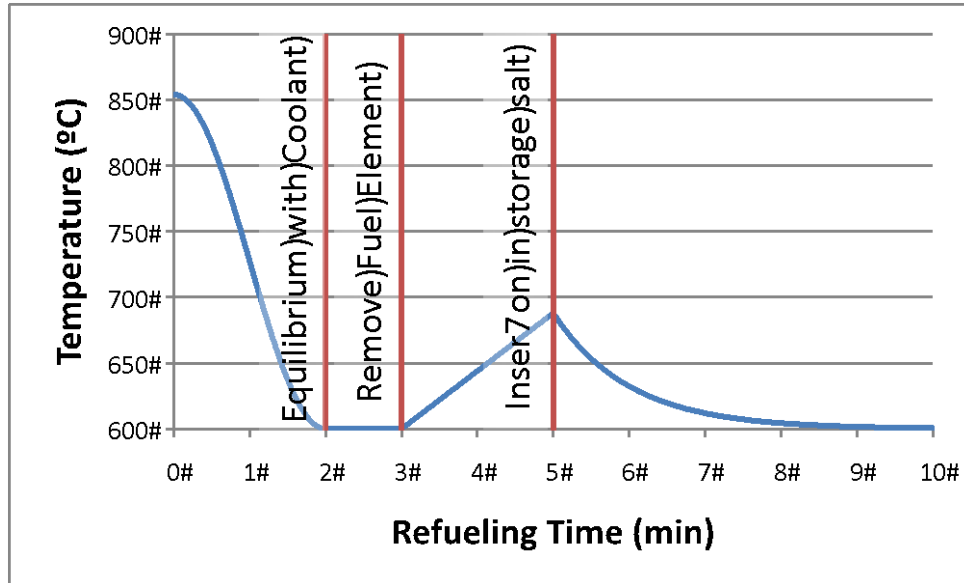


**Figure 1-10. Temperature Evolution in a 2011 AHTR Fuel Element During Refueling Transient**

## 2 FHR Fuel Fabrication and Performance

The FHRs use coated-particle fuels quite similar to those that have been developed for HTGRs. The coated-particle fuel is a uranium oxide or oxycarbide kernel coated with a series of layers that act as the cladding. The finished particles are approximately 800  $\mu\text{m}$  in diameter and are embedded in a graphite matrix that is the primary reactor neutron moderator and the structural form of the fuel. The graphite matrix can be molded into many forms including pebbles, hexagonal blocks, and plates. These coated-particle fuels have highly robust safety characteristics, with the ability to maintain their integrity up to temperatures of 1,600°C or more, many hundreds of degrees higher than the maximum temperatures that can be reached in FHR transients and accidents. Recent work to fabricate, irradiate, and test coated-particle fuel in the U.S. has been highly successful, and the complete capability to develop these fuels for use in FHRs currently exists in the U.S.

This chapter reviews the current status of coated-particle fuel technology, potential key issues for implementing particle fuel for the FHR design, and current fuel development needs.

### 2.1 Current Status of Coated-Particle Fuel Technology

The DOE's Next Generation Nuclear Plant (NGNP) initiative has supported a comprehensive fuel development project focused on the qualification of TRISO fuel for the Very High Temperature Reactor (VHTR) concept. The program has successfully demonstrated the capability to fabricate high-quality TRISO fuel particles on an engineering scale. Petti et al. (Petti et al. 2010) provided a general overview of the DOE's fuel development and qualification project, while the most recent NGNP technical development plan gives a more in-depth overview of the program (Simonds 2010).

The VHTR fuel project builds off the successful German coated-fuel program that demonstrated excellent performance with very few as-fabricated defective particles and fuel failures during irradiation testing. The NGNP TRISO fuel consists of a UCO fuel kernel surrounded by a porous buffer layer, and successive isotropic layers of dense inner pyrocarbon (IPyC), chemically vapor-deposited SiC, and a dense outer pyrocarbon (OPyC). The NGNP VHTR project focused on a prismatic core design and utilized cylindrical compacts instead of a pebble design. Because of similarities in construction and performance, lessons learned from the NGNP VHTR project and other historical fuel forms from gas-cooled reactor designs can be applied to the development of TRISO PB-AHTR fuel and the plate design of the ORNL AHTR. An International Atomic Energy Agency (IAEA) Technical Document provides an overview on the historic data from international efforts on coated-particle fuel (IAEA 1997).

For the NGNP fuel development project, ORNL established capabilities at laboratory scale with the intention to scale up production to an engineering scale through collaboration with General Atomics and Babcock and Wilcox. The initial fuel identified for the program was based on the historic German fuel utilizing similar fluidized bed-coating procedures. Petti et al. (Petti and Others 2004) provide a general overview of the specifications for each critical facet of the fuel fabrication process from kernel to compacting as well as technical justification for each

item. The following paragraphs summarize the fabrication approach for TRISO fuel and fuel compacts.

The specifications ensured that the final fuel form did not inhibit reactor operation. The design specifications for the kernel included physical properties such as composition, impurity concentrations, and density, because these values affect the fuel performance during operation; additional specifications included sphericity and diameter. The coating specifications included items such as thickness, density, anisotropy, and crystallite size for each layer. Quality assurance specifications focused on metrics such as the fraction of fabricated particles with missing layers and surface flaws that may lead to particle failure during operation and increased fission product release.

Coating specifications dictated the rate, temperature, and precursor gases for deposition to maintain consistent, high-quality TRISO layers. In general, the buffer layer was deposited using a blend of  $C_2H_2$  and argon; the IPyC and OPyC layers using a blend of argon,  $C_2H_4$ , and  $C_3H_6$ ; and the SiC layer using  $H_2$  and methyltrichlorosilane (MTS). As part of the NGNP VHTR advanced gas-cooled reactor (AGR) program, the specifics of the coating procedure are being investigated to tailor the microstructure to achieve optimal layer quality and microstructures. For example, a variant in the AGR-1 irradiation campaign included fuel with a SiC layer deposited using Ar/ $H_2$ /MTS. The particle specifications are generally tested through an interrupted coating process, where a coating batch is removed after successive steps and the physical properties of individual layers are tested to ensure that they fall within the critical range of specified values (Petti and Others 2004).

The knowledge base for the compacting step came from technologies developed for earlier reactors. The compacting step suspended the TRISO particles and graphite filler in a carbonaceous matrix in an appropriate shape for the reactor core. The two processes that have been predominantly used are the (1) overcoating and molding process, which was used to make pebble fuel compacts for the Dragon reactor, AVR, THTR, HTTR, and HTR-10; and (2) injection molding with thermoplastic resins method, which was used to make cylindrical fuel compacts for Peach Bottom and Fort St. Vrain reactors. Historically, the overcoating and molding process has produced fewer failed particles during compacting and as such was selected as the technology focus for the NGNP VHTR fuel development project.

The general compacting process consists of four steps: preparation of resin-coated filler powder, overcoating of TRISO particles, pressure molding of “green” compacts, and carbonization. The specifications and technical justifications for each stage can be found in detail in a report by Petti et al. (Petti and Others 2004). The resin-coated filler powder is added to promote adhesion of the powder to the TRISO particles during overcoating. Before overcoating, the TRISO particles are separated on a vibration table to remove abnormal particles. Overcoating protects particles during pressure molding because the coating dissipates stresses and deflects cracks from propagation into other particle layers. The thickness of the overcoating also dictates the available loading characteristics of the finalized fuel compact and helps to ensure that no particles are directly touching. After overcoating, the particles are blended with the resinated graphite powder to the appropriate volume fraction (35 vol% for AGR fuel compacts) and pressure molded in dies at 7 MPa at 160°C to 200°C to drive the polymerization and cross-linking of the resin. After pressure molding, the compact is ejected and carbonized at elevated

temperatures (900°C to 1,000°C) in an inert gas environment followed by a final heat treatment at 1,650°C to 1,850°C. The carbonization step converts the polymerized resin to elemental carbon and drives off water and hydrocarbons. The second thermal anneal completely removes deleterious gaseous contaminants that may have remained from the carbonization step. The compacting process is subject to quality specification and testing to ensure high-quality fuel. The specifications with defined critical limits include compact geometry, uranium loading, crush strength, compact density, matrix integrity, particle failure fraction, and impurity contamination.

The NGNP VHTR fuel development project has initiated a series of irradiation campaigns to test the performance of the TRISO fuel. Eight irradiations are planned for the program, designated AGR-1 through AGR-8. The irradiations are being conducted in the Advanced Test Reactor (ATR) at Idaho National Laboratory (INL). The AGR-1 campaign served as a shakedown test of the fuel produced in the laboratory setting. The UCO kernel fuel included a baseline and three fuel variants that served to test the performance of fuels with different coating layers at normal operating conditions. The irradiation was completed in November 2009 and experienced a peak burnup of 19%, a peak fast neutron fluence of  $4.5 \times 10^{25}$  n/m<sup>2</sup>, and a maximum time average volume average fuel temperature of ~1,250°C. On-line fission gas monitoring of the ~300,000 fuel particles detected no failures. The PIE of the AGR-1 particles is currently underway. Meanwhile the AGR-2 irradiation is nearing completion; the AGR-2 test is a performance test of the engineering scale fuel and will validate the performance of both uranium dioxide and UCO fuel types. AGR-3 and -4 will include designed-to-fail particles that will help the understanding of the fission product release behavior and distribution in the fuel elements and core. AGR-5 and -6 will validate fuel for use in the NGNP program, and AGR-7 and -8 will validate performance and fission product transport models currently being developed.

The PIE of AGR-1 is focusing on establishing protocol for the PIE of the future AGR experiments and is obtaining valuable information on particle evolution and performance. Information on particle behavior and fission product migration will support fuel model development with accurate data to validate codes such as PARTicle Fuel Model (PARFUME). PIE efforts include the following techniques:

- *Metrology* – Characterize shrinkage and swelling of the fuel.
- *Gamma scanning* – Determine if fission products have been released and if they are located in the fuel components.
- *Leach-Burn-Leach (LBL)* – Determine the number of defective fuel particles and distribution of retained fission products in TRISO layers by acid leaching the carbonaceous material surrounding the particles, burning the particles in air, and leaching a second time to determine if any particles were compromised during operation. The fission products in each stage are measured by gamma scanning.
- *Deconsolidated particle analysis*
  - *Irradiated Microsphere Gamma Analyzer (IMGGA)* – Measure fission product inventory of individual fuel particle to understand retention of individual fission products
  - *Electron and optical microscopy* – Investigate kernel and layer evolution and spatial distribution of fission products in irradiated fuel using energy dispersive

electron spectroscopy and wavelength dispersive spectroscopy, and correlate observations with fission product data from the IMGA

- *X-ray tomography* – Gain three-dimensional information on particle evolution and image entire kernel volume.
- *Safety testing* – Expose compacts to elevated temperatures to simulate accident conditions and determine fuel performance
  - Measure simultaneous release of fission products to determine release rates of specific fission products
  - Apply standard PIE techniques after testing to correlate with as-irradiated fuel performance.

Hunn et al. provide an in-depth overview of the PIE approach and methodology implemented at ORNL (Hunn and Others 2012). The findings from the initial PIE confirm the observation from on-line fission product release measurements that no defective particles existed, with LBL demonstrating that no exposed kernels and no defective SiC composites were present. However, release of some fission products was detected, with silver, europium, and palladium measured outside of the SiC layer as well as trace quantities of strontium, cerium, and samarium. The materialographic investigation showed segregation of fission product clusters at the IPyC/SiC interface and palladium and uranium penetration into bulk SiC, but no large penetration fronts. Buffer shrinkage was also commonly observed with buffer fractures in particles where the buffer remained bonded to the IPyC. In some cases kernel extrusion was observed at the fracture site. Figure 2-1 shows an isolated case where a crack was observed to propagate across the buffer/IPyC layer and extend a short distance into the SiC; however, the SiC layer remained intact. This phenomenon was observed in only one sample, and the frequency of these types of particles is unknown because the sampling and investigation of irradiated particles by scanning electron microscopy (SEM) is low.

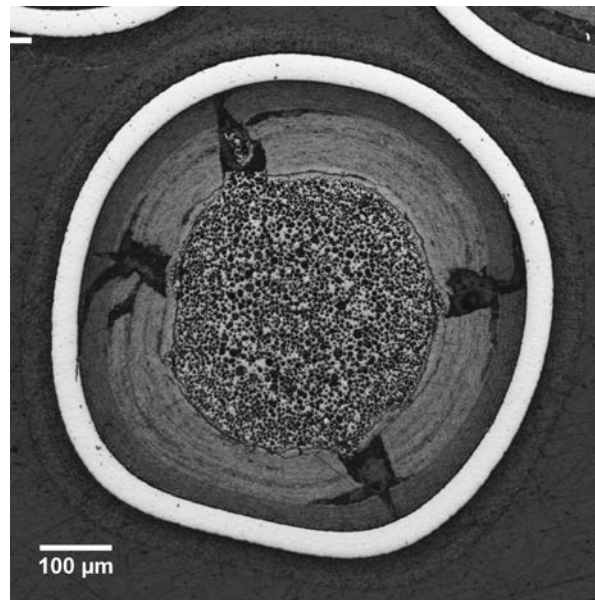


**Figure 2-1. Optical Cross Section of a Fuel Particle From AGR-1 PIE Campaign (Hunn and Others 2012)**

The NGNP VHTR fuel development project has demonstrated the ability to produce high-quality fuel based on the earlier German design. The AGR-1 irradiation campaign has shown that the particles remain intact with no failures observed. PIE of irradiated particles is currently being conducted, with initial protocols being developed for accurate determination of fuel performance. The FHR program can implement the lessons learned from this robust fuel development program to meet the needs of the reactor design.

## 2.2 Key Issues for FHR Fuels

The following subsections address key issues for FHR fuels, including candidate fuel geometries, unique operating conditions, and fuel qualification verification requirements.

### 2.2.1 Candidate FHR Fuel Geometries

FHRs use coated-particle high-temperature fuels originally developed for high-temperature gas-cooled reactors. The thicknesses of the TRISO layers have not yet been optimized for FHR fuel performance. The thermal hydraulic and neutronic performance of FHRs is not expected to be sensitive to the specific coated-particle fuel design. The current methodology has been to select representative values from literature; later on, when TRISO fuel performance tools are available, the fuel performance will be assessed, and the fuel design will be updated. Coated-particle fuel performance codes developed to date are not widely available.

The baseline fuel design utilizes two-phase low-enriched uranium ( $\text{UO}_{1.5}\text{C}_{0.5}$  fuel kernels enriched up to 19.9 wt%  $^{235}\text{U}$ ). The stoichiometry of the fuel kernel (ratio of oxygen and carbon) has little effect on reactor performance with respect to thermal hydraulics and neutronics. The ratio also has little effect on the thermal conductivity of the fuel kernel; furthermore, because the fuel kernel volume makes up only a small fraction of the active region volume, the kernel conductivity has little effect on the effective conductivity of the active region on the pebble scale. Carbon is a better neutron moderator than oxygen, but the effect of the carbon inside the kernel is very small because of the much larger amount of structural carbon around the kernel. However, the carbon concentration in the fuel kernel has a significant effect on the fuel performance, because it reduces the amoeba effect (Holcomb et al. 2011) by limiting CO production, but sufficient oxygen must be present to stabilize fission products in the kernel. Elevated kernel carbon/heavy metal ratios may limit the available oxygen necessary to stabilize metallic fission products in the kernel (Homan et al. 1977). Literature on the cost of coated-particle fuel suggests that fuel fabrication costs – the dominant cost for high-temperature reactor fuel – scale linearly with heavy metal loadings of fuel compacts. Therefore, fuel costs are minimized by maximizing burnup, which increases almost linearly with enrichment.

The function of the buffer region is to accept gaseous fission products and attenuate fission product recoils. The function of the SiC layer is to contain metallic fission products and provide structural support for the fuel particle. The IPyC layer serves as a structural component and gaseous fission product barrier. The IPyC layer also protects the buffer and kernel from chlorine attack during SiC deposition. The OPyC layer also serves as a structural component and protects the SiC layer during compacting. The thicknesses of the SiC layer are dictated by internal pressure generated during service and rate of attack by metallic fission products. The design of individual layers and fabrication specifics has been well vetted for the HTGR design. With

production of specifications to ensure that particle failures are below quality assurance standards without sacrificing fuel performance, the particle dimensions can be modified to accommodate changes in fuel performance requirements.

Figure 2-2 presents the geometry of the coated-particle fuel. The geometric and material definition is presented in Table 2-1. The following subsections lay out differences between annular pebble fuel and plate fuel.

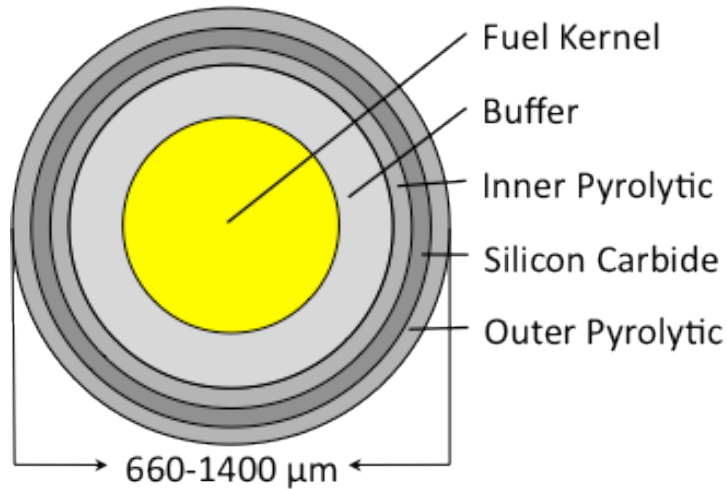


**Figure 2-2. Baseline PB-FHR Fuel Particle**

**Table 2-1. Geometric and Material Definition of the Baseline PB-FHR Coated-Fuel Particle**

Component	Dimension	Value	Material	Density, g/cc
Fuel kernel	Outer radius, $\mu\text{m}$	200	$\text{U}_{0.15}\text{C}_{0.5}$	10.5
Buffer	Outer radius, $\mu\text{m}$	300	Porous carbon	1.0
IPyC (inner pyrolytic)	Outer radius, $\mu\text{m}$	335	Pyrolytic carbon	1.87
Silicon carbide	Outer radius, $\mu\text{m}$	370	Silicon carbide	3.2
OPyC (outer pyrolytic)	Outer radius, $\mu\text{m}$	405	Pyrolytic carbon	1.87
Matrix	TRISO packing fraction, %	44	Graphite matrix	1.6

### *Annular Pebble Fuel*

Preliminary economic analyses indicate a high cost for particle fuel fabrication. The strategy to mitigate the impact of these fuel fabrications costs is to maximize burnup by using the

maximum allowable enrichment, 19.9 wt%,  $^{235}\text{U}$ , and using continuously fueled pebble fuel. A continuously refueled core can operate with low excess reactivity, maximizing the neutron economy and thereby maximizing burnup. Furthermore, this fuel cycle decouples the shutdown frequency from burnup to increase the flexibility of the fuel design and enhance the capacity factor.

One of the functional requirements of the pebble fuel elements is that they are buoyant in the liquid salt at operating and accident conditions. The buoyancy of these pebbles is controlled by the size and density of the inert low-density graphite core of the annular pebbles.

The only accident identified to date that can significantly stress the integrity of FHR systems is an anticipated transient without scram (ATWS), where shutdown is solely caused by the system's inherent temperature reactivity feedbacks. The characteristic average temperature of the fuel kernels limits the maximum temperature in ATWS transients. Therefore, using the annular fuel form to enhance heat transfer from the fuel mitigates the consequences of these ATWS accidents.

The fabrication and qualification of annual pebble fuel requires considerable development. While the fuel design exhibits similarities to the pebble fuel, in development the added complexity may require a complete irradiation and scale up program to qualify the fuel that will add considerable cost to the fuel development. Concerning buoyancy, the used pebble fuel geometries may be considered as alternatives, because the density of the graphite binder may be tailored to meet the fuel design needs. A prevailing concern is over-optimization of the TRISO construction. When considering the TRISO particle construction, a decision must be made on whether to use the particle design from the AGR project or to modify, for optimization, the construction to meet reactor needs. Changes to geometry and composition will require added qualification stages.

Figure 2-3 presents the geometry of the annular fuel pebble. The geometric and material definition is presented in Table 2-2.

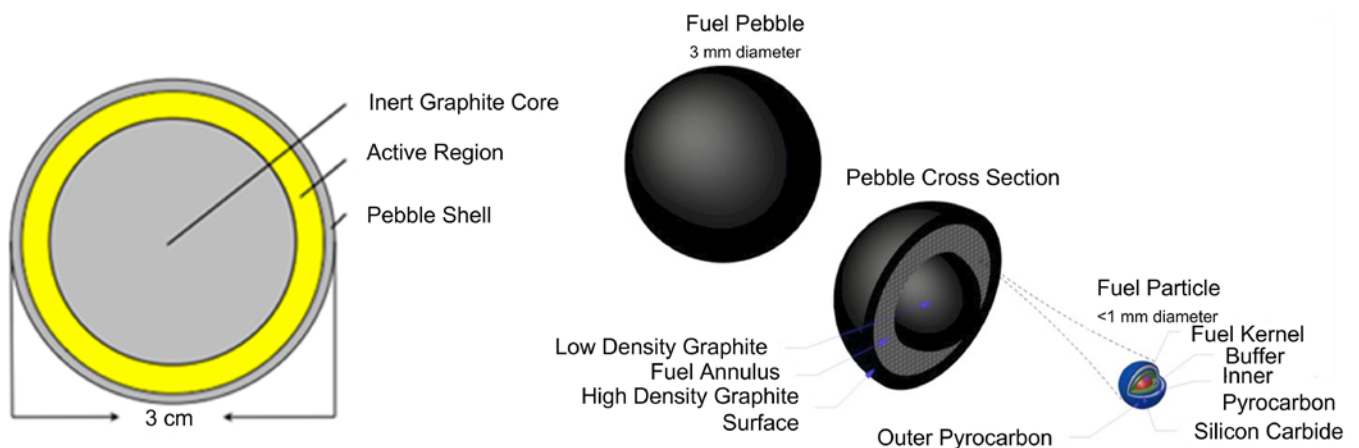


**Figure 2-3. Geometry of the Baseline PB-AHTR Fuel Pebble**

**Table 2-2. Geometric and Material Definition of the Baseline 2009 PB-AHTR Annular Fuel Pebble**

Component	Dimension	Value	Material	Density, g/cc
Inert graphite core	Outer radius, cm	1.25	Porous graphite	1.59
Active region	Outer radius, cm	1.40	TRISO + Matrix	-
Pebble shell	Outer radius, cm	1.50	Graphite	1.74

*Plate Fuel*

ORNL has been developing a fixed-fuel FHR variant to explore the possibilities of a large base-load electricity-generating FHR (Holcomb et al. 2011; Holcomb et al. 2012). The 2011 ORNL AHTR utilizes hexagonal fuel assemblies with fuel in slab geometry or plates of fuel; see Figure 2-4. These plates of fuel form low-resistance channels through which salt flows, enhancing passive cooling during LOFC transients.

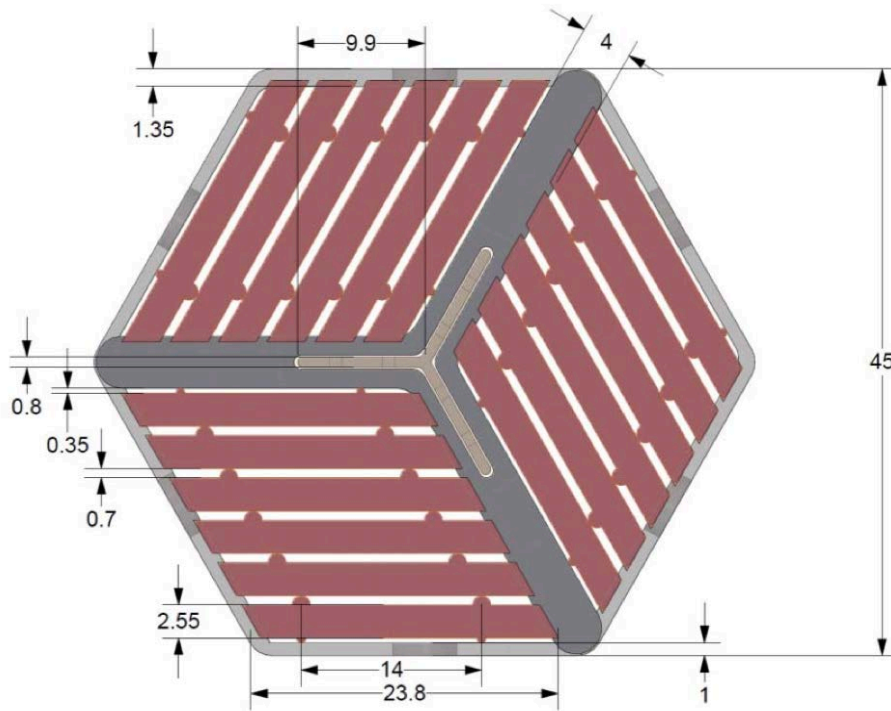


**Figure 2-4. Baseline 2011 AHTR Fuel Assembly with Dimensions in Centimeters**

In these plates, the coated-particle fuel is compacted into thin strips near the periphery of the plate surrounding an inert central matrix to minimize average fuel temperature; see Figure 2-5 (measurements in centimeters).

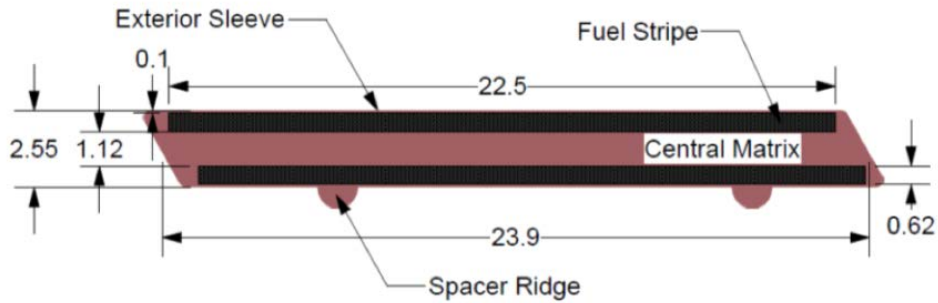


**Figure 2-5. Baseline 2011 AHTR Fuel Plate**

### 2.2.2 Unique FHR Operating Conditions

This subsection discusses typical differences between FHR and HTGR fuels from the perspectives of heavy metal loading (carbon/heavy metal ratio), power density and average/peak particle powers, and chemical environment (elimination of air ingress as an accident scenario, observation that chromium carbides may form on graphite surfaces, and possibility of beryllium carbides if excess beryllium metal is present; also absorption of oxygen/moisture as a potential source of chemical contamination in the primary loop).

The FHR IRP will use the annular pebble bed core (PB-FHR) as a baseline design. The existing 2009 design is 900 MWth, and UCB is studying designs with different power levels, ranging from 200 to 500 MWth, as the baseline for the commercial prototype. Whenever feasible, the following text compares the 2009 PB-AHTR baseline design, ORNL’s 2011 AHTR design, and the GT-MHR.

#### *Burnup*

Burnup is a key variable in determining the fuel performance in any nuclear fuel. Fission gas accumulated with increasing burnup stresses the TRISO layers and dictates the layer thickness requirements for safe operation. Radiation damage accumulated with increasing burnup degrades the thermal and mechanical properties of the coated particles’ constituents. The average discharge burnups for the 2009 PB-AHTR, 2011 AHTR, and GT-MHR are presented in Table 2-3.

**Table 2-3. Attainable Burnup in Various Reactors**

Factor	2009 PB-AHTR	2011 AHTR	GT-MHR (INL 2007)
Enrichment, percent	19.9	9	19.8
Burnup, MWd/Kg	220	73	140
Residence time, EFPD	1,071	360	425

Burnup can be decomposed into power/fluence, residence time and fuel loading. Power, fast fluence, and buildup fission gases are discussed in detail in subsections below. Residence time in a pebble bed reactor will be stochastic; under the baseline design, the pebble sorting machine will only measure burnup (by measuring  $^{137}\text{Cs}$  gamma activity). The distribution of burnups will peak at the center of the fixed fuel variant of the FHR because of the inherent flux shape of the finite core.

*Power*

Utilization of fluoride salts as a coolant enables natural circulation to remove passive decay heat; this process is much more effective than the combination of conduction and radiative heat transfer employed in modular HTGRs. This increased capacity for passive decay heat removal thereby allows the core to operate at a significantly higher power density than HTGR cores.

Furthermore, continuously circulated pebble fuel decouples the fuel burnup from the reactor shutdown frequency, so the pebble bed variants of FHRs can operate at higher power densities while maintaining criticality. Table 2-4 presents the power density characteristics for the 2009 PB-AHTR, 2011 AHTR, and GT-MHR.

**Table 2-4. Power in Representative Reactors**

Characteristic	2008 PB-AHTR	2011 AHTR	GT-MHR
Power, MWth	900	3400	600
Power density, MW/m <sup>3</sup>	16.2	12.9	6.6
Average power per particle, mW	80.7	25.4	-

The average power density does not completely define the characteristic power in an FHR. In the PB-AHTR, the neutron flux distribution is peaked toward the center of the reactor. Furthermore, the material vector that experiences this flux varies as a function of burnup. To completely understand the power densities of the pebbles, researchers calculated the power evolutions from beginning of cycle or end of cycle, assuming that a pebble was implemented immediately to the highest flux location in the center (highest power) or periphery (lowest power) radial position of the PB-AHTR and discharged after it reached the discharge burnup. Figure 2-6 compares the power evolutions of these hypothetical situations to the characteristic case (average flux experienced in the active region).

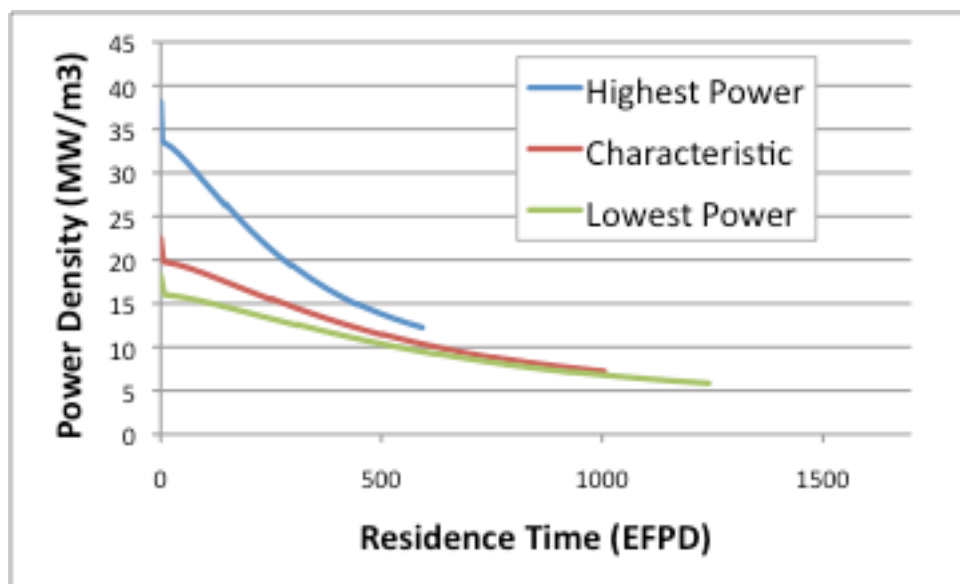


**Figure 2-6. Power Density Evolution of Pebble at Various Locations in the 2009 PB-AHTR**

*Temperature*

Characteristic temperatures are presented for the 2009 PB-AHTR, 2011 AHTR, and the GT-MHR in Table 2-5.

**Table 2-5. Temperatures in Various Reactors**

Characteristic	2009 PB-AHTR	2011 AHTR	GT-MHR (Simonds 2010)
Inlet coolant temperature, °C	600	650	590
Outlet coolant temperature, °C	700	700	950
Average kernel temperature, °C	711	844	850
Maximum kernel temperature, °C	770	854	1,250-1,350

Researchers calculated the temperature evolution for fuel particles in three representative locations in the core with a unit cell model for the 2009 PB-AHTR, assuming bulk coolant temperatures of 600°C, 650°C, and 700°C corresponding to the highest flux region, average flux region, and the periphery of the active region, respectively. The unit cell model assumes that the power distribution can be decomposed into a pebble scale and fuel particle scale. The power distribution is assumed constant in either the active region of the pebble or the kernel of the fuel particle, such that these two power distributions add up to the true power distribution as described by Stainsby et al. (Stainsby et al. 2009). The temperature distributions averaged on these two scales are superimposed to find the average kernel temperature. Researchers analyzed this unit cell heat transfer for every burnup state in each of the three characteristic locations. The resulting temperature evolutions are presented in Figure 2-7.

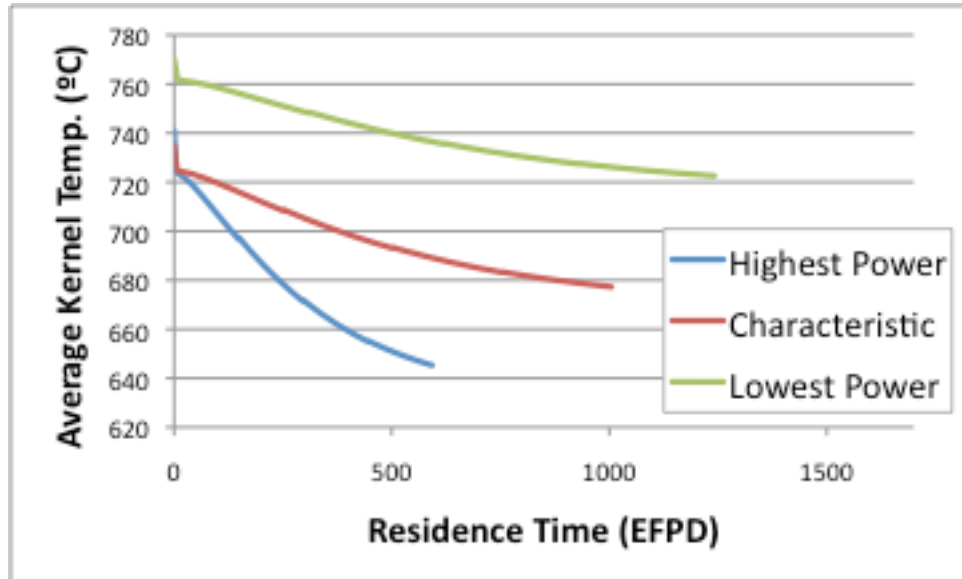


**Figure 2-7. Average Fuel Kernel Temperature Evolution of Pebble at Various Locations in 2009 PB-AHTR**

These average temperatures during normal operation have hundreds of degrees of margin until fuel failure starts to become an issue (at ~1,600°C). During ATWSs, the fuel and coolant reach elevated temperatures before their inherent feedback mechanisms stop the fission chain reaction, after which the fuel and coolant equilibrate to temperatures below the average fuel kernel temperature (Cisneros et al. 2012); see Figure 2-8.

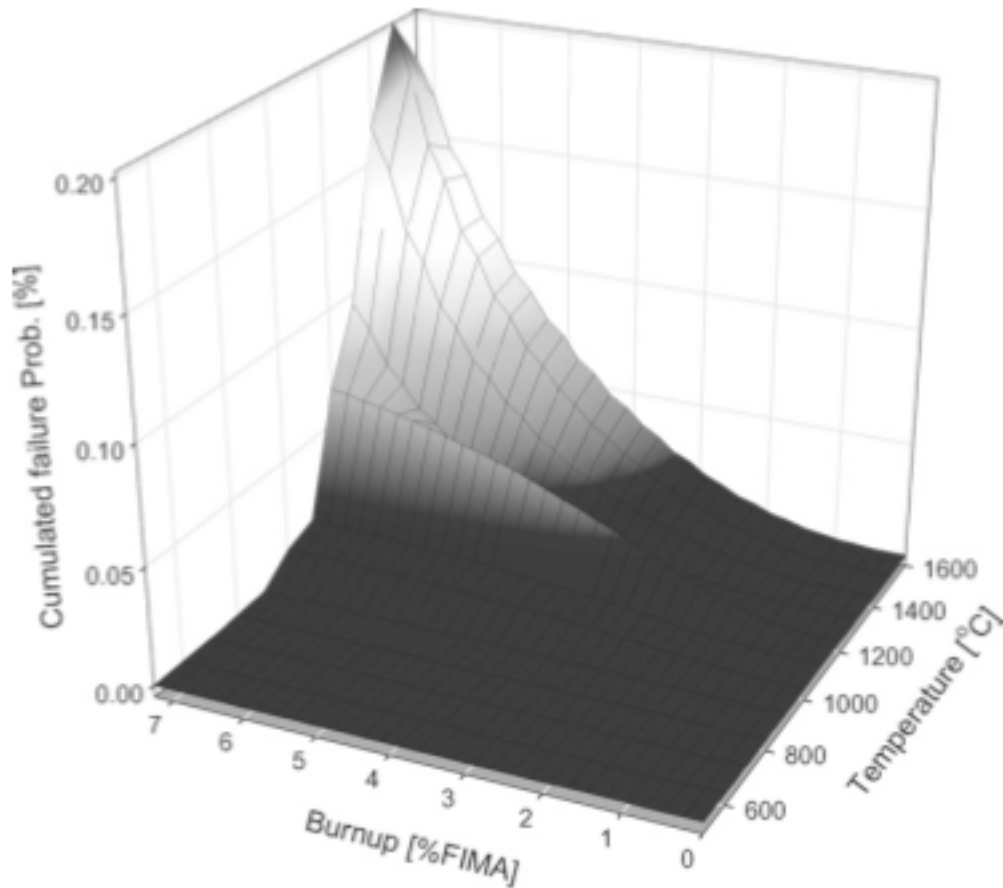


**Figure 2-8. Cumulative Failure Probability as a Function of Temperature and Burnup (Jeong, Jeong, and Chang 2009)**

The lower fuel operating temperature in FHRs should minimize the failure potential for TRISO particles. The role of temperature on fuel failure depends on the failure mechanism. TRISO fuel has many potential failure mechanisms, and the probability of failure is based on a multitude of variables. For intact particles, fuel would normally fail as a result of internal over-pressurization. The probability of failure for over-pressurization increases with temperature and burnup as the equilibrium pressure of the fission product gases xenon and krypton as well as CO/CO<sub>2</sub>, increase. In addition to temperature dependence, the probability of fuel failure caused by over-pressurization is tied to the dimensions and quality of the buffer and TRISO layers. An initial investigation into the critical limits for each fuel specification used the fuel performance code PARFUME, although the code is still in development, to support the qualification of NGNP VHTR fuel (Petti and Others 2004). The most significant parameter was the buffer thickness, because the buffer provides the free volume to accommodate fission product gases, and insufficient thickness can increase failure probability ~seven orders of magnitude. Other factors, such as SiC and IPyC thickness, IPyC anisotropy, and particle sphericity, can also have significant impacts on over-pressurization failure probability (Petti and Others 2004).

Intact particles can also fail by SiC fracture caused by irradiation-induced shrinkage cracking of the IPyC and propagation through the SiC layer. Fracture of the IPyC layer can cause a stress

concentration in the SiC layer and potentially lead to SiC failure. IPyC failure can be caused by shrinkage of IPyC and buffer layers from fast neutron irradiation. In the initial PIE of AGR-1, IPyC fracture was observed in isolated cases when the buffer and IPyC remained bonded; however, no complete failure were observed (Hunn and Others 2012). The onset of thermal creep at elevated temperature may change the risk of failure and degrade fuel performance.

Other temperature-dependent failure phenomena included attack of the SiC layer by metallic fission products. Historically, palladium attack on the SiC layer has been observed (Stansfield, Simon, and Baxter 1983). The penetration of palladium into the SiC reduces the layer's effective thickness and reduces the particle's overall strength. The attack by palladium ultimately limits fuel lifetime because continued attack may lead to catastrophic failure of the particle. Transport of metallic fission products to the IPyC/SiC interface and rate of attack depend on fuel temperature.

The amoeba effect occurs in situations where there is a temperature gradient across the fuel particle. Where sufficient oxygen is available and the temperature is sufficiently high, temperature gradient leads a gradient of the concentrations of CO and CO<sub>2</sub> across the kernel. This gradient results in the transport of carbon from the hot side to the cold side, ultimately leading to kernel migration in the particle. Adjustments in the kernel composition, particularly the C/U ratio, can limit the production of CO and CO<sub>2</sub> to minimize the amoeba effect. The amoeba effect can also be minimized through low power density designs and homogeneous fuel distribution, but high power density is a key design feature of FHRs (IAEA 1997).

Non-catastrophic failures include the release of metallic fission products from intact fuel particles. Fission products observed to be released from intact particles in the AGR-1 PIE in measurable quantities were silver, europium, palladium, strontium, cerium, and samarium (Hunn and Others 2012), while historically Cs was also observed to be released (IAEA 1997). The release has been modeled as diffusion dependent and is a function of the impurity species diffusion coefficient in the multiple layers. The diffusion coefficient follows an Arrhenius relationship that results in accelerated release at elevated temperatures. Fission products can also be released by recoil and knockout; however, this is a fuel geometry issue and not necessarily thermally driven because the release of a fission product by recoil and knockout depends on the mean free path of the energetic particle and the fission event's location within the kernel, such that the fission product can travel a sufficient distance to exit the particle. The design of the particle mitigates this effect through the implementation of the carbon buffer layer that attenuates fission product recoils.

Release of gaseous fission products such as xenon and krypton may also be observed during operation. The main source of gaseous fission products comes from heavy metal contamination in the graphite, because intact particles are not expected to release gaseous fission products. Because heavy metal contamination levels are a primary source of fission product release, specifications should be applied to keep heavy metal contamination to reasonable levels. The release of gaseous fission products from failed particles is expected to increase with increased temperature and burnup.

*Fast Flux*

Radiation damage degrades the thermal and mechanical properties of the constituents of the coated-fuel particles. The fast ( $> 0.1$  MeV) flux distribution in the 2009 PB-AHTR at equilibrium is presented in Figure 2-9.

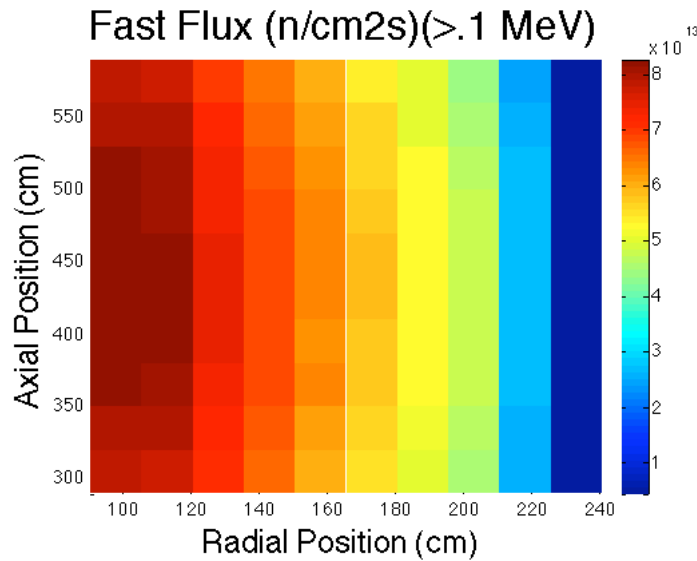


**Figure 2-9. Map of Fast Flux Intensity in the Active Region of the 2009 PB-FHR**

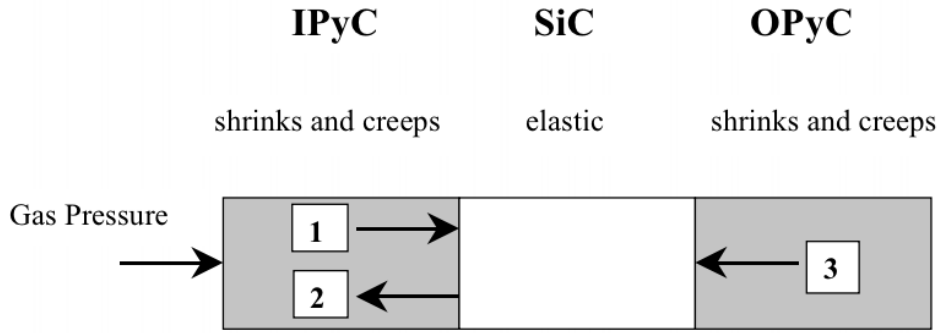
The fast fluences at end of life for the three cases described earlier are presented in Table 2-6.

**Table 2-6. Fast Fluence in the 2009 PB-AHTR at Various Locations**

Factor	Inlet	Characteristic	Outlet
Fast flux, n/cm <sup>2</sup> s ( $>0.1$ MeV)	$8.25 \times 10^{13}$	$4.93 \times 10^{13}$	$2.82 \times 10^{13}$
Residence time, EFPD	645	1,005	1,241
Fast fluence, n/cm <sup>2</sup> yr ( $>0.1$ MeV)	$4.22 \times 10^{21}$	$4.28 \times 10^{21}$	$8.89 \times 10^{20}$

*Fission Gases*

Gaseous fission products stress the coated-particle layers because these products accumulate in the buffer layer of the coated particle and generate internal pressure; see Figure 2-10.



- 1 Gas pressure is transmitted through the IPyC
- 2 IPyC shrinks, pulling away from the SiC
- 3 OPyC shrinks, pushing in on SiC

**Figure 2-10. TRISO Layer Behavior Under Irradiation (INL, Centre d’Etude Atomique, and Massachusetts Institute of Technology 2004)**

The inventory of fission gases increases with burnup. FHR fuel is optimized to high burnup because of high fuel fabrication costs. Therefore, such gaseous fission products might be more significant in FHR fuel compared to gas reactor fuel.

The accumulation gaseous fission products (hydrogen, helium, krypton, xenon, and radium) in a single characteristic TRISO particle in the 2009 PB-AHTR is presented in Figure 2-11. Krypton and xenon contribute the most to pressure on the particle layers.

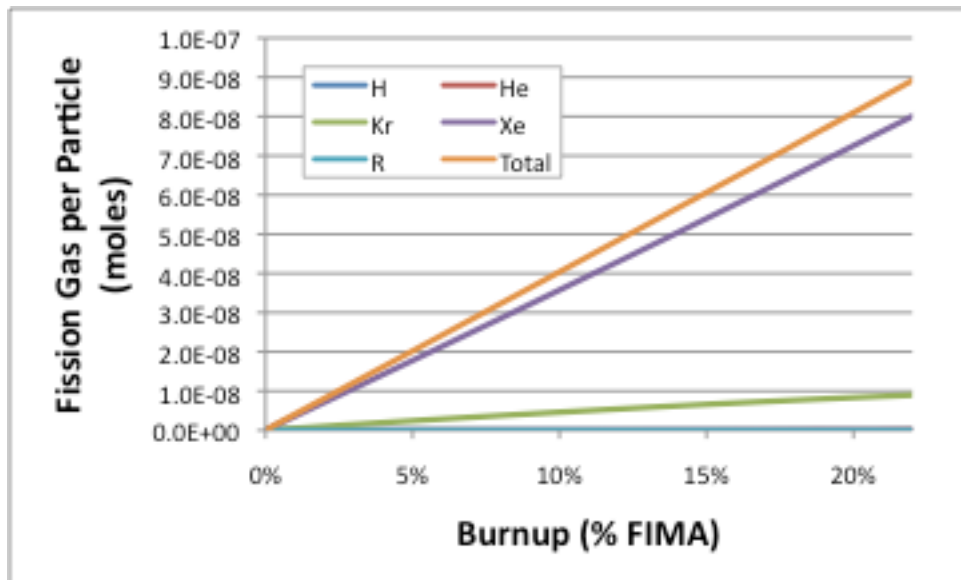


**Figure 2-11. Buildup of Fission Gases in the 2009 PB-AHTR in a Single TRISO Particle**

### 2.2.3 FHR Fuel Quality Verification Requirements

This subsection raises the question of whether FHR fuels need to have the same level of quality verification as HTGR fuels. In particular, it discusses whether FHRs could be licensed to allow higher defective particle fractions as a result of the different transport and release mechanisms for circulating activity in FHR transients and accidents, compared to HTGRs (where  $^{137}\text{Cs}$  absorption on graphite dust is a key safety issue because it can be mobilized during LOCAs). This level of defective particle fractions will dictate the level of sampling and quality assurance required to qualify the fuel for the FHR design. Actual defective particle fractions could be much lower, but the necessity to prove this using extensive destructive sampling is reduced.

Fission product release will increase the source term in the coolant. However, from the perspective of reactor safety the key issue is the fraction of fission products that could then be mobilized and released during an accident. Noble gas fission products released from FHR fuel are removed in the cover gas cleanup system, which is designed to maximize the recovery of tritium generated in the coolant. The remaining fission products either form stable fluoride salts with very low vapor pressures or deposit as noble metals on primary loop surfaces (particularly in the HX), on the cold end of the primary loop, and in the cold trap if used. Thus, the fraction of circulating activity that can be released during accidents in FHRs may be much lower than in HTGRs, potentially orders of magnitude lower. For this reason, the criteria for acceptable defective fuel particles may be established by other considerations, such as disposal criteria for used primary coolant salt.

Likewise, the failure fractions of FHR fuel particles may be different compared to HTGRs. The propensity for stress-induced failures varies at lower temperatures because thermal creep is not significant at lower operating temperatures.

The current approach for fuel qualification of the HTGR fuel incorporates an NQA-1 (nuclear quality assurance-1) quality assurance program for all stages of the manufacturing, handling, and shipping of the fuel. In some instances, sampling and destructive testing of the fuel are required to verify quality. All statistical sampling requires a 95% confidence level for every characteristic investigated (Petti and Others 2004). A similar program for FHR fuel development would ensure quality fuel is produced. Insight is needed into the level of sampling required for possible relaxed failure fracture standards. Additionally, lower quality fuel standards may not be accepted by regulators if high-quality TRISO fuel is demonstrated in other reactor designs.

## 2.3 Development Needs for FHR Fuel

Preliminary studies have been conducted regarding the testing program for FHR fuel. The 2010 UCB senior design class was charged with designing fuel qualification capsules for 2009 PB-AHTR annular fuel pebbles (Gomez et al. 2010). Students developed three conceptual designs of fuel qualification capsules based on those developed for the AGR program to be inserted into either 3-inch or 5.25-inch flux traps in the ATR at INL or the large-diameter removable beryllium locations in the High Flux Isotope Reactor (HFIR) at ORNL. Examples are shown in Figures 2-12, 2-13, and 2-14, respectively.

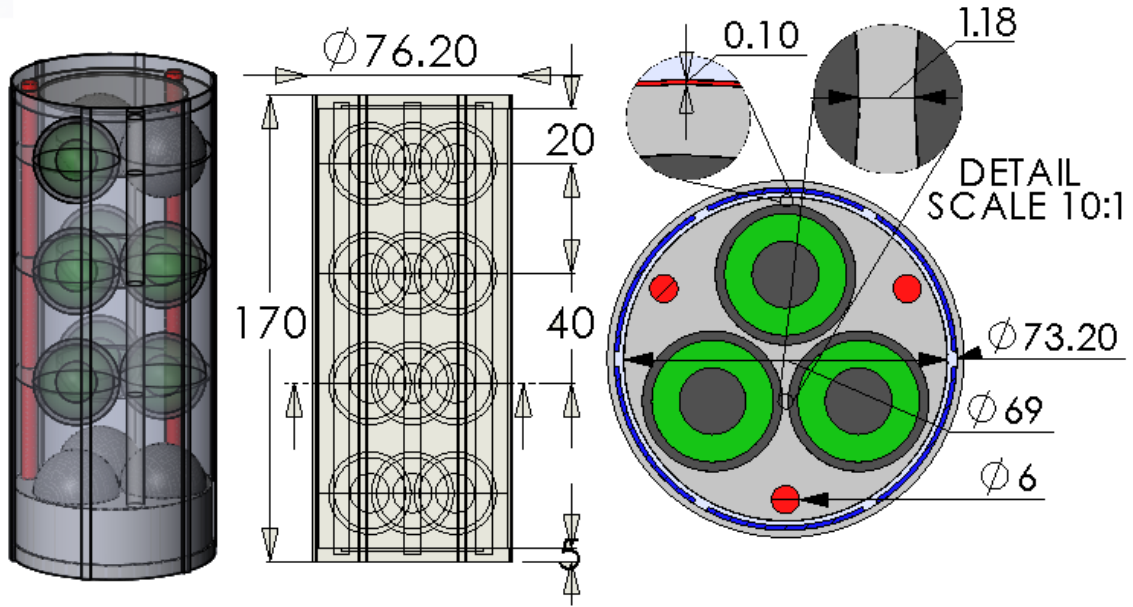


Figure 2-12. Fuel Qualification Capsule for 2009 PB-AHTR Fuel: ATR 3-Inch Location

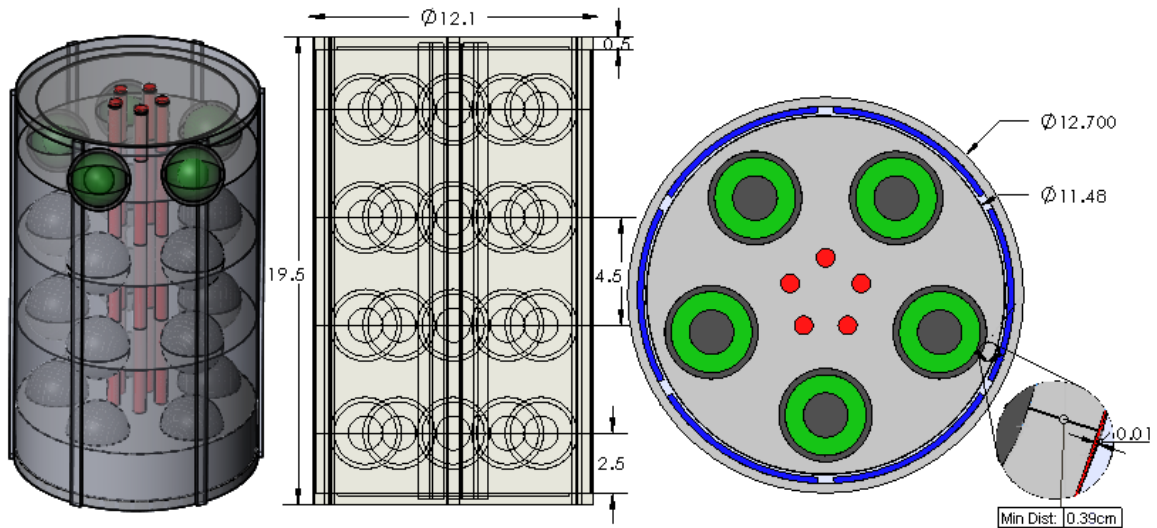
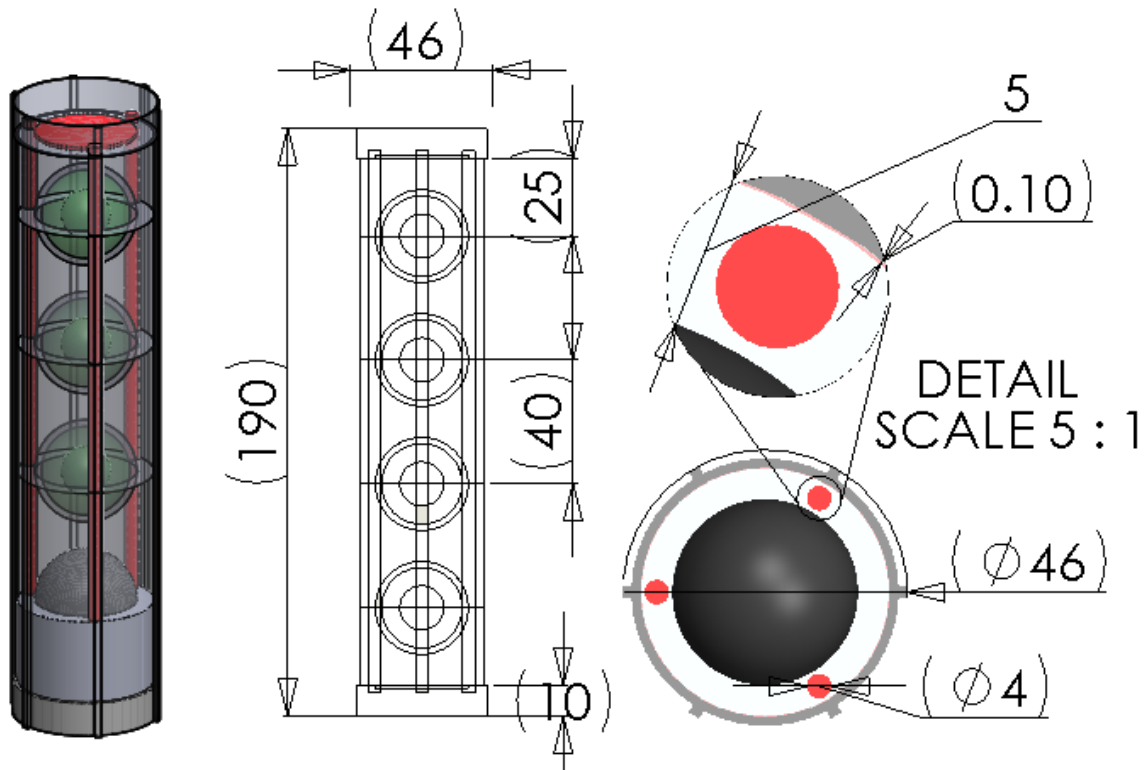


Figure 2-13. Fuel Qualification Capsule for PB-AHTR Fuel: ATR 5.25-Inch Location



**Figure 2-14. Fuel Qualification Capsule for PB-AHTR Fuel: HFIR Boron Removal Location**

Each of the irradiation locations in the ATR and HFIR can be instrumented with a dedicated gas feed to control the heat removal and insulation<sup>1</sup>; therefore, the fuel irradiation temperature can be tuned to match prototypical conditions of the PB-AHTR. Preliminary heat transfer analysis in the analysis code COMSOL Multiphysics confirms that the temperature profiles in these test trains are reasonable approximations of those in the PB-AHTR (Gomez et al. 2010).

Two group flux spectrums are given for the ATR and HFIR and compared against the PB-AHTR in Figure 2-15 (INL 2009)<sup>2</sup>. Note that only thermal and fast flux are reported for the ATR, and the energy limits were assumed based on flux distribution plots.

<sup>1</sup> See “Large Removable Beryllium Reflector Facilities” at <http://neutrons.ornl.gov/facilities/HFIR/in-vessel.shtml>. Accessed August 12, 2012.

<sup>2</sup> Ibid.

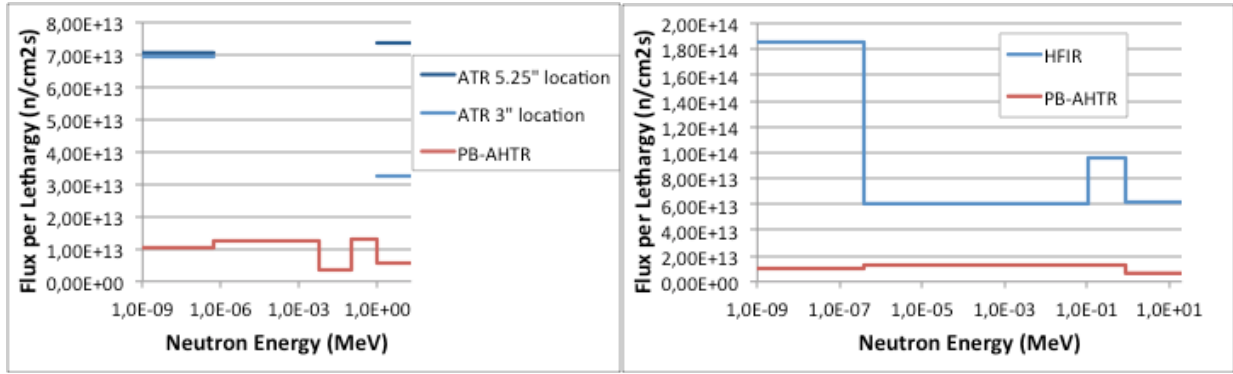


**Figure 2-15. Few Group Neutron Energy Spectrum Comparison Between ATR (left) and HFIR (right) and the 2009 PB-AHTR in the Active Region**

The energy spectrum can be softened by adding hafnium to the test train (Ellis 2011). The combination of high power density and low fuel loading in FHR coated-particle fuels enables rapid fuel qualification testing. Preliminary estimates of the time required for the qualification of the latest PB-FHR fuel design are presented in Table 2-7. The full power irradiation times to reach either the average thermal fluence (should be approximately proportional to burnup) and the fast fluence limit (should be approximately proportional to neutron damage) listed should give a first order indication on the length of the irradiation campaign required for fuel qualification – the energy limits of thermal and fast fluxes are taken to match the public information for each test reactor.

**Table 2-7. Fast Fluence in the 2009 PB-AHTR, ATR and HFIR at Various Locations**

Characteristic	Value
Power density, MW/m <sup>3</sup>	16.2
Total flux rate in active region of PB-AHTR, n/cm <sup>2</sup> s	2.77×10 <sup>14</sup>
Average residence time in PB-AHTR, EFPD	1,073
EFPD to reach average thermal fluence (< 0.4 eV) (HFIR)	57
EFPD to reach average fast fluence (> 0.111 MeV) (HFIR)	310
EFPD to reach average thermal fluence (10 <sup>-3</sup> eV < E < 0.537 eV) (ATR 5.25")	150
EFPD to reach average fast fluence (> 1 MeV) (ATR 5.25")	50
EFPD to reach average thermal fluence (10 <sup>-3</sup> eV < E < 0.537 eV) (ATR 3")	230
EFPD to reach average fast fluence (> 1 MeV) (ATR 3")	160

## 3 FHR Ceramic and Ceramic Composite Components

Like HTGRs, FHRs make extensive use of graphite as a structural material, but other materials are also important. The baseline FHR design assumes limited use of CFRC and SiC/SiC composite structures. The baseline design also assumes the use of CFRC for the core barrel assembly, which together with the reactor vessel creates the downcomer that guides flow to the core inlet and the use of SiC/SiC composites for structures in high neutron dose rate regions of the core, particularly for shutdown rod channels. This chapter reviews the current status of development for these materials, specific issues associated with their application to FHRs, and input from experts at the workshop on methods for in-service inspection and requirements for component testing.

### 3.1 FHR Graphite

The following subsections summarize the current status of graphite technology, including manufacturing, procurement, and other factors, and lays out unique operating conditions for FHRs related to the use of graphite in structures.

#### 3.1.1 Current Status of Graphite Technology

This subsection provides an overview of the current status of nuclear graphite technology, particularly in the United States. It provides references to current NGNP program activities as well as international activities. It also discusses the new ASME Division 5 treatment of graphite (see the second workshop white paper discussion on structural mechanics modeling for graphite components). Finally it briefly summarizes graphite experience from the MSRE and the Molten Salt Breeder Reactor (MSBR) programs.

Nuclear graphite is used as a moderator for high-temperature thermal reactors. Because of its high thermal conductivity and low chemical activity at elevated temperatures, it is considered an ideal moderator for molten salt reactors. However, before nuclear graphite can be used in a molten salt reactor certain issues must be addressed. This subsection provides a brief outline of current issues with nuclear graphite.

#### *Manufacturing*

Graphite is a highly engineered material made primarily of coke from petroleum or coal sources and petroleum-based tar. The petroleum industry is the main source for both starting materials. Coke must first be calcined at 1,300°C, then crushed and blended with tar. This mixture is extruded, molded, or pressed, and then baked at approximately 1,000°C. This process produces a very porous green billet. The green billet is then intruded with more tar and baked at 2,500°C to 2,800°C. Depending on the density needed, intrusion and baking steps may be repeated a number of times (Windes, Croson, and Roberts 2010). The entire process can take on the order of a few months to complete. While this is the standard approach for producing any graphite, nuclear graphite manufacturing has more stringent controls and requirements.

Nonnuclear graphite is primarily used in electrode refiners for metals or semiconductor materials (Windes, Croson, and Roberts 2010). Generally these materials will be processed

further and do not require very low impurity concentrations for the initial refining stage. Nuclear graphite, on the other hand, does need to have a very high degree of purity to prevent high concentrations of boron from lowering the reactivity to an unacceptable level. In addition, other elemental contamination could lead to the creation of long-lived activation products that will force the graphite blocks to be considered high-level waste at the end of the service life.

To produce nuclear graphite, either the raw material (coke and tar) or the final graphite piece must be baked with a halogen gas. This gas will act as a getter for metal impurities and allow metals to be removed from the carbon.

### *Procurement*

Currently four major graphite manufacturers are able to produce nuclear graphite in the quantities needed for use in a nuclear reactor: Graftech International, SGL, Toyo Tanso, and Carbone of America (Windes, Croson, and Roberts 2010). These four manufacturers have all shown willingness to produce nuclear graphite for the NGNP VHTR so long as the production quantity is large enough to justify the cost of gathering material and resources (around 100 tons worth). However, because of the stringent requirements and low market share of nuclear graphite, the petroleum industry is less willing to produce the needed raw materials (Windes, Croson, and Roberts 2010).

### *Neutron Radiation Damage*

Radiation damage in graphite results when neutrons interact with carbon atoms causing lattice displacement. The displaced atom can then knock other atoms off the lattice, known as secondary knock-on atoms (Windes, Croson, and Roberts 2010). The vast majority of these atoms will settle in vacancy locations. The very small percentage that settle in interstitial locations (between basal) will cause radiation damage. This damage will have an array of effects on the graphite, including changes in density and thermal conductivity. In FHRs, the thermal conductivity of structural graphite is not as important as it is for HTGRs, because decay heat is removed by natural circulation of salt rather than by thermal conduction through the graphite reflector structure to the reactor vessel. Only dimensional stability and mechanical strengths of graphite will be reviewed in this white paper.

Under neutron irradiation, graphite will become less dimensionally stable. At elevated temperatures, interstitial atoms will continue to be mobile. As more and more atoms settle between basal planes, the atoms will coalesce and form new basal planes. As the extra planes form, nano-cracks (termed Mrozowski) in the graphite structure close while the vacancies left behind collapse. This process causes a net densification of graphite. However, after all the Mrozowski are filled, a point called turnaround is reached, and graphite has the highest density. After turnaround, graphite will grow in the crystallographic c-direction. If the grains in the graphite have random orientations, the graphite is isotropic, and the graphite will grow uniformly in all directions. If the grains do not have random orientations, the graphite will grow preferentially in one direction and shrink primarily in a different direction. Dimensional changes in graphite are also temperature dependent. Figure 3-1 shows the volumetric changes in graphite as a function of dose and temperature, while Figure 3-2 shows the turnaround point. At energies greater than 1.0 MeV,  $1.0 \text{ dpa} = 0.78 \times 10^{21} \text{ n/cm}^2$  (Windes, Croson, and Roberts 2010).

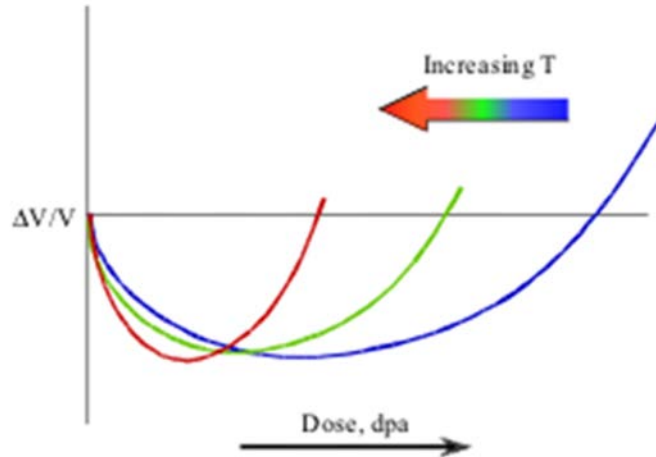


**Figure 3-1. Volumetric Response to Dose and Temperature of Generalized Graphite (Windes, Croson, and Roberts 2010)**

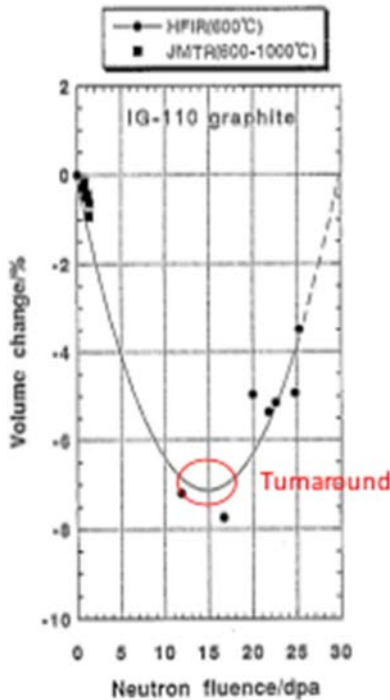


**Figure 3-2. Turnaround Point for Graphite (Windes, Croson, and Roberts 2010)**

*Strength*

Graphite increases in strength up to 2,000°C. The strength is the result of Mrozowski closing from thermal expansion. Irradiated strength changes in three parts. The first part changes at a very low dose (<1 dpa). This change will be a strength increase as a result from dislocations being pinned at lattice defect sites. As graphite reaches the turnaround point, the strength will increase because of a closure of the Mrozowski. Once turnaround is reached, graphite will expand and lose strength dramatically. Figure 3-3 shows how tensile strength will change as a function of temperature and dose.

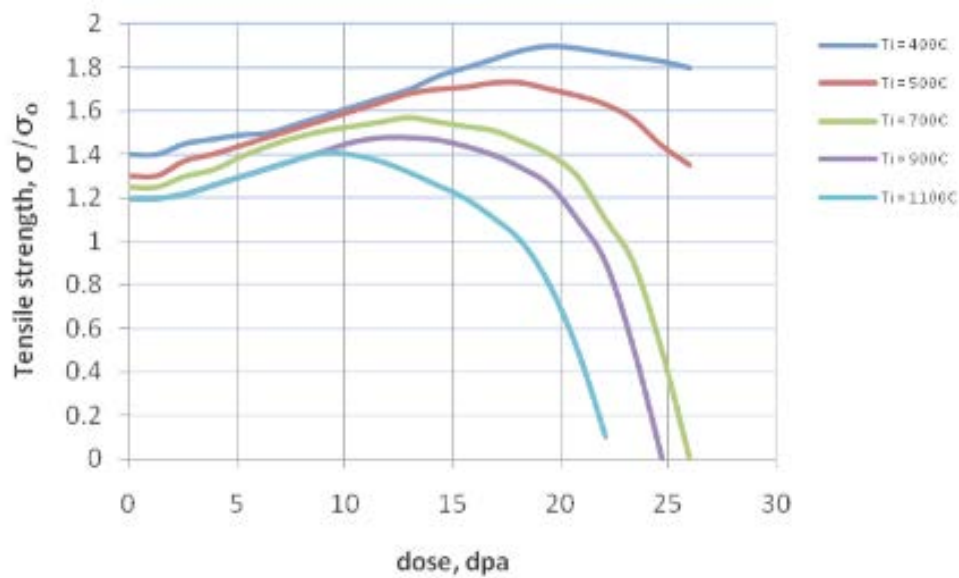


**Figure 3-3. Tensile Strength Response to Dose and Temperature of Generalized Graphite (Windes, Croson, and Roberts 2010)**

The Young's modulus will behave in the same manner as the tensile strength in elevated temperature and doses. Figure 3-4 shows these changes as a result from temperature and dose.

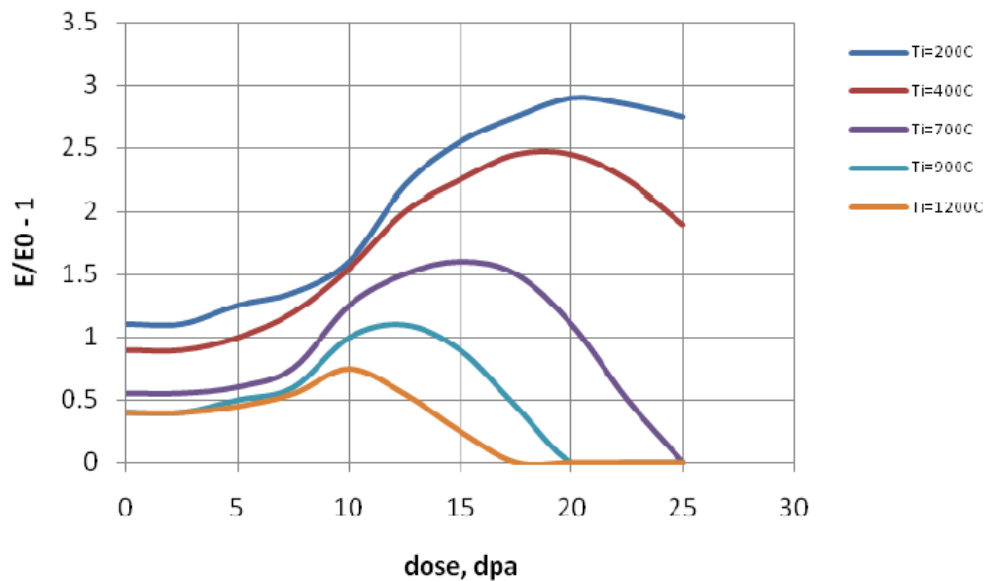


**Figure 3-4. Typical Young's Modulus Response to Dose and Temperature of Generalized Graphite (Windes, Croson, and Roberts 2010)**

#### *Experimental Data*

The VHTR program generated a significant amount of data for graphite. The VHTR program is conducting a major irradiation experiment called the Advanced Graphite Creep (AGC)

experiment. The AGC experiment will comprise six test trains. Also available is a baseline properties report from INL (INL/EXT-07-131652010). Each test train will have compressive and non-compressive samples. Figure 3-5 shows the test plan for the six test trains as well as two additional high-temperature vessel tests. Currently AGC-1 post irradiation characterization is partially complete, and AGC-2 has been pre-characterized. Rather than attempting to summarize the AGC-1, AGC-2, and the baseline properties report here, they are listed as references for further review (Carroll, Lord, and Rohrbaugh 2010; W. Swank 2011; D. Swank et al. 2010).

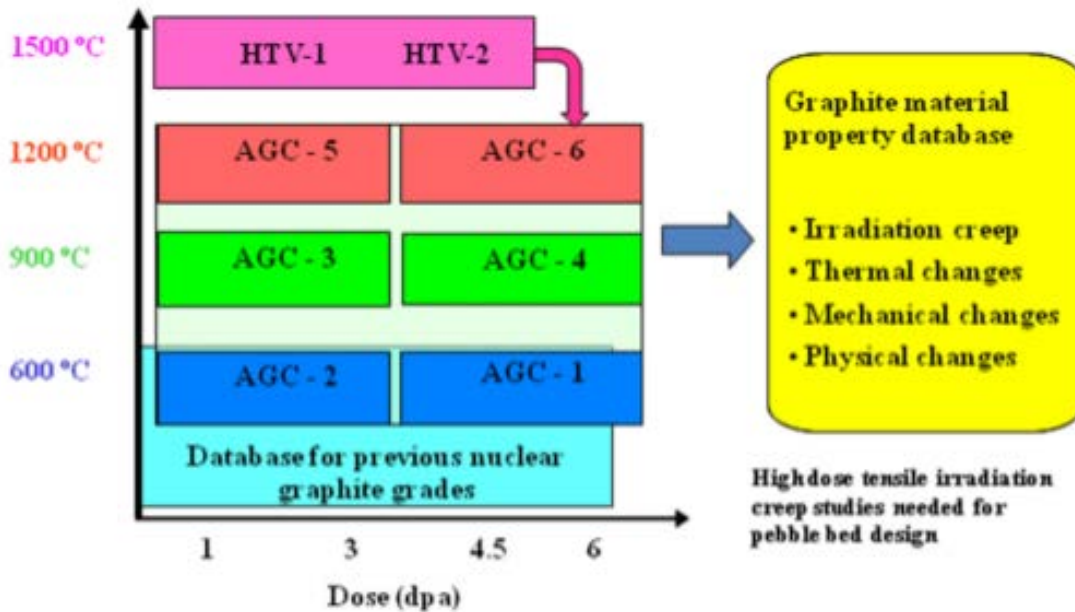


**Figure 3-5. NGNP VHTR Graphite Irradiation Test Plan (Bratton and Burchell 2005)**

Experimental data specifically for molten salt reactors are available from small scoping studies done for the MSRE at ORNL. The graphite used for the MSRE was CGB-grade graphite developed with ORNL. The graphite is described as highly dense anisotropic graphite sealed by chemical vapor deposition (CVD) to prevent the intrusion of liquid salt and  $^{135}\text{Xe}$ . In the MSRE, the uranium fluoride fuel was dissolved in the salt; thus, fission products including xenon were produced in the salt. In a molten-salt reactor, the xenon gas rapidly goes into the off-gas system. Xenon has a very high nuclear absorption cross section. To improve the neutronics, the xenon inventory in the reactor core was to be minimized. If there was molten salt trapped in pores in the graphite, the xenon would be trapped and act as a neutron poison. To avoid this, a CVD layer was added to the graphite so there was no molten salt in the graphite. At the time of the MSRE program, CGB-grade graphite was an advanced material. However, because of its anisotropic nature, it would not be considered a viable candidate for modern reactors. High-density graphite is needed for molten salt reactors to reduce salt attachment on the graphite. A few modern grades of graphite meet or exceed most of the material properties of CGB-grade graphite. Table 3-1 lists material properties for CGB-grade graphite and other modern grades of graphite. Because of the anisotropic nature of the graphite, the best material property will be chosen as a guide to compare to modern graphites.

As mentioned previously, modern graphites are much more isotropic. The isotropic nature of modern graphites will lead to a better radiation response. However, from a molten salt standpoint modern graphites will absorb more molten salt constituents because one final step in the manufacturing of CGB-grade graphite included a CVD treatment to seal open porosity. V. Bernardet et al. (Bernardet et al. 2009) found that NBG-17-grade graphite could be protected from molten salt impregnation by depositing a pyrocarbon layer on the surface. The potential need for similar CVD coating should be considered for FHRs.

**Table 3-1. Graphite Properties (Billot et al. 2004; Chi and Kim 2008; Simpkins et al. 1989; Briggs 1964)<sup>1</sup>**

Grade	CGB	IG-110	AXF-5Q	NBG-17
Bulk density, g/cm <sup>3</sup>	1.86	1.82	1.78	1.89
Close porosity, %	4	6.67	4	-
Open porosity, %	13.7	12.44	16	7
Total porosity, %	17.7	19.44	20	-
Thermal conductivity, W/m/K	193.84	139	95	143
CTE, 10 <sup>-6</sup> /K	15	4.8	7.9	4.7
Tensile strength, MPa	13.1	37	62	22
Flexural strength, MPa	29.6	54	86	32
Young's Modulus, GPa	22.06	10.8	11	11.9
Compressive strength, MPa	59.3	83.3	138	90
Ash content, ppm	41	<20	1700	180

#### *Salt Uptake by Graphite*

The CVD layer on MSRE graphite minimized possible salt uptake and the uptake of the fission product xenon in the graphite—not a concern for an FHR. Graphite generally is not wetted by the salt (Kasten et al. 1969). There are two other potential reasons to minimize salt uptake: (1) to minimize carryover of salt with the SNF and possibly simplify treatment before disposal and (2) to avoid the potential of unforeseen interactions of the salt or salt vapor with the

<sup>1</sup> See the POCO Graphite website <http://www.poco.com/tabid/89/defaults.aspx>. Accessed March 22, 2013. Additional information from Philippe Béghein, Gérard Berlioux, Bruno du Mesnildot, Frank Hiltmann, Marc Melin., NBG-17 An Improved graphite grade for HTR and VHTR. *Nuclear Engineering and Design*, In Press, Accepted 22 October 2011.

coated-particle fuel. Such interactions are not expected because of the outer carbon layer on the coated-particle fuel. A series of tests are underway to confirm this at UW.

#### *ASME Code Development*

ASME has drafted rules for HTGR graphite for core components, as a part of Section III of its Boiler and Pressure Vessel (BPV) Code. The U.S Nuclear Regulatory Commission (NRC) must research and possibly accept and endorse these codes. However, currently most codes for graphite stress analysis are proprietary in nature and vary widely. The NRC has initiated four tasks for approval of codes (Mohanty and Majumdar 2011):

- Task 1: Evaluate current graphite core stress analysis models and issue a technical letter report on them
- Task 2: Develop a finite-element stress analysis code and issue a technical letter report on it
- Task 3: Verify and validate the stress analysis method
- Task 4: Publish the methodology.

Argonne National Laboratory has completed Task 1 for HTGRs. Properties of interest in the HTGR program models are as follows:

- (a) Non-irradiated properties
  - i. Young's modulus versus temperature
  - ii. Elastic Poisson's ratio
  - iii. Coefficient of thermal expansion (CTE) versus temperature
  - iv. Thermal conductivity versus temperature
- (b) Irradiated properties as a function of temperature and irradiation dose
  - v. Dimensional change
  - vi. CTE
  - vii. Young's modulus
  - viii. Elastic Poisson's ratio
  - ix. Thermal conductivity
- (c) Irradiation creep as a function of temperature, dose, and stress
  - x. Creep law constants and variables
  - xi. Elastic Poisson's ratio in creep
- (d) Effect of oxidation on graphite mechanical properties
- (e) Interaction between irradiation creep and thermal expansion and dimensional change strains.

Data on many of these properties have been gathered by the baseline properties program at the INL. ABAQUS was chosen for heat conduction and stress analysis of components (Mohanty and Majumdar 2011). These properties will also apply to the graphite in a molten salt reactor; however, an additional section may be needed for molten salt reactors.

D. K. Morton, et al. (Morton et al. 2012) reported the development and future directions for the new BPV Section III, Division 5. The new code establishes a single-volume framework for high-temperature reactor design, fabrication, inspection, and testing, and provides a home for the new graphite rules.

### **3.1.2 Unique FHR Operating Conditions**

This subsection discusses unique issues for the FHR application of graphite as a structural material (primarily for neutron reflectors and upper-core support/outlet plenum structures). Chapter 5 (on salt corrosion and chemistry control) of this white paper discusses interactions with the coolant [uptake of moisture/oxygen during handling and release to the coolant, uptake of tritium, and corrosion interactions with coolant (e.g., formation of chromium carbides)].

Many of the functional requirements of the graphite structures subsystem can be achieved by maintaining the integrity of its BOL geometry. These requirements include the following safety-related regulatory design requirements:

- Maintain core and reactor vessel geometry
- Provide flow paths for primary coolant
- Maintain control and shutdown rod channel geometry.

The graphite structure geometry changes with increasing radiation damage and with thermal expansion, altering the alignment of control channels and affecting the integrity of this subsystem. Note that the core remains hot (~600°C) during downtime for maintenance in FHRs to keep the coolant molten and to minimize thermal cycling.

The specific operating environmental conditions with respect to temperatures, pressures, surface-to-volume ratios, and radiation damage for the 2009 PB-AHTR are presented here to illustrate operating conditions typical of FHRs. Figure 3-6 shows the 2009 PB-AHTR with the graphite structures subsystem highlighted in red.

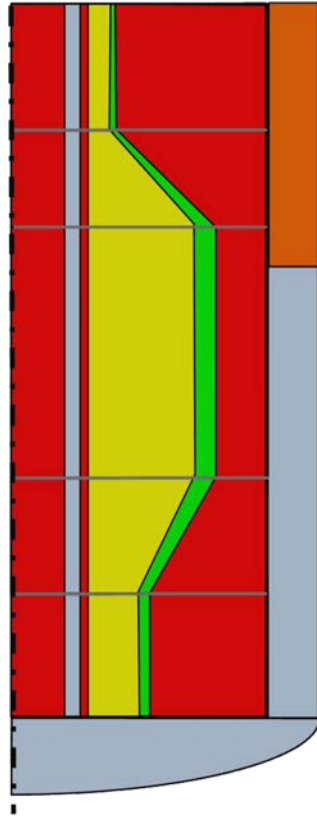


**Figure 3-6. 2009 PB-AHTR Core Geometry with Graphite Structures Subsystem Highlighted in Red**

*Temperature and Pressure in the Graphite Structures Subsystem*

Graphite structures in FHRs are directly exposed to the coolant in the core. Therefore, degradation mechanisms of the graphite structures subsystem are impacted by the temperature and pressure distributions of the coolant at the interface between the coolant and the graphite. In Chapter 1, Figures 1-3 and 1-5 show the bulk coolant temperature and the pressure distribution, respectively, in the 2009 PB-AHTR core under normal operating conditions.

Table 3-2 details the surface areas and coolant temperatures to which the inner and outer graphite reflectors are exposed. The variations in pressure along the interface between the coolant and the graphite reflectors are negligible (a few tens of kPas). Because of the pool-type configuration of the FHR, all pressures in the system are expected to be nearly at atmospheric pressure.

**Table 3-2. 2009 PB-AHTR Surface Areas of the Inner and Outer Reflectors Exposed to Coolant at Temperature T**

Inner Reflector		Outer Reflector	
A, m <sup>2</sup>	T, °C	A, m <sup>2</sup>	T, °C
<i>Inlet</i>			
1.80	600	3.13	601
1.80	601	3.13	601
1.80	601	3.13	603
1.80	601	3.13	604
1.80	601	3.13	607
1.80	602	3.47	610
1.80	604	3.80	614
1.80	604	4.13	620
1.80	606	4.80	628
<i>Mid-Core</i>			
1.88	607	5.03	634
1.88	608	5.03	639
1.88	617	5.03	643
1.88	628	5.03	649
1.88	639	5.03	654
1.88	648	5.03	659
1.88	658	5.03	663
1.88	669	5.03	667
1.88	679	5.03	678

Inner Reflector		Outer Reflector	
A, m <sup>2</sup>	T, °C	A, m <sup>2</sup>	T, °C
<i>Outlet</i>			
1.70	689	4.52	686
1.70	699	3.58	693
1.70	711	2.95	707
1.70	730	2.64	770
1.70	747	2.01	741
1.70	757	2.01	748
1.70	761	2.01	751
1.70	760	2.01	749
1.70	753	2.01	743

Some neutron and gamma energy from fission are deposited in the inner and outer graphite reflectors. Figure 3-7 presents the distribution of neutron and gamma heating in the inner and outer graphite reflectors, and Table 3-3 presents the average and maximum values of these energy deposition terms.

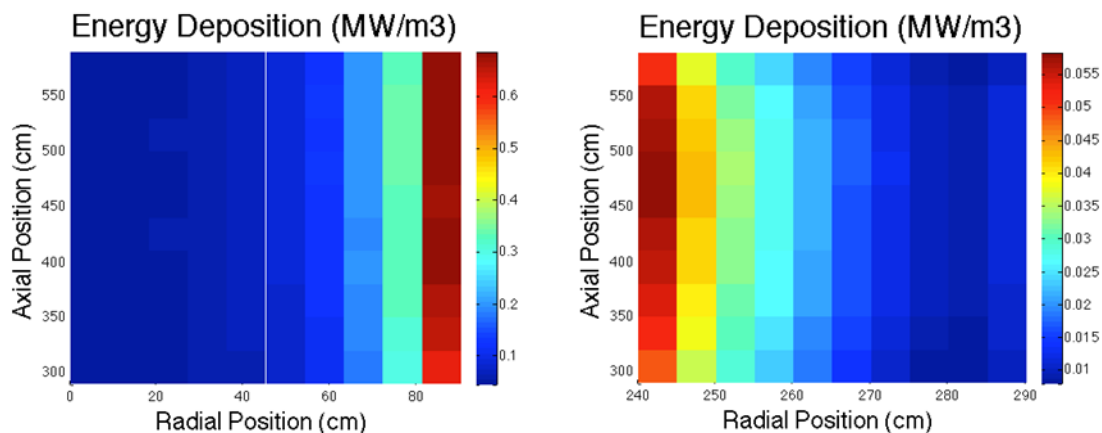


**Figure 3-7. Energy Deposition Rate for Inner (left) and Outer (right) Graphite Reflectors as a Function of R-Z Position in the Active Region of the 2009 PB-AHTR**

**Table 3-3. Energy Deposition Rate for the 2009 PB-AHTR Inner and Outer Graphite Reflector**

Factor	Inner Reflector	Outer Reflector
Average power, MW/m <sup>3</sup>	$2.51 \times 10^{-1}$	$2.23 \times 10^{-1}$
Maximum power, MW/m <sup>3</sup>	$6.84 \times 10^{-1}$	$5.82 \times 10^{-1}$

*Radiation Damage in the Graphite Structures Subsystem*

Radiation damage causes the geometry of the structures to deform and degrades the material properties of graphite structures in terms of mechanical strength and thermal conductivity. This subsection presents radiation damage in terms of dpa, fast neutron fluence (>0.1 MeV), and gas production.

Figure 3-8 presents the dpa fluence rate as a function of position (r-z) in the 2009 PB-AHTR inner and outer graphite reflectors adjacent to the active region of the core (i.e., the highest fast flux regions). The fluence rates suddenly drop, which might lead to internal stresses caused by the gradient of deformation rates. Detailed analysis is required to assess the impact of this gradient with respect to control rod alignment and internal stresses.

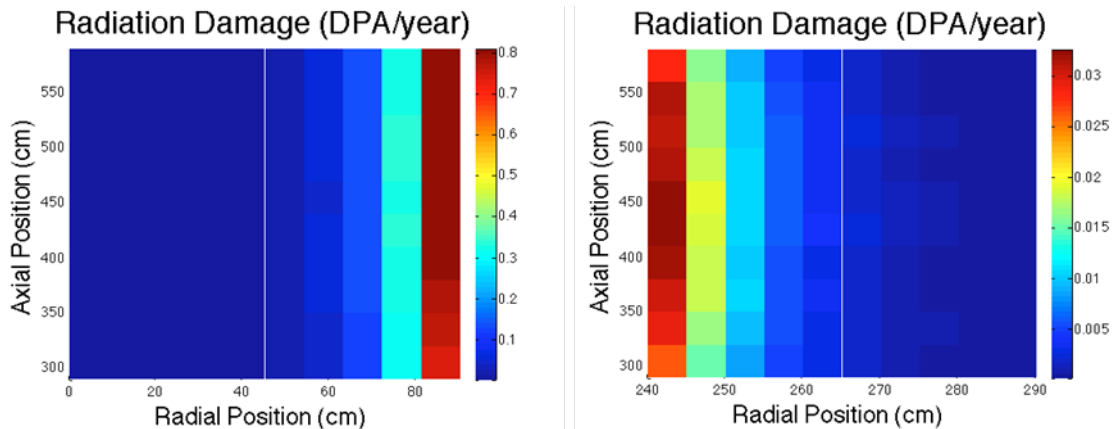


**Figure 3-8. Rates of dpa for Inner (left) and Outer (right) Graphite Reflectors as a Function of R-Z Position in the Active Region of the 2009 PB-AHTR**

A common design rule is that graphite structures should be able to survive until they accumulate 15 dpa (INL 2010). However, according to experts from ORNL at the workshop, the 15 dpa is too conservative. The nuclear graphite can be used up to 25 dpa. The maximum dpa will likely be one constraint on the power density of a pebble bed annular fuel FHR.

Ideally, the outer graphite reflector would last the life of plant, because the reflector would be so difficult to replace. Therefore, the baseline PB-AHTR utilizes a graphite pebble reflector to thermalize and attenuate high-energy neutrons before they damage the outer graphite reflector.

The inner graphite reflector must be in a region with sufficient importance to reactivity that when control elements are inserted into the control channels housed in this reflector, sufficient

reactivity worth will maintain subcriticality at cold zero power. This ability results in higher damage rates. However, the inner graphite reflector can be replaced periodically. These replacements will negatively impact the capacity factor of the plant, so they must be minimized by extending the replacement period.

The maximum dpa rates at the graphite reflector-pebble bed interface for the inner and outer reflector and time to reach 15 dpa are presented in Table 3-4.

**Table 3-4. Maximum Radiation Damage to the Inner and Outer 2009 PB-AHTR Graphite Reflector in Terms of dpa**

Factor	Inner Reflector	Outer Reflector
Maximum rate, dpa/yr	15.7	$3.31 \times 10^{-2}$
Replacement frequency, EFPY	0.96	453

Fast fluence is another commonly used metric for assessing radiation damage. Correlations for material properties and damage limits are given in terms of fast fluence if they are not given in terms of dpa. Figure 3-9 presents the fast flux profile in the 2009 PB-AHTR inner and outer graphite reflector, and Table 3-5 presents the maximum values of fast flux in the inner and outer reflector.

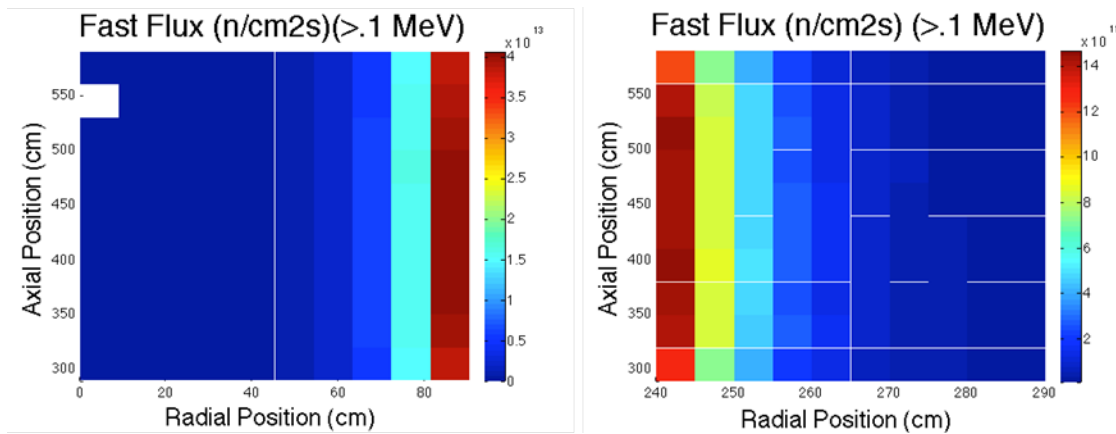


**Figure 3-9. Fast Flux in the Inner (left) and Outer (right) Graphite Reflectors as a Function of R-Z Position in the Active Region of the 2009 PB-AHTR**

**Table 3-5. Maximum Radiation Damage to Inner and Outer 2009 PB-AHTR Graphite Reflectors in Terms of Fast Flux (>0.1 MeV)**

Characteristic	Inner Reflector	Outer Reflector
Maximum fast flux, $n/cm^2 \cdot yr$	$3.85 \times 10^{20}$	$1.12 \times 10^{19}$

In addition, gas formation also causes radiation damage in structural materials. The gas (hydrogen or helium) formed in high-energy reactions can coalesce to form voids and bubbles in the graphite structure, degrading its material properties. Figure 3-10 presents the gas production rates in the 2009 PB-AHTR inner and outer graphite reflectors, and Table 3-6 presents the maximum values of gas production in the inner and outer reflectors.

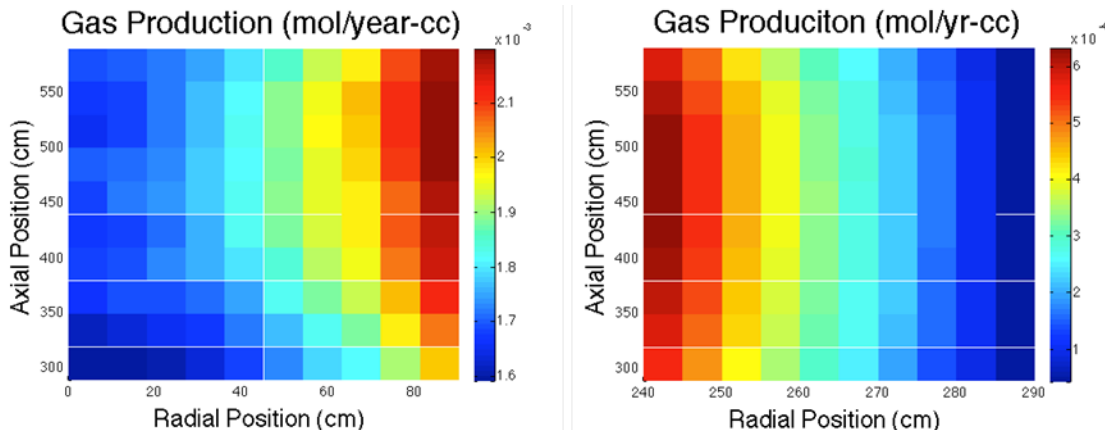


**Figure 3-10. Gas Production Rate in the Inner (left) and Outer (right) Graphite Reflectors as a Function of R-Z Position in the Active Region of the 2009 PB-AHTR**

**Table 3-6. Gas Production in the 2009 PB-AHTR Inner and Outer Graphite Reflector**

Characteristic	Inner Reflector	Outer Reflector
Maximum gas production, mol/yr-cc	$2.20 \times 10^{-3}$	$6.31 \times 10^{-4}$
Average gas production, mol/yr-cc	$1.93 \times 10^{-3}$	$2.98 \times 10^{-4}$

### 3.2 FHR Ceramic Composites

The following subsections summarize the current status of ceramic composites technology, including research and development in composites, composite joining issues, and ASME code qualification, as well as the unique FHR operating conditions that could influence the use of ceramic composites.

#### 3.2.1 Current Status of Ceramic Composites Technology

This subsection provides an overview of the current status of CFRC and SiC/SiC composite technologies, particularly in the United States. The primary goal is to provide references to current NGNP program activities as well as international activities. A second goal is to discuss possible approaches to ASME BPV Code treatment of composite structures.

##### *Research and Development in Composites*

Jean-Pierre Bonal et al. (Bonal et al. 2009) provide a detailed review of ceramic and ceramic composites for high-temperature nuclear power systems. Ceramic composites are being proposed for use as core internals in the next generation of gas-cooled nuclear reactors. The composites

specifically being considered are continuous fiber-reinforced materials of either carbon or silicon carbide fibers infiltrated with a similar matrix. Both materials have undergone significant study and development over the past two decades for fission and fusion energy applications.

The contrast between the two composite types is rooted in the relative maturity of the two systems and their responses to the expected irradiation environment. CFRC composites have a practical advantage over SiC/SiC composites, because they are a more mature commercial product and are available both “off the shelf” and in specialized architectures. Because carbon has self-lubricating characteristics, carbon composites are frequently used to make mechanical carbon bearings in chemical processing equipment (Phelps 2009). However, because of the anisotropic dimensional changes experienced by graphite under irradiation, CFRC composites are far more susceptible to irradiation-induced degradation than SiC/SiC composites (Bonal et al. 2009). An example of anisotropic dimensional change is densification parallel to the fiber axis and swelling perpendicular to the fiber axis in one-dimensional CFRC. Taken to the extreme, irradiation will cause large macroscopic changes to the CFRC composites. The effect of a high neutron dose (10 dpa) is seen to result in large dimensional changes in the fiber tows and a composite that is literally pulling itself apart. But interestingly, up to the point where these CFRC composites become friable, the mechanical properties such as strength and elastic modulus improve significantly (Bonal et al. 2009).

L. L. Snead et al. (Snead, Katoh, and Ozawa 2011) found that a three-dimensional CFRC composite exhibits continuous strengthening over about 32 dpa dose range at 800°C, but this process occurs with measurable loss of mass, increased volume, and for the highest dose studied, a large reduction in elastic modulus. While the balanced weave composite was orthogonally isotropic, a significant anisotropic dimensional change occurred under irradiation. Dimensional change was dominated by fiber dimensional change, and the overall shrinkage or swelling in a direction was determined by the extent to which intrinsic fiber shrinkage was capable of restraining swelling of matrix and fiber bundles.

For most composites now being considered in reactor applications, the neutron doses are low enough that the composite engineering properties of interest (strength, modulus, and fracture toughness) either are unaffected or are improved with irradiation and, for this reason, CFRC composites are primary candidates. However, some critical core components (such as control rod sleeves) have dose levels approaching the 10-dpa level, which likely exceeds the useful life of CFRC composites (Bonal et al. 2009). For the high-neutron-dose applications, SiC/SiC composites have a clear advantage over CFRC composites because of the inherent irradiation stability of the SiC crystal. The cubic SiC crystal undergoes an isotropic dimensional change under irradiation, with the dimensional change saturating at a modest level for the temperature range of interest for high-temperature reactors. Moreover, properties such as hardness, elastic modulus, and strength all undergo only modest changes and saturate at the same rate as the swelling (Bonal et al. 2009; Snead et al. 2007).

SiC/SiC composites can be manufactured by a variety of methods relying on the prefabrication of the preform of SiC fiber reinforcement. Once the SiC fiber preform is completed, the SiC matrix is produced within the reinforcement via chemical vapor infiltration (CVI), melt infiltration or polymer infiltration and pyrolysis (Vollman et al. 2008). Processes that leave residual silicon are not expected to produce SiC/SiC composites that are corrosion resistant

in fluoride salts. The current major manufacturers and brands are UBE Tyranno, Nippon-Carbon's Nicalon™ and Hi-Nicalon™ ranges, and Dow-Corning's Sylramic™ fiber. These fibers can be formed by a CVD process or derived from polymers using complex curing and pyrolysis steps to produce the desired properties. The production of the stoichiometric Nicalon Type S and Tyranno SA fibers has significantly improved the as-irradiated performance of composites (Katoh, Wilson, and Forsberg 2007).

Extensive research has been conducted at ORNL into the effects of neutron irradiation on Hi-Nicalon™, Hi-Nicalon™ Type S, and Sylramic™ fibers. Sylramic™ was found to be the poorest fiber in terms of radiation swelling and the degradation of mechanical properties following neutron irradiation. It is postulated that a contributory factor to this is that Sylramic™ fiber contains boron, which, under neutron irradiation, transmutes to helium (Vollman et al. 2008).

The ORNL report (Katoh, Wilson, and Forsberg 2007) listed in detail the irradiation effect issues for SiC/SiC composites and their constituents, as shown in Table 3-7 along with the present status of studies and assessments. All the issues are relevant to application of SiC/SiC composites to salt-cooled reactor fuel assembly; some of them are likely linked with the critical feasibility and/or critical design issues. Finally, the synergistic effects of neutron irradiation and chemical environment in salt-cooled reactors are unknown. This issue will also have to be examined.

**Table 3-7. Irradiation Effect Issues for SiC/SiC Composites (Katoh, Wilson, and Forsberg 2007)**

Issue	Status of Assessment
Irradiation effect on strength	<ul style="list-style-type: none"> <li>• No significant strength degradation confirmed up to 12 dpa at 750°C or 5 dpa at 1,100°C.</li> <li>• High-dose (&gt;10 dpa) irradiation effect on intrinsic mechanical properties of high-purity SiC has not been confirmed.</li> <li>• Anticipated structural instability of carbon interphase at high doses may cause issues with mechanical properties.</li> <li>• Constitutive models for mechanical properties of irradiated SiC/SiC composites are being developed.</li> </ul>
Thermal conductivity degradation	<ul style="list-style-type: none"> <li>• Fairly comprehensive experimental data for intrinsic thermal conductivity of irradiated high purity SiC have been published and/or are available for low doses (&lt;10 dpa) at 200°C to 1,500°C.</li> <li>• High-dose (&gt;10 dpa) data are not available.</li> <li>• Constitutive models for thermal conductivity of irradiated SiC/SiC are being developed.</li> <li>• Origin of thermal conductivity degradation is not exactly known.</li> </ul>
Point-defect swelling	<ul style="list-style-type: none"> <li>• Fairly comprehensive experimental data for irradiated high-purity SiC have been published and/or are available for low doses (&lt;~4 dpa) at 200°C to 1,000°C.</li> <li>• Higher dose data are not available.</li> <li>• Point-defect swelling is anticipated to cause secondary stress and/or deformation when a significant temperature gradient exists.</li> <li>• Source of point-defect swelling is not exactly known.</li> </ul>
Void swelling	<ul style="list-style-type: none"> <li>• High-purity, beta-phase CVD SiC has been confirmed to develop significant void swelling at &gt;1,200°C at &lt;10 dpa.</li> <li>• Fairly comprehensive data are available from neutron and ion irradiation experiments.</li> <li>• Little is known about driving/control mechanisms, effect of microstructures, high-dose phenomena, etc.</li> </ul>
Irradiation creep	<ul style="list-style-type: none"> <li>• Very little is known about irradiation creep phenomena and mechanisms for high-purity SiC. Steady-state irradiation creep is particularly unknown.</li> <li>• A study on transient irradiation creep in SiC has recently been initiated.</li> </ul>
Irradiation enhanced slow crack growth	<ul style="list-style-type: none"> <li>• Slow crack growth in SiC/SiC composites in oxidative, non-irradiation environment is being studied.</li> <li>• Recent modeling work suggests that fiber irradiation creep may dictate slow crack growth in SiC/SiC composites.</li> </ul>

Research and development on SiC/SiC composite materials and their application technologies is conducted for various nuclear and fusion energy applications, on small to medium scales, in the U.S., among the Generation IV International Forum (GIF) parties, and in the international fusion energy research communities. Table 3-8 lists the ongoing and recently finished programs involving research and development of SiC/SiC technologies for nuclear and fusion applications (Kato, Wilson, and Forsberg 2007). Most of the international partners in the GIF consider SiC/SiC composites to be viable materials for control rod sleeves and IHXs of VHTR and potentially for gas-cooled fast reactors (GFR) and other advanced reactor concepts (Kato, Wilson, and Forsberg 2007). More recently, substantial interest has emerged in the development of SiC/SiC composites for damage-tolerant fuels for LWRs.

**Table 3-8. Ongoing SiC/SiC Research and Development Activities for Nuclear Applications and Their Focuses (Katoh, Wilson, and Forsberg 2007)**

Envisioned System (component)	Country	Lead Contacts	Main Focus
VHTR (control rod, etc.)	U.S. (France, etc.)	L. L. Snead (U.S.) C. Colin (France)	<ul style="list-style-type: none"> <li>• Proof-of-principle irradiation</li> <li>• Test standard development</li> </ul>
LMR, VHTR (IHx)	Japan	S. Konishi (Japan)	<ul style="list-style-type: none"> <li>• Liquid metal loop compatibility testing</li> <li>• Production/shaping technology development for compact HX</li> </ul>
GFR (core assembly)	France, Japan	M. Le Flem (France) A. Kohyama (Japan)	<ul style="list-style-type: none"> <li>• Material processing and fundamental properties</li> <li>• Near-net shaping development</li> <li>• Conceptual core design</li> <li>• Irradiation effects</li> </ul>
GFR (fuel matrix)	Japan	T. Hinoki (Japan)	<ul style="list-style-type: none"> <li>• Fundamental technology development for SiC composite-matrix nitride fuel production</li> </ul>
LWR (fuel cladding)	U.S.	H. Feinroth (U.S.)	<ul style="list-style-type: none"> <li>• Feasibility assessment of SiC composite cladding nitride fuel for advanced LWR</li> </ul>
Fusion (blanket)	International	H. Hegeman (European Union) A. Hasegawa (Japan) Y. Katoh (U.S.)	<ul style="list-style-type: none"> <li>• Fundamental aspects of irradiation effects in SiC ceramics and composites, both experimental and theoretical modeling</li> <li>• Evaluation of SiC composites as Pb-Li flow channel insert material</li> </ul>

The natural thermal oxide of SiC is SiO<sub>2</sub>, which tends to form a scale on the SiC surface under highly oxidizing conditions. The oxidization of SiC is strongly promoted by the presence of water vapor in the atmosphere. In atmospheres containing high water vapor content, the protective SiO<sub>2</sub> layer reacts with the H<sub>2</sub>O to form Si(OH)<sub>4</sub>, which is volatile. In these

circumstances, the SiC is not protected, and continued oxidation leads to recession of the substrate (Vollman et al. 2008).

A study (Vollman et al. 2008) by General Atomics concluded that the control rods fabricated from FMI-222 C/C composites could withstand the nearly 1,000°C maximum temperature during normal operation and the 1,500°C maximum conduction cool down (CCD) temperature with an 8-year life. An alternate material choice of SiC/SiC composite could last the full lifetime of the reactor, but this is a longer-term alternative because additional technology development would be required to extend the temperature ceiling for SiC/SiC use above 1,400°C to accommodate the CCD maximum temperature of 1,500°C.

Studies by Katoh et al. (Katoh, Wilson, and Forsberg 2007) recommended, based on the analysis of requirements, composites of a continuous SiC fiber-reinforced, chemically vapor infiltrated SiC matrix (CVI SiC/SiC) as the primary option for further study on AHTR fuel cladding among various industrially available forms of SiC. The study further identified critical feasibility issues for the SiC-based AHTR fuel cladding to be (1) corrosion of SiC in the candidate liquid salts, (2) high-dose neutron radiation effects, (3) static fatigue failure of SiC/SiC, (4) long-term radiation effects including irradiation creep and radiation-enhanced static fatigue, and (5) fabrication technology of hermetic wall and sealing end caps. Considering the results of the issues analysis and the prospects of ongoing SiC research and development in other nuclear programs, participants in the third workshop recommended a path forward in this order of priority: (1) thermodynamic analysis and experimental examination of SiC corrosion in the candidate liquid salts, (2) assessment of long-term mechanical integrity issues using prototypical component sections, and (3) assessment of high-dose radiation effects relevant to the anticipated operating condition.

#### *Joining of SiC Composites*

Katoh et al. (Katoh, Wilson, and Forsberg 2007) provide an overview of the joining of SiC/SiC composites. Self-joining SiC and/or SiC/SiC is among the major near-term technical objectives for nuclear ceramics research and development. Currently, several joining methods, including diffusion bonding (by various approaches), transient eutectic phase (TEP) joining, and selective area CVD, are considered promising for radiation services. The diffusion bonding is typically facilitated by inserting thin metallic foil(s) between the joining surfaces of SiC. Because of the compatibility issues, the metallic foils should be selected from those elements that are corrosion resistant in flibe under neutron irradiation. The TEP joining takes advantage of reduced melting temperature for particular silica-bearing oxide systems (such as yttria-alumina-silica) to develop SiC-based joint material through the solution and re-precipitation process. The nano-powder infiltration and transient eutectoid (NITE) joint belongs to this category, in which the joint material is ideally identical with the matrix material for the NITE SiC/SiC composites.

The selective area CVD is obviously the method that produces the most radiation-resistant joint of SiC. Glass-ceramics joining is studied in the European Extremat program, and positive results on low-dose radiation performance have been reported (W. Swank 2011; Katoh et al. 2000). General issues for joining ceramics for nuclear applications include those associated with CTE mismatch, radiation stability and other performances of joint materials and interfaces, and practical applicability of the joining methods limited by requirements of temperature, pressure, and atmosphere for successful joining (Katoh, Wilson, and Forsberg 2007).

### *Selection of Ceramic Composites for the FHR*

Because of outstanding high-temperature performance of ceramic composites, SiC/SiC composites are being considered as the candidate material for control rod housing, and C/C composites are considered for the core barrel in the proposed FHR. Because the normal operating temperature range of the FHR is 600°C to 700°C, the selection of ceramic composites may be not required, and other high-temperature refractory alloys such as molybdenum alloys might be considered alternate materials for control rods. However, molybdenum alloys such as TZM (Mo-0.5Ti-0.1Zr) have radiation embrittlement problems at the FHR operating temperature range, and the weldability and fabricability are not that good (Zinkle et al. 2006; Leonard 2012).

Workshop participants agreed that it is very desirable to use SiC/SiC and C/C composites to make the control rod housing and core barrel, respectively, in the FHTR.

SiC/SiC composites can also be considered for FHR fuel fabrication. The IRP will design a test reactor, and one of the questions is how that test reactor would perform over several decades. One long-term test reactor option would be to test alternative fuels such as fuel-pin-type FHRs with SiC cladding and SiC-matrix coated-particle fuel. Composites can be used for alternative fuel forms that may have long-term economic or other benefits. The IRP has chosen graphite-matrix coated-particle fuels because the fuel exists today—there are no other near-term credible options. However, it is important to acknowledge these long-term options because the development of composites for the above applications is the stepping stone to some of these alternative fuel options. The test reactor could involve a broader possible set of fuels that might be tested over time. Appendix C shows some fuel options for the FHR program.

### *ASTM Code Qualifications*

The present knowledge about the availability and performance of both types of ceramic composites, carbon-fiber and SiC/SiC, provides a confidence that these materials are likely to perform as expected in nuclear reactor environments (Bonal et al. 2009). However, with no precedence for using ceramic composites within a nuclear reactor, standard test procedures by the American Society for Testing and Materials (ASTM) will be established from these mechanical and environmental tests. Close collaborations between the U.S. national laboratories and international collaborators (i.e., France and Japan) are being forged to establish both national and international test standards to be used to qualify ceramic composites for nuclear reactor applications (Windes et al. 2005). A program for composite qualification is currently under way to enable the use of these materials in the proposed NGNP gas-cooled reactor in 2021, according to the current NGNP development schedule (Bonal et al. 2009). The NGNP Composite Program conducts research and development for qualification and testing of the SiC/SiC composites, as the primary option, and C/C composites (Katoh, Wilson, and Forsberg 2007). The program comprises specific tasks for (1) confirmative feasibility issues for SiC/SiC including irradiation effect and fabricability, (2) key technical issues governing the lifetime envelope such as irradiation creep and time-dependent fracture, and (3) support to test standards and design code development in the framework of ASTM International and ASME (Katoh, Wilson, and Forsberg 2007).

### 3.2.2 Unique FHR Operating Conditions

This subsection discusses unique issues for FHR application of composites as structural materials (primarily for the core barrel assembly and for shutdown rod channels). It provides a brief review of expected neutron dose rates and of corrosion by the coolant.

CFRC composites are excellent candidates for FHRs because they have heat resistance, high strength, low thermal expansion, excellent thermal conductivity, and moderate resistance to neutron damage and are compatible with fluoride salts. Specifically, CFRC composites are a candidate material for the core barrel in the preliminary design of the FHTR and the baseline material for the fuel assembly structural material in the AHTR. CFRC composites would make an excellent core barrel because the CTE of CFRC composites matches the CTE of the outer graphite reflector much better than a steel core barrel would.

As discussed in earlier, the power density will be primary factor affecting the reflector graphite lifetime because of the maximum radiation damage limit of the structural graphite. SiC/SiC composites have significantly better resistance to radiation damage. Therefore, in evolutionary designs of FHRs, the central graphite reflector might be replaced with SiC/SiC shutdown channels.

The strategy for qualifying these ceramic composites is to first utilize them for non-safety-related applications in the FHTR to gain experience in a radiation environment, exposed to the fluoride salt. Then, as ASME high-temperature material design codes and experimental irradiation data become available, implement these composites accordingly.

The specific operating environmental conditions with respect to temperatures, pressures, surface-to-volume ratios and radiation damage for the 2009 PB-AHTR are presented below to describe operating conditions typical of FHRs. Figure 3-11 shows the 2009 PB-AHTR with the ceramic composite structures highlighted in red.

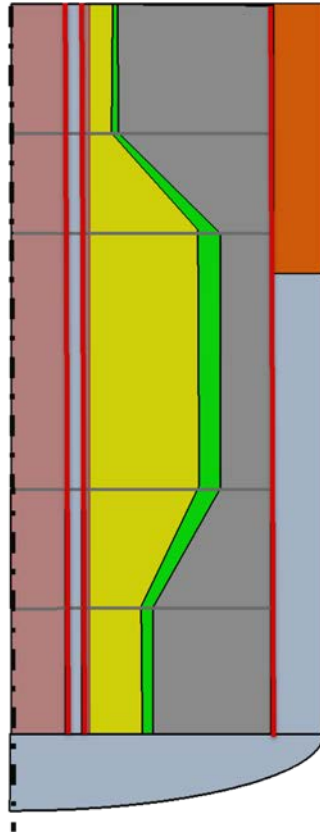


**Figure 3-11. 2009 PB-AHTR Core Geometry with Ceramic Composites Highlighted in Red**

*Temperature and Pressure for Composite Structures*

Composite structures in the 2009 PB-AHTR are directly exposed to the coolant flowing down the downcomer and bypassing the core through the control rod channels. Therefore, degradation mechanisms of the composites are impacted by the temperature and pressure distributions of the coolant at the interface between the coolant and the composites.

The temperature of the coolant flowing down the downcomer is the inlet temperature of the core: 600°C. During a LOFC transient, this temperature slightly rises to reach 631°C at the end of the transient, as shown in Figure 3-12. The thermal hydraulic model used to calculate these parameters is described in detail in Appendix D.

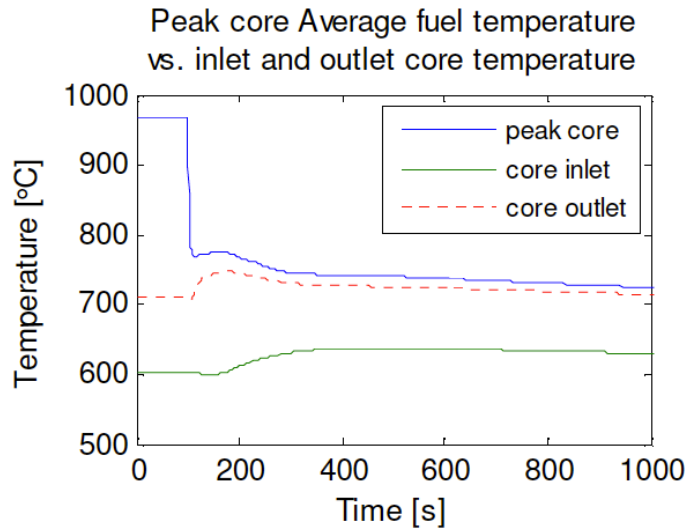


**Figure 3-12. Peak Core Average Fuel Temperature Compared to Inlet and Outlet Core Coolant Temperatures During a 2009 PB-AHTR LOFC Transient**  
(transient initiated at t=100s)

Temperature, pressure, and flow distributions in the control rod channels have not been modeled. However, because the control rod channels are near the surface of the inner graphite reflector, the temperature in these channels is limited by the coolant temperature along the inner reflector, which has a maximum value of 761°C, as seen in Table 3-2.

The variations in pressure along the interface between the coolant and the ceramic composites are negligible (a few tens of kPa). Because of the pool-type configuration of the FHR, all pressures in the system are expected to be close to atmospheric pressure.

#### *Radiation Damage for Composite Structures*

The same radiation damage metrics described earlier for graphite were calculated at UCB for the 2009 PB-AHTR CFRC composite core barrel, located outside the graphite reflector, and the SiC/SiC composite shutdown channel liners. The neutrons that reach the core barrel will have been moderated, reflected, and attenuated by both the graphite pebble reflector and the solid graphite reflector; therefore, there is little radiation damage to the core barrel. Conversely, the SiC/SiC liners are in a high neutron worth region of the core, and as a result they accumulate radiation damage at a high rate. Radiation damage and gas production rates are presented for the core barrel and shutdown channel liners in Table 3-9.

**Table 3-9. Radiation Damage and Gas Production Rates for Ceramic Composites in the 2009 PB-AHTR**

Component	Composite	Radiation Damage Rate, dpa/yr	Radiation Damage Rate, n/cm <sup>2</sup> /yr (>0.1 MeV)	Gas Production, mole/cm <sup>3</sup> yr
Core barrel	CFRC	4.27×10 <sup>-5</sup>	6.27×10 <sup>16</sup>	2.26×10 <sup>-13</sup>
Shutdown channel liner	SiC/SiC	2.38×10 <sup>-1</sup>	3.26×10 <sup>20</sup>	7.36×10 <sup>-8</sup>

The 2009 PB-AHTR design does not implement CFRC for fuel assemblies or the SiC/SiC composite for a central reflector, so the specific radiation damage rates were not calculated. However, the environments for the CFRC fuel assemblies and SiC/SiC central reflector should be similar to their PB-AHTR analogues, the pebble fuel (described in Chapter 2) and the inner graphite reflector (described in Section 3.1).

*Corrosion of Ceramic Composites (C/C and SiC/SiC) in Molten Salt*

Although there is a significant body of work on the behavior of SiC at high temperatures in various environments, the information on the compatibility of SiC in fluoride salts is very limited. Nishimura et al. (Nishimura et al. 2000) studied the performance of silicon carbide in flibe at 550°C. Some “black deposits,” identified as nickel silicide (Ni<sub>31</sub>Si<sub>12</sub>), on the surface of the SiC specimens were observed after exposures for 3 and 10 days. The nickel silicide was postulated as forming from a reaction between nickel and SiC. Such a reaction would give rise to a second reaction product, carbon, and an implied degradation of the SiC (Katoh, Wilson, and Forsberg 2007). As a result of this scarcity of data, the behavior of SiC in liquid fluoride salts can only be inferred from its behavior in other environments. Work needs to be performed to create a good thermodynamic foundation for the evaluation of SiC in liquid fluoride salts with respect to the basicity/acidity of the salt and low partial oxygen pressures expected in reactor systems. Experimental data need to be generated to support the thermodynamic analyses and to shed light on the corrosion effects in systems with varying temperatures (Katoh, Wilson, and Forsberg 2007).

The NGNP program (Vollman et al. 2008) found that adherence to stoichiometry and increased crystallinity improve the thermal stability of the fibers, with grades such as Sylramic™ exhibiting maximum use temperatures of 1,400°C. As mentioned before, a SiO<sub>2</sub> scale tends to form on the SiC surface under highly oxidizing conditions. The work of Gulbransen and Jansson (Gulbransen and Jansson 1972) demonstrated a critical oxygen pressure for the transition from active (formation of SiO<sub>2</sub> and CO with linear oxidation kinetics) at low oxygen potentials to passive (formation of self-healing SiO<sub>2</sub> with parabolic oxidation kinetics) oxidation of SiC. Antill and Warburton (Antill and Warburton 1971) demonstrated that active-to-passive oxidation of beta-SiC occurs below 10<sup>-6</sup> atm at 1,000°C. Katoh et al. (Katoh, Wilson, and Forsberg 2007) concluded that unless the SiC is thermodynamically stable in the liquid fluoride salt, control of the oxygen partial pressure is critical to long-term performance of SiC. Piyush Sabharwall et al. reported (Sabharwall et al. 2010) that in the uncoated C/SiSiC composites, the pure silicon

regions were selectively attacked in both flinak and  $\text{KCl-MgCl}_2$ . Pyrolytic carbon and SiC coating on the C/SiSiC composites was effective in eliminating the selective attack of the silicon phase in the C/SiSiC composite. Peterson et al. (Peterson, Forsberg, and Pickard 2003) reported that UCB thermodynamics calculations indicate that, with proper control of the salt fluorine potential, the rate of dissolution of the silicon may be acceptably low. CVI or CVD coating of the channel surfaces with carbon would result in a negligibly low corrosion rate, as long as the carbon layer remains mechanically intact. Based on the above research results, excess silicon during fabrication of SiC/SiC composites should be avoided for better corrosion performance in molten salt. As mentioned before, the production of the stoichiometric Nicalon Type S and Tyranno SA fibers have significantly improved the as-irradiated performance of composites (Katoh, Wilson, and Forsberg 2007). It is anticipated that stoichiometric SiC/SiC composites will have the best overall performance in molten salt corrosion and irradiation.

C/C composites, like graphite, oxidize rapidly at temperatures above  $\sim 600^\circ\text{C}$  in air or any oxidizing atmosphere. As with SiC/SiC, the presence of water severely exacerbates oxidation of C/C. C/C itself is very resistant to chemical corrosion and exhibits enormous high-temperature capability (Vollman et al. 2008). No data with respect to corrosion of C/C composites in a molten salt environment were found. Consequently, such corrosion data are apparently needed to validate lifetime predictions of behavior of C/C composite materials.

Assuming that the requirements for control rod materials are not too dissimilar between VHTRs and AHTRs, no critical issue has been identified associated with the fabrication of control rod components with CVI SiC/SiC. However, in case intrusion of liquid salt inside the control rod sheath is strictly prohibited, hermeticity becomes an issue (Katoh, Wilson, and Forsberg 2007).

In all cases, complex interactions between ceramic and metal components and the salt and any chemistry additions to the salt must be ultimately understood.

### **3.3 In-Service Inspection and Component Testing for Composites**

Workshop participants provided a number of suggestions and comments on in-service inspection options and component testing requirements. The following are the main suggestions and comments related to graphite and ceramic composite components including SiC/SiC and C/C.

#### **3.3.1 In-Service Inspection**

Suggestions for in-service inspection of FHR composites included the following:

- Monitor wear on ceramic/metallic interfaces to determine wear issues and the effects of vibrations.
- Monitor radiation damage. Monitor radiation dose by putting the coupon near graphite. Monitor weight change of the pebble, temperature change, and irradiation through the pebble.
- Monitor the impurities to determine when to replace the salt.

- Monitor dimension change. It is important to determine the position and condition of each component. A hole can be drilled through the graphite reflector wall to monitor thermal stress, dimensional change, and CTE, which would provide information on when the component needs replacing. It might be possible to measure dimensional changes macroscopically on large reactor components over 10 or 15 years. Laser inspection with very high precision can be used to detect cracks in ceramics in control rods.
- Visually observe materials in liquid salt (e.g., using a telescope).
- Measure temperature and flow rate (at different locations) based on the primary system pump.
- Monitor temperature distribution in the core before determining when to monitor salt.
- Monitor and control redox.
- Use coupons to measure vessel/mass change. It would be valuable to stress coupons. Consider the advantages of placing graphite coupons in locations where they can receive the highest dose.
- Monitor fission gases and radioactive contamination.
- Monitor important parameters including temperature, pressure, and level. It is easy to measure bulk temperature of the hot leg at the outlet of the pump and cold leg temperature at the outlet of the IHX with good mixing. Ultrasonic technology may be a good monitoring technique. Put trip signals as close to the core as possible, maybe by the outer reflector. A target flow meter might work in an FHR because the reactor uses a clear fluid. However, “optical access problems” will need to be solved, because if optical access to the top of the core can be obtained, graphite is a black body and good temperature measurements can be taken.
- Monitor geometry at the bottom of the bed for pebble insertion. A periscope can be used to see the bottom of the reactor vessel. A diamond window and precious metal mirror can also be used.
- Monitor fission products including cesium in coolant and noble gases in cover gas to detect broken pebbles or TRISO particles.
- Monitor  $^{10}\text{B}$  for shielding attack.
- Monitor the temperature distribution in the upper-core plenum.
- Consider using an un-fueled pebble as a material sample delivery device. Use non-fuel pebbles as a carrier to test materials. It is possible to discriminate based on weight, but the pebble cannot be forced to travel to a certain place. Flux can be measured by putting an activation material in the pebble.
- Provide flexibility to insert new instruments to test. On the FHTR, consider placing channels near the reflectors for inserting measurement instruments.
- Consider appropriate bonding methods for SiC/SiC composites.

- Use on-line monitoring or batch monitoring of activities. Chromium is the first thing to come off and can be used to indicate change. Neutron Activation Analysis (NAA) can also be helpful. Glow discharge mass spectrometry based on an argon beam can be used. Cyclic voltammetry can be used for on-line monitoring. Voltammetry is the best way to determine what's in the salt (composition).
- Monitor the pebble cooling of the pebble handling machine.
- Determine how to more accurately measure neutron flux. DOE currently has a high-temperature fission chamber program, but it is not intended for long life. Gamma thermometers, perhaps by GE, are also a possibility for flux profiling.
- Determine what accidents must be considered for the FHR design so that the precursors to the accidents can be measured to determine what trips the reactor.
- Emphasize cleaning the salt as well as redox control. If salt is clean, it will not wet the graphite. If the salt is dirty, then it will wet the graphite.
- Develop a map of what measurements must be taken to determine what instrumentation will be needed.
- Conduct surveillance testing for corrosion, irradiation, etc.
- Provide loose part monitoring systems. It is possible to listen for loose objects with a microphone, potentially even to detect loose fuel particles.
- Determine how to measure the temperature of the fuel. The fuel is far from the temperature limit, and it is difficult to add instrumentation to pebbles, but this is an important issue to consider. Determine what fuel temperature limits should be imposed. Time at temperature may be the most important metric.
- Monitor aging degradation of graphite and composites.

### 3.3.2 Component Testing Facility

Suggestions for the component testing facility included the following:

- Test the fuel handling system for the pebble bed reactor and salt-to-air HX.
- Test flow redistribution at the inlet of the annular core.
- Test the filling and emptying of the reactor to determine the best approach to fueling. Is it to insert the graphite balls and progressively fuel balls? Check the feasibility of radial zoning for the outer blanket of the graphite pebbles.
- Develop a way to detect leaks in the primary and intermediate loops.
- Verify approaches before building a commercial reactor. If the first FHR is a test reactor, the component testing facility may turn into a set of lab experiments rather than being a centralized facility. Should efforts focus on the requirements for the test reactor or for a commercial reactor?
- Test flow-induced vibration in the HX. Consider buckling and vibrations for thin parts. Determine whether scaling or full size is needed for experiments.

- Conduct tribology in the FHR environment.
- Determine how the reactor reaches criticality.
- Test the tritium removal system in the component testing facility.
- Determine how to isolate components for maintenance.
- Demonstrate beryllium safety.
- Determine to what extent the test reactor can be used as a component testing facility.
- Consider even flow distribution at the inlet (don't starve certain regions of the inlet of flow).
- Monitor pressure, flow, and temperature within the core.
- Discuss with industry the need for and amount of accuracy necessary in measurements (specification/margin).

## **4 FHR Metallic Structural Materials**

FHRs operate at high temperature using a low-pressure liquid coolant and thus share very close similarities with LMRs in the design of metallic structures, including their reactor vessels, core support structures, primary HXs, primary and intermediate coolant pumps, and DRACS. The design of these structures is complicated by the fact that they operate at sufficiently high temperatures for time-dependent creep deformation to be important. Accurate characterization of this time-dependent deformation requires extensive data that are expensive and time consuming to collect and which are currently available for only a small number of materials.

At the third FHR workshop, experts emphasized that only a single metallic structural material should be used in contact with the FHR coolant salts, to prevent electro-chemical interactions. This advice strongly increases the incentives to use a single material for all metallic structures in a given FHR design, although the use of bi-metallic or tri-metallic tubes in HXs, and/or a clad vessel and internal core support structures, also remains a possible approach. This chapter reviews the current status of candidate materials and input from experts at the workshop on methods for in-service inspection and requirements for component testing.

### **4.1 Current Status of Candidate Metallic Structural Materials for FHRs**

The selection criteria for FHR structural materials were a major focus of the third FHR workshop. Table 4-1 summarizes the key options for FHR structural materials, as discussed further in this section. The structural materials required for FHRs and those that have been studied and developed for NGNP largely overlap (INL 2010). The state of the art in high temperature reactor structural materials and the status of U.S. NGNP development efforts have been summarized in one of several INL white papers reviewing NGNP design and licensing issues (INL, PLN-3202). This NGNP work, and the new capabilities that have been developed under the NGNP program, provide an important foundation for FHR development.

**Table 4-1. FHR Constituents – Structural Materials**

Constituents	Candidates for IRP
<i><b>Metallic Components</b></i>	
Pressure vessels and piping	SS 316, Alloy N, Alloy 800H (clad), Alloy 617 (clad)
HXs	Alloy N, SS 316, Alloy 800H (clad)
Core internal structures	SS 316, Alloy N, Alloy 800H (clad)
<i><b>Ceramics</b></i>	
Reflectors	Graphite
Core internal structures	Graphite, baked carbon, CFRC, SiC/SiC composites
<i><b>Building Structures</b></i>	
Structures	Steel-concrete composites

The current NRC regulatory and policy statement framework for using metallic structural materials in reactors was established primarily for application to LWR technologies, but many elements are more generally applicable to HTGRs and FHRs as discussed in the NGNP white paper (INL, PLN-3202). A key issue for the design of FHRs and other high-temperature reactors (LMRs and HTGRs) is that key metallic components must operate at temperatures where creep occurs and where time-dependent behavior must therefore be considered. The requirement to consider time-dependent behavior greatly increases the complexity of the component design and requires extensive test data. Under joint work sponsored by the DOE and NRC, substantial progress has been made to develop a new Division 5 for Section III of the ASME BPV Code, which covers rules for the design, fabrication, inspection, and testing of components for use in high-temperature nuclear reactors. This new division makes several significant improvements relevant to FHRs.

For this IRP, the primary, intermediate, and DRACS pressure boundaries, as well as some reactor internal structures, will all be fabricated from the metallic materials listed in Table 4-1, which have existing and extensive property databases and are already included in ASME Section III (except Alloy N, which currently has only ASME Section VIII qualification). This IRP decision to use materials with existing ASME code qualification enables more rapid development of an FHTR and commercial prototype reactor (see Section 3.1).

The candidate materials for FHR metallic structures include Alloy N, 316 SS, Alloy 800H, and Alloy 617. Of these materials, all but Alloy N have been studied for NGNP application. Figure 4-1 presents ASME code-allowable stresses for several of these materials for 100,000 hours of operation at different temperatures.

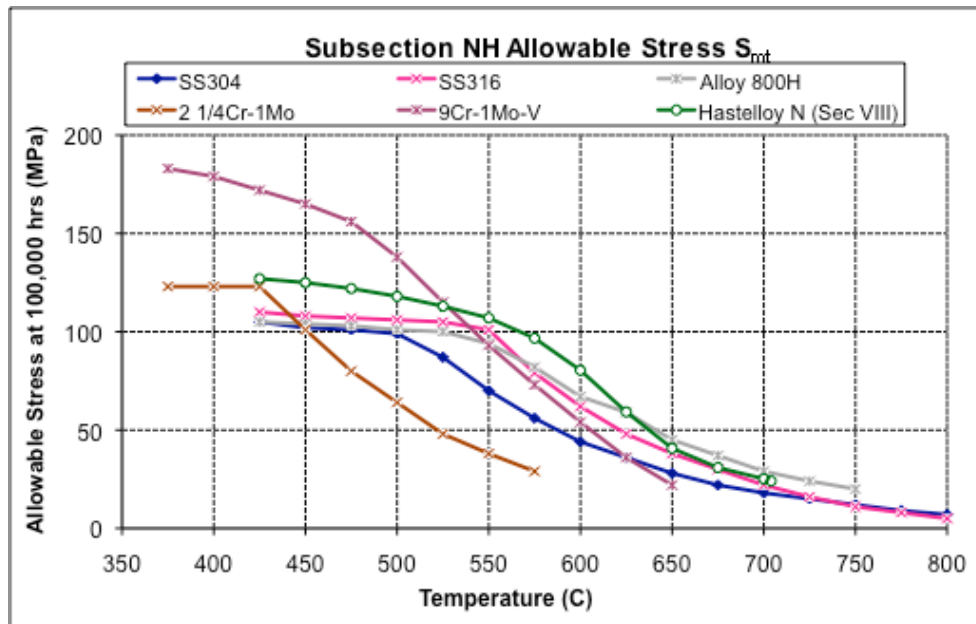


**Figure 4-1. ASME Code-Allowable Stresses for Several Structural Materials**

Alloy N was developed by ORNL specifically for the molten-salt reactor program and is an attractive candidate for FHR use because of its outstanding corrosion resistance with fluoride salts in the temperature range of interest for FHRs (Koger 1972). Extensive experience was gained with Alloy N in the manufacturing of HXs and other salt-loop components; this experiment was documented in a large number of ORNL reports. But Alloy N has relatively poor performance under neutron irradiation. It is a particularly good candidate material for FHR HXs, where its high corrosion resistance allows the use of thinner tube walls, resulting in more compact geometries, and for piping and other components in the intermediate and DRACS loops, which may use salts with higher corrosivity than flibe. Clark and Mizia (Clark and Mizia 2012) reported some preliminary results on the corrosion of diffusion-welded Alloy N in KF-ZrF<sub>4</sub> salt at different temperatures from 650 °C to 850°C.

316 SS is an attractive candidate material for use in FHRs because of its extensive experience for nuclear applications, its good tolerance for neutron irradiation compared to the high nickel superalloys like Alloy N and Alloy 800H, the large number of vendors who are qualified to fabricate nuclear-grade components with 316 SS, and the very well developed ASME Section III code case for high-temperature use. 316 SS has been shown to have excellent corrosion resistance with flibe if beryllium metal is used for controlling the salt fluorine potential (Keiser, DeVan, and Lawrence 1979). 316 SS may be an attractive structural material for FHR reactor vessels, because under power and normal shutdown conditions they will operate at the core inlet temperature. Because corrosion will be driven by solubility, little corrosion would be expected for the reactor vessel because it remains at the coldest temperature in the reactor system, and given the relatively thick cross section of the vessel, solubility-driven corrosion would not be an important degradation mechanism for the reactor vessel anyhow. The good tolerance of 316 SS to neutron irradiation would reduce the required neutron reflector thickness. With a pool design, the reactor vessel is the single most important element of the primary pressure boundary that

prevents LOCAs. In this case, the extensive experience base provided by 316 SS may also be of value, although the operating temperature for use in FHRs will be higher than that in most previous experience.

316 SS is allowed for use at temperatures up to 816°C (1,600°F) in Subsection NH and Code Case N-201-5, which comprise extensions to Subsections NB and NG, respectively. These parts of the ASME code cover Type 316H in terms of high-temperature strength, creep, and creep-fatigue effects up to a design life of 300,000 hours. However, the code does not address other key requirements associated with the design of these components, such as corrosion, thermal aging effects, and neutron embrittlement. Therefore, the qualification of this material will require some further evaluation to address these effects (INL 2010). The specifications, product forms, types, grades, or classes of 316 SS permitted in Subsection NH are listed in Table 4-2 (Natesan et al. 2008).

Other high-temperature alloys, such as Alloy 800H and 617, have favorable properties for high-temperature strength and creep resistance. However, these alloys have significant concentrations of constituents, particularly chromium, that have relatively high solubility in fluoride salts. For this reason, the use of these materials would also require the use of cladding or nickel plating. Cladding or plating may be a viable option for controlling corrosion, but overall fabrication costs will be higher than for materials (e.g., Alloy N and 316 SS) that would not require cladding. Alloy 617 also has 10% to 15% cobalt, which activates under neutron irradiation to produce  $^{60}\text{Co}$ , a strong gamma emitter.

Ren et al. (Ren et al. 2011) recently reviewed the performance of Alloy N for fluoride-salt, high-temperature reactor applications. Alloy N is a reasonably well-proven alloy for structural components that operate at temperatures less than or equal to 704°C in low neutron flux regions. According to researchers from ORNL during the third FHR workshop, Alloy N can tolerate less than or about 1 dpa. It will be problematic if irradiated above 2 or 3 dpa. In high neutron flux regions, high nickel alloys, because of their embrittlement characteristics, do not have acceptable performance, and thus current FHR designs do not employ structural alloys in their cores (Ren et al. 2011). Test results indicated that corrosion attack on Alloy N in molten fluoride salts at temperatures up to 704°C was less than 25  $\mu\text{m}/\text{yr}$  over 2 years. Alloy N also has good oxidation resistance in an air environment and may be used for continuous operations at temperatures up to 982°C.

**Table 4-2. Specifications, Product Forms, Types, Grades, or Classes of 316 SS Permitted in Subsection NH (Natesan et al. 2008)\***

Spec. No.	Product Form	Types, Grades, or Classes
SA-182	Fittings and forgings	F 316, F 316H
SA-213	Seamless tube	TP 316, TP 316H
SA-240	Plate	316, 316H
SA-249	Welded tube	TP 316, TP 316H
SA-312	Welded and seamless pipe	TP 316, TP 316H
SA-358	Welded pipe	316, 316H
SA-376	Seamless pipe	TP 316, TP 316H
SA-403	Fittings	WP 316, WP 316H, WP 316W, WP 316HW
SA-430	Forged and bored pipe	FP 315, FP 316H
SA-479	Bar	316, 316H
SA-965	Forgings	F 316, F316H

\* These materials shall have a minimum specified room temperature yield strength of 207 MPa and a minimum specified carbon content of 0.04%. For temperatures above 540°C, these materials may be used only if the material is heat-treated to a minimum temperature of 1,040°C and quenching in water or rapidly cooling by other means. Appendix X of Subsection NH provides non-mandatory guidelines on additional specification restrictions to improve performance when materials are used in the temperature range of 425°C to 595°C.

Although Alloy N was developed for nuclear applications and extensively investigated for nuclear reactor application during the MSRE program in an 8-MW test reactor at ORNL, it has not been codified into the ASME BPV Code Section III - Rules for Construction of Nuclear Power Plant Components, particularly not into Subsection NH - Class 1 Components in Elevated Temperature Service (Ren et al. 2011). This lack of codification means that the current qualification status of Alloy N does not allow it to be used for design and construction of any commercial nuclear reactors in the United States and Canada. During the workshop, experts agreed that it is important to perform creep tests in the relevant FHR flibe environment because creep can be influenced strongly by the sample's environment. Ren et al. (Ren et al. 2011) concluded that, to qualify an alloy for Subsection NH, certain behavioral features are required for preventing seven structural failure modes:

1. Ductile rupture from short-term loading
2. Creep rupture from long-term loading
3. Creep-fatigue failure

4. Gross distortion from incremental collapse and ratcheting
5. Loss of function from excessive deformation
6. Buckling from short-term loading
7. Creep-buckling from long-term loading.

While the corrosion rate of Alloy N measured during operation of the MSRE was relatively low, the review of Ignatiev and Surenkov (Ignatiev and Surenkov 2012) identified two problems with Alloy N. One is the radiation hardening from accumulation of helium at grain boundaries. Modified alloys with fine carbide precipitates within grains would hold the helium and avoid helium migration to grain boundaries. Reduction of the molybdenum concentration to 12% and the silicon content to 0.1% and the addition of a reactive carbide former such as titanium (about 2%) led to the formation of a fine carbide precipitate and an alloy with good resistance to embrittlement by helium. Ignatiev and Surenkov suggest that it is desirable to design well-blanked reactors in which the exposure of the reactor vessel wall to fast neutron radiation is limited. The second problem observed in the MSRE was tiny cracks on the inside surface of Alloy N piping caused by the fission product tellurium. While FHRs do not have significant concentrations of fission products in their primary coolant, tellurium attack can be controlled by controlling the fuel under reducing conditions, by adjusting the ratio of  $U^{+4}$  to  $U^{+3}$  in the salt (Ignatiev and Surenkov 2012). Ren et al. (Ren et al. 2011) also reported that tensile specimens exposed to the fuel salt and then tested to failure showed shallow surface cracks (150 to 250  $\mu\text{m}$ ) along the gage length at grain boundaries that connected to the salt-exposed surfaces. These cracks were also determined to be a result of the fission product tellurium.

Ignatiev and Surenkov (Ignatiev and Surenkov 2012) reported that 2% titanium addition would impart good resistance to irradiation embrittlement and 0% to 2% niobium addition would impart good resistance to intergranular tellurium embrittlement. Unfortunately, titanium-modified alloys developed so far even in conjunction with niobium were embrittled by tellurium as badly as standard Alloy N. Ren et al. (Ren et al. 2011) reported that modification of Alloy N with approximately 2% niobium significantly reduced the cracking, although it still did not totally prevent cracking (Ignatiev and Surenkov 2012). Ignatiev and Surenkov report that Alloy N modified with 1% to 2% niobium has good resistance to irradiation embrittlement and to intergranular cracking by tellurium. The mechanism of improved cracking resistance from the presence of niobium in the alloy is not known, but it is hypothesized that niobium forms surface reaction layers with the tellurium in preference to its diffusion into the metal along grain boundaries (Ignatiev and Surenkov 2012).

As to the selection of structural alloys for FHRs, because the cracking severity is influenced by the oxidation state of the salt and the salt could be made sufficiently reducing to prevent cracking in standard Alloy N, alloys containing titanium could be used to take advantage of their excellent resistance to irradiation damage if they were protected from cracking by tellurium. Even standard Alloy N could be used in part of the system where the neutron flux was very low (Ignatiev and Surenkov 2012). 316 SS and several other iron-based alloys were observed to resist intergranular embrittlement. It is possible that iron-based alloys can be used in molten salt if it is adequately reducing.

According to the review of Ignatiev and Surenkov (Ignatiev and Surenkov 2012), “the research toward finding a material for constructing [a fluid-fueled molten-salt reactor] that has

adequate resistance to irradiation embrittlement and intergranular grain-boundary cracking (IGC) by tellurium has progressed. ORNL findings suggest very strongly that [a molten-salt reactor] could be constructed of 1–2%-Nb modified Hastelloy N and operated very satisfactorily at 650°C (p 236).” A researcher at ORNL<sup>1</sup> reported that the national laboratory developed a new modified Hastelloy N alloy for molten salt reactors that solved both problems of irradiation embrittlement and IGC by tellurium, and it is anticipated that ORNL will make the alloy public soon.

Morton et al. (Morton et al. 2012) discussed the development and future directions for Section III, Division 5. In the near term, the ASME committees will focus on accommodating stakeholder needs, including corrections to allowable-stress tables, extension of design life to 60 years, and updating the Class B rules. Long-term activities will be stakeholder driven, and anticipated needs include new materials, less conservative and simplified analysis methods, consistent rules and allowable stresses over the full temperature range of operation, and, perhaps, a risk-informed, system-based code.

The ASME code qualification process for Alloy N will be time consuming and costly. Workshop participants suggested that, in addition to DOE, any parties interested should work together and start creating a code case for Alloy N, especially if China is involved.

Metallic structures may need to be shielded to keep neutron fluence negligible ( $\sim 10^{20}$ ) over the structures’ lifetimes to avoid having radiation effects at high temperatures for external materials and associated regulatory problems.

To combine the advantage of 316 SS and Alloy N, the option of using 316 SS or 800H with Alloy N or pure nickel cladding is also possible. This option may be an intermediate solution to avoid the time-consuming ASME code qualification process. Cold spray supersonic impingement of Alloy N or nickel on a base metal may be an option. However, the adhesion/compatibility at high temperatures between cladding and substrate has to be investigated. According S. Sham from ORNL, clad structure cannot take credit for the cladding thickness, and ratcheting, creep, and fatigue need to be considered for clad material.

Experiences of P. Hosemann<sup>2</sup> from UCB highlighted the potential impacts of freezing. His group spent tens of thousand dollars in replacing valves frozen from false positioning in the software, among other factors. He also suggested that loop operations should avoid using flanges in the design, unless where absolutely necessary because it can be very difficult to seal them at higher temperatures.

## **4.2 In-Service Inspection and Components for Metallic Components**

During the workshop, participants provided a number of suggestions and comments on in-service inspection options and component test requirements. The following are the main suggestions and comments related to metallic components. Some of the comments for graphite

---

<sup>11</sup> Private communication with Todd Allen (UW), August 2012.

<sup>12</sup> Communication with Peter Hosemann (UCB), August 2012

and ceramic composite components in Chapter 3 also apply to metallic components and are thus listed here too.

#### 4.2.1 In-Service Inspection

Suggestions for in-service inspection for metallic components included the following:

- Monitor wear on the ceramic/metallic interfaces to determine wear issues and the effects of vibrations.
- Monitor microcracking and pressure change in HXs. Develop a way to remove HXs to pull out coupons for corrosion and radiation monitoring.
- Measure temperature and flow rate (at different locations) based on the primary system pump.
- Monitor temperature distribution in the core before determining when to monitor salt.
- Monitor salt chemistry and control redox.
- Use coupons to measure vessel/mass change. A microphone can be used to listen for loose parts.
- Find a way to measure creep rate. It is unusual to measure creep on-line. Only a long-term rate can be measured. It is probably not practical on the reactor vessel. Normally creep is evaluated with models. For FHRs, focusing on areas where creep is expected would be a problem.
- Develop a general radiation monitoring program to look for radioactive contamination. Monitor fission gases.
- Monitor temperature, pressure, level, and flow. For temperature, the PBMR is going to use fiber optics. It is easy to measure bulk temperature of the hot leg at the outlet of the pump and cold leg temperature at the outlet of the IHX with good mixing. Ultrasonic could be used for monitoring. Put trip signals as close to the core as possible, maybe by the outer reflector. A target flow meter might work in an FHR because the reactor uses a clear fluid. However, “optical access problems” will need to be solved because if optical access to the top of the core can be obtained, graphite is a black body and good temperature measurements can be taken.
- Monitor  $^{10}\text{B}$  for shielding attack.
- Monitor the temperature distribution in the upper-core plenum
- It would be valuable to stress coupons.
- Design the HX to provide access for maintenance
- Conduct on-line monitoring or batch monitoring of activities. Chromium is the first to come off and can indicate changes. NAA is good. Glow discharge mass spectrometry based on an argon beam can be used. Cyclic voltammetry can be used for on-line monitoring. Voltammetry should be the base, which can be supplemented with optical absorption. Voltammetry is the best way to determine what’s in the salt (composition).

- Determine a way to more accurately measure neutron flux. DOE currently has a high-temperature fission chamber program, but it is not intended for long life. Gamma thermometers, perhaps by GE, are also a possibility for flux profiling.
- Determine what accidents must be considered for the FHR design so that the precursors can be measured to determine what trips the reactor. Start with possible accidents, and then determine what kind of measurements are needed to monitor to avoid them.
- Determine what fuel temperature limits should be imposed. Time at temperature may be the important metric. Determine what a spectrometer can't measure and then use appropriate other instruments instead.
- Develop flexibility to insert new instruments to test.
- Determine the power level to trip the reactor. What detection point will allow for a strong signal? What is the unintended reactivity insertion? How should trip limits be set? The peak temperature may be in the metallic structures.
- Design high-temperature HXs so that they are removable.
- Monitor cover gas carefully.
- Develop a map of what measurements must be taken to determine what instrumentation will be needed.
- Develop surveillance testing for corrosion, irradiation, etc.
- Partner with researchers and industry on optical systems to provide measurements in salts, remembering that this approach comes with its own set of issues.
- Monitor aging degradation of the reactor vessel.

#### **4.2.2 Component Testing Facility**

Suggestions for the component testing facility include the following:

- Test the salt-to-air HX.
- Test flow redistribution at the inlet of the annular core.
- Provide a way to detect leaks on primary and intermediate loops.
- Verify approaches before building a commercial reactor. If the first FHR is a test reactor, the component testing facility may turn into a set of lab experiments rather than being a centralized facility. Should efforts focus on the requirements for the test reactor or for a commercial reactor?
- Test HXs, pumps, and valves on a small scale.
- Determine where surrogate salts can be used instead of flibe. Only corrosion tests may need flibe but at a small scale.
- Test flow-induced vibration in the HX. Resonance would be a large problem, while buckling and vibrations are a large engineering concern. Consider buckling and

vibrations for thin parts. Determine whether scaling or full size is needed for experiments.

- Conduct tribology in the FHR environment.
- Test with salt, perhaps not in simulant fluid.
- Determine how the reactor reaches criticality.
- Test the tritium removal system in the component testing facility.
- Determine how to isolate components for maintenance.
- Test beryllium safety in the component testing facility.
- Determine to what extent the test reactor can be used as a CTF.
- Provide flibe for on-line chemistry monitoring.
- Consider even flow distribution at the inlet (don't starve certain regions of the inlet of flow).
- Monitor pressure, flow, and temperature.
- Discuss with industry the need for and amount of accuracy necessary in measurements (specification/margin).
- While the test reactor will be built first, construct the component testing facility to testing critical components, HXs, natural circulation, pumps, and valves. The component testing facility should be able to perform fundamental studies for the test reactor, and in turn the test reactor will validate the commercial reactor.

## 5 Salt Corrosion and Chemistry Control

The intermediate loop of the MSRE operated for over 24,000 hours without any detectable corrosion of structures in the loop. The low corrosion rates of pure salts in the MSRE intermediate loop suggest equally low corrosion rates may be possible for the clean salts in the FHR intermediate and DRACS loops. However, the same cannot be said for the primary system. The FHR primary coolant is clean relative to the MSRE where the uranium was dissolved in the salt, but it can continuously pick up impurities during operations. Neutron irradiation of the lithium creates tritium and thus converts LiF into  ${}^3\text{HF}$ , which is corrosive. Refueling operations with new fuel could add impurities. While new fuel will be cleaned, the heatup and cooldown of the fuel over time may allow impurities in the graphite to diffuse out. Lastly, some leaky fuel is expected over the reactor lifetime. Developing methods to control salt chemistry for these loops, demonstrating through experiments that corrosion rates will be acceptably low, and developing methods to perform on-line monitoring of salt chemistry and in-service inspection of structures is critical to the successful development of FHR technology. This chapter reviews the existing experience base in salt corrosion and chemistry control, new research that may be needed, and FHR-specific issues.

Was and Allen<sup>1</sup> introduced the different salts for nuclear reactors: “Salts are chosen for a specific application based on the optimization of a number of specific properties such as melting point, vapor pressure, density, heat capacity, viscosity, thermal conductivity, and cost ” (Williams, Toth, and Clarno 2006). Delpech and co-workers outlined the uses of a number of salts in nuclear systems (Delpech et al. 2010):

- LiF-BeF<sub>2</sub> (66-33mol%) (flibe) was studied at ORNL for the development of the MSRE and the MSBR and has also been considered as a breeder blanket material for fusion power plants. In recent times, flibe has also been chosen as the primary coolant for FHRs.
- LiF-NaF-KF (46.5-11.5-42 mol%) (flinak) is a candidate for secondary cooling loops for high-temperature gas-cooled reactors.
- LiF-ThF<sub>4</sub>-UF<sub>4</sub> is being studied as a salt for a fast spectrum molten salt reactor by the Centre National de la Recherche Scientifique (National Center for Scientific Research, CNRS) in France

Additionally, three other salts are in current consideration for nuclear system use:

- KCl-MgCl<sub>2</sub> and 58%KF-42%ZrF<sub>4</sub> are both being evaluated as candidates for secondary cooling loops for high-temperature gas-cooled reactors.
- Molten LiCl-KCl is used in electrochemical processes for recycling nuclear fuel (Till, Chang, and Hannum 1997).

---

<sup>1</sup> Was, G. S., and T. R. Allen. “Corrosion Issues in Current and Next Generation Nuclear Reactors,” to be published in *Materials for Advanced Nuclear Systems*, J. Stubbins and I. Robertson, editors, World Scientific Publishing Company.

In the IRP FHR program, flibe salt was selected as the primary coolant, and flinak or 58%KF-42%ZrF<sub>4</sub> was selected as a candidate for the intermediate loop. During the workshop, researchers from ORNL suggested using 58%KF-42%ZrF<sub>4</sub> salt in the intermediate loop because it would be less difficult to separate from flibe if an HX leaks.

## 5.1 Review of Previous Work in Salt Corrosion and Chemistry Control

The following subsections discuss corrosion in molten fluoride salts, the effects of added materials on corrosion, salt purity standards, and the differences between flibe and flinak. Specific bodies of work are discussed in Sections 5.2 and 5.3.

### 5.1.1 Corrosion in Molten Fluoride Salts

Molten fluoride salts corrode structural materials in a number of ways, including general corrosion, impurity-driven corrosion, dissimilar metal- and temperature gradient-driven corrosion, and stress corrosion cracking from fission product exposure.

#### *General Corrosion*

Molten fluoride salts generally corrode structural alloys through dissolution of alloying components, corresponding to the free energy of formation of specific compounds. According to the Gibbs free energy of formation, among major alloying elements such as nickel, iron, and chromium, chromium is one of the most stable fluoride compounds of all alloying constituents of typical high-temperature structural alloys, which makes it the most vulnerable to corrosive attack. These alloys usually require large quantities (15 to 25 at%) of chromium to maintain passivation in oxidizing environments. Studies have shown that the corrosion products in molten salt environments tend to be soluble in the corroding media (Manly 1960; ASM International 2003; Adamson, Crouse, and Manly 1961).

#### *Impurity-Driven Corrosion*

Impurities in the salts are known to cause corrosion issues, where compounds such as HF, FeF<sub>2</sub>, and NiF<sub>2</sub> act as oxidants (Williams and Toth 2005). From an alloy corrosion perspective, such reactions lead to the attack of alloying constituents with fluoride compounds having a more negative Gibbs free energy of formation, ΔG, usually chromium. Such a reaction is



Impurity-driven corrosion generally originates with water. By introducing water into a molten salt, a disassociated fluoride can react with it, producing an oxide or hydroxide and hydrofluoric acid gas, as shown in Equations 5-2 to 5-4. This hydrofluoric acid can then fluorinate metals that are exposed to the molten salt and convert them into metal difluorides. The metal difluorides can then dissolve into the salt, exposing more bare metal. To stop these reactions, all the water, oxides, and hydroxides must be removed from the salt. Water-induced corrosion includes HF generation (Equation 5-3) and corrosion of metal by HF (Equation 5-4). During the workshop V. Ignatiev questioned how much impurity-driven corrosion needs to be characterized before investigating other factors driving corrosion.





where M = Ni, Fe, Cr, etc.

#### *Dissimilar Metal- and Temperature-Gradient-Driven Corrosion*

Was and Allen<sup>1</sup> reported that because the dissolution rate and thermodynamic driving forces of cations depend on local conditions, metallic ions can be transported throughout closed loop systems. This transport can be caused by temperature gradients, where dissolution occurs in a hot leg and deposition in a cold leg of a system. Similarly, corrosion potential gradients can preferentially transport ions from one surface to another (Koger and Litman 1971). An example is the transport of chromium from a steel component through a salt with deposition onto a graphite crucible. This mechanism has been shown to significantly increase the chromium dissolution rate in capsule experiments (Olson et al. 2011) and might have implications for FHR concepts that use metallic containers and graphite structural and moderating materials.

#### *Fission Product-Driven Stress Corrosion Cracking*

In molten salt-cooled reactors that dissolve the fuel into the flowing salt, fission products will accumulate in the salt throughout the fission process. As an example, at high enough concentrations, the tellurium concentration can increase and react with structural steel (Delpech et al. 2010) to form  $Ni_yTe_x$  or  $Cr_xTe_y$ . These compounds form at grain boundaries and are brittle, leading to an intergranular attack (Williams, Toth, and Clarno 2006).

Generally, preventing the movement of chromium becomes the focus of eliminating structural alloy corrosion in molten salt systems. This process is accomplished through limiting the diffusion of chromium out of the alloy or adjusting the reduction/oxidation potential of the salt into a reducing tendency to prevent chromium fluoride compounds from forming.

In the past several years, researchers at UW studied corrosion and corrosion control by redox control of structural alloys in different salt systems including flinak and KCl-MgCl<sub>2</sub> systems. Flinak is a candidate fluorine salt for IHXs; the corrosion mitigation by redox control can also help understand the corrosion mitigation in flibe, which is toxic and more difficult to handle in corrosion testing. Some typical results on corrosion study at UW are reviewed in Section 5.2.

#### **5.1.2 Effect of Additional Materials on Corrosion**

Non-structural materials such as graphite can have an accelerating effect on chromium attack in molten salt systems. In some scenarios, graphite can act as a sink for chrome dissolved into the molten salt. Depending on the surface area of the graphite, the effect can cause severe degradation of chromium.

Table 5-1 lists the testing parameters for two static corrosion tests performed at UW in flinak at 850°C. Alloy 800H when tested in a graphite crucible experienced a weight loss about 100 times greater than an equivalent test performed in an 800H crucible (Figure 5-1). The method by which graphite increases chromium attack is explained in following subsections.

---

<sup>1</sup> Was, G. S., and T. R. Allen, "Corrosion Issues in Current and Next Generation Nuclear Reactors," to be published in *Materials for Advanced Nuclear Systems*, J. Stubbins and I. Robertson, editors, World Scientific Publishing Company.

**Table 5-1. Testing Parameters and Weight Loss for Two Static Corrosion Tests at 850°C**

Alloy	Salt	Crucible Material	Duration, h	Weight Loss, mg/cm <sup>3</sup>
800H	Flinak	Graphite	500	28.6 ± 2.6
800H	Flinak	800H	500	0.15 ± 0.22

**Incoloy-800H (20 at% Cr) in a graphite crucible with FLiNaK\*  
Cross section and EDS chromium depletion map**

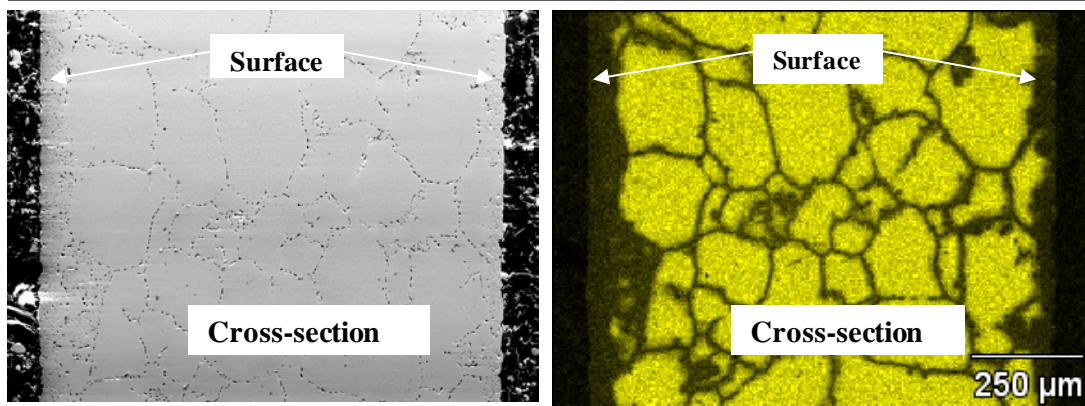


**Figure 5-1. Chromium Depletion Through the Thickness of the 800H Sample Exposed to Flinak at 850°C in a Graphite Crucible**

### 5.1.3 Salt Purity Standards

A commercial FHR must have proper corrosion control to ensure a long operational life. A passive chemistry control system can be implemented by using noble construction materials. Active chemistry control systems can be employed through a chemical treatment process. These processes must eliminate impurities that could corrode infrastructure, absorb neutrons, change the heat transfer characteristics of the salt, or alter the hydrodynamics of the salt. Chemical treatments must also work on a large scale with industrial-grade salts that could contain significant amounts of impurities. Fortunately, a joint batch production and purification process was developed and documented in great detail during the Aircraft Reactor Experiment (ARE) and MSRE (Ozeryanaya 1985; Adhoum et al. 2006; Liu et al. 2011; Liu et al. 2010). Acceptable limits for impurities in a fluoride salt, created by these programs, are shown in Table 5-2. The chemistry control process at ORNL was based on three reversible reactions shown as Equations 5-2, 5-3 and 5-4 (Adhoum et al. 2006).

**Table 5-2. Acceptable Impurity Levels for the MSRE (Adhoum et al. 2006)**

<b>Impurity</b>	<b>Weight Percent</b>	<b>Parts Per Million</b>
Water	0.1	1,000
Cu	0.005	50
Fe	0.01	100
Ni	0.0025	25
S	0.025	250
Cr	0.0025	25
Al	0.015	150
Si	0.01	100
B	0.0005	5
Na	0.05	500
Ca	0.01	100
Mg	0.01	100
K	0.01	100
Li (Natural)	0.005	50
Zr (Natural)	0.025	250
Cd	0.001	10
Rare Earths (Total)	0.001	10

#### **5.1.4 Differences Between Flibe and Flinak**

Because flibe and flinak come from the same family of molten fluoride salts, it is in some ways appropriate to treat flinak as a flibe surrogate because of its ease in handling and production. However, flibe and flinak have some key chemistry differences that can influence corrosion properties, in addition to vastly different neutronic properties. Some of the major differences between the two fluids are outlined by D. F. Williams (Williams and Toth 2005).

Some studies performed during the Aircraft Nuclear Propulsion project to determine the preferred oxidation state of various dissolved alloy constituents found that flinak exhibited a unique preference for M(III) oxidation states, whereas flibe and NaF-ZrF<sub>4</sub> typically preferred M(II), where M = Fe, Cr. Williams suggests that the unique flinak preference could provide for a stronger corrosive driving force because of the variation in preferred cation state [M(II/III)] with temperature (Olson et al. 2009). The preference for a M(III) oxidation state may also contribute to the chromium carbide plating process observed in UW flinak corrosion tests.

## **5.2 Previous Work at UW**

The UW has conducted a number of studies on corrosion and corrosion control. The following subsections provide an overview of static immersion corrosion testing, then delves into additional details on material corrosion and thermal hydraulic studies and work on molten salt/graphite interactions.

### **5.2.1 Static Immersion Corrosion Test Overview**

Static immersion corrosion tests are a common method for quickly and easily establishing a relative baseline alloy effectiveness comparison in a corrosive medium. Opposed to a dynamic (or flowing) corrosion test, static tests are cheaper and can be quickly fabricated and executed because they don't rely on complicated components like pumps or lengthy trace heat, both of which become problematic at high temperatures. A static test typically only needs four basic components: (1) a static test crucible, (2) the corrosive medium, (3) the corrosion target material, and (4) a source of heat. Static corrosion testing has no established standards. Components are designed to simulate the intended application of the corrosive medium and target material. According to the ASTM International Standard Practice for Laboratory Immersion Corrosion Testing of Metal, "Corrosion testing by its very nature precludes complete standardization."

Because of the necessarily small scale of static corrosion tests, some emergent corrosion effects cannot be adequately studied in this form factor; these include galvanic effects created by large material surface area ratios, thermal gradient effects, flow-assisted corrosion effects, and effects dependent on the separation distance between two different materials in the corrosive medium. Nevertheless, the static corrosion tests discussed in the following subsections were designed and carried out with immersion testing suggestions of ASTM International, NACE International, and ASM International in mind.

### **5.2.2 Material Corrosion and Thermal Hydraulic Studies at UW**

The first round of corrosion studies performed at the UW consisted of exposing a breadth of high-temperature alloys to flinak salt at 850°C. Studies found that the extent of corrosion correlated to the chromium content of the alloys, whereby high-chromium-containing alloys experienced higher attack in flinak salt. Pure nickel was shown to resist corrosion the best. Corrosion was also shown to be strongly dependent on material interactions. The studies also examined the impact of two different crucible construction materials (graphite and 800H) on the corrosion of 800H. Under the same testing conditions, area-specific weight loss of the 800H sample exposed to flinak salt was approximately 100 times as great when tested in a graphite crucible than the 800H crucible. Finally, a study compared the corrosion characteristics of flinak

procured through several sources and showed that all sources produced uniform corrosion results (Delpech et al. 2010; Olson et al. 2009).

Complementary work developed and characterized protective nickel-plating techniques for high-chromium alloys. Results showed that the nickel-plating layer reduced the diffusion of vulnerable species (chromium, iron) from the substrate into the flinak bath. However, the plating layer may not be mechanically stable, because void formations were observed (Olson et al. 2011). Thermal hydraulic-forced convection studies have been performed in molten flinak circulation loops dating back to the 1950s through the 1980s. Ambrosek at UW collected a cumulative literature review in 2009 (J. Ambrosek et al. 2009). Of note was the wide discrepancy in measured thermal conductivity of the molten salt, which impacted forced convection experiments taken from literature. Ambrosek recalculated a number of literature heat transfer coefficients using the same thermal conductivities and found the values in agreement with the Dittus-Boetler correlation within 15%.

However, Ambrosek noticed that the literature-based data concerning a nickel-based Inconel alloy varied greatly from data collected using 316 SS tubes. Corrosion product radiation effects may be the source of the discrepancy, whereby alloy-dependent chromium dissolution into the salt may affect the radiative absorption coefficient.

As a part of his dissertation research, Ambrosek constructed a forced-convection molten salt loop. Currently, this loop has only measured chloride salt heat transfer coefficients, but studies in fluoride salts are planned (J. W. Ambrosek 2011). Some work has been started at UW to study how the ultraviolet-visible spectral properties of molten flinak change with corrosion product concentration. Understanding the corrosive properties of molten salts has a far-reaching impact beyond knowing which alloy is best for which purpose. Furthering the understanding of molten salt corrosion will also benefit the study of molten salt heat transfer and physical property measurement.

The most recent corrosion work being performed at UW involves exposing a limited selection of candidate alloys to a larger variety of salts and chemistry conditions. 316L and Alloy N have been tested in 316L stainless steel static systems containing flinak and a metallic redox agent (either zirconium or sodium) plus samples of graphite, with the goal of observing chemical interactions between materials that may be present together in a realistic reactor environment. Metallic redox agents show promising results for 316L stainless steel, where SEM/energy-dispersive X-ray spectroscopy analysis detects less chromium attack when these redox agents are present. However, secondary effects such as plating, interdiffusion, and dealloying must be considered if such a system is to be used at a larger scale.

More static tests are in initial stages of completion, building on the lessons learned in the aforementioned flinak tests. Valuable experience has been gained in how to properly apply redox agents, as well as how to analyze the results and determine the effectiveness. This experience will be applied to future tests performed in flibe with controlled additions of metallic beryllium as a redox agent, including studies of the effects of different methods of beryllium metal redox control on graphite and ceramic composite structural materials. It is important for these corrosion experiments to include graphite, because graphite is an essential structural material for the primary loop.

### 5.2.3 Molten-Salt/Graphite Interaction Overview

The following subsections outline issues associated with molten salt/graphite interactions, including the issues involving the graphite itself, carbide alloying effects, graphite damage through oxidation by zirconium, and graphite damage through alkali intercalation.

#### *Graphite*

Graphite plays an important role in the nuclear industry. FHR and other high-temperature Generation IV reactor designs use nuclear-grade graphite in critical roles where the material is expected to maintain geometry under high neutron flux, high temperature, and challenging chemical conditions (Flanagan, Holcomb, and Cetiner 2012). Additionally, previous work has shown that graphite can have an important influence on the corrosion characteristics of structural alloys in molten salt and can depend very strongly on the methods used to control the salt chemistry. Therefore, it is necessary to understand how graphite will behave when several materials are present in a high-temperature molten salt system, using different methods for chemistry control, to identify potential operational issues in a full-scale molten salt reactor system. The graphite used in all tests for the IRP project is POCO Graphite grade AXF-5Q with flinak molten salt.

#### *Carbide Alloying Effect*

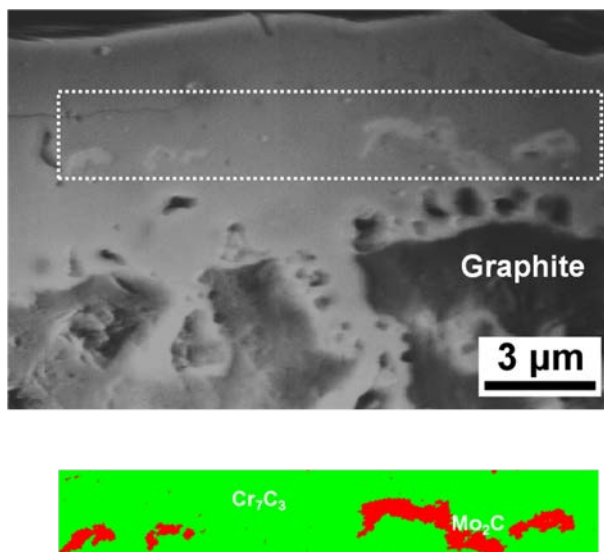
One phenomena pertaining to graphite in systems not containing a redox agent is an electrochemical alloying effect, where the graphite sample will emerge covered in a silver-colored coating. For the 316L samples in contact with these graphite pieces, weight loss and chromium depletion also increase.

Figure 5-2 shows the change in visual characteristics of graphite samples tested with 316L. X-ray diffraction identified the coating on graphite and was found to match with  $\text{Cr}_7\text{C}_3$  carbide. A cross-sectional SEM micrograph of graphite samples (Figure 5-3) shows surface  $\text{Cr}_7\text{C}_3$  formation approximately 10  $\mu\text{m}$  thick.



**Figure 5-2. Typical Graphite Coupon Appearance Before Exposure to Flinak at 850°C for 1,000 hours (left) and After Cleaning Showing the Presence of the Chrome Carbide Coating (right)**

(The length is shorter because a cross section of the sample has been taken)



**Figure 5-3. Cross-Sectional SEM Micrograph of Graphite Coupon Tested with 316L in Flinak at 850°C for 1,000 Hours (top) and Electron Backscatter Diffraction Analysis Phase Distribution Map of the White Dotted Rectangle on the SEM Micrograph (bottom)**  
(Green and red phases represent Cr<sub>7</sub>C<sub>3</sub> and Mo<sub>2</sub>C, respectively)

Additionally, some bright particles could be found in Cr<sub>7</sub>C<sub>3</sub> and can be identified as molybdenum carbide (Mo<sub>2</sub>C). The Cr<sub>7</sub>C<sub>3</sub> and Mo<sub>2</sub>C plating process occurs through the nonelectric transfer of chromium and iron from 316L to electropositive graphite as described by Ozeryanaya (Ozeryanaya 1985). According to Ozeryanaya, electronegative metals would dissolve into the molten salt bath at low oxidation states (i.e., Cr<sup>2+</sup> or Mo<sup>2+</sup>) then undergo simultaneous oxidation and reduction at the surface of the electropositive material, provided an alloy could be formed between the dissolved and electropositive species. An example of the carbiding process is shown in Equation 5-5.



This effect accelerates the dissolution of chromium and iron contained in 316L when graphite is present, which had been reflected on its weight change result. The formation of small amounts of Mo<sub>2</sub>C on graphite implies molybdenum in the 316L sample and crucible would still be corroded by flinak, even though molybdenum is more noble compared to chromium, iron, or nobelium based on the fluoride formation free energy.

#### *Graphite Damage Through Oxidation by Zirconium*

In all systems where graphite was contained in conjunction with an excess of zirconium, the graphite piece was damaged and broken up into several pieces within the salt. This result can be explained by the dissociation of ZrO<sub>2</sub>. The process is as follows:



The graphite sample was initially corroded by HF (Equation 5-6), which was generated by the reaction of water and salt, to form CF<sub>4</sub>. The ZrO<sub>2</sub> crystals growing on the sample would be

corroded by  $\text{CF}_4$  and then generated  $\text{CO}_2$  gas (Equation 5-7) (Devilliers et al. 1983). The porous surface of the coatings on 6-Zr-Gr and N-Zr-Gr samples can also indicate the formation of gaseous  $\text{CO}_2$  released from the dissociation of  $\text{ZrO}_2$ . Another possible reason for reduced  $\text{ZrO}_2$  formation is that the oxygen coming from water contamination was consumed by the formation of  $\text{CO}$  or  $\text{CO}_2$  as a result of the oxidation of the graphite sample.

#### *Graphite Damage Through Alkali Intercalation*

In one study, researchers added 1.5-g metallic sodium as a redox agent to several corrosion crucibles to observe its effect on alloy corrosion. Metallic sodium had an even greater damaging effect on graphite than zirconium. Following the completion of the static corrosion tests containing sodium and graphite, no remaining graphite pieces were visible. Once researchers took crucible cross sections, they discovered small black particles dispersed throughout the salt. Researchers suspect that these black particles represent broken up graphite (Figure 5-4).



**Figure 5-4. Graphite Particle Dispersion Within Frozen Flinak in a Crucible Containing 316L, Graphite, and Metallic Sodium Held for 1,000 Hours at 850°C**

Because of the highly damaging effect of sodium on graphite, researchers felt it is necessary to explore this mechanism further. Examining literature pertaining to this industrial process is a practical way to gain insight in the graphite degradation of the present work because of the shared fluoride salt chemistry and high operational temperature.

To understand the carbon anode degradation mechanics of the Hall–Héroult process, Adhoum et al. electrochemically characterized graphite intercalation in molten  $\text{NaF}$  with metallic sodium addition at 1,025°C (Adhoum et al. 2006). Intercalation is a reversible process where molecules are inserted between layers of other molecular structures. Coincidentally, Adhoum used POCO grade AXF-5Q graphite as his graphite electrode (the exact grade of graphite used in the present work). Through cyclic voltammetry techniques and X-ray diffraction analysis, researchers showed that sodium can successfully intercalate with the graphite electrode to cause interstitial expansion and eventual erosion.

In a similar study, D. Liu showed that a nearly identical process can occur in a system of metallic potassium dissolved in  $\text{KF}$  at 890°C (Liu et al. 2011). Although no metallic potassium

was present in the test systems, potassium reduction is thermodynamically favorable because NaF is slightly more stable than KF. Such a reaction would occur until equilibrium is reached between KF, NaF, sodium, and potassium,



The two processes of alkali intercalation explained by Adhoum and Liu are likely the cause of graphite degradation in the present work conducted for the IRP project. Following eventual detachment of the graphite sample from the mounting rod, the broken up graphite likely floated to the top of the salt pool as a result of density effects, as shown in Figure 5-5.

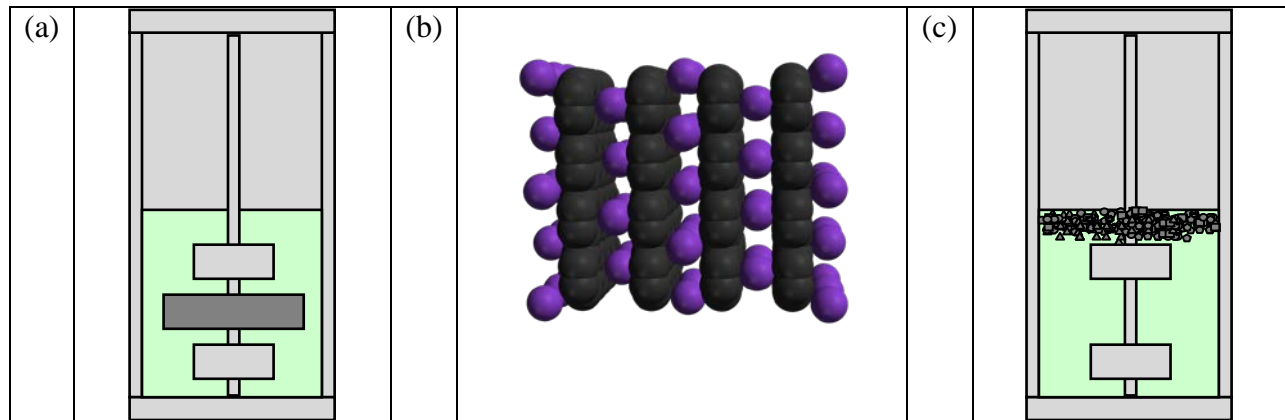


**Figure 5-5. Graphite Intercalation Process by Alkali Metallics in Molten Flinak: (a) Beginning of Corrosion Test, (b) Alkali Uptake Between Layers of Graphene, (c) Complete Graphite Erosion**

An unintended consequence of the erosion process is that graphite undergoes an order of magnitude growth in surface area – akin to using graphite powder in the test instead of a solid graphite piece. Numerous effects in this galvanic system are highly sensitive to the surface areas of individual components, especially the carbide alloying effect described previously. Some results suggest graphite intercalation in a flinak system may have severe consequences for corrosion characteristics of 316L and Alloy N.

### 5.3 Previous MSRE/MSBR Work

Additional work on corrosion and corrosion control was conducted for the MSRE and MSBR. The following subsections discuss efforts related to passive and active corrosion control, MSRE flibe production, and MSRE salt purity analysis.

#### 5.3.1 Passive Corrosive Control

Corrosion reduction techniques generally fall into two categories: passive and active. In passive protection, damage to the molten salt system is prevented through mechanically separating the molten salt from the vulnerable material through the use of noble alloys like pure nickel or nickel coatings. Development of passive nickel coatings for corrosion prevention in flinak at UW are described by Olson (Olson et al. 2009; Olson et al. 2011). However, it is not practical to rely only on a passive system because the general ability and aggressiveness of

molten salts to corrode is preserved and it is generally not possible to construct a practical fluoride salt system from noble metals because of cost or strength restrictions.

### 5.3.2 Active Corrosion Control

Active systems seek to directly influence the reactions that govern the rate of corrosion through the use of molten salt chemistry control systems and corrosion-resistant structural alloys. Numerous active corrosion control systems have been employed with success during the MSRE. The ARE and MSRE saw the creation and fine-tuning of what is now called Alloy N, a Ni-Mo-Cr alloy specially created to resist corrosion in molten fluoride salts (Briggs 1962; McCoy et al. 1970). The alloy relies on a high concentration of nickel and molybdenum, both of which provide excellent resistance to molten salt corrosion (Hurst and Lyon 1960). Scientists also developed and implemented a redox control method based on altering the  $U^{4+}/U^{3+}$  ratio in the MSRE.

Chromium content has been kept low in Alloy N, which has been shown to be beneficial to molten salt corrosion resistance in conjunction with a high nickel matrix (Sohal et al. 2010). However, chromium is kept at a high enough level to preserve hot air oxidation resistance (Haynes International 2012). Corrosion of Alloy N in hot molten fluoride salt exposure has been studied in abundance, with good results indicating little corrosion. Another important active corrosion chemistry control technique developed during the ARE and MSRE projects is batch purification. While making a new batch of salt, specially selected gases were bubbled through the mixture to remove unwanted moisture and metallic impurities. Researchers found that a sparge mixture of hydrofluoric acid (HF) and hydrogen ( $H_2$ ) was optimal in eliminating salt impurities while not inadvertently damaging the salt containment vessel. Following HF/ $H_2$  treatment, impurities in the melt were vaporized out of the mixture, or the precipitates were mechanically filtered (Shaffer 1971; Grimes 1967). More recent studies at an ORNL/Inconel loop (Briggs 1963a) showed that an HF- $H_2$  sparge can reduce the corrosive effects of molten salts (Calderoni et al. 2009). Reducing sulfur concentrations was also important to maintain the integrity of the structural alloys (Briggs 1963b; Shaffer 1971).

In the MSRE, researchers dissolved the uranium fuel in the flibe salt as the  $U^{4+}/U^{3+}$  redox couple, with the desired ratio being 100:1. J. R. Engel (formerly of the ORNL MSRE chemistry control team) discussed how the coolant redox condition became increasingly oxidizing as a result of the imbalance of the fission product valences compared to the uranium valences<sup>1</sup>. Eventually, the  $U^{4+}/U^{3+}$  ratio would exceed 100:1, and then beryllium rods in the alloy cages were lowered into the pump-bowl via the sampler/enricher for up to hours at a time. This approach reduced some of the  $U^{4+}$  back to  $U^{3+}$  and returned the ratio of  $U^{4+}/U^{3+}$  back to 100:1.

Like the FHR primary loop, the MSRE secondary loop consisted of clean flibe. To keep the salt sufficiently clean, any intrusion of oxygen or water must be kept to a minimum. The MSRE accomplished this via a pure helium overpressure of 5 psi.

---

<sup>1</sup> Personal communication between J. R. Engel and C. F. Forsberg, August 2012.

### 5.3.3 MSRE Flibe Production

With no commercial source of flibe, all the salt at ORNL had to be produced onsite. Between the MSRE and the ARE, 72,000 kg of fluoride salts were produced in batch sizes of about 2 ft<sup>3</sup> from commercially available sources. To fill both the primary and secondary loop of the MSRE, around 200 ft<sup>3</sup> of salt were required. Isotopically pure Li<sub>7</sub>F was obtained from the Y-12 Plant onsite. BeF was procured from a major beryllium manufacturer as an intermediary product to beryllium metal (Adhoum et al. 2006).

To produce and purify flibe, a scientist in a plastic fresh-air suit weighed each constituent and loaded it on a hopper inside of an atmospherically controlled room. The air inside of the room cycled through a filtration system three times per minute. These extreme safety measures ensured that employees would not be exposed to elevated levels of beryllium, which can cause Chronic (CBD) or Acute Beryllium Disease (Briggs 1962). This disease is caused by a hyperactive response by the white blood cells of the body to inhaled beryllium particles, which causes pneumonia-like symptoms, lung cancer, or even death (Hurst and Lyon 1960). The current U. S. Department of Labor Occupational Safety and Health Administration (OSHA) permissible exposure limits for beryllium are 2 µg/m<sup>3</sup> as an 8-hour time-weighted average, 5 µg/m<sup>3</sup> as a ceiling not to be exceeded for more than 30 minutes at a time, and 25 µg/m<sup>3</sup> as a peak exposure never to be exceeded. Section 6.2 discussed beryllium safety in greater detail.

The hopper then transferred salt into a 6-ft-long, 12-inch Iron Pipe Size (IPS), 304L SS preliminary treatment vessel lined with 1/8-inch-thick commercially pure, nickel 200. Next, the salt was melted and then sparged with an Ar-H mixture. The heat and gas sparge worked together to remove water from the salt. This pretreated salt was then moved to the primary chemical reactor, which was of similar construction to the introductory vessel.

The primary chemical reactor, shown in Figure 5-6, was also constructed of a 6-ft-long, 12-inch IPS, 304L SS pipe lined with a 1/8-inch-thick nickel sheet. Located on the lid of the vessel was an elongated nickel 200 tube, which terminated in a flanged loading port, gas outlets, and a nickel 200 transfer line. The nickel transfer line was positioned 1/8 inch from the bottom of the chamber. The nickel transfer line connected to a smaller, 3-ft-long receiving vessel that housed various gas introduction ports. Between the reaction vessel and receiver vessel was a 0.0015-inch sintered nickel filter and a chamber used to sample salt for purity testing.

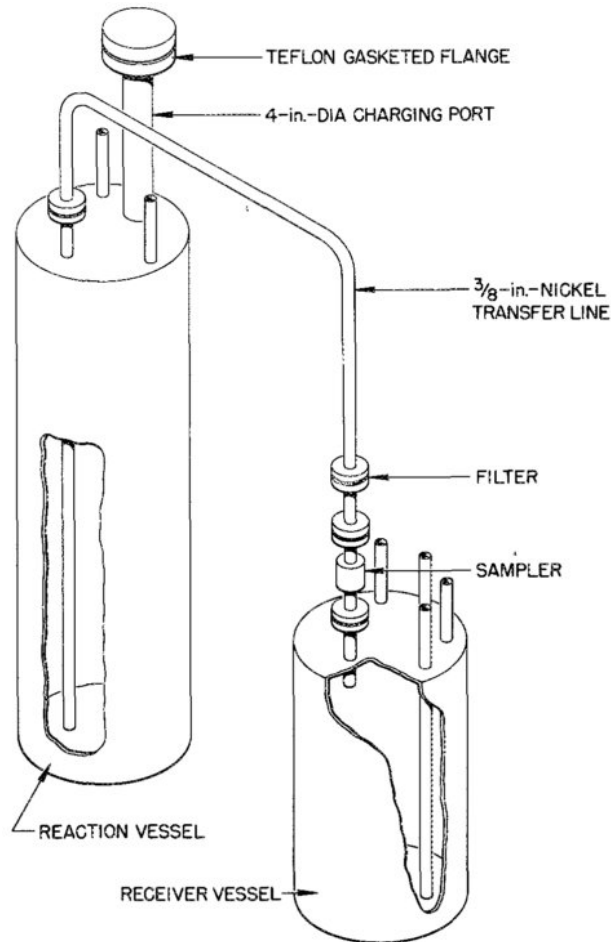


**Figure 5-6. ORNL's Batch Fluoride Salt Primary Chemical Reactor**

A 1:5 ratio by volume mixture of anhydrous hydrofluoric acid and hydrogen gas was then fed into the empty receiving vessel, forced through the nickel transfer line, and sparged into the melted, pretreated salt at 600°C to 750°C (Devilliers et al. 1983; McCoy et al. 1970). This hydrofluorination process caused the reactions shown in Equations 5-1 to 5-3 to reverse. Hydrogen reacted with metal fluorides and caused the metals to precipitate out. Oxides and hydroxides reacted with the hydrofluoric acid to form water vapor. The water immediately vaporized and was removed through a gas outlet along with unreacted hydrofluoric acid and hydrogen gas. By monitoring the hydrofluoric acid and water in the effluent stream, the purity of the salt could be back tracked. Once the hydrofluoric acid inlet and outlet concentration matched, researchers assumed that all of the hydroxides and oxides were removed. At a flow rate of 2.5 L/min, the hydrofluorination step took between 30 and 100 hours. After the hydrofluorination process was complete, a final sparge at 700°C of just hydrogen gas further precipitated any metal difluorides. Additionally, a metal reducing agent such as beryllium or zirconium was added at this time. The hydrogenation process ended once hydrofluoric acid, which was created during the process, was found at a high enough level in the effluent stream.

After the sparging with gas produced the desired results, the next step of the purification process began to remove precipitates by decantation and filtration. First, precipitated metals in

the salt were allowed to settle to the bottom of the reaction chamber. Pressurization of the reaction vessel then pumped the mix to the receiving vessel. During the transfer, the mix flowed through a sintered nickel filter that removed any remaining precipitate. The salt then flowed into a sampler that captured a small amount of the melt for chemical analysis. Once all the purified salt was moved to the receiving vessel, a blanket of dry argon was injected into the container to prevent any contact with air or moisture.

#### **5.3.4 MSRE Salt Purity Analysis**

Determining the concentration of impurities listed in Table 5-2 in raw and purified salt is of great importance in determining if the final product is suitable for use in a reactor. To do this, ORNL used chemical and radiological methods. Beryllium was determined by photoneutrons, chromium by amperometric methods, iron by an o-Phenanthroline titration, water through Karl Fischer titration, and nickel through dimethylglyoxime titration (Hurst and Lyon 1960). Researchers repeated these methods numerous times for each sample, reducing error to 5% for radiological determinations and 15% for chemical methods (J. M. Harp 2012). The methods taken to find other containments have not yet been found in literature. Detailed tables of MSRE salt batches and purities can be found in *Chemical Aspects of MSRE Operations* (Thoma 1971).

### **5.4 New Work Needed for Salt Corrosion and Chemistry Control**

Even with the experience gained by studies at UW and ORNL, new work will be needed in salt corrosion and chemistry control in initial operations and pebble treatment as well as primary and intermediate loop chemistry control.

#### **5.4.1 Initial Operational Concerns and Pebble Treatment**

The FHR concept borrows many ideas from the MSRE, but it also presents unique challenges concerning its solid fuel, secondary loop chemistry, and modernization. Addressing all of these issues is paramount to building an FHR that operates with long-term success.

The first issue that must be investigated is the insertion of pebble fuel into the reactor's core. These pebbles will have been exposed to humid air during manufacturing and will contain water vapor, oxides, and fabrication residues on their surfaces. When inserted into the primary loop, these pebbles could introduce unwanted contaminants that could corrode the structural metal of the FHR. What needs to be determined is how much impurity a pebble can carry, how these impurities can be removed, how much of the residual impurity can dissolve into the salt, and the corrosion potential of these dissolved impurities. If pebble fuel contaminants are found to be of concern over the reactor's lifetime, it will be important to determine how to clean the fuel and primary coolant.

Several options exist for cleaning the fuel. The simplest would be to borrow methods from sodium-cooled reactors. To prepare fuel for sodium work, fuel was pre-dipped into a separate bath of sodium. Similar to sodium reactors, an FHR could bathe its fuel in molten flibe salt before introduction into the primary loop in the reactor. The salt has the potential to absorb oxide, oil, and water through chemical reactions. The salt bathing system could use salt that is on its way to re-purification from the primary loop.

If major contaminants are not found in excess on the fuel, less sophisticated methods could be used for cleaning. A high-temperature bake in an inert atmosphere may remove excess water and oils but would not remove oxide contaminants. That process requires fluorination. After baking, pebbles would need to be kept in a dry, inert atmosphere until being moved into the reactor. If it is found that the water is the main source of concern with the pebbles, and that oxides are less important, this treatment could be viable.

If oxides are found to be a large portion of the impurities introduced into the reactor, chemical treatments might be applicable. Pebbles could be prefluorinated, or pickled, before they went into the reactor with a suitable chemical agent, such as nitrogen trifluoride or hydrogen fluoride. Both of these reactions would have to be done at a high temperature, which would help bake off any water created during the reaction. If these reactions are to be considered, the effect of exposing pyrolytic graphite to these gases needs to be explored. If excessive damage occurs during these treatments, other options will have to be considered.

#### **5.4.2 Primary Loop Chemistry Control**

The MSRE saw success in using a variety of active chemistry control techniques. In addition to relying on a noble structural alloy (Alloy N) and chemical purification systems, the MSRE also depended on a uranium  $U^{+3}/U^{+4}$  redox couple to help control corrosion. The FHR will not be able to take advantage of this approach. Flibe needs to be shown to work in scenarios where a dissolved salt redox couple cannot be used, or a new rare-earth fluoride redox couple needs to be found and made suitable. To answer these questions, more information is needed about solubility limits of redox metals in molten salt.

Previous subsections of this white paper established modes of damage to graphite materials present in a flinak static test system. It is important to stress that damage occurred in chemical environments that are very different from what would be encountered in the FHR. If impurities can be reliably controlled and there is no introduction of abundant extraneous redox materials, graphite damage will be maintained at a minimum.

Another FHR-relevant issue is how to monitor the purity of the salts in real time. The solutions to this problem may have changed over the 50 years since the MSRE. Chemistry control of the primary coolant is only as good as the ability to monitor the coolant in real time at operating conditions. The proposed baseline monitoring system when the FHR is operating would combine NAA with spectroscopy. This system would have a fast response and should be reliable because similar systems are used in other industries.

The neutron flux in the core will activate most but not all impurities in the coolant. The coolant, flibe, has an extremely low activation and thus provides low gamma-ray background radiation levels. Measurement of the energy of the gamma rays should allow detection of most impurities to low levels.

The second on-line instrument could be a spectrometer. The molten salts are transparent over a wide frequency range, and thus a spectrometer can be used to identify many impurities to low levels. Many of the impurities have colorful chemistries that are easy to identify. In the last decade, spectrometers with fiber optic cables have become a standard instrumentation in many chemical plants because of their high sensitivity to impurities in optically transparent fluids.

No detailed coolant monitoring study has been done to determine if impurities of concern could not be measured by these two techniques at the required level of sensitivities. Neutron activation will not work when the reactor is shut down, so other instrumentation or grab samples with laboratory analysis will also be required.

To measure contaminants that are not easily identified through NAA or spectrophotometric methods, other techniques will have to be used. As mentioned before, ORNL had such techniques, many which revolved around wet chemical titrations. These chemical titrations require time and a strong chemical understanding—many are outdated as well. Measurements of metallic constituents could possibly be replaced with inductively coupled plasma mass spectrometry (ICP-MS) or inductively coupled optical emission spectrometry (ICP-OES). Both of these techniques are quick and accurate under the right chemical conditions and do not require a plethora of chemical knowledge or techniques. They do, however, require that the samples be dissolved and suspended in an aqueous solution, something that does not come naturally to most fluoride salts.

Currently, strong mineral acids are used to digest fluoride salts into molecules that can dissolve into water. Less than a gram of fluoride salt is added to a few milliliters of nitric or hydrochloric acid and then digested in a pressure vessel for a few hours at temperatures beyond the acid's boiling point. As of now, the correct temperature, acid, and molar ratios are being determined to cause a complete dissolution of all chemicals in the salt. This approach has proved difficult, as certain acids will allow a chemical equilibrium of partially dissolved salts. For this technique to work flawlessly, the proper conditions for complete dissolution need to be determined.

### **5.4.3 Intermediate Loop Chemistry Control**

Because of the shared fluoride chemical similarities of primary and intermediate loop salts, techniques that are developed for the primary loop can likely be adopted for use with the intermediate loop. Of course, the redox agent will have to be appropriate to whichever secondary molten salt mixture is selected.

Previous work at UW showed that zirconium can have a beneficial effect on the corrosion of 316L; however, the salt chemistry could be affected by the formation of zirconium fluoride. The effect of small quantities of zirconium fluoride dissolved in eutectic flinak has not been studied. Similar to adding beryllium to flibe, the appropriate quantity of zirconium to add must be determined. As observed in UW static tests, if too much zirconium is available, then there will be negative plating and dealloying processes. Also observed in these experiments was the formation of zirconium oxide coatings on metal surfaces; these coatings require further study because they may provide a useful diffusion barrier to tritium if they remain stable over long periods of time. If a zirconium fluoride-based eutectic salt is to be used, metallic zirconium would be a more viable option because the salt will still remain in a binary mixture condition. Researchers at UW are planning to measure redox potential of metallic zirconium in  $\text{KF-ZrF}_4$  salt. This measurement could provide more understanding of the electrochemical property of fluoride salt and could help evaluate the benefits of redox agent to mitigate alloy corrosion.

In addition to the metallic zirconium technique, liquid alkali baths may be a potential corrosion control method. The use of alkali metals for redox control would cause damage to

graphite, but this is not a concern for the intermediate loop because it does not have graphite structures. Such a system may be simple to implement and would be driven by buoyancy effects between the flinak salt and alkali bath mixture. The system could divert a portion of salt from the loop by spraying it into the high-temperature alkali bath, allowing it to settle, and then collecting it from the bottom once a composition gradient is established. A suitable K:Na ratio will need to be found such that flinak chemistry does not change during the cleaning process as a result of undesirable reduction/oxidation reactions.

## 5.5 FHR Coolant Chemistry – Considerations for Failed Fuel and Accident Conditions

In all reactor types, whether LWRs, helium-cooled reactors, sodium-cooled fast reactors, or the FHR discussed here, the coolant redox potential when fuel fails or during an accident determines whether the fuel and fission products will solubilize, precipitate, or volatilize. Determining the ideal redox potential must account for desired normal operating conditions and postulated accident scenarios. This ideal potential may be somewhat of a compromise. A redox potential that minimizes corrosion in the salt during normal operation may not be the best potential during an accident. This section discusses potential possible fission products and additional redox considerations for FHRs.

### 5.5.1 Possible Fission Products of Concern

A number of fission products and inventories are expected for UO<sub>2</sub>-fueled LWRs. Because the FHR is a thermal-spectrum reactor, the FHR fission product distribution inventory is expected to be similar. Radioactive cesium and radioiodine are the two most important fission products to consider in the event of a large release. Nuclides such as <sup>133</sup>Xe and <sup>131</sup>I are released in greater total activities than the nuclides of cesium, but their half-lives are relatively short (<sup>131</sup>I has a half-life of 8 days, and <sup>133</sup>Xe has a half-life of 5 days). Thus, both isotopes will disappear from the environment shortly after their release. The half-life for <sup>134</sup>Cs is 2 years, and the half-life for <sup>137</sup>Cs is 30 years. Consequently, radiocesium will exist in the environment for a number of years, and its dose will be delivered over a longer period of time.

In addition to the nuclides listed in Table 5-3, TRISO fuel experiments in a helium coolant loop in the ATR at INL have shown that several metallic fission products may migrate through failed fuel, and in some cases, intact fuel as well (J. Harp). For intact fuel, silver (<sup>110m</sup>Ag) can be released from intact fuel particles at sufficiently high temperatures. One of the concerns with radioactive silver is that it would condense in cooler parts of the plant, such as HXs. Small fractions of other condensable fission products such as <sup>137</sup>Cs, <sup>134</sup>Cs, <sup>144</sup>Ce, <sup>90</sup>Sr, and <sup>154</sup>Eu were also observed. A summary of potentially troublesome metallic fission products is found in Table 5-4. The relative stabilities of fission product fluorides are discussed in Subsection 5.5.2.

One of the principle concerns is that if the redox potential is too reducing, fission products, particularly cesium, will remain in the metallic state rather than being dissolved in the coolant as a fluoride. Cesium metal is volatile, with a melting point of 28°C and a boiling point of 671°C. If the fission product cesium were to exist in metallic form in the coolant, it would rapidly boil away. In contrast, cesium fluoride is a more stable compound, melting at 682°C and boiling at

1,251°C. A redox potential that promotes the dissolution of key fission products in the coolant is desirable if there are fuel failures or during an accident.

**Table 5-3. Fission Product Inventories for Four Plants (Beahm et al. 1992) Based on the Total Core**

Element, kg	Grand Gulf (BWR), 1,071 MWe	Peach Bottom (BWR), 1,140 MWe	Sequoyah (PWR), 1,160 MWe	Surry (PWR), 839 MWe
I	17.7	16.6	15.2	12.4
Cs	244.8	230.3	184.7	145.7
Te	37.1	34.9	31.7	25.4
Sr	66.7	62.7	60.9	47.6
Ba	112	105	77.7	61.2
Ru	621	584	470	369
Ce	221	208	167	131
La	1,724	2,404	1,313	855
Noble Gases	439	413	347	273

**Table 5-4. Metallic Fission Products Known to Escape from Intact TRISO Fuel Particles in the VHTR (J. Harp)**

Migratory Fission Product Nuclides	Melting Point, °C	Boiling Point, °C
<sup>110m</sup> Ag	962	2163
<sup>144</sup> Ce	798	3442
<sup>134</sup> Cs	28	671
<sup>137</sup> Cs	28	671
<sup>154</sup> Eu	822	1,527
<sup>90</sup> Sr	769	1,382

### 5.5.2 Data and Discussion

In the MSRE, the uranium fuel was dissolved in the flibe salt as the  $U^{4+}/U^{3+}$  redox couple. Researchers made use of beryllium as a reductant in the MSRE to shift the ratio  $U^{4+}:U^{3+}$  to 100:1 and favor a reducing potential (Beneš and Konings 2012). Because of the buffering capacity of the  $U^{4+}/U^{3+}$  redox couple, a steady, reducing environment could be maintained (Williams, Toth,

and Clarno 2006; Beneš and Konings 2012). This approach is not suitable for the FHR, which will operate with a clean coolant without a fission product inventory.

Clean flibe has little or no buffering capacity. Metallic beryllium would need to be immersed in the flibe to maintain a reducing environment. Furthermore, the potential created by beryllium major-metal control would be more reducing than the potential created by the  $U^{4+}/U^{3+}$  redox couple in the MSRE. As discussed below the U(IV)-U(III) couple is less reducing (and their associated fluorides are slightly less stable) than the Be(II)-Be(0) couple. A general rule that indicates whether a material will be noble in a molten salt is that the Gibbs free energy of formation for the salt should be  $>80$  kJ/mol-K (20 kcal/mol-K) less than that of the free energy of formation for the fluoride of the material in question (Ignatiev and Surenkov 2012). Applying this logic to soluble fission products, for example for cesium, the Gibbs free energy of formation for CsF should be at least 80 kJ/mol-K more negative than the free energy of formation for the salt. If the redox scheme used in the FHR is too reducing, then fission products (like cesium) released from damaged fuel will not be soluble.

Another consideration is the solubility of the redox couple in the salt. Fluoride couples for redox control are fully soluble in the coolant, resulting in a uniform redox potential everywhere in the system. A potential drawback to the use of beryllium major-metal for redox control is that the metal has low solubility in flibe. The redox conditions near the beryllium metal may be desirable, but the redox conditions in the coolant away from it may not be desirable. Providing an excess of beryllium metal may also damage the graphite. One option might be to use the Ce(IV)/Ce(III) couple, using beryllium metal to fix the ratio of Ce(IV):Ce(III) (Olander 2002). This approach would be analogous to the use of the  $U^{4+}/U^{3+}$  redox couple in the MSRE.

Table 5-5 shows the standard electrode potentials for a number of redox couples in flibe. Couples with more positive potentials are more likely to acquire electrons and be reduced. These are the oxidants. Couples with more negative potentials are more likely to give up electrons (be oxidized) and act as reductants.

For general interest, Figure 5-7 depicts the relative stability of structural metals nickel, iron, and chromium. This figure illustrates the fact that chromium is the least stable element in nickel-based alloys like Alloy N. The formation free energies of some fluorides are listed in Table 5-6 as a further illustration of relative stability.

Figure 5-8, from Baes (Baes Jr. 1974), gives a rough idea of the relative stability of selected fluorides including the fuel constituents of the MSRE (uranium, plutonium, and thorium), along with key structural elements (nickel, iron, and chromium). This figure also includes alkali metals, such as cesium and rubidium, and alkaline earth metals, such as strontium and beryllium. This figure should be viewed very cautiously, however, because it represents heats of formation ( $\Delta H^f$ ) and not Gibbs free energies of formation ( $\Delta G_{\text{Gibbs}} = \Delta H - T\Delta S$ ). Thus, Figure 5-8 may not be an accurate representation of stabilities, which are more often judged based on the Gibbs free energy of formation.

**Table 5-5. Electrochemical Measurements of Redox Couples in Chlorides and Fluorides, Measured at 496°C (Del Cul, Williams, and Toth 2002)**

Redox Couples	Standard Electrode Potential, V	
	LiCl-KCl at 450°C Reference Couple Cl <sub>2</sub> /Cl <sup>-</sup>	2LiF-BeF <sub>2</sub> (flibe) at 700°C Reference Couple HF/H <sub>2</sub>
Li(I)-Li(0)	-3.62	-2.56
Mg(II)-Mg(0)	-2.88	—
Be(II)-Be(0)	—	-1.765
Zr(IV)-Zr(0)	-2.13	-2.084
Sm(III)-Sm(II)	-2.035	-1.355
Yb(III)-Yb(II)	-1.68	—
U(IV)-U(III)	-1.55	-1.045
V(III)-V(II)	-1.07	—
Eu(III)-Eu(II)	-0.86	—
Cr(II)-Cr(0)	-1.75	-0.39
Fe(II)-Fe(0)	-1.49	-0.011
Mo(III)-Mo(0)	-0.603	0.053
Ni(II)-Ni(0)	-1.17	0.473

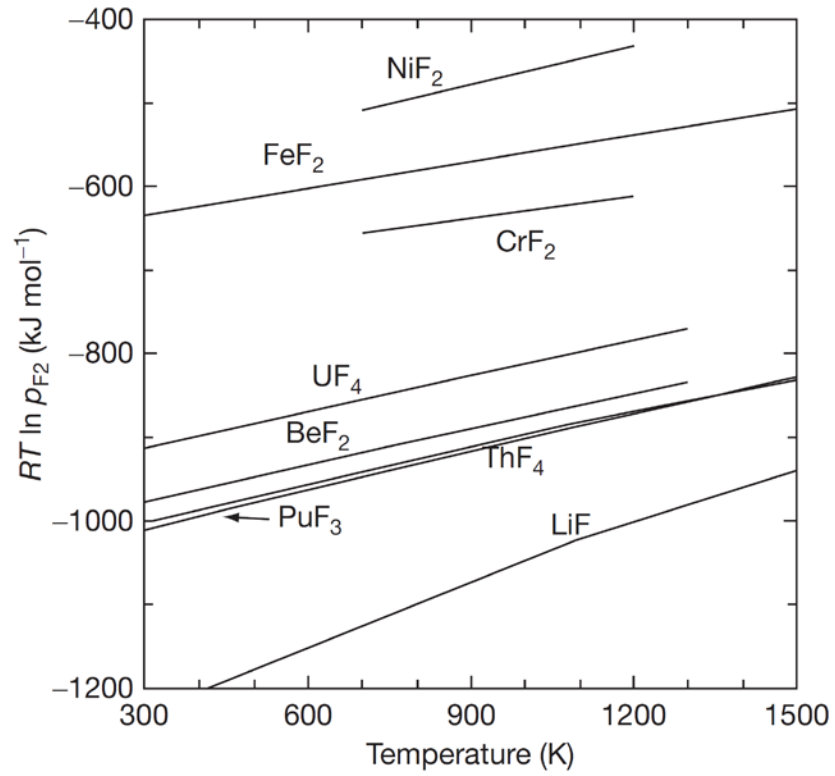


**Figure 5-7. Stability of Selected Metal Fluorides**  
 (More negative indicates increasing stability of the fluoride (Beneš and Konings 2012))

**Table 5-6. Gibbs Free Energy of Formation of Fluorides at 727°C (1,000K) (Keiser, DeVan, and Manning 1977)**

Compound	Gibbs Free Energy of Formation per Gram-Atom of Fluorine	
	kJ	kcal
LiF	-523	-125
BeF <sub>2</sub>	-448	-107
UF <sub>3</sub>	-410	-98
CrF <sub>2</sub>	-314	-75
FeF <sub>2</sub>	-280	-67
HF	-276	-66
NiF <sub>2</sub>	-230	-55
MoF <sub>6</sub>	-209	-50

Because Figure 5-8 is a questionable representation of relative stabilities, and many of the data reported in the literature are for fixed temperatures and do not include fission products, a calculation using the HSC Chemistry software package was performed at MIT. Figure 5-9 shows the results of the calculation as a plot of the Gibbs free energy of formation for various fluorides as a function of temperature. The calculation included the major fission products expected to be mobile in the TRISO fuel. Fission products, such as strontium, barium, and cerium, form sufficiently stable fluorides that they would be expected to be stable in even the most reducing environment. Fission product fluorides such as CsF and EuF<sub>3</sub>, on the other hand, have stabilities very similar to BeF<sub>2</sub>. In fact, above 1,100°C, CsF is less stable than BeF<sub>2</sub>, indicating that accident conditions with coolant temperatures approaching 1,100°C may drive cesium into the volatile reduced state of cesium metal. Europium could present a similar problem over a wider temperature range, owing to the similarity between the Gibbs free energy of formation between BeF<sub>2</sub> and EuF<sub>3</sub>. The MSRE program relied on UF<sub>4</sub> as the principle redox agent. This approach allowed CsF to remain stable up to 1,600°C. This option is not available for the FHR. The data in Figure 5-9 and the general lack of data for clean flibe further illustrate the need for a detailed study of the thermodynamics of the flibe coolant and its possible fission product and impurity constituents at normal and off-normal conditions.

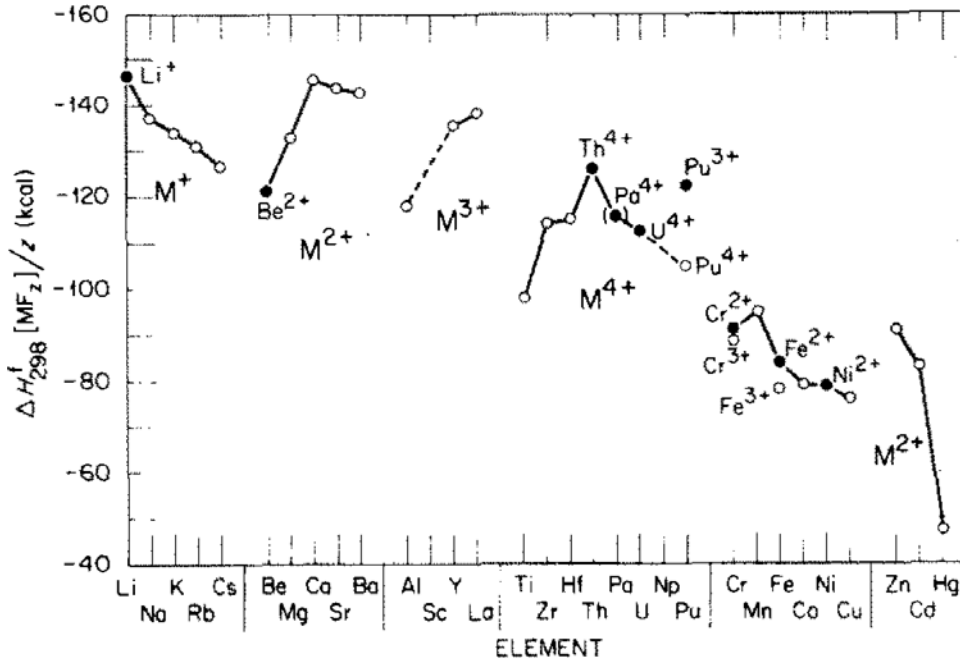


**Figure 5-8. Relative Stability of Fluoride Compounds of the Various Elements, Indicated Approximately by the Heat of Formation per Mole of Fluoride at an Unknown Temperature (Baes Jr. 1974)**

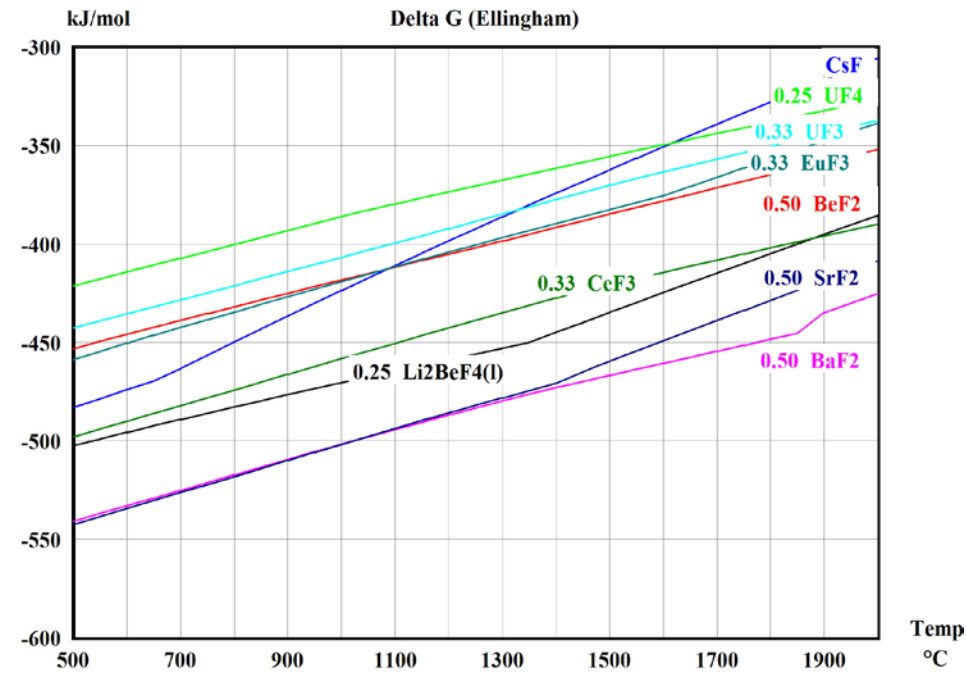


**Figure 5-9. Stability via the Gibbs Free Energy of Formation of Select Fluoride Compounds**

(Fission products europium and cesium may not be stable fluorides at all temperatures using beryllium for redox control. Calculated with HSC Chemistry v.6.0.)

**Table 5-7. Approximate Relative Stability of Fluoride Indicated by the Gibbs Free Energy of Formation (Grimes 1967). These data are for the pure crystalline solid, not for the formation of molten fluorides in molten mixtures.**

Compound	Gibbs Free Energy of Formation at 727°C, kcal/F atom	Melting Point, °C
<i>Structural Metal Fluorides</i>		
CrF <sub>2</sub>	-74.0	1,100
FeF <sub>2</sub>	-66.5	930
NiF <sub>2</sub>	-58.0	1,330
<i>Diluent Fluorides</i>		
CaF <sub>2</sub>	-125	1,330
LiF	-125	848
BaF <sub>2</sub>	-124	1,280
SrF <sub>2</sub>	-123	1,400
CeF <sub>3</sub>	-118	1,430
YF <sub>3</sub>	-113	1,144
MgF <sub>2</sub>	-113	1,270
RbF	-112	792
NaF	-112	995
KF	-109	856
BeF <sub>2</sub>	-104	548
ZrF <sub>4</sub>	-94	903
AlF <sub>3</sub>	-90	1,404
SnF <sub>2</sub>	-62	213
PbF <sub>2</sub>	-62	850
BiF <sub>3</sub>	-50	727
<i>Active Fluorides</i>		
ThF <sub>4</sub>	-101	111
UF <sub>4</sub>	-95.3	1,035
UF <sub>3</sub>	-100.4	1,495

Aside from radiological concerns, a few fission products are also of concern from a materials standpoint. Cesium and rubidium are known to form compounds with graphite at high temperatures (Grimes 1967). Other high-yield fission products with unstable fluorides include molybdenum, niobium, rubidium, technetium, and tellurium. Molybdenum may form carbides and adhere to the graphite moderator (Grimes 1967). Another issue that received a lot of attention during the MSRE project was tellurium embrittlement of Alloy N by intergranular corrosion.(Ignatiev and Surenkov 2012) Fortunately, by keeping a sufficiently reducing potential, such embrittlement can be mitigated (Ignatiev and Surenkov 2012).

## 5.6 In-Service Inspection and Component Testing for Salt Corrosion

During the workshop, experts provided a number of suggestions and comments on in-service inspection options and component testing requirements.

### 5.6.1 In-Service Inspection

Suggestions for in-service inspection for salt corrosion monitoring included the following:

- Conduct on-line impurities monitoring to determine when to replace the salt.
- Use chromium as an indicator for on-line monitoring of activities. If something changes, then more detailed analysis can be performed.
- Use NAA, GD-MS based on an argon beam and cyclic voltammetry for impurities monitoring.
- Consider using the INL-developed on-line salt impurity measurement method. Using a Venturi nozzle to atomize the metal might be a good approach for sampling small melts of salts to directly generate 5- to 10- $\mu\text{m}$  particles. This size particle could be vaporized in an ICP-OES system that is capable of measuring sensitivity to impurities at the parts per million level or better.
- Watch cation concentrations.
- Add removable corrosion coupons and radiation monitoring coupons to the HX. Look at corrosion and neutron irradiation in 1 to 2 years.
- Add the factor of stress on coupons when monitoring corrosion and radiation damage to an alloy.
- Determine where to place the coupons in the test reactor.
- Visually observe materials in liquid salt (e.g., using a telescope).
- Monitor redox. Electrochemical probes in the salt can be used. But implementation of on-line redox potential measurement technique depends on the salt used.
- Consider ways to measure redox. A reliable reversible reference electrode for molten salt doesn't exist, so redox measurement may be a challenge. Zirconium, beryllium, and  $\text{NF}_3$  are possible redox agents. A bubble mixture of  $\text{H}_2$  and HF can be used to measure redox.

- Use multiple methods to monitor salt. Each method should be used for some elements in the sample.
- Consider electrochemistry for monitoring salt. It is cheap and easy and probably practicable.
- Use voltometry to determine the composition of the salt (best method).
- Determine which impurities are able to be measured.
- Monitor  $^{10}\text{B}$  for shielding attack.
- Monitor oxygen, cesium, and fission gases and contamination in released cover gas.
- Develop a way to provide volume control.
- Determine whether an external inventory of salt to inject/extract continuously is needed and allow for chemistry control of part of the inventory continuously if so.
- Emphasize cleaning of the salt as well as redox control. If salt is clean, it will not wet the graphite. If the salt is dirty, then it will wet the graphite.
- Verify what can be detected with a spectrometer.
- Conduct surveillance testing for corrosion, irradiation, etc.

### 5.6.2 Component Test Facility

Suggestions related to corrosion monitoring for the component test facility included the following:

- Test how salt fills and drains from the primary and secondary systems.
- Consider normal and off-normal salt chemistry
- Focus on salt instead of surrogates, but provide centralization.
- Determine which tests can be performed without flibe to reduce component testing facility cost.
- Consider beryllium control and exclusion from large components for testing.
- Determine to what extent the test reactor can be used as a component testing facility. On-line chemistry monitoring needs flibe. It may not end up in the component testing facility.
- Consider whether flinak would be better than flibe as a primary coolant.

## 6 Tritium and Beryllium Control

The use of flibe ( ${}^7\text{Li}_2\text{BeF}_4$ ) as the primary coolant for FHRs brings major advantages, including negative coolant void and temperature reactivity feedback, high fuel utilization, and excellent forced convection and natural circulation heat transport. These major advantages are balanced by two key disadvantages, the need to manage hazards associated with tritium and beryllium. This chapter reviews these hazards and methods to manage them.

### 6.1 FHR Tritium Control

Tritium ( $\text{H}_3$ ) is produced continuously in FHRs from neutron reaction with the primary coolant, and given the radioactive nature of the isotope, the release to the atmosphere and to water must be controlled. Tritium is an emitter of low-energy beta particles and has a half-life of 12.3 years. Its radiation does not readily penetrate skin, but ingesting or inhaling more than the dose limit can increase the risk of cancer<sup>1</sup>. When tritium decays inside the body, the low-energy electron it emits can break bonds in chemical structures in cells. In humans, tritium has a relatively short biological half-life of about 10 days.

Tritium is produced primarily within the primary coolant of FHRs by neutron irradiation. It is produced in significant quantities, higher than in the average PWR<sup>2</sup> but lower than in heavy water reactors like CANDUs. Tritium permeates through high-temperature metals easily. Permeation through pipes within heat exchangers is significant at the operating temperature of the FHRs, which ranges between 600°C to 700°C. Tritium can therefore permeate through the IHX. Tritium is an isotope of hydrogen and can cause embrittlement in metals as it diffuses through. The control of tritium in the FHR will vary significantly from PWRs or CANDUs because of the chemical characteristics of the coolant (water has high solubility for tritium oxides, while flibe has very low solubility), quantities of tritium produced, the unique power conversion system, and the high operating temperatures. The following subsections discuss tritium production, the transport pathways, methods by which tritium permeation could be mitigated, and potential tritium recovery systems.

#### 6.1.1 FHR Tritium Source Term

${}^6\text{Li}$  is a primary contributor to tritium production in the initial operating period of the coolant. At steady state,  ${}^9\text{Be}$  and  ${}^7\text{Li}$  reactions become the most important, with reactions on  ${}^{19}\text{F}$  producing tritium at much lower rates.

The main contributor to tritium production is  ${}^6\text{Li}$  neutron interactions, where the  ${}^6\text{Li}$  comes from the residual  ${}^6\text{Li}$  in the initial enriched lithium, and from neutron reactions with beryllium as discussed below.

---

<sup>1</sup> NRC, “Backgrounder on Tritium, Radiation Protection Limits, and Drinking Water Standards” at <http://www.nrc.gov/reading-rm/doc-collections/fact-sheets/tritium-radiation-fs.html>. Accessed March 22, 2013.

<sup>2</sup> NRC, “Curies of Tritium Released in Liquid Effluents” at <http://www.nrc.gov/reactors/operating/ops-experience/tritium/faqs.html#normal>. Accessed March 22, 2013.



A chemical balance of the above reaction is given in equation (6-2)



During steady-state operation, neutron interactions with  ${}^9\text{Be}$  produces  ${}^6\text{He}$ , which beta decays into  ${}^6\text{Li}$  and can be displayed like this:



Thus, tritium is also continually created from the steady-state production of  ${}^6\text{Li}$ , as shown in Equation 6-1.

During steady-state operation, neutron interactions with  ${}^7\text{Li}$  also produce tritium:



Because  ${}^9\text{Be}$  and  ${}^7\text{Li}$  are major constituents in the primary salt, Equations 6-3 and 6-5 are the dominant reactions that produce tritium during steady-state operation (Figure 6-1).<sup>1</sup>

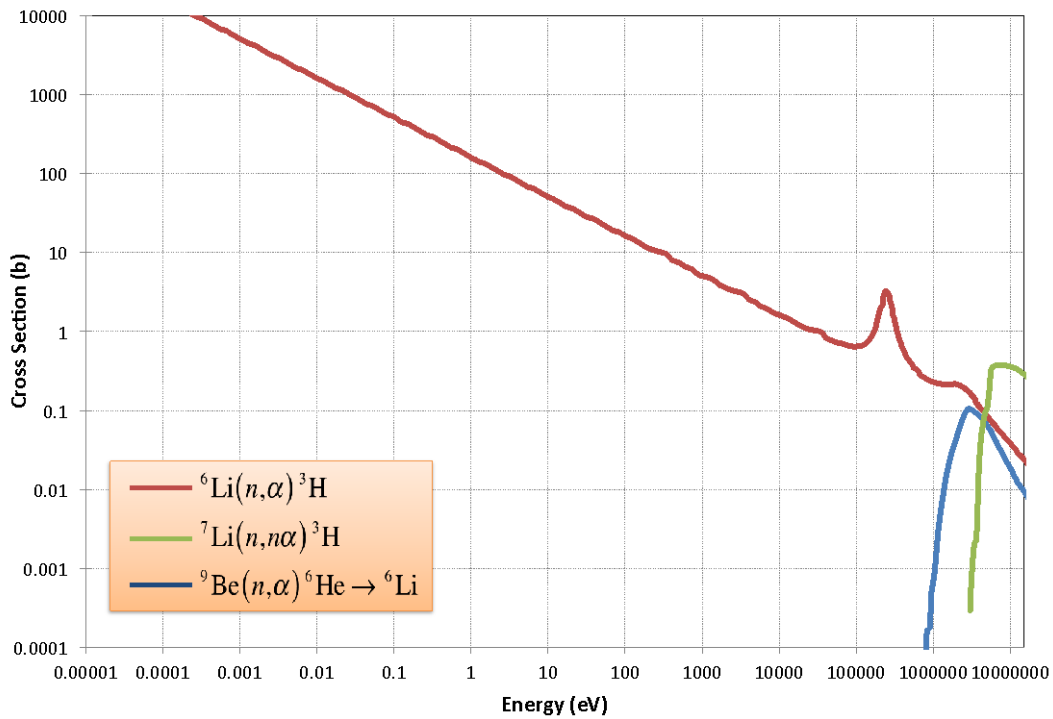


**Figure 6-1. Cross Sections for (n.alpha) Reactions for  ${}^6\text{Li}$ ,  ${}^7\text{Li}$ , and  ${}^9\text{Be}$**

<sup>1</sup> Holcomb, D. E., unpublished paper.

The time it takes the reactor to reach the equilibrium isotopic composition depends on the initial salt inventory as depicted in Figure 6-2. Until steady state is reached, the larger the flibe inventory the higher the tritium emissions will be. With the minimum salt inventory, it takes about 4 years to attain equilibrium isotopic composition of lithium. This should be accounted for when designing the tritium management system.

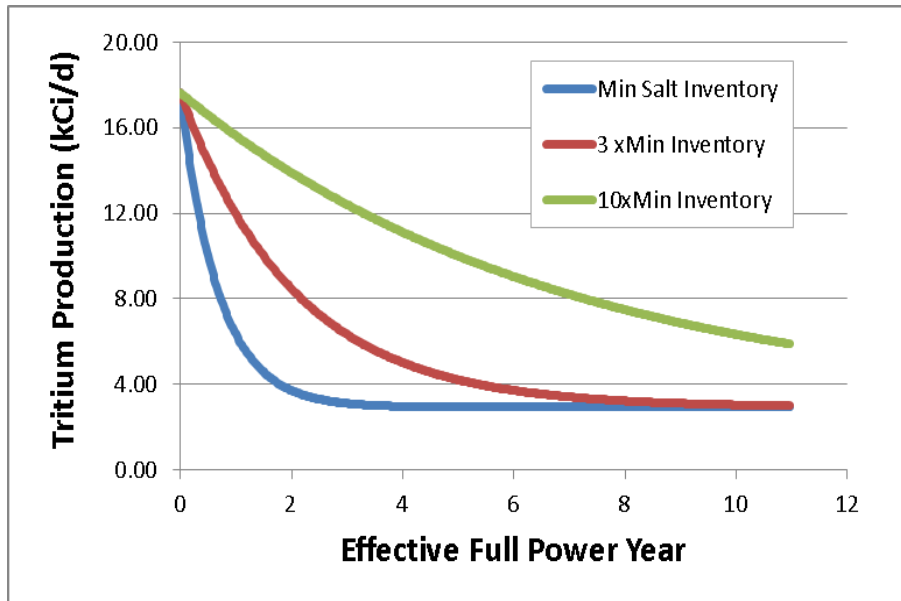


**Figure 6-2. 900 MWth PB-FHR Tritium production rate**

Section 3.1 in the FHR White Paper 4 (‘Preliminary Fluoride Salt-Cooled High Temperature Reactor (FHR) Development Roadmap and Test Reactor Performance Requirements’) gives an overview of current and possible future lithium enrichment capabilities.

### 6.1.2 Comparison of Tritium Production in FHRs to PWRs and CANDUs

Table 6-1 provides a rough comparison of the various tritium production reaction rates during steady-state operation.

**Table 6-1. Equilibrium Tritium Production Rates for Different Types of Reactors**

Reactor	Reactor Power (GWe)	Total Tritium Production (Ci/day)	Relative Tritium Production (Ci/GWe day)
PB-AHTR (Berkeley FHR)	0.410	2508	6119
PWR (average)*	1.000	1.99	1.99
CANDU (Darlington)	3.512	53100	15100
MSR	1.000	2420	2420
PBMR	0.133	1794	13488

\*From NRC website at <http://www.nrc.gov/reactors/operating/ops-experience/tritium/faqs.html#normal>. Accessed March 3, 2013.

Table 6-1 shows that a tritium removal process is necessary if cumulative FHR environmental tritium release values are to be maintained close to PWR releases. It should also be noted that while PWRs release their tritium effluents both into bodies of water (primarily blow-down of water from the spent fuel pool and reactor coolant chemistry and volume control systems) and the air (primarily evaporation of water from the spent fuel pool), FHRs using open air Brayton cycles will release the majority of tritium into the air, likely in the chemical form of hydrogen gas molecules, while FHRs using steam Rankine cycles will release tritium dominantly as a water liquid effluents.

CANDU reactors often have a tritium removal facility onsite. The tritium is produced as a by-product. As an example, the reactor site at Darlington, Ontario has four units, with a total electrical output of 3512 MWe. This site can produce around 19.3 MCi of tritium in a year. The tritium is extracted from the heavy water and stored in steel containers placed within a cement structure onsite. It is stored as tritium gas absorbed on titanium metal. At equilibrium a 410-MWe PB-FHR produces about 2508 Ci of tritium per day, and potentially several times as much during the first few years of operation. This is of the same order of magnitude as the rate of tritium production in CANDUs. This implies that a tritium removal system is absolutely necessary for the FHR.

NRC and EPA establish limits for tritium concentration in water effluents to groundwater, for tritium concentration in air effluent, and maximum worker dose. Table 6-2 summarizes the regulatory limits on tritium concentration in air and water effluents. However, there are no established cumulative tritium release limits that the authors of this document have been able to find. Liquid and gaseous releases of tritium from PWRs result in offsite exposures that are a small fraction of permissible doses, so achieving a release rate comparable to PWRs should be a reasonable target for the design the tritium control system. From a regulatory point of view, the total offsite radioactivity emissions are the only limit for cumulative offsite releases of tritium.

**Table 6-2. United States Regulatory Constraints on Tritium Concentration in Air and Water Effluents**

	Regulation	Annual Radiation Dose		Effluent Concentration			
		(mrem)	(mSv)	Air		Water	
				( $\mu\text{Ci/ml}$ )	(Bq/ml)	( $\mu\text{Ci/ml}$ )	(Bq/ml)
Limit	10 CFR 20.1301(a)1	100	1	-	-	-	-
	Table 2 of Appendix B to 10 CFR 20	50	0.5	$1 \times 10^{-7}$	$3.7 \times 10^{-3}$	$1 \times 10^{-3}$	37
Standard	10 CFR 20.1301(e)	25	0.25	$(5 \times 10^{-8})^a$	$(1.85 \times 10^{-3})^a$	$(5 \times 10^{-4})^a$	$(18.5)^a$
ALARA	Appendix I to 10 CFR 50	15	0.15	$(3 \times 10^{-8})^a$	$(1.11 \times 10^{-3})^a$	-	-
		3	0.03	-	-	$(6 \times 10^{-5})^a$	$(2.22)^a$
Drinking Water	EPA standard	4	0.04	-	-	$2 \times 10^{-5}$	0.74

a. Calculated by assuming the linear relationship between the annual dose of 50 mrem and the values in Table 2 of Appendix B of 10 CFR 20.

ALARA = as low as reasonably achievable  
 CFR = Code of Federal Regulations  
 EPA = U.S. Environmental Protection Agency

In agreement with these assumptions, L. Hu reported on MIT controls for tritium release from their experimental nuclear reactor:

1. There is no regulatory limit on tritium release through air in terms of activity. However, an environmental impact statement will have to justify that such routine releases will not result in radiation dose to workers or the general public exceeding the regulatory dose limit. Note that a dilution factor is typically applied to offsite releases (e.g., through a stack) to account for dilution of such releases, which can range from 1000s to 10,000s.
2. Tritium release through sewage discharge is 5 Ci/year, as specified in 10 CFR 20, Appendix B. Therefore, it is necessary to ensure that whatever is released is significantly less than the concentration limits imposed by the NRC and results in significantly lower offsite doses than the limits imposed by the NRC for routine releases.

### 6.1.3 FHR Tritium Transport

In general, transport processes depend on solubility and diffusivity in the molten salt, dissociation at the surface and diffusion in contacting materials, mass transport, and possibly recombination at gas-melt interfaces (Calderoni et al. 2008). The interaction of hydrogen with flibe is complex because of the structure of ionic liquids with electrochemical processes critical in determining transport properties. The chemical behavior of flibe is determined by the fluorine potential in the molten salt, which is affected by the radiation environment, reactions with contacting materials, and impurities (Calderoni et al. 2008). The chemical behavior of tritium

begins with TF; this species is generated by the reaction of LiF with a neutron (Nishimura et al. 2001). TF then interacts with impurities in the coolant and structural materials, resulting in the creation of HT or T<sub>2</sub> (Suzuki, Terai, and Tanaka 1998a). This change enables tritium to permeate through structural materials, particularly high-temperature metals. The rate-determining process is from HT migration from a flibe surface to a metal surface (Suzuki, Terai, and Tanaka 2000). Thus, the rate of this permeation depends on the structural materials. However, the conversion to HT limits the corrosion caused by TF (Nishimura et al. 2000). Additionally, it is easier to recover tritium from coolant as HT than as TF, because the form of the tritium makes it easier for a sweep gas to be used (Suzuki, Terai, and Tanaka 1998b). The form of tritium in this system depends largely on the concentration of H<sub>2</sub>. As the partial pressure of H<sub>2</sub> in the system increases, the concentration of TF in flibe decreases significantly (Suzuki, Terai, and Tanaka 1998a). With redox control for corrosion, tritium will take the chemical form HT rather than corrosive TF.

At 427°C to 704°C (800°F to 1,300°F), tritium tends to diffuse through the metal walls of the reactor equipment and piping into the surroundings. Measurements of the tritium distribution in the MSRE indicated that about 20% of the tritium escaped from the reactor system in this way (Briggs 1972). In the early 1970s, ORNL also constructed and was testing intermediate loop heat transfer systems in a Molten Salt Coolant Facility (McNeese 1976), where researchers injected hydrogen mixed with small quantities of tritium to study tritium transport in molten-salt reactor intermediate loops.

Tritium has low solubility in the flibe coolant and rapidly diffuses out of the system through metallic materials because of their relatively high hydrogen permeability. This factor means the tritium can be transported into the intermediate loop and then into the power conversion fluid. The permeability highly depends on the material. For example, vanadium and niobium have high permeability, while molybdenum, palladium, and yttrium absorb tritium at high rates (Edao et al. 2010). Accordingly, metallic materials may be coated with barriers to reduce tritium diffusion. Such diffusion barriers can reduce the amount of tritium transported to the power conversion system and other areas of the FHR facility. The largest metallic surface area with which the salt comes into contact is within the heat exchangers. The heat exchangers are also the metallic components exposed to salt at the highest temperature, which is 700°C during normal operation. The reactor vessel comes in contact with the salt at the lowest temperature of the coolant in the system, which is 600°C during normal operation. Any piping that transports salt that is not integral to the reactor vessel will also be metallic but the piping surface area will be insignificant compared to that of the heat exchanger.

Tritium diffusion in liquid is very fast. Fusion scientists at INL put molten lithium in the gap between the double-walled HX, and it absorbed tritium very well. It is necessary to know tritium steady-state partial pressure because it affects production rates and permeation rates. HT is better than HTO. Petti from INL pointed out that using Henry's law, tritium permeation on a nickel system is lower than predicted by Sievert's law. Most of tritium will go through HXs, and a little tritium will go out of the reactor vessel, so a trap is needed. It is possible to design the HX so that tritium can be directed appropriately. Recently, INL has developed and verified simulation methods for tritium transport in VHTRs (Oh and Kim 2009).

### 6.1.4 FHR Tritium Barriers

Metallic and ceramic barriers have been studied to reduce tritium permeation. In addition to reducing permeation of hydrogen, the barriers must survive the same conditions of corrosion, irradiation, mechanical stresses, etc. as the base structural materials. Their effectiveness depends on their subjected irradiation field and their corrosion resistance in the coolant. It is thought that irradiation and corrosion effects will reduce but not eliminate the effectiveness of barriers (Hollenberg et al. 1995). Some of the barriers studied are shown in Table 6-3. These results are primarily for un-irradiated materials. Permeability highly depends on fluence, and barrier quality is greatly reduced if a high dose is received. This problem is not a concern for FHRs, because all metallic structural materials are well-shielded from neutrons.

**Table 6-3. Tritium Permeation Barriers and Their Associated Effectiveness**

Barrier	Base Metal	PRF
Al <sub>2</sub> O <sub>3</sub>	SS316, MANET, TZM, Ni, Hastalloy-X	10 to >10,000
TiC, TiN, TiO <sub>2</sub>	SS316, MANET, TZM, Ti	3 to >10,000
Cr <sub>2</sub> O <sub>3</sub>	SS316	10 to 100
Si	Steels	10
BN	304SS	100
N	Fe	10 to 20
Er <sub>2</sub> O <sub>3</sub>	Steels	40 to 700

Permeability reduction factors (PRF) range from ~3 to 10,000 for un-irradiated materials such as aluminide (Al<sub>2</sub>O<sub>3</sub>) and titanium ceramics (TiN, TiC, TiO<sub>2</sub>), and from 3 to 150 for irradiated samples (Hollenberg et al. 1995; Perujo and Forcey 1995). The PRF is a ratio of the tritium permeation rate without the coating to the rate with a barrier coating. Some of the barriers that have been proposed include gold,  $\beta$ -SiC, ZrO<sub>2</sub>, and Er<sub>2</sub>O<sub>3</sub> (erbia) (Causey et al. 1993). The most effective permeation barriers are ceramics. For example, SiC has a very low tritium diffusivity and solubility, much lower than reported for tritium in metals. Many ceramics are not viable in molten salts because they dissolve in the salt, and many of the base metals themselves are not stable. But, oxide barriers would be effective if they were used on the secondary side of the HX facing steam, carbon dioxide, helium or air (depending on the power cycle). A PRF of 100 can be achieved at 600°C if a Cr<sub>2</sub>O<sub>3</sub> barrier is used (Hollenberg et al. 1995). Another possible barrier with a similar PRF is erbia (Er<sub>2</sub>O<sub>3</sub>), but the amount of research on the effectiveness of this barrier is much less (Chikada et al. 2009). One of the key issues with the permeation barriers is their long-term stability. While they may reduce the permeability for a short period of time, their effectiveness after years of use is not well known. This issue is especially valid for FHRs because of the high temperatures at which the reactor and power cycles operate.

An alternative is to use double-walled tubes in place of the single-walled tubes, particularly for application to steam generators for FHRs using the steam Rankine cycle. Research on double-walled steam generators has been primarily conducted for the use of liquid metal fast breeder reactors to ensure no interactions between the sodium and water. A small space between the tubes allows some gas flow. The Japan Atomic Energy Agency has proposed the use of the tubes in the steam generators of future sodium fast reactors (SFR) (Hayafune 2011). Double-walled tubes have also been examined as tritium permeation barrier systems for use in Li-Pb fusion energy system HXs, eliminating the necessity for an intermediate loop. In such a system, a PRF of  $>10^3$  was calculated, along with an increase of  $\sim 25\%$  surface area (Schluderberg et al. 1983).

Tritium transport and management should be one of the key technology developments in the test reactor. Double-walled HXs (although difficult to manufacture) with sweep flow may help to remove tritium. Based on experiences of D. Petti of INL, an accident scenario will not present different tritium release pathways. Tritium barriers have been studied for 30 years in fusion. While they perform well in a laboratory setting, once they go through heat cycles they could crack and cease working. According to D. Holcomb from ORNL, it would be interesting to develop an alloy that will inherently grow an alumina layer, but no one has been able to do this. Tritium is easier to manage in a closed power conversion system. SiC is a theoretical solution, but practically, it would be difficult to qualify SiC/SiC composites for use in the FHR primary pressure boundary.

### **6.1.5 FHR Tritium Management and Recovery**

FHRs produce about a 1000 times more tritium than PWRs do as liquid effluent, as shown in Table 6-1. Ideally, the PB-FHR would be designed to maintain tritium emissions close to currently operating PWRs. Some options for the tritium recovery system are discussed in this section. A large allowable tritium concentration in the primary loop is desirable because this permits the use of a side stream to remove tritium. To achieve this, tritium barriers with large PRFs are desirable, allowing for a higher allowable concentration of tritium in the primary loop. The tritium barrier would be on the primary side of the IHX or coiled tube air heaters (CTAH). Additionally, a smaller removal system or a bypass flow could be used because the driving concentration is much larger.

A tritium recovery system extracts the tritium from the primary or intermediate coolant. This system would serve the dual purpose of lowering the tritium partial pressure in the primary and intermediate loops and allowing the tritium to be extracted. Extracted tritium could be stored and sold, allowed to decay to  $^3\text{He}$  and sold, or discarded. One of the first steps in such a process would be to contact the primary coolant with a redox agent like beryllium metal or beryllium carbide, so that any hydrogen fluoride (HF or TF) is reduced to hydrogen gas (HT or  $\text{T}_2$ ). It is desirable to minimize the amount of HF in the coolant because, although it is soluble in most fluoride salts, it is extremely corrosive to the piping material. Tritium shows very little solubility in fluoride salts and therefore can generate high tritium partial pressure. This high partial pressure can create a large driving potential for mass transfer through metallic structures such as IHXs and power conversion HXs. It can also result in mass transfer to the cover gas and to any gas that might be sparged into the coolant or contacted with coolant in a stripping column to recover tritium. The approach to tritium recovery will also vary depending on the power

conversion system that is employed, with closed gas Brayton cycles being able to provide effective tritium isolation at higher primary coolant tritium partial pressures than steam and open air cycles.

For FHRs, it is likely that the tritium removal system will be designed as a joint system with chemistry control, because salt chemistry plays an important role in the performance of the tritium removal system, and because both functions would likely be performed on a side-stream of the salt flow.

Many methods have been proposed to isolate and extract the tritium from fluoride salt coolants. The MSRE program at ORNL in the late 1960s implemented a combination of sodium fluoride and sodium fluoroborate as the intermediate coolant (MacPherson 1985). This intermediate coolant had a relatively high solubility for tritium and was able to adequately trap the tritium, which was then separated using a gas purge system.

Another proposed method for tritium recovery involves gas sparging in the intermediate loop. Inert gas is bubbled through the intermediate coolant and strips it of any dissolved gases, hydrogen being the main gas. The MSBR program proposed that helium bubbles could be injected into the primary and intermediate coolants, and then recovered from a side-stream of the salts to allow tritium to be stripped (Perujo and Forcey 1995). ORNL studied bubble generators and separators for this purpose (Rosenthal, Briggs, and Kasten 1969; Rosenthal, Briggs, and Kasten 1970a). ORNL also studied adding hydrogen to dilute the tritium and coating HXs to reduce tritium releases by various ratios. The effort concluded that some combinations of these methods could reduce tritium releases by factors of 10 to 100 or more (Rosenthal, Briggs, and Kasten 1970b). ORNL developed modeling tools for predicting tritium transport in the MSBR (Briggs and Nestor 1975). Subsequently, extensive work by the fusion research community on tritium recovery and control included studies on the generation and transport of tritium from flibe in reactors (Suzuki, Terai, and Tanaka 2000).

Alternatively, the primary salt may be contacted with counter-flowing gas in a spray column or packed column. The tritium can then be separated from the inert gas using conventional techniques. The effectiveness of this method depends on how well the gas bubbles are dispersed into the coolant or how effectively the spray or packed column generates large liquid surface areas, which determines the area available for mass transfer. Experiences from INL showed that sparging is a slow process. A solid getter could also be used to extract the tritium from the fluoride salt, with dissolved tritium being absorbed into the matrix of the getter (Andrews and Forsberg 2012).

Experience from the MSRE showed that a significant amount of tritium was absorbed in the graphite surfaces on the graphite blocks. The PB-FHR could possibly use graphite surfaces to limit the tritium that remains within the coolant. In PB-FHR, the surface area of the graphite pebble fuel is 9800 m<sup>2</sup>, which is one fourth of the surface area of the salt-to-air heat exchangers. The fuel pebbles are continuously recirculated through the PB-FHR core. It is important to understand if the fuel pebbles can represent a sufficiently large absorber of tritium from the core. If so, then fuel recirculation can be an important mechanism of tritium control.

## 6.2 FHR Beryllium Control

Flibe, the baseline primary coolant for FHRs, contains beryllium. Alternative coolants could use enriched zirconium fluoride ( $ZrF_4$ ), at the expense of less desirable neutronic and thermal hydraulic properties, if affordable zirconium enrichment methods were available. This section reviews beryllium control issues for FHRs, including the 2008 UCB Senior Design Project report that included a study of FHR beryllium control (Fei et al. 2008). That project developed the design and configuration of a FHR heating, ventilation, and air conditioning system to facilitate beryllium control and emphasized the need to closely integrate the radiation control program with the beryllium control program.

### 6.2.1 Beryllium Health Effects and Standards

Beryllium and beryllium-containing compounds, including beryllium fluoride, are recognized by the International Agency for Research on Cancer (IARC) as a Group 1 carcinogen, meaning there is sufficient evidence of carcinogenicity in humans (IARC 2012). The toxicity of beryllium and beryllium-containing compounds is also recognized by the United States government in 10 CFR Part 850 Chronic Beryllium Disease Prevention Program (Schepers 1964). Additionally, the potential for beryllium fluoride to cause harm in both humans and monkeys at a wide range of particulate levels has been documented under controlled circumstances (Anon.).

The ability of beryllium and beryllium-containing compounds to cause illness is well documented. In the 1940s, during the industrial beginning of beryllium extraction and processing, workers were exposed to levels of beryllium in the air greater than  $1,000 \mu\text{g}/\text{m}^3$  (Cummings et al. 2009). Some of these workers displayed short-term onset symptoms such as skin rashes, ulcers, weight loss, tiredness, breathing difficulties, and coughing. Other indications of their beryllium exposure were inflammation of their nose, throat, trachea, and lungs. The reaction of the human body to exposure to high concentrations of airborne beryllium was deemed to cause Acute Beryllium Disease (ABD). The exact mechanism of contracting ABD is under debate because there are few to no documented cases. In 1949, to prevent excess inhalation and production of beryllium dust, the U.S. Atomic Energy Commission took action by limiting its contractor's daily weighted average exposures to less than  $25 \mu\text{g}/\text{m}^3$ . Also around this time, beryllium's secondary disease, CBD, was discovered (Cummings et al. 2009).

The DOE defines CBD as a granulomatous lung disease that is caused by the body's immune system response (similar to an allergic reaction) to inhaled dust or fumes containing beryllium metal, alloys, beryllium compounds or mixtures, or insoluble beryllium salts. This immune system response is in contrast to ABD in that it is a hyper activity of the white blood cells in the body, as opposed to just chemical irritation (Anon.). CBD is marked by many of the same symptoms as ABD, except they can become known as long as several years after an exposure. Frequently reported symptoms include one or more of the following: dyspnea (shortness of breath) on exertion, cough, fever, night sweats, and chest pain and, less frequently, arthralgias (neuralgic pain in joints), fatigue, weight loss, and appetite loss (Anon.). On physical examination, a doctor may find signs of CBD, such as rales (changes in lung sounds), cyanosis (lack of oxygen), digital clubbing, or lymphadenopathy (enlarged lymph nodes). A radiograph (X-ray) of the lungs may show many small scars. Examination of the lung tissue under the microscope may show granulomas, which are signs of damage caused by the body's reaction to

beryllium (Anon.). Figure 6-2 shows a chest X-ray of a beryllium worker hired on 2 March 1979 and a follow up on 13 February 1997, showing reduced lung volumes and a bilateral interstitial infiltrate. The worker left the plant in 1999 because he had CBD.

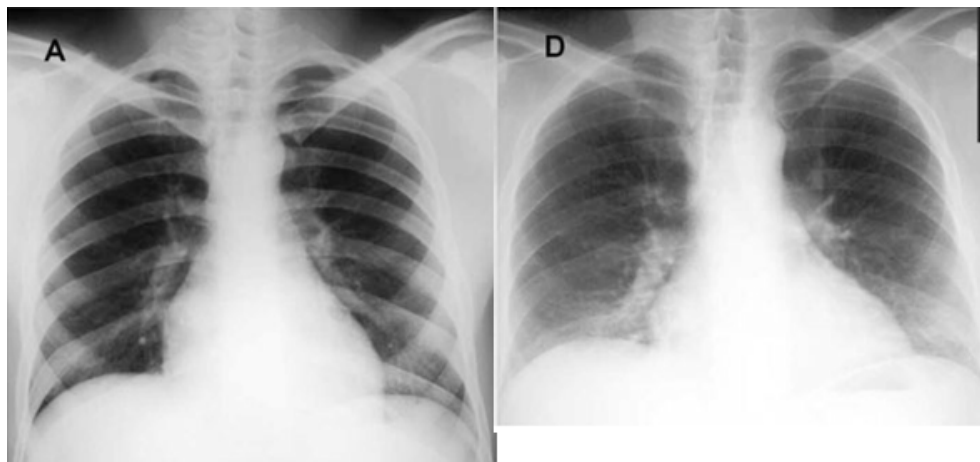


**Figure 6-2. Chest Radiographs of Worker Involved in the Production of Beryllium Metal from Beryllium Fluoride: (A) Before Being Hired; (D) Follow-Up**

The body's immune system response to beryllium is often called beryllium sensitization. Sensitization means that the person was exposed to beryllium and that his or her body has become hypersensitive to it (Anon.). This sensitivity ultimately makes the individual more likely than others to get CBD, but the individual may never get CBD or may get a mild case of CBD especially if the individual's exposure was low. Sensitivity to beryllium is unpredictable and highly individual. Experts believe that a test, known as the beryllium lymphocyte proliferation test (Be-LPT) shows abnormal results in individuals who have become sensitized to beryllium. Studies have shown that practically all individuals with CBD also are sensitized (Anon.). On the other hand, many individuals that are sensitized to beryllium do not have CBD.

CBD is a lifelong disease; there is no known cure (Schepers 1964). Prednisone or other corticosteroids are the most specific treatment currently available (Schepers 1964). They are directed at suppressing the immunological reaction and can be effective in diminishing symptoms of CBD. Other symptomatic treatment, such as oxygen, inhaled steroids, or bronchodilators, may be prescribed and can be effective in selected cases. Note, however, that some individuals sensitized to beryllium are asymptomatic and not physically impaired. However, once an individual has become sensitized, it is medically prudent to prevent additional exposure to beryllium (Cummings et al. 2009; Anon.).

Since the DOE implemented airborne standards for beryllium in 1949, more studies have changed the standards for beryllium in the work place. Different organizations have different standards for what is acceptable during an 8-hour work day (Table 6-4). In order from most strict to least strict, Materion and California OSHA allow an 8-hour work day average of  $0.2 \mu\text{g}/\text{m}^3$ . The National Institute for Occupational Safety and Health (NIOSH) recommends an average of  $0.5 \mu\text{g}/\text{m}^3$  (Anon.). OSHA has the highest allowable average concentration of  $2 \mu\text{g}/\text{m}^3$  (Anon.). All of these values are achievable, and many modern beryllium workplaces find themselves with less than  $1.0 \mu\text{g}/\text{m}^3$ . By improving control methods, the Oak Ridge Y-12 Plant and the Rocky

Flats Machine Shop were able to reduce their beryllium level averages from greater than 1.0  $\mu\text{g}/\text{m}^3$  to less than 0.3  $\mu\text{g}/\text{m}^3$  out of an average of greater than 1,600 combined samples (Anon.).

**Table 6-4. Workplace Beryllium Standards ( $\mu\text{g}/\text{m}^3$ ) as Dictated by Different Organizations**

OSHA*			California OSHA**		NIOSH***
PEL	Ceiling	Peak	PEL	Ceiling	REL
2	5	25	0.2	25	0.5

\*OSHA=Occupational Safety and Health Administration; PEL=8-hr time-weighted average Permissible Exposure Limit; Ceiling=not to be exceeded except for peak limit; Peak=30-minute maximum duration concentration above ceiling limit.

\*\*PEL=same as for OSHA; Ceiling=not to be exceeded at any time.

\*\*\*NIOSH=National Institute for Occupational Safety and Health; REL=8-hr time-weighted average Recommended Exposure Limit.

### 6.2.2 Beryllium Fluoride Health Effects

Beryllium fluoride is a clear-to-off-white, water soluble solid and is commonly the precursor to pure beryllium metal used in all modern beryllium production facilities (Materion 2011a). To produce beryllium, ore is converted to the chemical form of ammonium tetrafluoroberyllate. This ammonium tetrafluoroberyllate can be heated in a fluoride furnace to release ammonium fluoride gas, leaving beryllium fluoride nuggets (Materion). These nuggets (Figure 6-3) are then transferred to a reduction furnace, where they are reacted with magnesium metal to yield pure beryllium pebbles. This industrial process is currently carried out in Elmore, Ohio, at the Materion (formerly Brush-Wellman) Beryllium Pebble Plant. Here, workers routinely heat and reduce large quantities of beryllium fluoride to metal (Materion).



**Figure 6-3. Beryllium Fluoride Nugget Obtained from Materion**

The toxicity of beryllium fluoride is potentially different than that of beryllium metal. Beryllium metal is insoluble, so its presence in the lungs is likely much more detrimental than the water-soluble beryllium fluoride, which could be removed (Materion 2011b). Additionally,

most of the DOE's working beryllium guidelines are tailored to beryllium metal, because it is used in numerous nuclear applications. No sections in the DOE's beryllium worker protection program directly address the use of beryllium fluoride. However, the gaps in the DOE's literature can be filled with industrial health studies related to the production of beryllium metal through the ammonium tetrafluoroberyllate process, which does use beryllium fluoride.

In 1964 G. W. H. Schepers studied how to determine the effect of soluble beryllium salts, including beryllium fluoride, on the respiratory system and general health of rhesus monkeys (Schepers 1964). The study compared results to those of non-soluble salts to contrast the effect of particulate versus soluble beryllium compounds. Researchers periodically weighed and X-rayed fifteen monkeys, fed them strict diets, and exposed them to different concentrations of beryllium salt aerosols for different times. Their health was compared to twenty control monkeys that were exposed to the same conditions without beryllium exposure. During tests, monkeys were exposed to 953.5  $\mu\text{g}/\text{m}^3$  of airborne  $\text{BeF}_2$ , which corresponded to 184  $\mu\text{g}/\text{m}^3$  of beryllium, for anywhere from 7 to 13 days. The author reported that

“Anorexia was a marked feature in the monkeys exposed to the beryllium fluoride aerosol. This symptom appeared by the end of the third day of exposure and fluoride refusal commenced after six days. Anorexia persisted in the monkeys that continued to inhale  $\text{BeF}_2$ , but in the two animals transferred to normal air, decisive recovery took place within a week (p 2).”

Over the course of the exposure to beryllium fluoride, the monkeys lost a maximum of 20% of their initial body weight. On return to normal air, the monkeys recovered to 10% less than their initial body weight. Monkeys who were never exposed gained an average of 10% of their initial body weight. Monkeys exposed to other salts lost their appetites, although the effect was less pronounced than with beryllium fluoride.

The secondary observable effect of beryllium fluoride exposure was dyspnea, or difficulty in breathing. The author notes that “[dyspnea] developed most rapidly in the monkeys in the  $\text{BeF}_2$  chamber, and on continued exposure they suffered marked air hunger. When these groups of animals were returned to normal air a moderate recovery was noted in the group exposed to beryllium fluoride (p 3).”

Although monkeys in this test were exposed to airborne levels of beryllium that were nearly seven and a half times higher than the DOE standard imposed in 1949, the results show that a severe reaction, including anorexia and dyspnea, leading to chemical pneumonitis and eventually death, is possible with beryllium fluoride.

Case studies on humans have shown the negative effects of beryllium fluoride under acceptable airborne conditions. In 2008, K. J. Cummings, et al., performed two case studies on workers who were exposed to beryllium fluoride as well as other beryllium compounds at a beryllium manufacturing plant while reducing the beryllium fluoride with magnesium (Cummings et al. 2009). The first case detailed a 20-year-old male nonsmoker who started his employment at the beryllium production plant on March 12, 1979. All of his pre-employment health screenings showed healthy lung functions. This individual was transferred from ceramic and alloy fabrication, where he exhibited normal pulmonary function, to the metal production

department to operate the reduction furnace on December 31, 1979 (Figure 6-4). On January 12, 1980, he was documented for rashes at the plant's medical office, followed by shortness of breath, chest pain, 2.7-kg weight loss, and a nonproductive cough on March 29, 1980. Over the course of his tenure, he experienced reoccurring symptoms but continued to work. Eventually he transferred out of the furnace group and back into the alloy division, where he was without symptom until 1999, when he left the plant as a result of the onset of CBD.

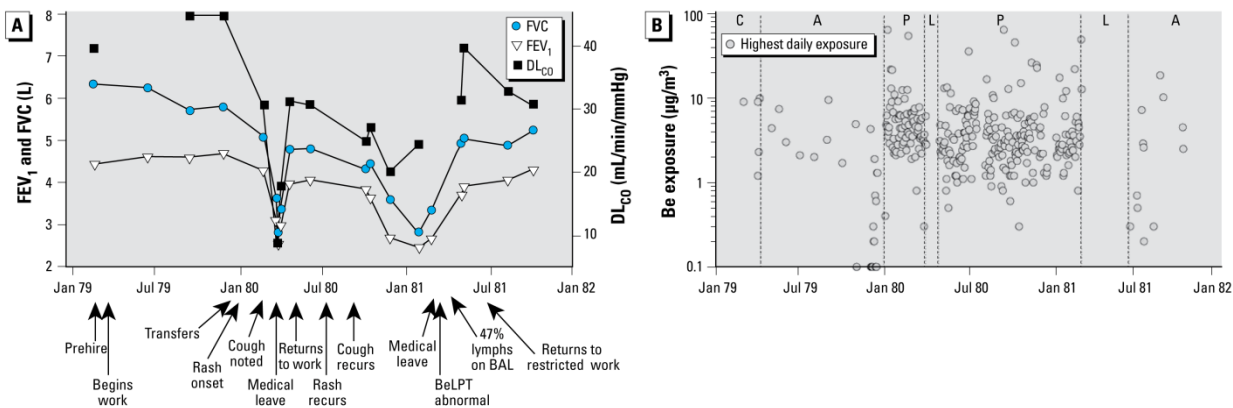


**Figure 6-4. Summary of Lung Function and Beryllium Exposure of Case 1 : (A) Results of Pulmonary Function Tests Before, During, and After Two Episodes of Acute Work-Related Illness. (B) Time-Weighted Average Airborne Beryllium Exposures in Patient's Departments During This Time.**

[Abbreviations: A, alloy department exposures (beryllium metal, beryllium oxide, copper); C, ceramics department exposures (beryllium oxide); L, medical leave; P, metals production department exposures (beryllium metal, beryllium oxide, beryllium fluoride, ammonium beryllium fluoride, ammonium fluoride, magnesium fluoride).]

The second case study presented by K. J. Cummings et al. tells a similar story. A healthy 25-year-old male smoker began operating the fluoride furnace at the beryllium production plant on May 11, 1981. On May 22, 1981, the employee reported rashes on his wrists and forearms followed by fatigue, shortness of breath, and a nonproductive cough on June 26, 1981. During the course of his employment at the fluoride furnace, none of the air samples exceed 20 µg/m<sup>3</sup>, and most were less than 10 µg/m<sup>3</sup>. Symptoms continued to present themselves after he was laid off on October 16, 1981. In 1984, he returned to the plant as a janitor, restricted from the furnace area. He left the plant in 1992 because of CBD.

Both of these cases illuminate the effects of beryllium fluoride in conjunction with other beryllium compounds on sensitive individuals in a commercial setting. Both individuals began their employment as healthy individuals and were medically monitored regularly throughout and after their employment. Both were exposed to very modest levels of beryllium, which tended to be below the peak and ceiling levels required by modern DOE standards, yet they ignored their symptoms and continued to work around beryllium, eventually resulting in CBD (Anon.). Currently there are no studies available for workers exposed to just beryllium fluoride.

### 6.2.3 Previously Used Beryllium Fluoride Control Methods

A wealth of information is available on how to protect personnel from beryllium and beryllium fluoride exposure. These techniques are highly situational and depend on many variables. Currently, information and control techniques cover handling flibe in large batches for the MSRE, in a glove box, and in contained melting operations (Shaffer 1971). Other general guidelines for handling beryllium and beryllium-contaminated items have been provided by Materion<sup>1</sup>. More situation information from Materion could detail the process of melting beryllium fluoride. This information could be highly valuable for creating handling guidelines that are commercially successful, timely, and safe.

The first and arguably most important source of information for proper handling of flibe and its component salts are documents from the MSRE (Figure 6-5). A paper written by J. H. Shaffer details the operation of a fluoride salt preparation plant that ultimately produced 126,000 lb of fluoride salt mixtures (Shaffer 1971). The main production facility was able to handle full powder production and large amounts of aerosols. To do this, the room cycled its air three times a minute while keeping it at negative pressure. To enter the room, workers were required to remove all their clothing except underwear and don a plastic fresh air suit. On exiting, workers showered in the suit and then removed the suit. These extreme safety measures were needed for the handling of powdered fluoride salts.



**Figure 6-5. An MSRE Employee Measuring Quantities of Salt for Production of Flibe**

Additional beryllium control information is documented in N. E. Bolton and T. C. Whitson, *Revised Beryllium Control Program for the MSRE*. This document is an unpublished internal

---

<sup>1</sup> Materion Brush, Inc., “Interactive Guide to Working Safely with Beryllium and Beryllium-Contaminated Materials,” at <http://www.berylliumsafety.com>. Accessed August 9, 2012.

document referenced in a few manuscripts. Parts of this document are reproduced in *MSRE Design and Operations Report Part IX: Safety Procedures and Emergency Plans* by A. N. Smith (Smith 1965). General guidelines are included in the Smith paper. A. N. Smith reported that “It is recognized that there will be short periods of an operational nature when the concentration will be relatively high. Acute exposure for workers without respiratory protection should not exceed  $25 \mu\text{g}/\text{m}^3$  and the time limit for such exposure should be less than 30 min.” Additionally, guidelines allowed continuous or chronic exposure of less than  $2 \mu\text{g}/\text{m}^3$  for an 8-hour, 5-day week. Around the entire building, guidelines stipulated  $0.01 \mu\text{g}/\text{m}^3$ . Surface contamination on walls, floors, and equipment in beryllium-contaminated zones was kept at less than  $25 \mu\text{g}/\text{ft}^2$ , and equipment moved from these areas had to have less than  $4 \mu\text{g}/\text{ft}^2$  of surface contamination. To ensure these standards were met, the MRSE used 15 permanent air-sampling stations. These stations also checked the atmosphere in the radiator stack while the reactor operated and in the coolant pit during shutdown (Smith 1965).

Recently, ORNL transferred 350 kg of flibe from one large container to several smaller containers for use in FHR research. All of the salt was in solid form, except some powders that formed when vapor condensed on cold legs during melting. The transfer process required adapting and opening the main container of flibe by removing flanges and Swageloks. This work was performed inside a walk-in fume hood with full protective suits and respirators. After finishing, workers swiped surfaces and sent the swipes to industrial hygienists for analysis. Afterwards, workers cleaned contaminated surfaces with 409<sup>TM</sup>, double-bagged contaminated supplies, and sent them to a landfill.

Facilities at INL also have worked with flibe albeit in a glove box. Operational procedures and controls for this experiment involved wearing gloves and respirators when opening the glove box to atmosphere, followed by wiping surfaces in and around the glove box to send to an industrial hygienist. Respirators were outfitted with air samplers that could also be analyzed by an industrial hygienist. After a certain procedure had been completed and found not to cause contamination, the procedure was deemed safe and did not require personal protective equipment (PPE). Once again, all contaminated items were double-bagged (Calderoni et al. 2009).

#### **6.2.4 Potential Beryllium Controls for the FHR**

Beryllium controls from the FHR should be modeled on previous successful work, specifically that from the MSRE and from DOE’s Chronic Beryllium Disease Prevention Program (10 CFR Part 850). All of these methods should mainly revolve around minimizing dust production and movement. Moreover, the FHR should have two distinct forms of monitoring: individual medical surveillance and environmental monitoring. By implementing successful patterns and surveillance, beryllium fluoride can be handled safely.

Beryllium controls in the FHR will depend largely on the form of beryllium fluoride handled. If beryllium fluoride can be obtained in large, solid form, less stringent protection will be needed. On the other hand, if beryllium fluoride can only be found in powder form, strict protection will be needed. Currently, beryllium fluoride has been obtained by UW in solid chunk form. By using solid chunks, the potential for aerosol production is much less than that of a powder beryllium fluoride. In this case, a fluoride production facility should keep a negative pressure in respect to the rest of the plant, air which moves in and out should use high-efficiency particulate air (HEPA) filters, and workers who may come in contact with solid beryllium should

wear Tyvek<sup>®</sup> suits and a respirator. Respirators should be equipped with an inline air monitor that measures the amount of beryllium a worker inhaled. No other work, other than beryllium work, should be performed in this room. Any object that comes out of this room should be cleaned to the MSRE's recommended standards. Painting tools with distinct "beryllium contamination colors" could also help that prevent the spread of beryllium around the plant. Beryllium fluoride will likely be melted in the same room where beryllium metal will be added as a reducing agent. As long as the beryllium metal is not machined in any way, or treated in a way that produces dust, the metal can be handled without using PPE.

Inside the beryllium room, salts should be able to be melted and sent to a purification system, and then on to the reactor, all within piping. Any fumes created from melting the salt should be adequately filtered and vented. After the salt components have been melted, all beryllium work should be self contained and not require a person to handle the salt at any time. Two layers of metal should separate an unprotected employee from the flibe at all stages. The only times these areas should present a beryllium danger is during repair after operation. These areas should be constantly swipe monitored and air monitored for any potential contamination.

Around the FHR building, several continuous air monitoring stations should be placed at critical points that can determine the amount of atmospheric beryllium. These stations should be tested regularly and be kept below the MSRE's limit of  $0.1 \mu\text{g}/\text{m}^3$ . Swipes should be regularly taken to ensure no buildup of beryllium-containing dust.

It may be advisable to have an in-house analytical facility capable of fast turnaround times on beryllium swipes and air monitors. This capability would allow beryllium-contaminated equipment or areas to be deemed safe without the long lead time associated with sending samples to offsite labs. Swipes and air monitors can potentially be analyzed using ICP-MS or ICP-OES, which is a candidate technique for determining the purity and composition of salts.

Workers should also be monitored by a medical professional who knows the limits of beryllium exposure. A Materion document outlines the extent of the company's medical testing. Basic lung function tests should be done when an employee begins a beryllium-related job at the FHR and at the end of the job. Quarterly function monitoring should be offered during the extent of the job. Chest X-rays should be mandatory at the beginning of the job, every third year of the job, and on exit. Voluntarily, they should be offered every year. A blood lymphocyte proliferation test should be offered voluntarily to any employee but should be mandatory for all employees who directly handle beryllium fluoride. Direct handlers should receive a BeLPT after their first, second, and third year, followed by every third year thereafter, and then one on exit. Other employees who have spent time in an area where they might be exposed to an atmosphere with levels of beryllium greater than  $0.1 \mu\text{g}/\text{m}^3$  should have a BeLPT every 3 years. These tests can provide employees an early indication of abnormalities before employees develop CBD.

Other questions still exist, such as how to design a beryllium room with its eventual decontamination and disassembly in mind, how to monitor beryllium in a timely fashion, and how to minimize beryllium-related operating costs. All of these questions have the potential to be answered by Materion, which has performed all of these duties with a commercial vision in

mind. When designing a commercial beryllium fluoride contamination area, Materion should be consulted.

### 6.2.5 Expert Discussion on Beryllium Control

Comments on beryllium control from experts participating in the third workshop included the following:

- BeF<sub>2</sub> has a much higher volatility than LiF in flibe and thus is more prone to evaporate into cover gas spaces.
- Beryllium condenses on cool or hot surfaces.
- It is important to enforce regulations on proper use of protective equipment.
- The flanges/seals don't seal well at the temperatures and chemistry planned for the FHR. Swagelocks don't work well. It is important to use welds.
- It is helpful to design for few penetrations.
- Because workers exhibited beryllium diseases, limits on permissible air concentration have been reduced over time. Use of PPE is very important because incorrect use accounts for a lot of the overexposure. Sometimes excessive exposure is not detected by external dosimeters, because of improper use of PPE.
- Flibe was treated like beryllium at INL. Across the DOE complex, there had been discussion about moving the OSHA and DOE standards down to ~0.2 ug/m<sup>3</sup>. Use this standard.
- Containment should use an inert atmosphere so that people are fully dressed in PPE when they go in; maintenance should also be considered in design.
- NIOSH has a stricter limit (0.5 ug/m<sup>3</sup>) than OSHA, and it is used for DOE fusion safety. Review how the MSRE handled beryllium and then consider what would have to change to accommodate more stringent regulations today.

The Joint European Tokamak (JET) facility in the United Kingdom provides relevant information on methods and costs of implementing beryllium (and tritium) controls in facilities. The total cost of implementing beryllium controls in JET was estimated to be \$382,000 per year from 1995 to 2004 (Campling and Patel 2006). If a 410-MWe FHR plant were to have similar beryllium control costs, they would contribute approximately 0.012 cents/kWhr to the cost of electricity production, a small amount of the total.

## 7 References

- Adamson, G. M., R. S. Crouse, and W. D. Manly. 1961. *Interim Report on Corrosion by Zirconium-Base Fluorides*. Oak Ridge, Tennessee: Oak Ridge National Laboratory.
- Adhoum, N., J. Bouteillon, D. Dumas, and J. C. Poignet. 2006. "Electrochemical Insertion of Sodium into Graphite in Molten Sodium Fluoride at 1025°C." *Electrochimica Acta* 51 (25): 5402–5406.
- Ambrosek, J., M. Anderson, K. Sridharan, and T. Allen. 2009. "Current Status of Knowledge of the Fluoride Salt (FLiNaK) Heat Transfer." *Nuclear Technology* 165: 166–173.
- Ambrosek, J. W. 2011. *Molten Chloride Salts for Heat Transfer in Nuclear Systems*. Madison, Wisconsin: University of Wisconsin-Madison.
- Andrews, N., and C. Forsberg. 2012. "Tritium Management in Fluoride-Salt-Cooled High-Temperature Reactors (FHRs)." In *Tritium in Fission and Fusion — II Transactions of the American Nuclear Society, Vol. 107, San Diego, California, November 11–15, 2012*, 107:391–395. American Nuclear Society.
- Anon. *Chronic Beryllium Disease Prevention Program; Final Rule*.
- Antill, J. E., and J. B. Warburton. 1971. "Active to Passive Transition in the Oxidation of SiC." *Corrosion Science* 11 (6): 337–342.
- ASM International. 2003. "Corrosion by Molten Nitrates, Nitrites, and Fluorides." In *ASM Handbook Volume 13A: Corrosion: Fundamentals, Testing, and Protection*, ed. S.D. Cramer and B. S. Covino Jr., 124–128. ASM International.
- Baes Jr., C. F. 1974. "The Chemistry and Thermodynamics of Molten Salt Reactor Fuels." *Journal of Nuclear Materials* 51 (1): 149–162.
- Bardet, P., E. Blandford, M. Fratoni, A. Niquille, E. Greenspan, and P. F. Peterson. 2008. "Design, Analysis and Development of the Modular PB-AHTR." In *Proceedings of ICAPP '08 (International Congress on Advances in Nuclear Power Plants)*, 1–18. American Nuclear Society.
- Beahm, E. C., C. F. Weber, T. S. Kress, and G. W. Parker. 1992. *Iodine Chemical Forms in LWR Severe Accidents*. Washington, D.C.: U.S. Nuclear Regulatory Commission.
- Beneš, O., and R. J. M. Konings. 2012. "Molten Salt Reactor Fuel and Coolant." In *Comprehensive Nuclear Materials*, 359–389. Elsevier B.V.
- Bernardet, V., S. Gomes, S. Delpeux, M. Dubois, K. Guérin, D. Avignant, G. Renaudin, and L. Duclaux. 2009. "Protection of Nuclear Graphite Toward Fluoride Molten Salt by Glassy Carbon Deposit." *Journal of Nuclear Materials* 384 (3) (February): 292–302. doi:10.1016/j.jnucmat.2008.11.032. <http://linkinghub.elsevier.com/retrieve/pii/S0022311508007642>.
- Billot, P., L. J. Seran, M. T. Cabrilat, H. Burlet, A. Terlain, and J. P. Bonal. 2004. "CEA R&D Programme on Structural Materials for Future Gas-Cooled Nuclear Systems." In *Basic Studies in the Field of High-temperature Engineering Third Information Exchange Meeting: Ibaraki-ken, Japan, 11-12 September 2003*, 58. Paris: OECD Publishing. <http://www.oecdbookshop.org/oecd/display.asp?lang=EN&sf1=identifiers&st1=92-64-01601-5>.
- Bonal, J.-P., A. Kohyama, J. van der Laan, and L. L. Snead. 2009. "Graphite, Ceramics, and Ceramic Composites for High-Temperature Nuclear Power Systems." *MRS Bulletin* 34: 28–34.

- Bratton, R., and T. Burchell. 2005. *NGNP Graphite Testing and Qualification Specimen Selection Strategy*. Idaho Falls: Idaho National Laboratory.
- Briggs, R. B. 1962. *Molten-Salt Reactor Program Semiannual Progress Report for Period Ending February 28, 1962*. Oak Ridge, Tennessee: Oak Ridge National Laboratory.
- . 1963a. *Molten-Salt Reactor Program Semiannual Progress Report for Period Ending January 31, 1963*. Oak Ridge, Tennessee: Oak Ridge National Laboratory.
- . 1963b. *Molten-Salt Reactor Program Semiannual Progress Report for Period Ending July 31, 1963*. Oak Ridge, Tennessee: Oak Ridge National Laboratory.
- . 1964. *Molten-Salt Reactor Program Semiannual Progress Report for Period Ending July 31, 1964*. Oak Ridge, Tennessee: Oak Ridge National Laboratory.
- . 1972. “Tritium in Molten-Salt Reactors.” *Reactor Technology* 14 (4): 335–352.
- Briggs, R. B., and C. W. Nestor. 1975. *A Method for Calculating the Steady-State Distribution of Tritium in a Molten-Salt Breeder Reactor Plant*. Oak Ridge, Tennessee: Oak Ridge National Laboratory.
- Calderoni, P., P. Sharpe, M. Hara, and Y. Oya. 2008. “Measurement of Tritium Permeation in Flibe (2LiF–BeF<sub>2</sub>).” *Fusion Engineering and Design* 83 (7-9): 1331–1334.
- Calderoni, P., P. Sharpe, H. Nishimura, and T. Terai. 2009. “Control of Molten Salt Corrosion of Fusion Structural Materials by Metallic Beryllium.” *Journal of Nuclear Materials* 386-388: 1102–1106.
- Campling, D., and B. Patel. 2006. “Sampling and Analysis of Beryllium at JET: Policy Cost and Impact.” *Journal of ASTM International* 3 (1).
- Carroll, M., J. Lord, and D. Rohrbaugh. 2010. *Baseline Graphite Characterization : First Billet*. Idaho Falls: Idaho National Laboratory.
- Casino Jr., W. A. 2006. “Investigation of an Alternative Fuel Form for the Liquid Salt Cooled Very High Temperature Reactor (LS-VHTR).” In *Proceedings of ICAPP '06 (International Congress on Advances in Nuclear Power Plants)*. La Grange Park: American Nuclear Society.
- Causey, R. A., W. R. Wampler, J. R. Retelle, and J. L. Kaae. 1993. “Tritium Migration in Vapor-deposited B-silicon Carbide.” *Journal of Nuclear Materials* 203 (3): 196–205.
- Chi, S.-H., and G.-C. Kim. 2008. “Comparison of 3MeV C<sup>+</sup> Ion-Irradiation Effects Between the Nuclear Graphites Made of Pitch and Petroleum Cokes.” *Journal of Nuclear Materials* 381 (1-2) (October): 98–105. doi:10.1016/j.jnucmat.2008.08.001. <http://linkinghub.elsevier.com/retrieve/pii/S0022311508004327>.
- Chikada, T., A. Suzuki, Z. Yao, D. Levchuk, H. Maier, T. Terai, and T. Muroga. 2009. “Deuterium Permeation Behavior of Erbium Oxide Coating on Austenitic, Ferritic, and Ferritic/Martensitic Steels.” *Fusion Engineering and Design* 84 (2-6): 590–592.
- Cisneros, A. T., R. O. Scarlat, M. Laufer, E. Greenspan, and P. F. Peterson. 2012. “Pebble Fuel Design for the PB-FHR.” In *Proceedings of the International Congress on Advances in Nuclear Power Plants (ICAPP '12)*. American Nuclear Society.
- Clark, D. E., and R. E. Mizia. 2012. *Diffusion Welding of Alloys for Molten Salt Service – Status Report*. Idaho Falls: Idaho National Laboratory.
- CNSC. 2010. *Evaluation of Facilities Handling Tritium*. Ontario, Canada: Canadian Nuclear Safety Commission.
- Del Cul, G. D., D. F. Williams, and L. M. Toth. 2002. “Redox Potential of Novel Electrochemical Buffers Useful for Corrosion Prevention in Molten Fluorides.” In

- Thirteenth International Symposium On Molten Salts*, Abstract #1441. Pennington, New Jersey: Electrochemical Society.
- Cummings, K. J., A. B. Stefaniak, M. A. Virji, and K. Kreiss. 2009. “A Reconsideration of Acute Beryllium Disease.” *Environmental Health Perspectives* 117 (8): 1250–1256.
- Davis, C. B. 2005. *Implementation of Molten Salt Properties into RELAP5-3D/ATHENA*. Idaho Falls: Idaho National Laboratory.
- Delpech, S., C. Cabet, C. Slim, and G. S. Picard. 2010. “Molten Fluorides for Nuclear Applications.” *Materials Today* 13 (12): 34–41.
- Devilliers, D., M. Vogler, F. Lantelme, and M. Chemla. 1983. “Mass Spectrometric Analysis of Thermal Decomposition Products of Graphite Fluorides and Electrogenerated Carbon-Fluorine Compounds.” *Analytica Chimica Acta* 153: 69–82.
- DOE’s Chronic Beryllium Disease Prevention Program 1999, Final Rule, 10 CFR Part 850.
- Duderstadt, J. J., and L. J. Hamilton. 1976. *Nuclear Reactor Analysis*. New York: Wiley and Sons.
- Edao, Y., S. Fukada, S. Yamaguchi, Y. Wu, and H. Nakamura. 2010. “Tritium Removal by Y Hot Trap for Purification of IFMIF Li Target.” *Fusion Engineering and Design* 85 (1): 53–57.
- Ellis, R. J. 2011. “Comparison of Calculated and Measured Neutron Fluence in Fuel/Cladding Irradiation Experiments in HFIR.” *Transactions of the American Nuclear Society* 105: 808–810.
- Fei, T., D. Ogata, K. Pham, M. Solom, C. Zhao, C. Xu, A. Cheng, et al. 2008. *A Modular Pebble-Bed Advanced High Temperature Reactor*. Berkeley: University of California, Berkeley.
- Flanagan, G. F., D. E. Holcomb, and S. M. Cetiner. 2012. *FHR Generic Design Criteria*. Oak Ridge, Tennessee: Oak Ridge National Laboratory.
- Forsberg, C. 2008. “Fuel Geometry Options for Salt-Cooled Advanced High-Temperature Reactors.” In *Proceedings of ICAPP '07*, Paper 7405. American Nuclear Society.
- Forsberg, C. W., L.-W. Hu, P. F. Peterson, and T. Allen. 2012. *Fluoride-Salt-Cooled High-Temperature Reactors (FHRs) for Power and Process Heat*. MIT-ANP-14th ed. Cambridge, Massachusetts: Massachusetts Institute of Technology.
- Forsberg, C. W., K. A. Terrani, L. L. Snead, and Y. Katoh. 2012. “Fluoride-Salt-Cooled High-Temperature Reactor (FHR) with Silicon-Carbide-Matrix Coated-Particle Fuel.” In *American Nuclear Society Annual Meeting Transactions*, Paper 6514. American Nuclear Society.
- Galvez, C. 2011. “Design and Transient Analysis of Passive Safety Cooling Systems for Advanced Nuclear Reactors”. University of California, Berkeley.
- Galvez, C., R. Wang, S. Margossian, S. Dionisio, and P. F. Peterson. 2010. “Modeling and Transient Simulation of the PB-AHTR Using RELAP5.” In *Proceedings of the ICAPP 10*, Paper 10138. American Nuclear Society.
- Gomez, J., M. Hay, J. Lee, and B. Tam. 2010. *Design of Fuel Testing and Qualification Capsules for the Pebble Bed Advanced High Temperature Reactor*. Berkeley: University of California, Berkeley, Thermal Hydraulics Laboratory.
- Greene, S. R., J. C. Gehin, D. E. Holcomb, J. J. Carbajo, D. Ilas, A. T. Cisneros, V. K. Varma, et al. 2010. *Pre-Conceptual Design of a Fluoride-Salt-Cooled Small Modular Advanced High-Temperature Reactor (SmAHTR)*. Oak Ridge: Oak Ridge National Laboratory.

- Grimes, W. R. 1967. *Chemical Research and Development for Molten-Salt Breeder Reactors*. Oak Ridge, Tennessee: Oak Ridge National Laboratory.
- Gulbransen, E. A., and S. A. Jansson. 1972. "The High-Temperature Oxidation, Reduction, and Volatilization Reactions of Silicon and Silicon Carbide." *Oxidation of Metals* 4 (3): 181–201.
- Guymon, R. H. 1973. *MSRE Systems and Components Performance*. Oak Ridge, Tennessee: Oak Ridge National Laboratory.
- Harp, J. M. 2012. "AGR-1 Capsule Fission Product Inventory Measurements". Idaho Falls: Idaho National Laboratory.
- Harp, Jason. "AGR-1 Capsule Fission Product Inventory Measurements."
- Hayafune, H. 2011. "Double-Walled-Straight-Tube Steam Generator for Future SFRs in Japan." In *Technical Meeting on Innovative Heat Exchanger and Steam Generator Designs for Fast Reactors*. Vienna, Austria: International Atomic Energy Agency.
- Haynes International. 2012. "Hastelloy(R) N Alloy". Kokomo, Indiana: Haynes International.
- Holcomb, D. E., D. Ilas, A. L. Qualls, F. J. Peretz, V. K. Varma, E. C. Bradley, and A. T. Cisneros. 2012. "Current Status of the Advanced High Temperature Reactor." In *Proceedings of the International Congress on Advances in Nuclear Power Plants (ICAPP '12)*, 911–919. American Nuclear Society.
- Holcomb, D. E., D. Ilas, V. K. Varma, A. T. Cisneros, R. P. Kelly, and J. C. Gehin. 2011. *Core and Refueling Design Studies for the Advanced High Temperature Reactor*. Oak Ridge, Tennessee: Oak Ridge National Laboratory.
- Hollenberg, G. W., E. P. Simonen, G. Kalinin, and A. Terlain. 1995. "Tritium/Hydrogen Barrier Development." *Fusion Engineering and Design* 28: 190–208.
- Homan, F. J., T. B. Lindemer, E. L. Long Jr., T. N. Tieg, and R. L. Beatty. 1977. "Stoichiometric Effects on Performance of High-Temperature Gas-Cooled Reactor Fuel from the U-C-O System." *Nuclear Technology* 35 (2): 428–441.
- Hong, R., S. Huber, K. Lee, P. Purcell, S. Margossian, and J.-D. Seelig. 2009. *Reactor Safety and Mechanical Design for the Annular Pebble-bed Advanced High Temperature Reactor*. Berkeley: University of California, Berkeley.
- Huddar, L. 2011. *Risk Assessment and Risk Management of Tritium Transport and Release in FHRs Using Open Air Brayton Cycle*. Berkeley: University of California, Berkeley.
- Hunn, J. D., and Others. 2012. *AGR-1 Irradiated Compact 6-1-1 PIE Report: Evaluation of As-Irradiated Fuel Performance Using Leach Burn Leach, IMGA, Materialography, and X-Ray Tomography*. Oak Ridge, Tennessee: Oak Ridge National Laboratory.
- Hurst, R., and R. N. Lyon. 1960. "Series IV: Technology, Engineering, and Safety, Vol. 2." In *Progress in Nuclear Energy*, ed. C. M. Nicholls, 164–179.
- IAEA. 1997. *Fuel Performance and Fission Product Behaviour in Gas Cooled Reactors*. Vienna, Austria: International Atomic Energy Agency.
- IARC. 2012. "Beryllium and Beryllium Compounds." *IARC Monographs on the Evaluation of Carcinogenic Risks to Humans* 42: 95–117.
- Ignatiev, V., and A. Surenkov. 2012. "Material Performance in Molten Salts." In *Comprehensive Nuclear Materials*. Elsevier B.V.
- Ingersoll, D. T., C. W. Forsberg, and P. E. MacDonald. 2007. *Trade Studies for the Liquid-Salt-Cooled Very High-Temperature Reactor: Fiscal Year 2006 Progress Report*. Oak Ridge: Oak Ridge National Laboratory.

- INL. 2007. *Next Generation Nuclear Plant Pre-Conceptual Design Report*. Idaho Falls: Idaho National Laboratory.
- INL. 2009. *NGNP Licensing Plan*, PLN-3202.
- . 2009. *FY 2009 Advanced Test Reactor National Scientific User Facility Users' Guide*. Idaho Falls: Idaho National Laboratory.
- . 2010. *NGNP High Temperature Materials White Paper*. Idaho Falls: Idaho National Laboratory.
- INL. *FY 2007 Graphite Technology Development Plan*, INL/EXT-07-131652010.
- INL, Centre d'Etude Atomique, and Massachusetts Institute of Technology. 2004. *Development of Improved Models and Designs for Coated-Particle Gas Reactor Fuels: Final Report Under the International Nuclear Energy Research Initiative*. Idaho Falls: Idaho National Laboratory.
- Jeong, H., Y. H. Jeong, and S. H. Chang. 2009. "Model Development for the Estimation of Fission Product Release Under Normal and Accident Conditions in a HTGR." *Nuclear Engineering and Design* 239 (6): 1066–1075.
- Kasten, P. R., E. S. Bettis, W. H. Cook, W. P. Eatherly, D. K. Holmes, R. J. Kedl, C. R. Kennedy, et al. 1969. *Graphite Behavior and Its Effects on MSBR Performance*. Oak Ridge, Tennessee: Oak Ridge National Laboratory.
- Katoh, Y., M. Kotani, A. Kohyama, M. Montorsi, M. Salvo, and M. Ferraris. 2000. "Microstructure and Mechanical Properties of Low-Activation Glass-Ceramic Joining and Coating for SiC/SiC Composites." *Journal of Nuclear Materials* 283: 1262–1266.
- Katoh, Y., D. F. Wilson, and C. W. Forsberg. 2007. *Assessment of Silicon Carbide Composites for Advanced Salt-Cooled Reactors*. Oak Ridge, Tennessee: Oak Ridge National Laboratory.
- Keiser, J. R., J. H. DeVan, and E. J. Lawrence. 1979. "Compatibility of Molten Salts with Type 316 Stainless Steel and Lithium." *Journal of Nuclear Materials* 85-86: 295–298.
- Keiser, J. R., J. H. DeVan, and D. L. Manning. 1977. *The Corrosion Resistance of Type 316 Stainless Steel to Li<sub>2</sub>BeF<sub>4</sub>*. Oak Ridge, Tennessee: Oak Ridge National Laboratory.
- Koger, J. W. 1972. *Evaluation of Hastelloy N Alloys After Nine Years Exposure to Both a Molten Fluoride Salt and Air at Temperatures from 700 to 560°C*. Oak Ridge, Tennessee: Oak Ridge National Laboratory.
- Koger, J. W., and A. P. Litman. 1971. *Mass Transfer Between Hastelloy N and Haynes Alloy No. 25 in a Molten Sodium Fluoroborate Mixture*. Oak Ridge, Tennessee: Oak Ridge National Laboratory.
- Leonard, K. J. 2012. "Radiation Effects in Refractory Metal and Alloys." In *Comprehensive Nuclear Materials*, ed. R. Konings. Elsevier Ltd.
- Li, L., C. Galvez, A. T. Cisneros, and P. F. Peterson. 2010. *Coupled RELAP5-3D and MCNP5 Baseline Core Model of the Annular Pebble Bed Advanced High Temperature Reactor (PB-AHTR)*. Berkeley: University of California, Berkeley.
- Liu, D.-R., W.-X. Li, Z.-H. Yang, S.-L. Qiu, and Y.-T. Luo. 2011. "Electrochemical Investigation on Kinetics of Potassium Intercalating into Graphite in KF Melt." *Transactions of Nonferrous Metals Society of China* 21 (1): 166–172.
- Liu, D.-R., Z.-H. Yang, W.-X. Li, S.-L. Qiu, and Y.-T. Luo. 2010. "Electrochemical Intercalation of Potassium into Graphite in KF Melt." *Electrochimica Acta* 55 (3): 1013–1018.

- MacPherson, H. G. 1985. "The Molten Salt Reactor Adventure." *Nuclear Science and Engineering* 90: 374–380.
- Manly, W. D. 1960. "Metallurgical Problems in Molten Fluoride Systems." *Progress in Nuclear Energy* 2: 164–179.
- Materion. "Designing and Fabricating Beryllium". Elmore, Ohio: Materion.
- . 2011a. "MSDS No. M12, Beryllium Fluoride". Elmore, Ohio: Materion.
- . 2011b. "Potential Health Effects from Exposure to Water Soluble Beryllium Compounds". Elmore, Ohio: Materion.
- McCoy, H. E., R. L. Beatty, W. H. Cook, R. E. Gehlbach, C. R. Kennedy, J. W. Koger, A. P. Litman, and C. E. Sessions. 1970. "New Developments in Materials for Molten-Salt Reactors." *Nuclear Applications and Technology* 8: 156–169.
- McNeese, L. E. 1976. *Molten-Salt Reactor Program Semiannual Progress Report for Period Ending February 29, 1976*. Oak Ridge, Tennessee: Oak Ridge National Laboratory.
- Mohanty, S., and S. Majumdar. 2011. *HTGR Graphite Core Component Stress Analysis Research Program – Task 1 Technical Letter Report*. Lemont, Illinois: Argonne National Laboratory.
- Morton, D. K., J. E. Nestell, T. D. Burchell, and T.-L. Sham. 2012. "Section III , Division 5 – Development and Future Directions." In *Proceedings of the ASME 2012 Pressure Vessels and Piping Division Conference, PVP2012*. American Society for Mechanical Engineers.
- Natesan, K., M. Li, S. Majumdar, R. K. Nanstad, and T.-L. Sham. 2008. *Code Qualification of Structural Materials for AFCI Advanced Recycling Reactors*. Lemont, Illinois: Argonne National Laboratory.
- Nishimura, H., A. Suzuki, T. Terai, M. Yamawaki, S. Tanaka, A. Sagara, and O. Motojima. 2001. "Chemical Behavior of Li<sub>2</sub>BeF<sub>4</sub> Molten Salt as a Liquid Tritium Breeder." *Fusion Engineering and Design* 58-59: 667–672.
- Nishimura, H., T. Terai, T. Yoneoka, S. Tanaka, A. Sagara, and O. Motojima. 2000. "Compatibility of Structural Candidate Materials with LiF–BeF<sub>2</sub> Molten Salt Mixture." *Journal of Nuclear Materials* 283-287, P: 1326–1331.
- Oh, C. H., and E. S. Kim. 2009. *Development and Verification of Tritium Analyses Code for a Very High Temperature Reactor*. Idaho Falls: Idaho National Laboratory.
- Olander, D. 2002. "Redox Condition in Molten Fluoride Salts: Definition and Control." *Journal of Nuclear Materials* 300 (2-3): 270–272.
- Olson, L. C., J. W. Ambrosek, K. Sridharan, M. H. Anderson, and T. R. Allen. 2009. "Materials Corrosion in Molten LiF–NaF–KF Salt." *Journal of Fluorine Chemistry* 130 (1): 67–73.
- Olson, L. C., K. Sridharan, M. Anderson, and T. Allen. 2011. "Nickel-Plating for Active Metal Dissolution Resistance in Molten Fluoride Salts." *Journal of Nuclear Materials* 411 (1-3): 51–59.
- Ozeryanaya, I. N. 1985. "Corrosion of Metals by Molten Salts in Heat-Treatment Processes." *Metal Science and Heat Treatment* 27 (3): 184–188.
- Perujo, A., and K. S. Forcey. 1995. "Tritium Permeation Barriers for Fusion Technology." *Fusion Engineering and Design* 28: 252–257.
- Peterson, P. F., C. W. Forsberg, and P. S. Pickard. 2003. "Advanced CSiC Composites for High-Temperature Nuclear Heat Transport with Helium, Molten Salts, and Sulfur-Iodine Thermomchemical Hydrogen Process Fluids." In *Second Information Exchange Meeting on Nuclear Production of Hydrogen*. Argonne, Illinois: Argonne National Laboratory.

- Petti, D. A., J. Maki, J. Hunn, P. Pappano, C. Barnes, J. Saurwein, S. Nagley, J. Kendall, and R. Hobbins. 2010. "The DOE Advanced Gas Reactor Fuel Development and Qualification Program." *JOM* (September): 62–66.
- Petti, D. A., and Others. 2004. *Preliminary AGR Fuel Specifications*. Idaho Falls: Idaho National Laboratory.
- Phelps, G. H. 2009. "Mechanical Carbon in Chemical Processing Equipment." *Chemical Engineering* (January): 46–78.
- Ren, W., G. Muralidharan, D. F. Wilson, and D. E. Holcomb. 2011. "Considerations of Alloy N for Fluoride Salt-Cooled High Temperature Reactor Applications." In *Proceedings of the 2011 ASME Pressure Vessels and Piping Conference, PVP2011*, Paper 57029. American Society for Mechanical Engineers.
- Rosenthal, M., R. B. Briggs, and P. R. Kasten. 1969. *Molten-Salt Reactor Program Semiannual Progress Report for Period Ending August 31, 1968*. Oak Ridge, Tennessee: Oak Ridge National Laboratory.
- . 1970a. *Molten-Salt Reactor Program Semiannual Progress Report for Period Ending August 31, 1969*. Oak Ridge, Tennessee: Oak Ridge National Laboratory.
- . 1970b. *Molten-Salt Reactor Program Semiannual Progress Report for Period Ending February 28, 1970*. Oak Ridge, Tennessee: Oak Ridge National Laboratory.
- Rosenthal, M., P. Haubenreich, and R. Briggs. 1972. *The Development Status of Molten-Salt Breeder Reactors*. Oak Ridge, Tennessee: Oak Ridge National Laboratory.
- Sabharwall, P., M. Ebner, M. Sohal, P. Sharpe, M. Anderson, K. Sridharan, J. Ambrosek, L. Olson, and P. Brooks. 2010. *Molten Salts for High Temperature Reactors: University of Wisconsin Molten Salt Corrosion and Flow Loop Experiments – Issues Identified and Path Forward*. Idaho Falls: Idaho National Laboratory.
- Schepers, G. W. 1964. "Biological Action of Beryllium. Reaction of the Monkey to Inhaled Aerosols." *Industrial Medicine and Surgery* 33: 1–16.
- Schluderberg, D. C., J. H. Huang, L. Pong, and D. K. Sze. 1983. "Thermal and Mechanical Design of a Double-Walled Steam Generator". Madison, Wisconsin: Fusion Technology Institute, University of Wisconsin.
- Shaffer, J. H. 1971. *Preparation and Handling of Salt Mixtures for the Molten Salt Reactor Experiment*. Oak Ridge: Oak Ridge National Laboratory.
- Simonds, J. 2010. *Technical Program Plan for the Next Generation Nuclear Plant/Advanced Gas Reactor Fuel Development and Qualification Program*. Idaho Falls: Idaho National Laboratory.
- Simpkins, J. E., R. A. Strehlow, P. K. Mioduszewski, and T. Uckan. 1989. "Control of Water Absorption by Purification of Graphite." *Journal of Nuclear Materials* 162-164 (1): 871–887.
- Smith, A. N. 1965. *MSRE Design and Operations Report, Part IX, Safety Procedures and Emergency Plans. Engineering & Technology*. Vol. 4. Oak Ridge, Tennessee: Oak Ridge National Laboratory. doi:10.1049/et.2009.1706. <http://digital-library.theiet.org/content/journals/10.1049/et.2009.1706>.
- Snead, L. L., Y. Katoh, and K. Ozawa. 2011. "Stability of 3-D Carbon Fiber Composite to High Neutron Fluence." *Journal of Nuclear Materials* 417 (1): 629–632.
- Snead, L. L., T. Nozawa, Y. Katoh, T.-S. Byun, S. Kondo, and D. A. Petti. 2007. "Handbook of SiC Properties for Fuel Performance Modeling." *Journal of Nuclear Materials* 371 (1-3)

- (September): 329–377. doi:10.1016/j.jnucmat.2007.05.016.  
<http://linkinghub.elsevier.com/retrieve/pii/S0022311507007623>.
- Sohal, M. S., M. A. Ebner, P. Sabharwall, and P. Sharpe. 2010. *Engineering Database of Liquid Salt Thermophysical and Thermochemical Properties*. Idaho Falls: Idaho National Laboratory.
- Stainsby, R., M. Worsley, A. Grief, F. Dawson, M. Davies, P. Coddington, J. Baker, and A. Dennier. 2009. “Development of Local Heat Transfer Models for Safety Assessment of High Temperature Gas-Cooled Reactor Cores--Part I: Pebble Bed Reactors.” *Journal of Engineering for Gas Turbines and Power* 132 (1): 012906–012914.
- Stansfield, O. M., W. A. Simon, and A. M. Baxter. 1983. *Fuel Performance Models for High-Temperature Gas-Cooled Reactor Core Design*. GA Technologies.
- Suzuki, A., T. Terai, and S. Tanaka. 1998a. “Change of Tritium Species in Li<sub>2</sub>BeF<sub>4</sub> Molten Salt Breeder Under Neutron Irradiation at Elevated Temperature.” *Journal of Nuclear Materials* 258-263, P: 519–524.
- . 1998b. “In-Situ HT Release Behavior from Molten Li<sub>2</sub>BeF<sub>4</sub> Salt.” *Fusion Engineering and Design* 39-40: 781–785.
- . 2000. “Tritium Release Behavior from Li<sub>2</sub>BeF<sub>4</sub> Molten Salt by Permeation Through Structural Materials.” *Fusion Engineering and Design* 51-52: 863–868.
- Swank, D., J. Lord, D. Rohrbaugh, and W. E. Windes. 2010. *AGC-2 Graphite Preirradiation Data Package*. Idaho Falls: Idaho National Laboratory.
- Swank, W. 2011. *AGC-1 Post-Irradiation Examination Status*. Idaho Falls: Idaho National Laboratory.
- Thoma, R. E. 1971. *Chemical Aspects of MSRE Operations*. Oak Ridge, Tennessee: Oak Ridge National Laboratory.
- Till, C. E., Y. I. Chang, and W. H. Hannum. 1997. “The Integral Fast Reactor-An Overview.” *Progress in Nuclear Energy* 31 (1/2): 3–11.
- Vollman, R., R. Phelps, D. Carosella, J. Saurwein, J. Taylor, J. Shoesmith, A. Donaldson, P. Andrews, and J. Jun. 2008. *NGNP Composites R&D Technical Issues Study*. Oak Ridge, Tennessee: Oak Ridge National Laboratory.
- Williams, D. F., and L. M. Toth. 2005. *Chemical Considerations for the Selection of the Coolant for the Advanced High-Temperature Reactor*. Oak Ridge, Tennessee: Oak Ridge National Laboratory.
- Williams, D. F., L. M. Toth, and K. T. Clarno. 2006. *Assessment of Candidate Molten Salt Coolants for the Advanced High-Temperature Reactor (AHTR)*. Oak Ridge: Oak Ridge National Laboratory.
- Windes, W. E., D. V. Croson, and G. Roberts. 2010. *Graphite Technology Development Plan*. Idaho Falls: Idaho National Laboratory.
- Windes, W. E., P. A. Lessing, Y. Katoh, L. L. Snead, E. Lara-Curzio, J. Klett, C. Henager Jr., and R. J. Shinavski. 2005. *Structural Ceramic Composites for Nuclear Applications*. Idaho Falls: Idaho National Laboratory.
- Zinkle, S. J., J. T. Busby, K. J. Leonard, L. L. Snead, D. T. Hoelzer, T. S. Byun, and M. Li. 2006. “Refractory Alloys for Nuclear Applications.” In *Topical Meeting on Nuclear Fuels and Structural Materials for the Next Generation Nuclear Reactors, 2006 ANS Annual Meeting*. La Grange Park: American Nuclear Society.





**Table A-1. Reactor Functional Requirements Related to Thermal Hydraulic Modeling of the Core**

Subsystem Functional Requirements		Related Metrics	
<i>Primary Coolant</i>			
1	Provide negative temperature feedback	RDC 2	Coolant to fuel temperature difference; temperature distribution in the core
2	Coolant remains in liquid phase	RDCs 3, 5	Minimum coolant temperature
3	Maintain low temperature for coolant in vicinity of reactor vessel and other core metallic components	RDC 5	Maximum outlet coolant temperature
4	Provide sufficient flow to maintain 100°C core temperature rise		Core temperature rise
5	Control reflector by-pass leakage		Minimize core pressure drop
<i>Graphite Reflectors</i>			
6	Provide thermal inertia		Maximize heat transfer flux/coefficient with graphite blocks
<i>Fueling Stand-Pipe</i>			
7	Prevent primary coolant inventory loss	RDC 4	Minimize core inlet pressure (ie core pressure drop)
<i>Fuel Subsystem</i>			
8	Transfer heat to the coolant	RDC 3	Predict temperature drop across the fuel element; predict core pressure drop during natural circulation
9	Fuel element manufacturability (and fuel qualification requirements)		Fuel element geometry should respect manufacturability limits
10	Provide the first barrier to radionuclide emission	RDC 1	Predict peak fuel temperature
11	Provide negative temperature reactivity feedback	RDC 2	Minimize average fuel temperature
12	Minimize difference between average fuel and coolant temperatures at full power operation (for ATWS response)		Minimize coolant to fuel temperature difference

In summary, the primary objectives for this optimization study are: (1) to minimize the difference between the average fuel temperature and the bulk fluid temperature, (2) to minimize core pressure drop during forced circulation, and (3) to maximize heat transfer with the graphite reflectors during transients.

Subsequently, the objectives of thermal-hydraulic modeling of the core are: (1) to predict the coolant and fuel temperature distribution in the core, during forced and natural circulation, and (2) to predict pressure drop in the core during forced and natural circulation.

The following metrics are determined by sub-systems external to the core, and are not considered in this analysis: (1) minimum coolant temperature, (2) maximum outlet coolant temperature, and (3) core temperature rise.

## A.2 COMSOL Model

Optimal results have been obtained by changing the positions of inlet and outlet faces and ports, and changing the mass flow rate distribution among the inlets and outlets.

The final geometry of the model is shown in Figure A-2, and details on the locations and dimensions of the outlet ports are provided in Table A-2.

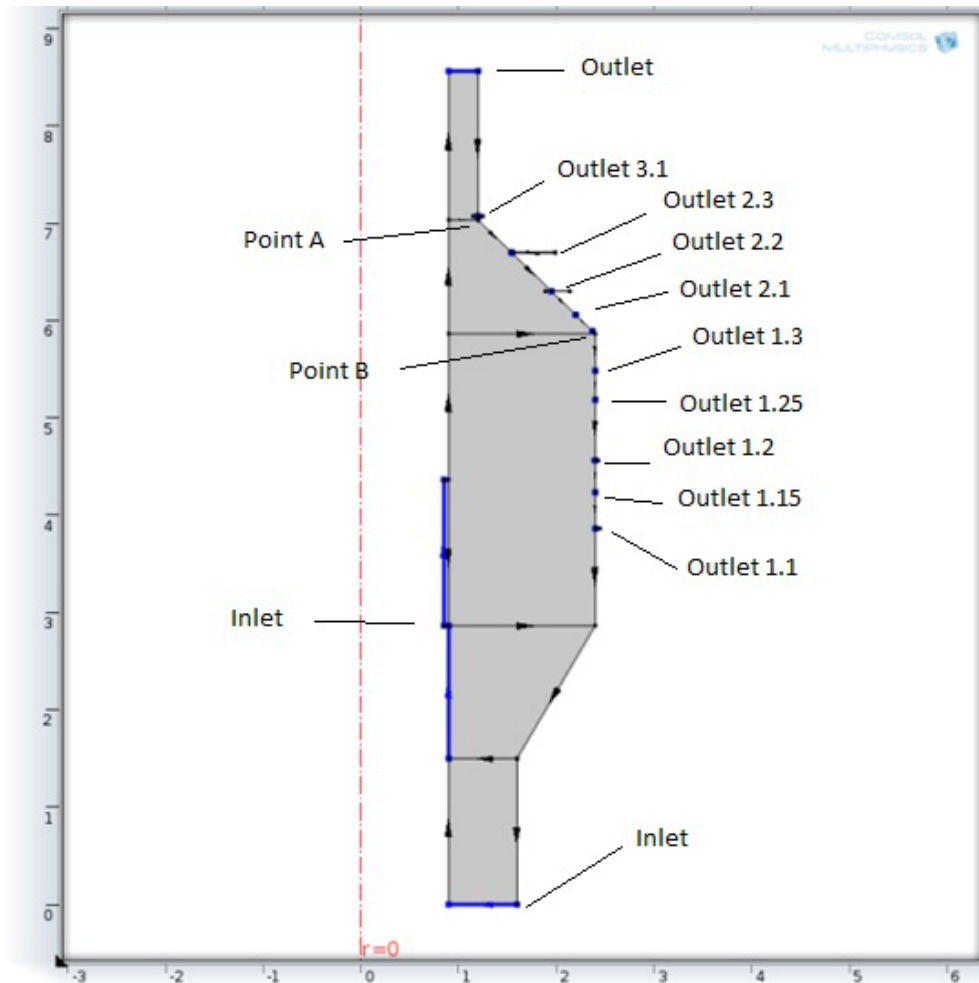


**Figure A-2. Geometric Configuration of the Annular PB-AHTR Core as Modeled in COMSOL Multiphysics**

**Table A-2. Detailed Positions and Dimensions of the Outlet Ports in the COMSOL Multiphysics Model of the Annular PB-AHTR Core**

<b>Port</b>	<b>Position</b>	<b>Width</b>
Outlet 1.1	2 m from Point B	0.005 m
Outlet 1.15	1.63 m from Point B	0.001 m
Outlet 1.2	1.26 m from Point B	0.003 m
Outlet 1.25	0.65 m from Point B	0.001 m
Outlet 1.3	0.38 m from Point B	0.003 m
Outlet 2.1	0.08 m from Point B	0.002 m
Outlet 2.2	0.45 m from Point B	0.008 m
Outlet 2.3	0.88 m from Point B	0.01 m
Outlet 3.1	0.1 m from Point A	0.005 m

Results obtained with this model are shown in Chapter 1.

## Appendix B Neutronic Model for FHR

UCB has been developing methods to analyze the neutronics performance of FHRs. The baseline design for the commercial prototype, PB-FHR, and the FHR test reactor (FHTR), utilize continuously refueled pebble fuel. The continuously refueled depletion problem is challenging because there are not many widely distributed tools to analyze these systems. Furthermore, the concentration of  ${}^6\text{Li}$  equilibrates in the salt coolant as it is constantly being removed in (n,T) reactions and generated in (n, alpha) reactions on the  ${}^9\text{Be}^1$ . UCB has developed a tool to analyze these systems at their equilibrium state ( $k_{\text{effective}} = 1$ , with no control elements engaged) BEAU<sup>2</sup>. The most developed design that the FHR IRP has access to is the 900MWth PB-AHTR as described in “Fuel Design for the PB-FHR” so this design will be used to generate environmental parameters used for corrosion and degradation models. This appendix describes the neutronics model used to generate the power distribution and radiation damage environment for the thermal hydraulics model, fuel performance and materials degradation models.

### B.1 TRISO Geometry

FHRs use coated-particle high temperature fuels originally developed for high temperature gas-cooled reactor. The TRISO layer thicknesses of the PB-FHR fuel are not optimized for fuel performance. The thermal hydraulics and neutronics performance of the PB-FHR are not expected to be sensitive to the specific coated-particle fuel design. The current methodology has been to select representative values from literature – later on when TRISO fuel performance tools are available, the fuel performance will be assessed and the fuel design will be updated. Coated-particle fuel performance codes developed are not well distributed.

The baseline fuel design utilizes LEU  $\text{UO}_{1.5}\text{C}_{0.5}$  fuel kernels enriched to 19.9w%  ${}^{235}\text{U}$ . The stoichiometry of fuel kernel (ratio of oxygen and carbon) have little effect on reactor performance with respect to thermal hydraulics and neutronics. There is little effect on the conductivity of the fuel kernel; furthermore, the fuel kernel volume makes up only a small fraction of the active region volume so there is little effect on the effective conductivity of the active region on the pebble scale. Carbon is a better neutron moderator than oxygen, but the effect on moderation is likely swamped by the moderation of the structural carbon – this is a 0.5-1 increase in the carbon to heavy metal ratio whereas the baseline fuel design has a ratio of 300. However, the carbon to heavy metal ratio has a significant effect on the fuel performance, because it reduces the amoeba effect. Literature on the cost of coated-particle fuel suggest that fuel fabrication costs – the dominant cost for high temperature reactor fuel – scale linearly with heavy metal loadings of fuel compacts. Therefore, fuel costs are minimized by maximizing burnup, which increases almost linearly with enrichment.

The function of the buffer region is to accept gaseous fission products. The silicon carbide layer’s function is to contain the fission products. The inner and outer pyrolytic carbide layers function to interface between the silicon carbide layer and the buffer as well as the silicon carbide layer and the graphite matrix, respectively. The thicknesses of these particle coatings are taken as constant values from literature for the previous design analysis. The thicknesses of the silicon carbide layer is dictated by the ability to coat pebbles.

### B.1.1 Neutronics Model

To accurately account for the well-known double heterogeneity self-shielding effect, continuous energy Monte Carlo code, MCNP5 version 1.51 with ENDF VII nuclear data, is used to perform neutron transport. The model developed explicitly models the fuel kernels, but homogenizes the TRISO layers and graphite matrix. These kernels are models on a simple cubic lattice as shown in Figure B-1.

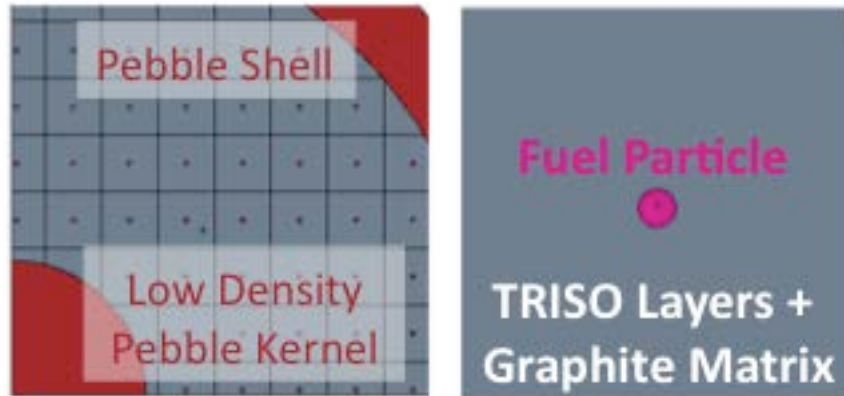


**Figure B-1. MCNP5 Model of TRISO Particles: (left) Pebble Scale Model with TRISO Particles in a Simple Cube Lattice; (right) a Single Unit Cell of a TRISO Particle with the TRISO Layers and Graphite Matrix Homogenized Together**

## B.2 Pebble Geometry

Preliminary economic analyses indicate a high cost of particle fuel fabrication. The strategy to mitigate the impact of these fuel fabrications costs is to maximize burnup by using the maximum allowable enrichment, 19.9w%,  $^{235}\text{U}$  and using continuously fueled fuel, the pebble fuel. A continuously refueled core can operate without any excess reactivity, maximizing the neutron economy and thereby maximizing burnup. Furthermore, this fuel cycle decouples the shutdown frequency from burnup to increasing the flexibility of the fuel design and enhancing the capacity factor.

One of the functional requirements of the pebble fuel elements is that they are buoyant in the liquid salt at operating conditions. The buoyancy in these pebbles is controlled by the size and density of the inert low-density graphite core of the annular pebbles.

The only credible accident to stress the integrity of FHR systems are anticipated transients without scram, ATWS, events that shutdown because of the systems inherent temperature reactivity feedbacks. The characteristic average temperature of the fuel kernels limits the maximum temperature in ATWS transients. Therefore, using the annular fuel form to enhance heat transfer from the fuel mitigates the consequences of these ATWS accidents.

### B.2.1 Neutronics Model

The pebbles are well-mixed with respect to burnup within the PB-AHTR core. The neutronics of the system are mostly dependent on the aggregate flux spectrum and composition of the pebble bed rather than any specific burnup. This well-mixed pebble bed is modeled by a

lattice of face centered cubic unit cell of pebbles with 4 different burnup states (low-, low-intermediate- high-intermediate- and high- burnup) as shown in Figure B-2. Each pebble has only one type of fuel kernel with a single composition corresponding to a give burnup state. This composition is the time averaged composition of averaged over one fourth of the residence time in the PB-FHR (i.e. this composition represents all the pebbles with burnups in this residence time bin). More details of this model are discussed in the fuel cycle analysis section.

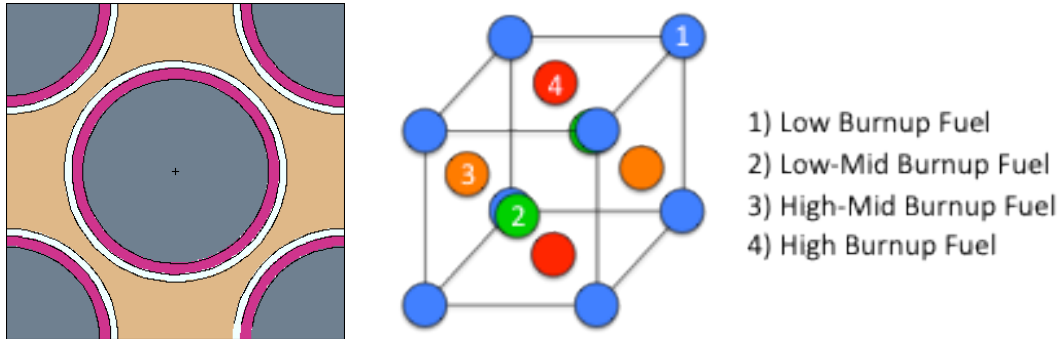


**Figure B-2. FCC Pebble Unit Cell Model: (left) MCNP5 Model of Annular Fuel Pebbles: (orange) Flibe, (white) Pebble Shell, (pink) Active Region, and (grey) Inert Pebble Core; (right) Burnup States Within an FCC Unit Cell Model**

### B.3 Full Core Geometry

The PB-AHTR can be segmented into 5 axial regions: entrance, expansion, active, converging and defuel chute. The goals of the core configuration are to concentrate the fission energy production in the active region, enable control of the nuclear chain reaction and efficiently transfer the heat from the pebbles to the secondary loop. This core configuration originally was developed for an NE170 senior design class (Hong et al. 2009).

The core has a wide active region to promote neutron multiplication. The expansion and converging region connect the entrance and defueling chute to the active region. The entrance region must be thick enough to establish radial pebble zones (the minimum thickness of these radial pebble zone scales with pebble size rather than reactor size). The defueling chute is size to prevent bridging and jamming.

The PB-AHTR must utilize either a blanket of fertile thorium pebbles or a graphite pebble reflector to extend the lifetime of the outer graphite reflector to the life of plant. Preliminary analyses envision that the outer solid graphite reflector would be arduous to replace so it must last the life of plant, 60-80 EFPD – whereas it is feasible to replace the inner solid graphite reflector. Trade design studies show that there is little gain in terms of fuel utilization or reduction in fuel costs from utilizing a thorium blanket rather than a graphite pebble reflector. Therefore, the baseline configuration of the PB-AHTR utilizes a graphite pebble reflector. Experiments and computational simulation show that these pebble bed radial zones occupy constant cross sectional area fractions of the pebble bed, the minimum cross section area graphite pebble blanket for the PB-AHTR core consists of 21% of the cross sectional area and will enable the graphite reflector to survive to 170 years, assuming a maximum radiation damage limit of 15

DPA. During this workshop, experience of experts from ORNL show graphite can be used up to 25DPA (15DAP is too conservative).

### B.3.1 Physical System

Figure B-3 presents the geometry of the annular fuel pebble. The geometric and material definition is presented in Table B-1.

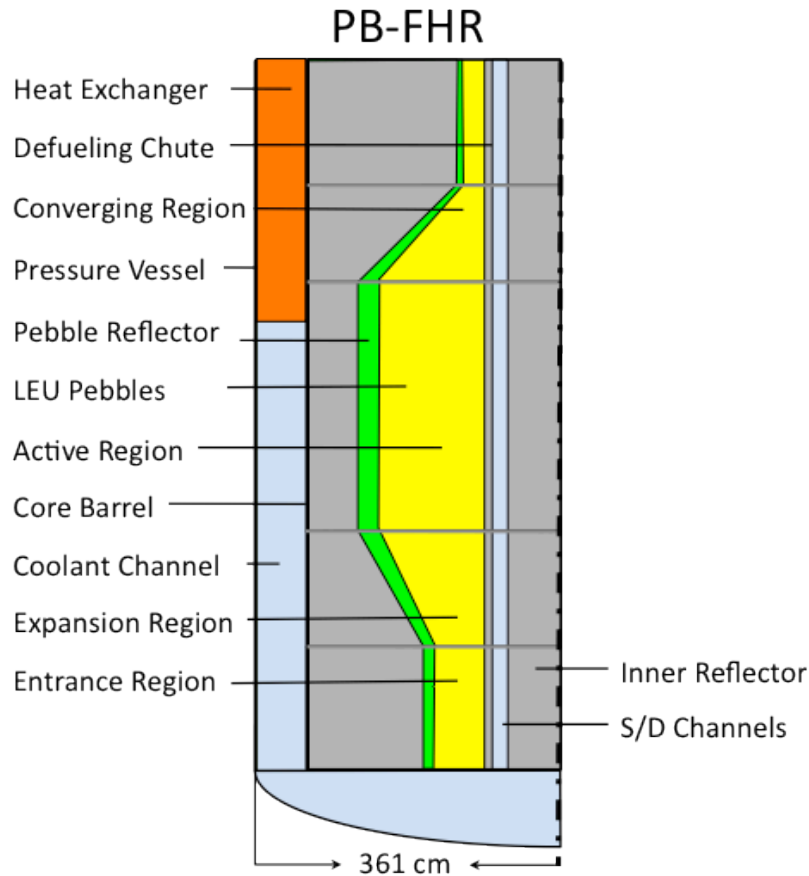


Figure B-3. Baseline PB-FHR Full Core Geometry

Table B-1. Geometric and Material Definition of the Baseline PB-AHTR Full Core

Core Component	Component Dimension	Dimension Value
Inner graphite reflector	Outer radius, cm	90
Pebble bed (entrance)	Outer radius, cm	160
	Height, cm	150
Pebble bed (expansion region)	Expansion angle, degrees	60

Pebble bed (active region)	Outer radius, cm	240
	Height, cm	300
Pebble bed (converging region)	Converging angle, degrees	45
Pebble bed (defueling chute)	Outer radius, cm	120
	Height, cm	150
Outer graphite reflector	Outer radius, cm	300

### B.3.2 Neutronics Model

The TRISO particle and pebble models are implemented into a full-core neutronics model. Everything in the active region is modeled at a single characteristic temperature. The graphite pebble reflector and the active pebble bed are assumed have a perfect interface, composed of cylindrical and conical surfaces that “clip” pebbles as well as TRISO particles. The pebbles in graphite pebble reflectors are also modeled explicitly in a FCC unit cell similar to the LEU pebbles. Figure B-4 presents the geometry of the full-core PB-AHTR MCNP5 model.

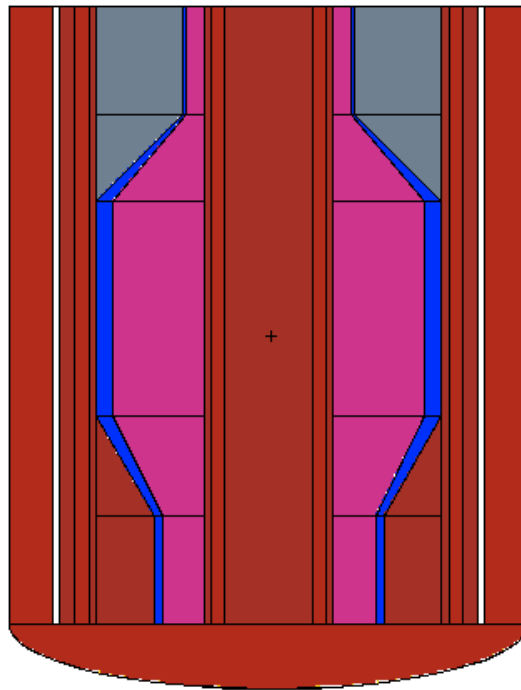


**Figure B-4. MCNP5 Model of Full Core PB-AHTR**

The equilibrium state of the PB-AHTR was determined using BEAU as described in Section B.4. The radiation damage distribution, neutron and gamma heating and tritium source terms were then calculated using this equilibrium MCNP5 model using flux multiplier tallies.

## B.4 Fuel Cycle Analysis

UCB has developed a coupled neutron transport and transmutation framework to identify the equilibrium state of a continuously refueled nuclear power system, Burnup Equilibrium Analysis Utility (BEAU). BEAU runs continuous energy Monte Carlo neutron transport using MCNP5 to calculate the neutron multiplication factor, flux distribution and system- and burnup- specific cross sections. BEAU then controls the depletion analysis using ORIGEN to follow a control volume of fuel through the core. BEAU depletes the control volume fuel under constant flux with the system- and burnup specific cross sections in each burnup state, advancing the fuel from low burnup states to high burnup states, as shown in Figure B-5. The material composition vector evolutions over each time step are collapsed to a single equilibrium composition vector by a time-weighted average as shown in Figure B-6. The well-mixed pebble bed is approximated by a repeated FCC unit cell with 4 burnup states as shown in Figure B-6. BEAU also searches iteratively for the fuel cycle parameters (fission neutron source and cycle length) to impose a target  $k$  at a given power using the algorithm shown in Figure B-7.

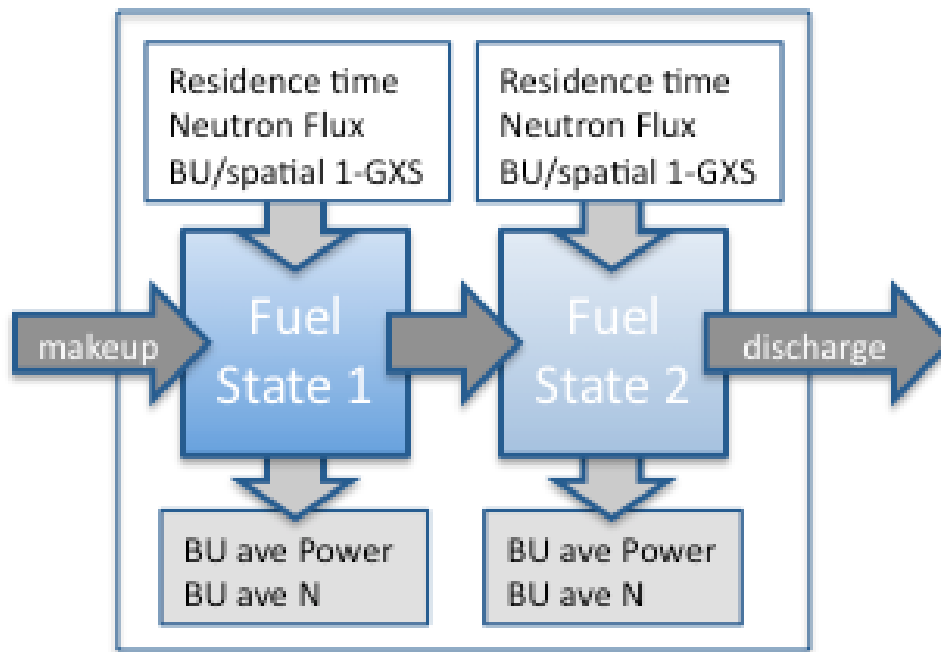


**Figure B-5. Simplified Transmutation Flow Chart for a Two Burnup State System: (dark gray) Fuel Composition Flow, (white) Independent Parameters Supplied from Fuel Cycle Search and Neutron Transport, (light gray) Dependent Parameters Supplied from Transmutation Analysis**

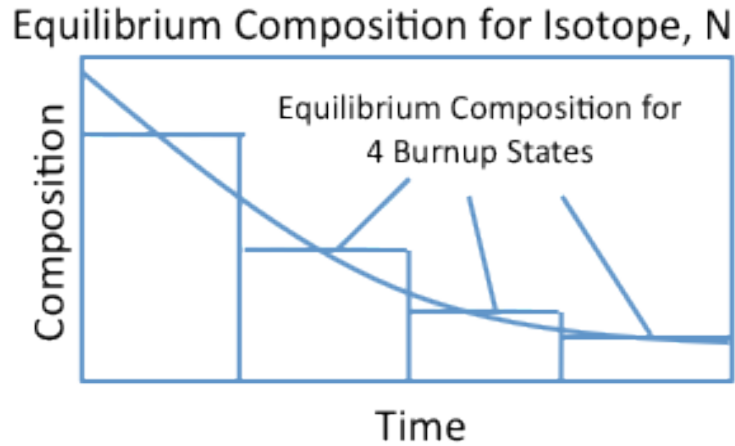


**Figure B-6. Continuous Composition Evolution Divided into Four Burnup States**

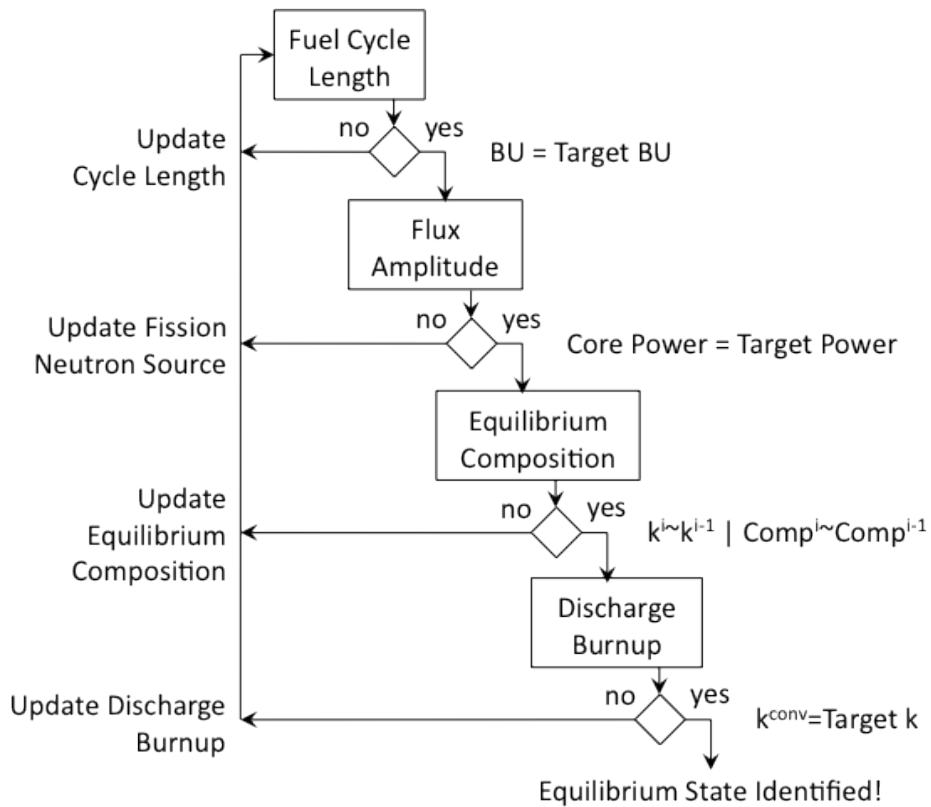


**Figure B-7. BEAU Iterative Equilibrium Depletion Algorithm**

## Appendix C Fuel Options

The FHR is a new reactor concept—about a decade old. Its characteristics are a consequence of combining a high-temperature fuel with a high-temperature low-pressure fluoride salt. There are several candidate fuels. The near-term option is the graphite-matrix coated-particle fuel because of its (1) demonstrated high-temperature capability and (2) compatibility with high-temperature salts. In the longer term, there are other candidates that use SiC as a major structural material. Silicon carbide has received attention because of the radiation resistance of SiC and its inert characteristics. Silicon carbide could have major advantages for some types of FHRs. The major SiC research programs are associated with fusion, high-temperature gas-cooled reactors, and more recently as a cladding material for light-water reactors.

The IRP of MIT, UCB, and UW is developing a preconceptual design of a commercial FHR and a Fluoride-salt-cooled High-temperature Test Reactor (FHTR). The preconceptual design of the commercial FHR will be based on graphite-matrix coated-particle fuel because that is the only option today. However, the design of the test reactor should consider both near-term testing and long-term testing. This appendix is a first effort to define the possible range of future FHR fuels that might be tested in a FHTR. Our evaluation is separated into fuels in terms of materials and geometries.

### C.1 Fuel Material

#### C.1.1 Graphite-Matrix Coated-Particle Fuel

Graphite-matrix coated-particle fuel is the leading option for FHR fuel as it is the only fuel with demonstrated high-temperature capabilities and near-term availability (Greene et al. 2010). In this fuel type, fuel microspheres (TRISO particles) are encased in a graphite matrix, which can be shaped into many forms including pebbles, plates, and cylindrical compacts. The graphite serves as both a structural component and as the primary neutron moderator. Modern versions of this type of fuel have evolved from similar fuels that have been demonstrated in several helium-cooled high-temperature reactors. Peach Bottom Unit 1, the Fort St. Vrain Reactor (FSVR), the Arbeitsgemeinschaft Versuchsreaktor (AVR), the Thorium High-Temperature Reactor (THTR), and more recently, the Chinese HTR-10 pebble-bed prototype reactor and the Japanese High-Temperature Test Reactor (HTTR) have all successfully demonstrated variations of graphite-matrix coated-particle fuel (C. Forsberg 2008).

#### C.1.2 SiC-Matrix Coated-Particle Fuel

Silicon-carbide-matrix (SiCm) coated-particle fuel is a variation of graphite-matrix coated-particle fuel that replaces graphite with SiC. Only limited work has been done on this advanced fuel at ORNL. The objectives of this substitution are to exploit SiC's resistance to radiation damage and to create a fuel form that is more robust under accident and repository conditions. In a reactor, graphite first shrinks and then swells as a function of fast neutron fluence. SiCm fuel provides much more dimensional stability under irradiation, as can be seen in the Figure C-1.

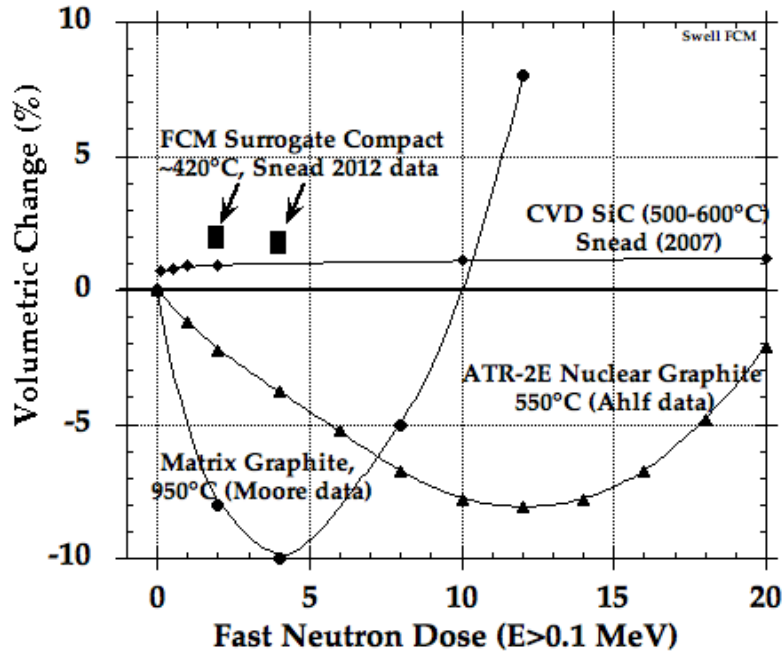


**Figure C-1. Dimensional Change Contrast of CVD SiC and FCM Fuel with Nuclear Graphite ATR-2E and Matrix Graphite (C. W. Forsberg, Terrani, et al. 2012)**

SiCm fuel provides less moderation than graphite-matrix fuel, and if the power density of the TRISO particles and loading are unchanged, the core power density will be about 30% lower if SiCm fuel is used instead of graphite-matrix fuel. The lower power density subsequently results in lower peak fuel temperatures. Additional moderation can be achieved in SiCm fuel by increasing the thickness of the graphite layers in the TRISO fuel kernels and/or embedding graphite microspheres into the SiCm. The use of SiCm in place of graphite-matrix fuel will also require changes to certain reactor systems, particularly the refueling system, as the density of SiCm coated-particle fuel is greater than the density of the salt, so the fuel will not be buoyant (C. W. Forsberg, Terrani, et al. 2012).

### C.1.3 SiC Pin Fuel

The longer-term option may exist to create an FHR with a pin-type fuel assembly. The graphite and moderator would be separated from the fuel. Conceptually this would be similar to the British Advanced Gas-Cooled Reactors with graphite matrix and pin type fuel assemblies. The fuel would be in pellet form. This is a longer-term option because the SiC pin must not only provide structural support but *it must be a sealed container for fission product gases*. While SiC has been developed as the cladding for coated particle fuel, the joining technology does not yet exist for sealed tubes. Major work is underway to develop this type of pin for light-water reactor fuel; thus, the future of this option will be strongly dependent upon progress for advanced LWR fuels.

## C.2 Fuel Geometry

### C.2.1 Pebble Fuel

Pebble fuel is comprised of coated-particle fuel kernels embedded in spherical graphite elements. The pebble diameter is typically around 6 cm. Pebbles are arranged stochastically. Pebbles are added to the core until criticality is reached. Successful use of pebble fuel has been demonstrated in several high-temperature helium-cooled reactors: the Chinese HTR-10 and the German AVR and THTR (C. Forsberg 2008).

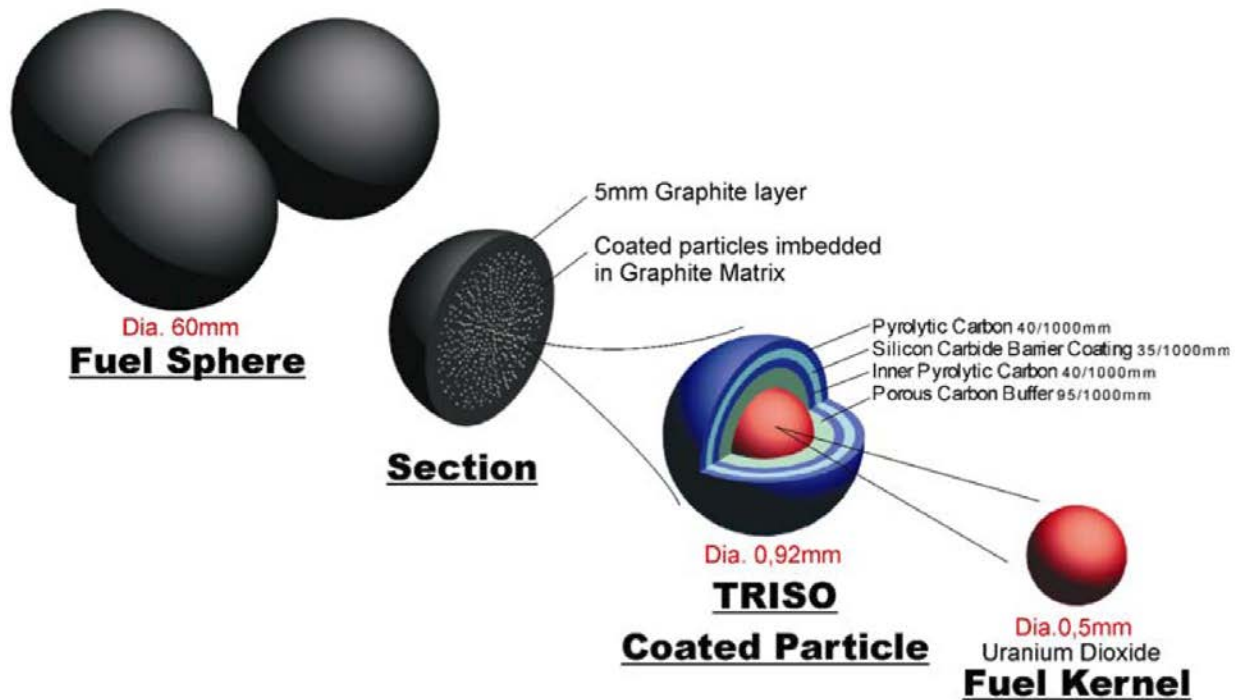


Figure C-2. Composition of Pebble Fuel (C. Forsberg 2008)

Pebble fuel has several advantages over other geometries: (1) lower fabrication costs than other geometries because there is no complex geometry internal to the fuel; (2) ability to perform on-line refueling; and (3) less complex, and likely lower cost, refueling systems (C. W. Forsberg, Hu, et al. 2012). These advantages—primarily the less-complex refueling requirements—led to the inclusion of pebble fuel in the baseline design of the commercial FHR.

Preliminary economic analyses indicate that particle fuels will have high fabrication costs. Continuous refueling may be able to offset high fabrication costs by maximizing burnup (i.e. decreasing the amount of fuel required for producing a given amount of energy). Pebble fuel is the only fuel geometry under consideration that allows continuous refueling, which allows improved neutron economy and higher burnup because the reactor can operate without any excess reactivity.

The same property of pebble fuel that enables continuous refueling is not without drawbacks. The stochastic movement of pebbles means that instrumentation cannot be attached or inserted

directly into the fuel. Additionally, if graphite-matrix fuel is used, the pebbles will float freely in the coolant salt because the density of the fuel is lower than that of the salt. In contrast, the fuel in all of the other geometries is static, meaning that the fuel can be prevented from floating by adding weights or directly attaching the fuel to the surrounding structures (C. Forsberg 2008).

#### *Advantages*

- Demonstrated technology
- Continuous and less complex refueling
- Potentially higher capacity factor with on-line refueling
- Higher burnup than in other fuel geometries

#### *Disadvantages*

- Instrumentation cannot be located directly in the fuel
- Low flexibility in fuel-to-carbon-to-coolant ratio.

### **C.2.2 Plate Fuel**

Graphite-matrix coated-particle plate fuel is a fixed (static) fuel that is under development at ORNL. This fuel variant is composed of plates (slabs) of graphite-matrix coated-particle fuel arranged into hexagonal fuel assemblies. The fuel in each plate is located in fuel stripes on both sides of the plate. This results in lower peak temperatures relative to a plate of uniform fuel distribution. The space between the plates provides low-resistance channels for coolant flow, which enable increased passive cooling during loss of forced circulation scenarios.

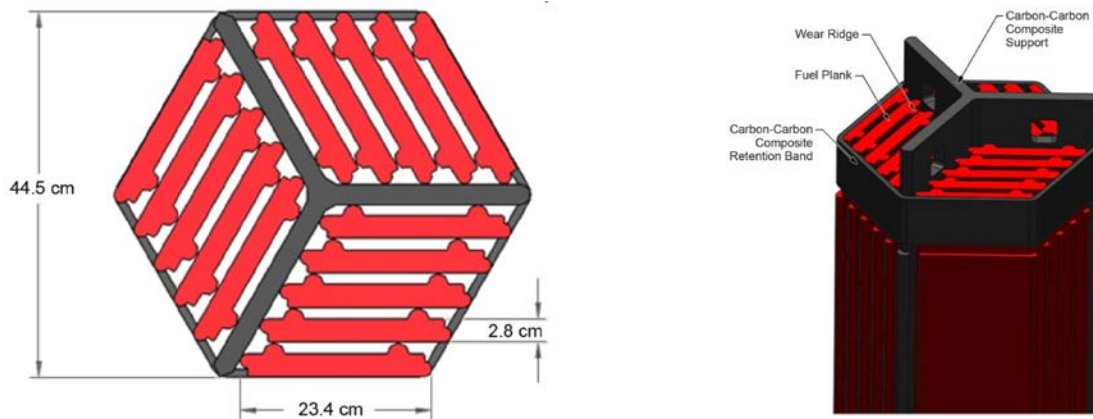


**Figure C-3. Hexagonal Plate Fuel Assembly (Greene et al. 2010)**

Plate fuel uses the same materials as pebble fuel, but arranged into a different geometric form. The similarity between pebble and plate fuel appears to indicate that plate fuel should not be significantly more difficult to manufacture than pebble fuel, but unlike pebble fuel, plate fuel allows high flexibility in the fuel-to-carbon-to-coolant ratio. However, because plate fuel is fixed in place, lower burnup at the top and bottom of each fuel plate contributes to a lower average burnup relative to pebble fuel, which achieves uniform burnup through the continual movement of the fuel through the core (Greene et al. 2010).

### Advantages

- High flexibility in fuel-to-carbon-to-coolant ratio
- Instrumentation can be located directly in the fuel
- Enhanced passive cooling capabilities

### Disadvantages

- No prior experience with manufacturing plate fuel.

### C.2.3 Prismatic-Block Fuel

Prismatic-block fuel was originally developed for use in high-temperature gas-cooled reactors (HTGRs). In this implementation, fuel microspheres are encased in a graphite matrix, which is shaped into the form of annular fuel compacts. The compacts in the FSVR were not annular, but the more recent HTTR (Japan) incorporated annular fuel compacts. The annular compacts were designed to decrease the peak fuel temperature by keeping the center of the fuel element, where the peak temperature would otherwise occur, free of fuel.

At FSVR, these compacts are loaded into fuel channels in the graphite block. Coolant flows through separate channels in the graphite blocks. In the Japanese HTTR, the compacts are loaded into hollow, cylindrical sleeves that are placed in channels in large prismatic blocks of graphite. Coolant flows between these sleeves and the graphite block (see figure)

Coolant channels in a salt-cooled reactor can be made smaller than in gas-cooled reactors because of salt's superior heat transport properties relative to gas. Prismatic-block fuel has a large base of operating experience (in Peach Bottom Unit 1, the FSVR, and the HTTR) and the technology is considered fully developed for use gas-cooled reactors (C. Forsberg 2008; Casino Jr. 2006).

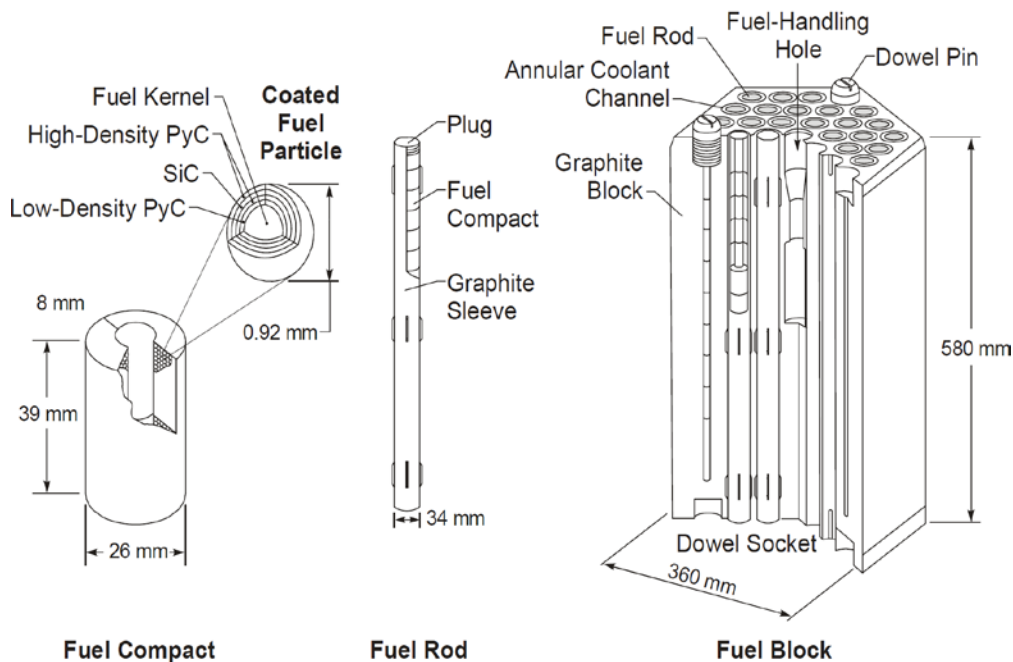


Figure C-4. HTTR Prismatic-Block Fuel (C. Forsberg 2008)

### Advantages

- Large base of operational and fuel-fabrication experience
- High flexibility in fuel-to-carbon-to-coolant ratio
- Instrumentation can be located directly in the fuel

### Disadvantages

- Complicated refueling requirements.

## C.2.4 Pin Fuel

Pin-type fuel, comprising  $\text{UO}_2$  fuel pellets surrounded by SiC or high-nickel alloy (e.g. Alloy N, also called Hastelloy®-N and INOR-8) cladding, has been considered for use in FHRs. Fuel pins are typically arranged in clustered assemblies, in which multiple concentric rings of fuel pins and a single central support pin are held in place by a grid structure and are moved as a single unit. The core is arranged as a square lattice array of clustered fuel assemblies surrounded by blocks of graphite moderator. This arrangement of clustered assemblies and graphite moderator has been thoroughly demonstrated in the United Kingdom's fourteen Advanced Gas Reactors (AGRs) that used carbon dioxide gas as the coolant.

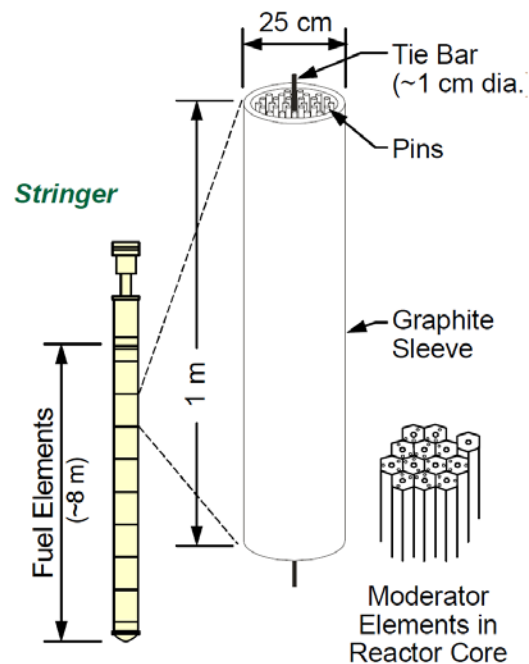


**Figure C-5. Pin-Type (“stringer”) Fuel (Ingersoll, Forsberg, and MacDonald 2007)**

In AGRs, stainless steel is used for cladding and for the grid structure that holds each assembly together. For use in FHRs, these components could be constructed of SiC or metal. The British did limited work on using SiC for this application. The challenges include sealing pins to hold in fission gases and demonstrating the performance of SiC in this application. If metal is used, it would require a high-nickel alloy clad for corrosion resistance. Historically high-nickel alloy clad has not been considered viable because of neutron absorption that creates alpha

particles resulting in helium inclusions that weaken the clad. Recent advances in centrifuge technology may allow isotopic separation of nickel isotopes to create nickel-alloy clad without helium buildup. Either option involves major technical uncertainties and a long development program. The SiC option would be strongly preferred because of its much higher temperature capability. SiC is being considered as an advanced cladding material for LWRs. If it is successfully developed for this application, it could become a candidate for an FHR with pin fuel assemblies.

The economic advantages of using pin-type fuel are using pellets rather than coated particle fuel and use of the existing fuel fabrication infrastructure—factors that resulted in Areva looking at a pin-type fuel for FHRs. Commercial facilities have decades of experience in producing pin-type fuel assemblies at predictable costs. There is no equivalent infrastructure for any other fuel form (C. Forsberg 2008; Casino Jr. 2006).

The second major incentive for using pin-type fuel is the physical decoupling of fuel and moderator in the core. Graphite lifetime in a reactor is limited by fast neutron fluence, but in typical FHR configurations, the fuel is depleted long before the limit on graphite lifetime is reached. This results in unnecessary graphite waste production in configurations in which the moderator and fuel are inseparable (as is the case with pebble fuel and, because of refueling practicalities, prismatic-block fuel). The separation of fuel and moderator also simplifies refueling operations. The moderator blocks can be fastened in the core to counteract their buoyancy, thereby enabling maintenance and refueling without the complication of fuel-block movement (Casino Jr. 2006).

#### *Advantages*

- Low fabrication cost
- Lower graphite waste production
- High flexibility in fuel-to-carbon-to-coolant ratio
- High flexibility in axial fuel enrichment and radial fissile loadings
- Instrumentation can be located directly in the fuel

#### *Disadvantages*

- No operational experience with pins in high-temperature fluoride-salt environment
- Major R&D to demonstrate feasibility.

## Appendix D Thermal Hydraulic Modeling of the PB-AHTR Core in RELAP5

At this point on the development path of the FHR design, all thermal-hydraulic analyses of the primary loop have been performed using the RELAP5 systems analysis code. This Appendix describes the PB-AHTR model in RELAP5. Results from this model are used in Chapter 4. More details on thermal-hydraulic modeling of the FHR can be found in the second FHR Workshop White Paper.

Figure D-1 shows a PB-AHTR plant nodalization diagram that has been used for modeling in RELAP5, with the major sub-systems indicated.

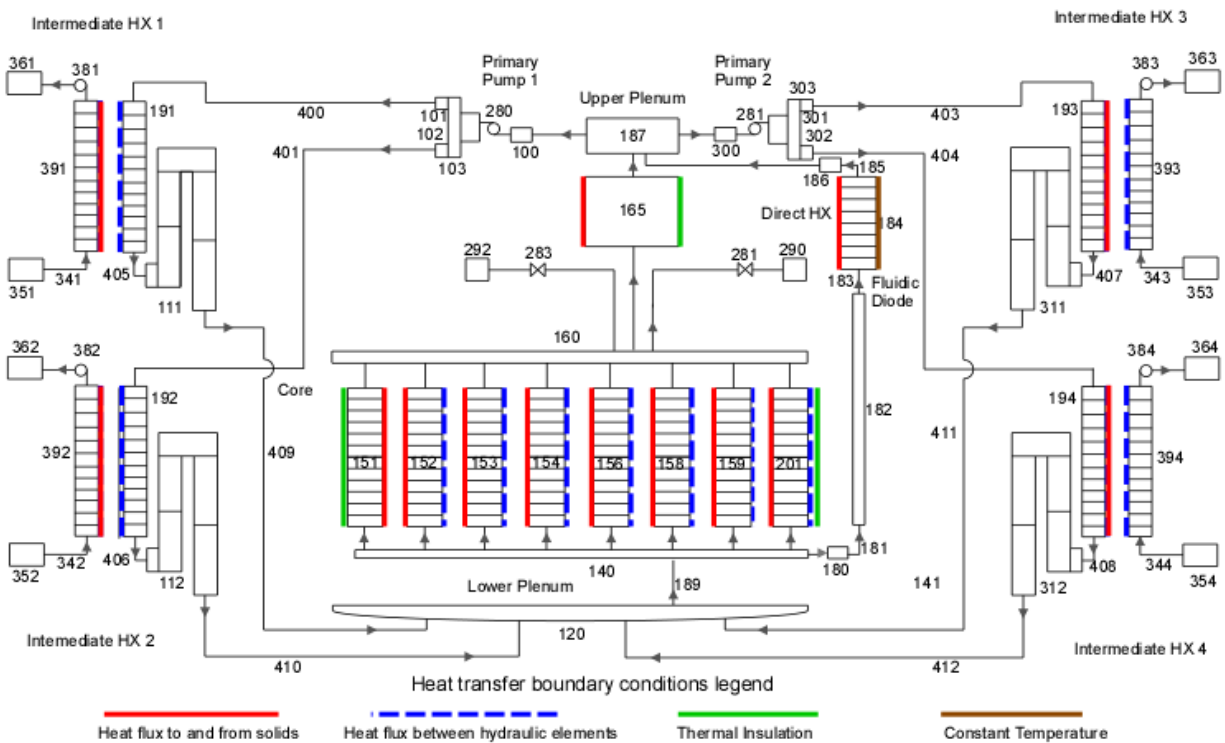


**Figure D-1. Schematic of the Modular PB-AHTR RELAP5 Model**  
(Logical junctions are highlighted and do not take physical space. The positions of the components are not to scale (Galvez et al. 2010).)

The baseline design for this model is a 900MWth pebble channel assembly (PCA) type PB-FHR core. Although the design is expected to significantly evolve during the development path of this project, this model serves as a first proof of principle regarding the capability to model the FHR using RELAP5.

Flibe is used as the primary coolant, while flinak – which has also been implemented into RELAP5 (Davis 2005) – is used as the secondary coolant. Friction losses across the pebble-bed are calculated using Ergun’s correlation, which is the most common correlation for porous media flow, while convective heat transfer between the coolant and the pebbles is characterized by the

Wakao correlation (see second FHR Workshop White Paper. The design of the IHX and the DHX is derived from the heat exchanger design of the MSBR developed at ORNL in the 1970s, while the design of the NDHX is based on a helical heat exchanger. According to these designs, relevant heat transfer correlations are also implemented into RELAP5 (Galvez 2011). In this model, the DRACS heat exchanger (DHX) is considered as an assembly of 1000 2.5 cm tubes, divided into baffled circular bundles, modeled as one single pipe with the same heat transfer characteristics as the whole heat exchanger, and divided into 6 axial elements. The IHX is considered as an assembly of 9465 0.3428 cm tubes, also divided into baffled circular bundles and modeled as one single pipe with the same heat transfer characteristics as the whole heat exchanger, divided into 12 axial elements.

Overcooling transients have not been considered in thermal-hydraulic analyses of the FHR in RELAP5 so far, and at this point, the code is not able to properly model this phenomenon. Similarly, the capacity to properly model bypass flow in the graphite reflectors has not been developed in RELAP5, because of the complexity of graphite blocks geometry changes under thermal transients.

Despite these limitations in the modeling capabilities of RELAP5 for the FHR, preliminary results for the transient response of the system to a LOFC have been obtained, which are presented in Chapter 3 as an example of the capabilities that are expected from the thermal-hydraulic modeling of the FHR.